DETERMINATION OF THE MODAL PROPERTIES OF COMPLEX STRUCTURES INCLUDING NON-LINEAR EFFECTS

BY

GEOFFREY R, TOMLINSON

A THESIS SUBMITTED FOR THE DEGREE OF DOCTOR OF PHILOSOPHY OF THE UNIVERSITY OF SALFORD, DEPARTMENT OF MECHANICAL AND AERONAUTICAL ENGINEERING

MAY 1979

CONTENTS

Page No.

SECTION2 - THE EIFECTS OF MODAL COUPLING IN LIGHTLY DAMPED STRUCTURES

ACKNOWLEDGEMENTS

The author wishes to express his thanks to Dr. J.H. Hibbert, of the Mechanical Engineering Department, Salford University for his help and advice, and to Dr. J. Mather, Manchester Polytechnic, for his support throughout the course of the project.

Thanks are also extended to Dr. J. Cox, of the Mechanical Test Department, British Aerospace, Preston for the advice and facilities extended during the course of the work.

Finally, my sincere thanks to my wife, Margaret, for her patient preparation of this dissertation.

PUBLICATIONS

During the course of the work two papers were accepted for publication. The details of these are shown below and proof copies of the papers are given in Appendix VIII.

1. G R Tomlinson 1979
   Journal of Sound and Vibration 63 -3, 1-14.
   Force Distortion in Resonance Testing of Structures with Electra-Dynamic Vibration Exciters.

2. G R Tomlinson and J H Hibbert 1979
   Journal of Sound and Vibration 64 -3, l-10
   Identification of the Dynamic Characteristics of a Structure with Coulomb Friction.

SUMMARY

This dissertation is concerned with the determination of such modal properties as natural frequencies and modal damping of lightly damped linear and non-linear structures.

The material is presented in three sections, the first of which analyses in detail the problems that are encountered when using electro-dynamic vibration exciters to harmonically excite a structural resonance in order that the modal properties can be accurately determined.

The second section of the work deals with the effect of modal interaction and different damping distributions on the ability to excite the normal modes of vibration of linear structures, and the influence of these on the resulting modal properties.

The results from this work and those of the first section are used to develop a rig which includes a non-linear friction device on which normal mode tests are conducted. This constitutes the final section of the work which is devoted to the theoretical and experimental identification of the modal properties of non-linear systems using normal mode methods.

INTRODUCTION

The work described in this dissertation was instigated through contacts with the Department of Mechanical Test, British Aerospace, Warton, Preston. One of the functions of this Department is to carry out Ground Resonance Tests on military aircraft. These tests employ steady state forced vibration procedures using multiple exciter inputs to excite the normal modes of aircraft in order to accurately determine such modal properties as normal mode frequencies, damping ratios, generalised masses and stiffnesses.

However, problems arise in the forced vibration testing of these complex structures due to the effects of non-linearities such as friction, non-linear stiffnesses and backlash. As a result of these problems the author became involved in a research project which was concerned with the identification of the damping ratios and natural frequencies (the properties of generalised mass and stiffness be'ing excluded from the identification process) of non-linear structures employing multi-point excitation methods.

However, initial experimental tests, employed to 'practise' the art of multi-point normal mode excitation procedures, which were carried out on rigs which had low damping properties revealed problems relating to the effects of the vibration exciters which the author had not expected. These problems resulted in a considerable effort being spent on their investigation and eventual solution before any work employing multi-point excitation methods on structures with and without controlled non-linearities could be carried out.

Thus the overall programme of work is presented in three sections. The first section deals with the effects of using electro-dynamic vibration exciters to vibrate a structure. This work analyses in detail the constraints that these exciters impose upon a vibration test programme and reveals the cause of the harmonic input force distortion which arises when vibration tests are carried out on lightly damped

structures, which, although reported by other researchers, have never been satisfactorily explained.

The second section of the work is devoted to an area which has recently received considerable attention, that of the effect of a modal damping matrix with off-diagonal terms which causes modal interaction. This was a further problem with which the author was confronted in the initial testing stage and the results of this investigation have produced criteria which enhance the existing knowledge of the effects of modal interaction on the ability to excite the normal modes of vibration of linear damped structures.

The final section exploits the information obtained from the work described in the earlier sections to investigate the effects of two commonly occurring structural non-linearities, Coulomb friction and non-linear stiffness. A considerable part of this section concentrates in particular on the effect of Coulomb friction, since this had proved to be a problem on swing-wing aircraft at British Aerospace, and the work has produced an original identification procedure using multi-point excitation methods which is supported by extensive experimental work.

NOMENCLATURE

Definition of Greek symbols used in the text is listed below, other nomenclature which is used is defined the first time it is introduced, and where possible, it is consistent throughout, although in some cases it has been necessary to use the same symbol to describe more than one variable.

α	Constant representing the maximum armature displacement.
β	Ratio of adjacent natural circular frequencies.
β_1	Ratio of excitation frequency to test structure natural frequency.
γ	Co-ordinate system.
δ	Structural (hysteretic) damping factor.
δ^*	Equivalent structural damping factor.
ε_δ	Percentage error in the modal damping factor.
ε_ω	Percentage error in the transverse normal mode frequency.
ζ	Viscous damping ratio.
ζ_1	Test structure viscous damping ratio.
ζ_2	Vibration exciter viscous damping ratio.
λ	Normalising constant.
ν	Non-linear stiffness coefficient.
$\underset{\sim}{\xi}$	Matrix of modal damping coefficients.
$\underset{\sim}{\xi}_n$	Matrix of modal coupling damping coefficients whose leading diagonal is zero.
$\underset{\sim}{\xi}_d$	Diagonal matrix of modal damping coefficients.
σ	Surface integral.
ϕ	Phase angle between input force and output displacement.
$\underset{\sim}{\Phi}$	Modal matrix.
ψ	Magnetic flux linkage.
$\underset{\sim}{\Psi}$	Transformation matrix.
ω	Excitation frequency.
ω_1	Test structure natural circular frequency.
ω_2	Vibration exciter natural circular frequency.

ω_b	Natural circular frequency of vibration in the transverse (bending) mode.
ω_n	Normal mode frequency of vibration.
ω_t	Natural circular frequency of vibration in the torsional mode.
$\omega_{j,k}$	Natural frequency of vibration in the j^{th} and kth mode respectively.
Ω	Ratio of excitation frequency to normal mode frequency.

SECTION 1

FREQUENCY RESPONSE TESTING OF LIGHTLY DAMPED STRUCTURES

1. FREQUENCY RESPONSE TESTING USING ELECTRO-DYNAMIC VIBRATION EXCITERS

1.1 INTRODUCTION

The use of electro-dynamic vibration exciters in the frequency response testing of structures is almost universal. These exciters are very simple in their basic design and construction (1) and due to their ease of application, particularly in the ability to attach and orientate these on the test structure, they are the type of vibration exciter most commonly used in forced vibration tests. There are two basic modes of operation with such exciters, these being related to the reference used as the input to the structure.

In order to excite a structural resonance, a harmonic force is injected into the structure under test. In order to establish the resonant condition of the structure, it is necessary to have some knowledge of the phase of the input force with respect to the output response, particularly if the structure is lightly damped when accurate determination of peak amplitudes is difficult.

This can be done in two ways. The first, and most commonly used mode of operation, is to use a force gauge which is inserted between the vibration exciter and the test structure, which gives an output voltage proportional in magnitude and phase to the force being injected into the structure at that point. The second method is to measure the input current, in magnitude and phase, to the vibration exciter from the oscillator and amplifier. Reference to the basic equations of motion of an electro-dynamic exciter (2) shows that the force delivered by the vibration exciter is proportional to the current flowing through the coil of the exciter armature. There are fundamental differences between these two approaches since the latter approach involves the structure plus the vibration exciter characteristics whereas with the first approach one is dealing with the virgin structure. Although the use of a force gauge appears to be the most obvious

choice to provide the reference input force source, problems arise when the structure under test is lightly damped. Under these conditions the force signal around the resonant regions reduces in magnitude and, particularly at the fundamental resonance, becomes considerably non-linear.

This aspect of the effects of electro-dynamic vibration exciters on a system under test has received considerable attention. For example, the work by Taylor et al (3), and Holmes (4) discusses means of compensating for the exciter mass, stiffness and damping characteristics, which may be very significant if the structure is lightly damped. However, no reference is made to the problems of harmonic force distortion which occur in the resonance testing of lightly damped structures.

The problem of harmonic force distortion is one which seems to have received little attention in terms of understanding exactly what is the cause of this, or the manner in which the frequency spectrum of the input force varies, particularly near the structural resonance. The reason for this is due to the fact that techniques for removing unwanted harmonics e.g. the use of tracking filters (5) have been long established and present day techniques based on digital filtering methods are often taken for granted when using sophisticated equipment. Nevertheless, most researchers in the field of vibration testing will undoubtedly have at some time observed on an oscilloscope the output from a force transducer in the region of a structural resonance when the magnitude of the force signal has reduced considerably and has displayed considerable non-linear harmonic distortion. These effects have been analysed in detail and the theoretical predictions confirmed by carrying out an extensive experimental programme and analogue computer simulation study.

In order to understand fully the implications of using either the input current as a reference input force source or using a force gauge directly, a further analysis relating to the effects of a typical electro-dynamic vibration exciter on

choice to provide the reference input force source, problems arise when the structure under test is lightly damped. Under these conditions the force signal around the resonant regions reduces in magnitade and, particularly at the fundamental resonance, becomes considerably non-linear.

This aspect of the effects of electro-dynamic vibration exciters on a system under test has received considerable attention. For example, the work by Taylor et al (3), and Holmes (4) discusses means of compensating for the exciter mass, stiffness and damping characteristics, which may be very significant if the structure is lightly damped. However, no reference is made to the problems of harmonic force distortion which occur in the resonance testing of lightly damped structures.

The problem of harmonic force distortion is one which seems to have received little attention in terms of understanding exactly what is the cause of this, or the manner in which the frequency spectrum of the input force varies, particularly near the structural resonance. The reason for this is due to the fact that techniques for removing unwanted harmonics e.g. the use of tracking filters (5) have been long established and present day techniques based on digital filtering methods are often taken for granted when using sophisticated equipment. Nevertheless, most researchers in the field of vibration testing will undoubtedly have at some time observed on an oscilloscope the output from a force transducer in the region of a structural resonance when the magnitude of the force signal has reduced considerably and has displayed considerable non-linear harmonic distortion. These effects have been analysed in detail and the theoretical predictions confirmed by carrying out an extensive experimental programme and analogue computer simulation study.

In order to understand fully the implications of using either the input current as a reference input force source or using a force gauge directly, a further analysis relating to the effects of a typical electro-dynamic vibration exciter on

the response of a single degree-of-freedom system has been carried out. The analysis covers not only the modifications which occur in the interpretation of the resonant condition due to using the input current as a force reference, but also the importance of relating the output response to the input response of a test system in order to measure the true system characteristics.

1.2 ANALYSIS OF THE HARMONIC FORCE DISTORTION ENCOUNTERED WITH ELECTRO-DYNAMIC VIBRATION EXCITERS

Experimental tests (described in the following Chapter) had shown that the non-linearities occurring in the input force signal in the region of a structural resonance of a lightly damped structure were predominantly due to second harmonic effects and the origin of these was the electro-dynamic vibration exciter. This was indicated by the fact that although the input current to the exciter, the motion of the armature of the vibration exciter and the output response were sinusoidal throughout the tests, the input force signal displayed considerable harmonic distortion as the resonant condition of the structure was approached.

Thus having isolated the source of the harmonic distortion as the vibration exciter it was necessary to know in detail something of the vibration exciter characteristics. The underlying theory of electro-dynamic exciters, which distinguishes them from electro-magnetic exciters, is that the force generated by the exciter is assumed to be proportional to the input current, the constant of proportionality being a function of both the armature coil design and the magnetic field structure (7).

In the case of electro-dynamic exciters, the magnetic flux field is assumed constant which results in an equation for the force generated being given as:

$$F = BlNi \quad \ldots\ldots\ldots\ldots\ldots\ldots \quad (1)$$

where, l= coil length in the flux field
B = flux density
N = number of turns of length 1,
i = current

However, if the magnetic field structure does not produce a uniform flux density field, then equation (1) does not hold true and one must resort to the fundamental electromagnetic equations which allow for variations in the magnetic flux field.

1.2.1 CHARACTERISTICS OF THE VIBRATION EXCITER MAGNETIC FLUX FIELD

The voltage V which results when a coil is oscillated in a magnetic flux field is given as (8):

$$V = \frac{d\psi}{dx} \cdot \frac{dx}{dt} \quad \ldots\ldots\ldots\ldots\ldots\ldots\ldots (2)$$

where $\frac{d\psi}{dx}$ is the rate of change of flux linkage with respect to the instantaneous displacement within the magnetic flux field and $\frac{dx}{dt}$ is the instantaneous velocity. To be able to derive a characteristic of the magnetic flux field behaviour it was required to be able to identify the behaviour of $\frac{d\psi}{dx}$ in equation (2).

In order to examine the characteristics of the vibration exciter magnetic flux field, two vibration exciters with similar characteristics were connected armature to armature via a rigid link as shown in Figure 1. One of the exciters was used to 'drive' the other exciter, whose armature was open-circuited, with a constant peak-to-peak amplitude at a given frequency, the amplitudes being measured by a non-contact displacement transducer. By superimposing a d.c. bias voltage onto the drive signal, the mean position of the open-circuit exciter armature (i.e. the static equilibrium point about which the vibration takes place) could be varied throughout its working displacement range for that

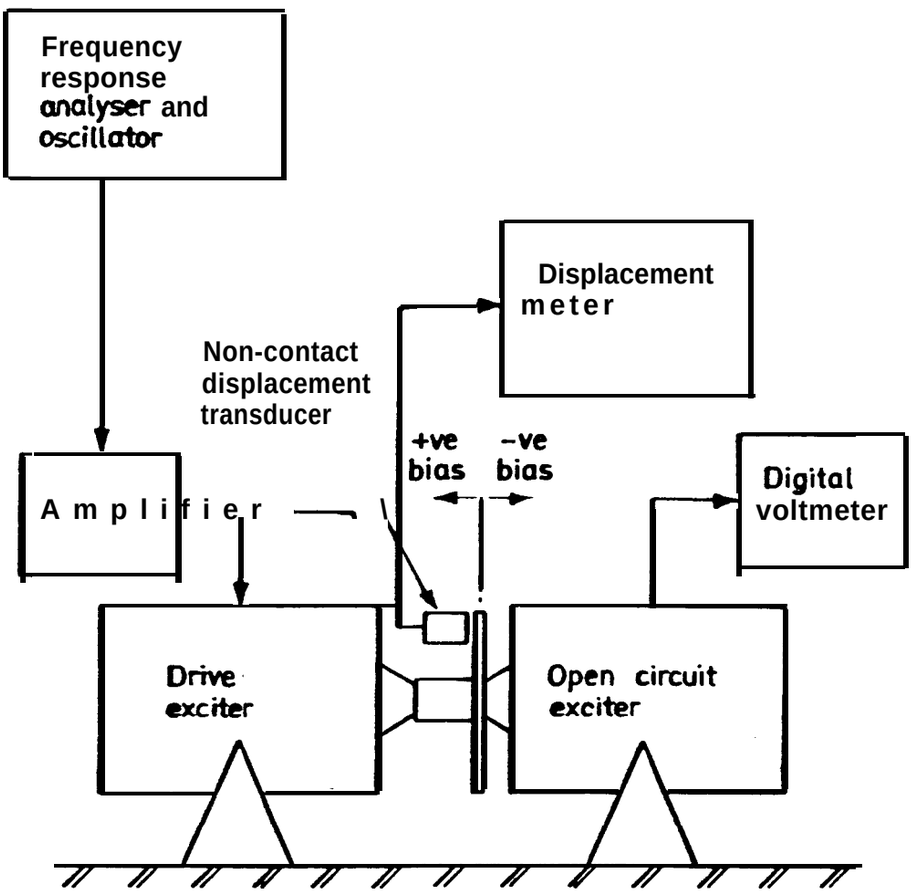

FIGURE 1

MEASUREMENT OF VIBRATION EXCITER MAGNETIC FLUX FIELD CHARACTERISTICS.

particular exciter model. For each mean position of the open-circuited exciter armature a constant peak-to-peak amplitude of vibration was applied, this amplitude representing 15% of the rated maximum peak-to-peak displacement range of the exciter. Tests were carried out at different frequencies (for the same mean armature positions and amplitudes of vibration) and the results from tests carried out at 30 Hz and 60 Hz are shown on Figure 2. These curves, which are even functions with a square-law characteristic, are related to the back emf generated by the velocity of the armature and the position of the armature in the flux field.

The characteristics of Figure 2 show that the assumption of a constant magnetic field is invalid and that there is a variation in the magnetic field structure which is related to the position of the exciter armature in the magnetic field. In the case of lightly damped structures where the amplitudes of vibration are large and the level of the input forces are small, the normal governing electro-dynamic equations are inapplicable.

Since, for each test the velocity was constant, the characteristics of Figure 2 must represent $\frac{d\psi}{dx}$. The characteristics of the curves of Figure 2 are given by:

$$C\{1 - \alpha(x_o + x)^2\} \quad . . . . . \quad (3)$$

$$\therefore \frac{d\psi}{dx} = C\{1 - \alpha(x_o + x)^2\} \quad . . . . . \quad (4)$$

where $\sqrt{\alpha}$ = constant

$$= \frac{1}{\text{maximum rated peak displacement of the exciter}}$$

$$\geq \frac{1}{(x_o + x} \quad .. \quad .. \quad .. \quad .. \quad .. \quad .. \quad (5)$$

due to the constraints imposed by the exciter design, i.e.

the armature 'bottoms' on the centre pole magnet if,

$$(xo + x) \geq \frac{1}{\sqrt{\alpha}}$$

where x_o = mean position of the armature
x = instantaneous peak displacement of the armature
C = constant related to the maximum back emf generated

Thus the back emf generated as a result of the motion of the armature in the magnetic flux field of Figure 2 is:

$$v_B = \frac{d\psi}{dx} \cdot \frac{dx}{dt} = C\{1 - \alpha(x_o + x)^2\}\dot{x} \quad \ldots \quad (6)$$

If the well-known basic equations of motion (see Appendix I) of an electro-dynamic vibration exciter are modified to include the terms of equation (6) one gets an expression for the armature equation of motion:

$$\ddot{x} + \frac{kx}{m} + \frac{K}{mR}\{1 - \alpha(x_o + x)^2\}\dot{x} = \frac{k_F}{mR}v\cos\omega t \quad \ldots \quad (7)$$

where the constant K is a combination of the force current constant k_F and the back emf constant k_B, (it is generally assumed that these quantities are equal since the electrical power developed in the armature is equal to the mechanical power absorbed by the armature).

Equation (7), which represents the equation of motion of the armature of the vibration exciter, is a non-linear second order differential equation. If the solution of this equation was obtained in terms of the amplitude of vibration 'x' then the effect of the square law terms $(x_o + x)^2$ would be negligible compared to the fundamental component and the output displacement would have virtually no harmonic distortion.

However, it is not the amplitude of vibration which is under

observation but the force delivered by the exciter to produce this motion. To examine the validity of equation (7), a model of a single degree-of-freedom system excited by an electro-dynamic vibration exciter, whose equation of motion is governed by equation (7) was analysed on an EAL 380 Analogue Computer.

1.3 SIMULATION STUDY OF HARMONIC FORCE DISTORTION

The physical model of the system used in the simulation is shown on Figure 3, and the equation of motion for this two-mass single degree-of-freedom system, assuming that steady state vibration is about the zero mean, i.e. $x_0 = 0$, $(x = X_1 = X_2)$ is:

$$\ddot{x} + \left\{\frac{c_1}{m_1+m_2} + \frac{K}{R(m_1+m_2)}(1-\alpha x^2)\right\}\dot{x} + \frac{(k_1+k_2)x}{m_1+m_2} = \frac{k_F v \cos\omega t}{m_1+m_2} \qquad (8)$$

The analogue computer block diagram used to simulate equation (8) is shown on Figure 4. The physical quantities used in the simulation were obtained from the tests carried out on a cantilever beam detailed in Chapter 2 and from the data supplied by the manufacturers of the vibration exciter.

The photographs on Plate 1 show the results of the simulation exercise and a set of experimental results from tests carried out on a cantilever beam (detailed in Chapter 2). It can be seen that the behaviour of the force trace is almost identical in both cases. The centre set of traces of the experimental results also show the input current to the exciter at resonance and it can be clearly seen that no harmonic distortion is apparent. The results of the analogue simulation produced the identical force input behaviour as was obtained during experimental testing whereby the force input signal approached a minimum at resonance, with second harmonic distortion becoming predominant. Above and below

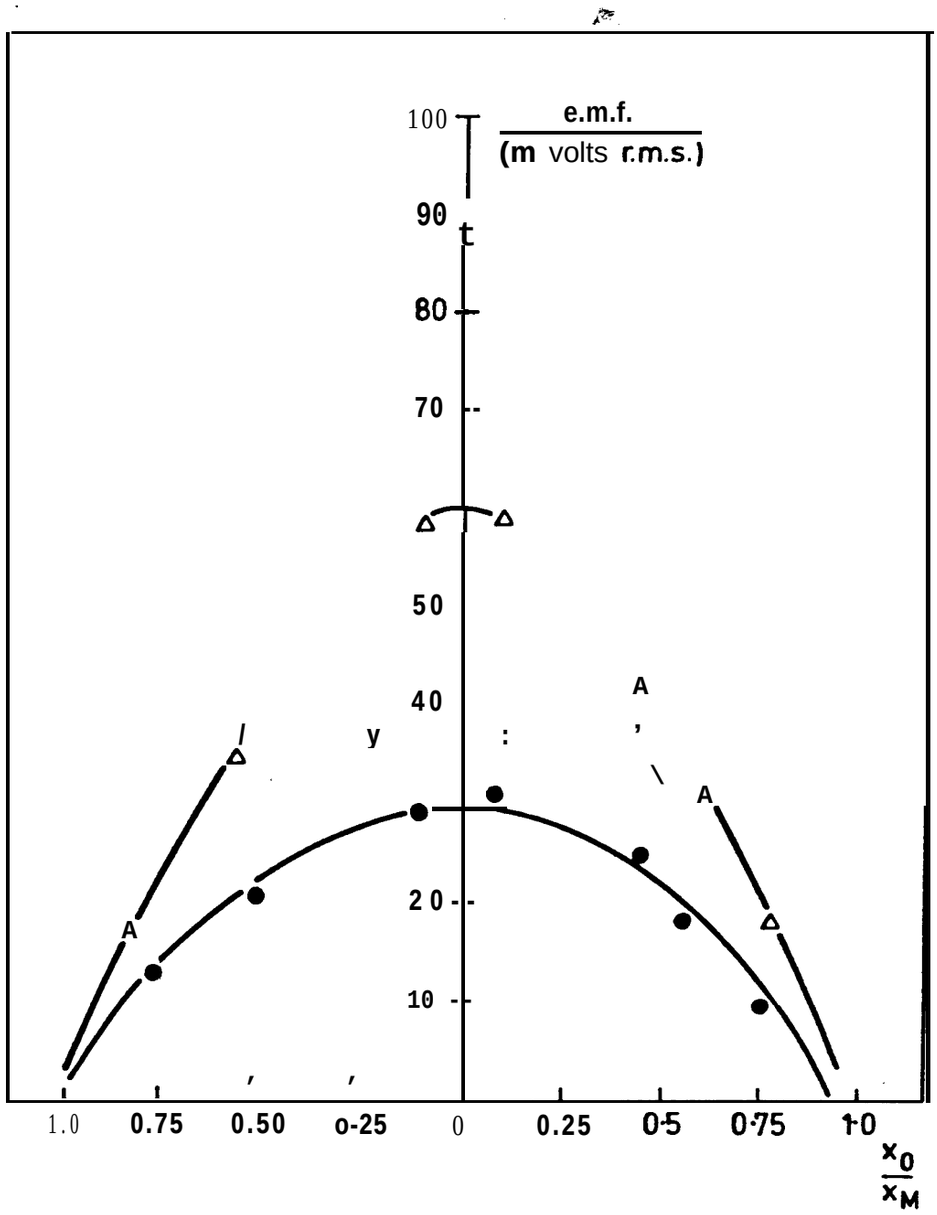

FIGURE 2

BACK e.m.f. GENERATED AS A FUNCTION OF THE OPEN-CIRCUIT EXCITER ARMATURE POSITION

x_O **IS THE ARMATURE MEAN POSITION**
x_M **IS THE MAXIMUM ARMATURE DISPLACEMENT**

A **EXCITATION FREQUENCY 60 Hz**
● **EXCITATION FREQUENCY 30 Hz**

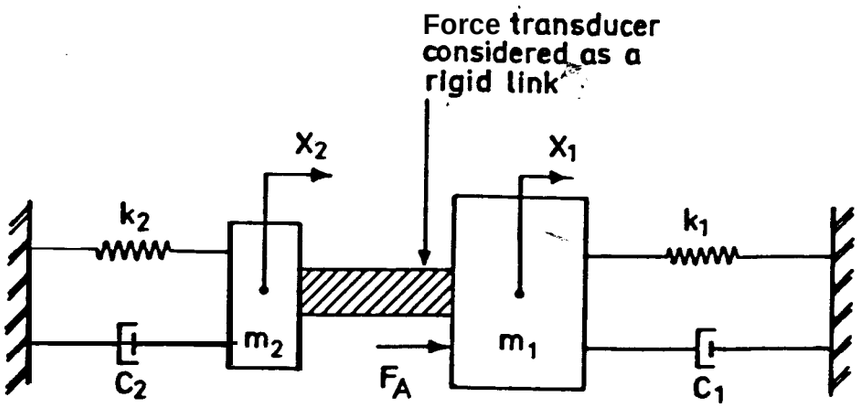

FIGURE 3

PHYSICAL MODEL OF A SINGLE DEGREE-OF-FREEDOM STRUCTURE EXCITED BY AN ELECTRO-DYNAMIC EXCITER

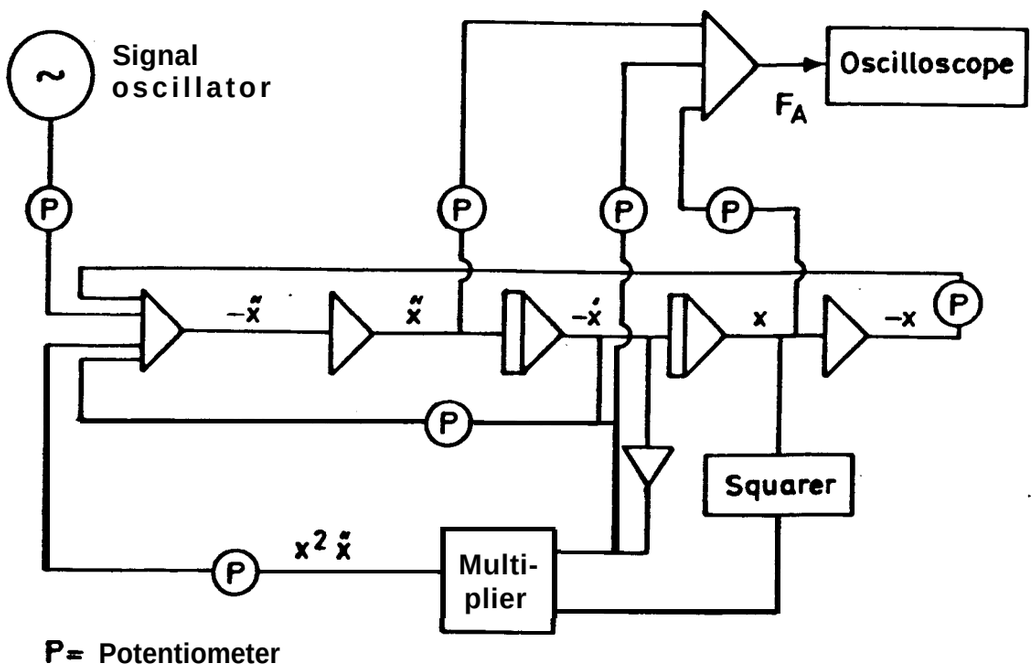

FIGURE 4

ANALOGUE COMPUTER SIMULATION DIAGRAM

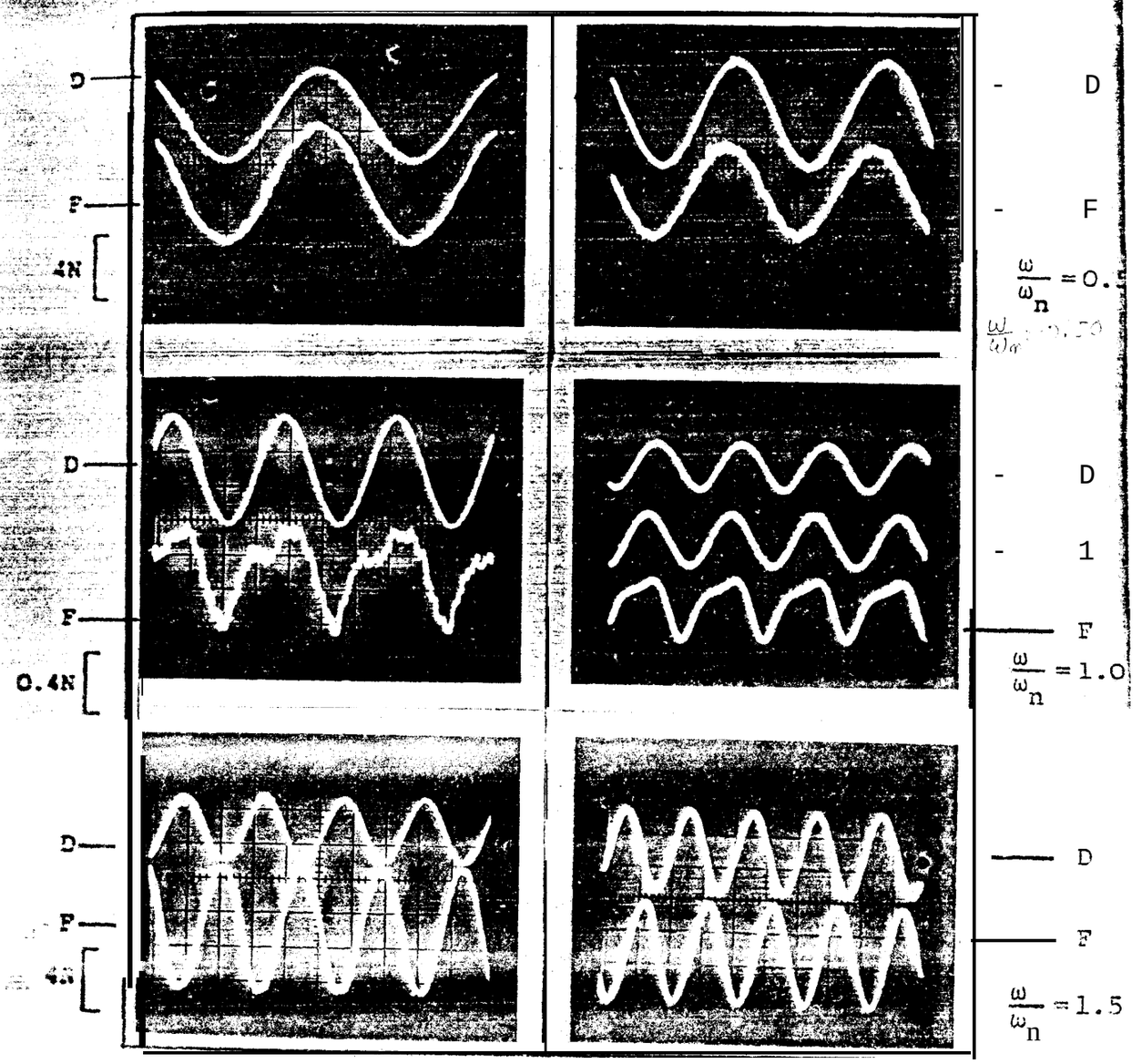

ANALOG SIMULATLCN EXPERIMENTAL RESULTS

PLATE 1

COMPARISON OF SIMULATED AND EXPERIMENTAL RESULTS SHOWING TRE HARMONIC FORCE DISTORTION AT RESONANCE.

D - OUTPUT DISPLACEMENT OF STRUCTURE
I - INPUT CURRENT TO EXCITER
F - INPUT FORCE TO STRUCTURE

the resonant condition the force input signal is predominantly the fundamental component and displays negligible amounts of harmonic distortion.

In each of the traces shown on Plate 1 the resulting displacement response is given and it can be seen that no harmonic distortion is present, the displacement being in phase with the force below resonance, changing to 180^{o} out of phase above resonance, which is the case for a single degree-of-freedom system. The 90^{o} phase change at resonance cannot be readily discerned due to the high level of second harmonic distortion of the force signal.

1.4 THEORETICAL ANALYSIS OF THE HARMONIC DISTORTION MAGNITUDES

Having established that due to the square law characteristics of the flux field the harmonic distortion was predominantly second harmonic in nature, an analysis of the harmonic distortion magnitudes likely to be experienced when testing systems which bebave basically as a single degree-of-freedom system (i.e. well separated resonant frequencies) was carried out. With reference to Figure 3 it can be assumed that the total force generated by the vibration exciter is represented by a harmonic series:

$$F_A = \sum_{n=1}^{\infty} F_{A_n} e^{j\ (n\omega t+\phi_n)}, n = 1, 2\ .\ ....\infty\ ..\quad ..\qquad (9)$$

where $F_{A_n} = F_n e^{j(n\omega t+\phi_n)} - (m_2 D^2 + c_2 D + k_2)xe^{j(n\omega t+\phi_n)}$ (10)

and F_n = magnitude of n^{th} harmonic component
ω = excitation frequency
ϕ_n = phase angle between n^{th} force and displacement component

The force F_{A_n} reacts against the test structure to give:

$$F_{A_n} = (m_1 D^2 + c_1 D + k_1) x e^{j(n\omega t+\phi_n)} \quad .. \quad .. \quad (11)$$

$$\therefore \quad e^{j(n\omega t+\phi_n)} (F_n - m_2 D^2 x - c_2 D_x - k_2 x) =$$

$$(m_1 D^2 + c_1 D + k_1)\ x e^{j(n\omega t+\phi_n)} \quad .. \quad .. \quad .. \quad (12)$$

For harmonic motion $Dx = jn\omega x$

$$\therefore F_{A_n} = \frac{(k_1 - m_1 n^2\omega^2 + jc_1 n\omega) . F_n e^{j(n\omega t+\phi_n)}}{\{(k_1+k_2) - (m_1+m_2)n^2\omega^2 + (c_1+c_2)jn\omega\}} \quad (13)$$

and introducing the notation:

$$\omega_2^{\,2} = \frac{k_2}{m_2} \text{ (vibration exciter natural frequency)}$$

$$\omega_1^{\,2} = \frac{k_1}{m_1} \text{ (structure natural frequency)}$$

$$\frac{m_2}{m_1} = m', \quad \frac{k_2}{k_1} = k', \quad \beta_n = \frac{n\omega}{\omega_1}$$

$$\frac{c_1}{k_1} = \frac{2\zeta_1}{\omega_1}, \quad \frac{c_2}{k_2} = \frac{2\zeta_2}{\omega_2}$$

equation (13) becomes:

$$F_{A_n} = \frac{(1-\beta_n^{\,2}+j\beta_n\ \zeta_1)\ F_n e^{j(n\omega t+\phi_n)}}{\{(1+k') - \beta_n^{\,2}(1+m') + j(2\zeta_1\beta_n+2\zeta_2 n\frac{\omega}{\omega 2}k')\}} \quad (14)$$

At the structural resonant frequency, $\omega = \omega_1$ and $\beta_1 = 1$, thus the fundamental harmonic force component is:

$$F_{A_1} = \frac{(j2\zeta_1)\ F_1 e^{j(\omega t+\phi_1)}}{\{(1+k') - (1+m') + j(2\zeta_1+2\zeta_2\frac{\omega_1}{\omega_2}k')\}} \quad .. \quad (15)$$

the second harmonic force component is:

$$F_{A_2} = \frac{(-3+j4\zeta_1)\ F_2 e^{j(2\omega t+\phi_2)}}{\{(1+k') - 4(1+m') + j(4\zeta_1+4\zeta_2\frac{\omega_1}{\omega_2}k')\}} \quad .. \quad (16)$$

substituting for $\frac{\omega_1}{\omega_2}k' = \sqrt{m'k'}$ in equations (15) and (16) gives for the ratio of the second harmonic component to the fundamental:

$$\frac{F_{A_2}}{F_{A_1}} = \frac{F_2 e^{j(\omega t+\phi)}}{F_1} \frac{(-3+j4\zeta_1)}{j(2\zeta_1)} \frac{\{(k'-m')+j(2\zeta_1+2\zeta_2\sqrt{m'k'})\}}{\{(k'-4m'-3)+j(4\zeta_1+4\zeta_2\sqrt{m'k'})\}} \quad (17)$$

Equations similar to equation (17) may be written for the higher harmonics but the effects of these are obviously lower than the second harmonic contribution.

An equation similar to equation (17) was developed by Asher (9) who based his original equations of motion on the somewhat dubious assumption that 'the force transducer stiffness was similar to (and in certain cases less than) the stiffness of the structural system under test'. He gave an equation for the ratio of F_{A_2}/F_{A_1} as:

$$\frac{F_{A_2}}{F_{A_1}} = \frac{F_2}{F_1} \frac{(-3+j4\frac{\zeta_1}{\omega_1})}{j^2\frac{\zeta_1}{\omega_1}} \frac{\left\{-k' - j\frac{\zeta_1}{\omega_1}(\frac{k'}{m'}-1)\right\}}{\left\{(12-\frac{3k'}{m'}-4k')-j\frac{4\zeta_1}{\omega^1}(\frac{k'}{m'}-4)\right\}}. \quad (18)$$

where all the symbols have the same definition apart from k' which was given as:

$$k' = \frac{\text{force transducer stiffness}}{k_1} \quad .. \quad .. \quad .. \quad (19)$$

Unfortunately, equation (18) has no practical significance since the use of a force transducer which has a stiffness less than or equal to the structural stiffness would lead

to extreme difficulties in resonance testing. Another factor which eluded Asher is that his equations do not allow for the fact that the vibration exciter effects are minimised when the vibration exciter natural frequency coincides with the structural natural frequency ($k' = m'$ in equations (14) to (17)) as shown in Appendix II, and thus the effects of the harmonic distortion are also minimised.

Normally in resonance testing, the vibration exciter is chosen so that its mass and stiffness effects will have a minimal effect on the structure under test, and in these cases we have the following conditions:

$$m' < k' << 1 \quad . \quad . \quad . \quad . \quad . \quad . \quad . \quad . \quad . \quad . \quad . \quad . \quad . \quad . \quad (20)$$

Equation (17) can then be approximated, for the case of lightly damped structures, to:

$$\left|\frac{F_{A_2}}{F_{A_1}}\right| = \frac{k'}{2\zeta_1}\left|\frac{F_2}{F_1}\right| \quad . \quad . \quad . \quad . \quad . \quad . \quad . \quad . \quad . \quad . \quad . \quad . \quad . \quad . \quad . \quad (21)$$

Equation (21) indicates that for the second harmonic distortion to be less than 100%, the stiffness ratio $k' \leqslant 2\zeta_1$. For lightly damped structures, where the equivalence $2\zeta = \delta$ (δ being the structural damping factor) can be made then $k' \leqslant \delta$ and since structural damping forces increase with stiffness, the stiffer the structure the lower will be the harmonic force distortion.

The reason behind the harmonic distortion becoming predominant at a system resonance is easily shown by considering equation (14). Equation (14) represents the harmonic force components applied to the system under test. If one assumes that the exciter is being driven by a high output impedance amplifier then electrical damping effects can be ignored (3, 4). Also if one considers the mechanical damping of the

exciter to be negligible, equation (14) for the modulus of the fundamental and second harmonic force component respectively reduces to:

$$|F_{A_1}| = \frac{\left\{(1 - \beta_1{}^2)^2 + (\beta_1 2\zeta_1)^2\right\}^{\frac{1}{2}} |F_1|}{\left\{((1 + k') - \beta_1{}^2(1 + m'))^2 + (2\zeta_1\beta_1)^2\right\}^{\frac{1}{2}}} \quad (22)$$

and $$|F_{A_2}| = \frac{\left\{(1 - 4\beta_1{}^2)^2 + (4\beta_1\zeta_1)^2\right\}^{\frac{1}{2}} |F_2|}{\left\{((1 + k') - 4\beta_1{}^2(1 + m'))^2 + (4\zeta_1\beta_1)^2\right\}^{\frac{1}{2}}} \quad (23)$$

Equation (22) is shown plotted on Figure 5 as a function of the frequency ratio (β_1) for different values of the system damping ratio for the cases when the system natural frequency is greater and less than the exciter natural frequency.

Inspection of equation (23) shows that the magnitude of the second harmonic content is almost constant. Since the magnitude of the fundamental harmonic approaches a minimum at the resonant condition, as shown by Figure 5, the ratio of the second (and the higher harmonics) to the fundamental harmonic at this point is a maximum.

Figure 5 also shows that the force characteristic is 'inverted' when the condition of the system natural frequency changes from a value above to a value below that of the exciter natural frequency.

1.5 SOME PITFALLS ENCOUNTERED DURING THE RESONANCE TESTING OF LIGHTLY DAMPED STRUCTURES

The work detailed in the above sections has shown that the mass and stiffness properties of an electro-dynamic exciter can affect the force being injected into a system under test.

It is commonly thought that if a constant current source is used to drive an electro-dynamic vibration exciter then the

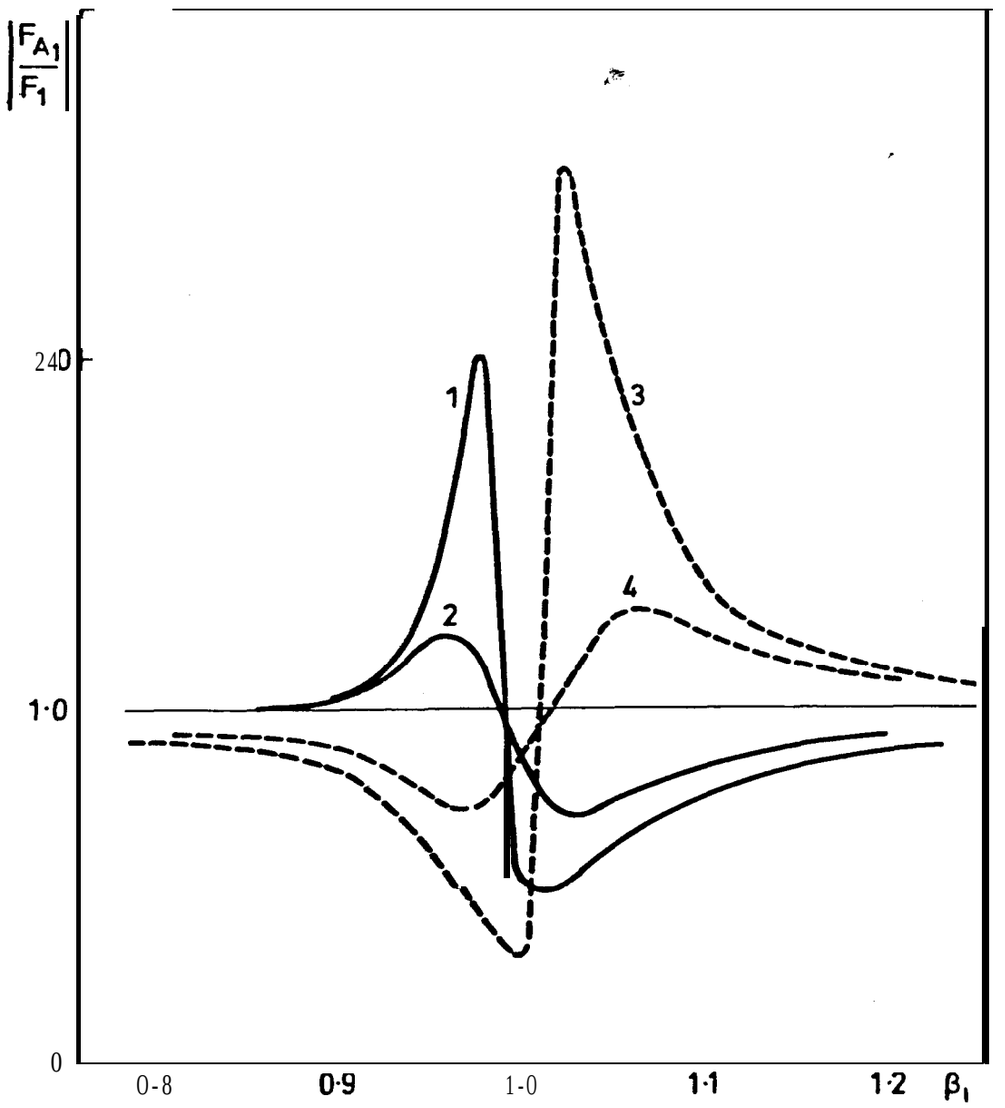

FIGURE 5

THEORETICAL CURVES FROM EQUATION (22) SHOWING INPUT FORCE VARIATION AT A STRUCTURAL RESONANCE FOR:

1. $\zeta_1 = 0.01$ } $m' = 0.175$, $k' = 0.14$, $\omega_1 > \omega_2$
2. $\zeta_1 = 0.05$ }
3. $\zeta_1 = 0.01$ } $m' = 0.005$, $k' = 0.06$, $\omega_1 < \omega_2$
4. $\zeta_1 = 0.05$ }

β_1 **IS THE FREQUENCY RATIO,** ω/ω_1

F_{A_1} **IS THE FORCE DELIVERED TO THE STRUCTURE**

F_1 **IS THE FORCE DELIVERED BY THE EXCITER**

force exciting the test structure is also constant in magnitude (and phase with respect to the oscillator).

However, the results of experimental tests (Chapter 2, Section 2.3) showed that this is not the case if the system under test is lightly damped. These effects have been noted by other researchers and means of compensating for these have been suggested (3, 10). An analysis of why there is such a large variation in the magnitude and phase of the input force has been carried out and is presented in Appendix II.

This analysis is based on the model of Figure 3 and considers a constant input current source being fed to the exciter coil which produces a force to excite a structure.

However, the force which is developed must also accelerate the additional masses of the exciter and its connections to the structure under test. This results in an equation relating the exciter and structural natural frequency to the force, (F), generated as a result of the input drive current. This equation, given in Appendix II, A.II.13 is:

$$k_2 X \left(\left(\frac{\omega_1}{\omega_2}\right)^2 - 1 \right) = F \sin\phi \quad \ldots\ldots\ldots\ldots \quad (24)$$

where the symbols have the usual meaning, and

ϕ = phase angle between the force F and the actual resultant force applied to the test structure.

Equation (24) shows that the actual force which is applied to the test structure is only in phase with the force delivered by the exciter when one or more of the following conditions arise:

(a) $\phi = 0$
(b) $\omega_1 = \omega_2$
(c) $X = 0$

Condition (b) is impractical since this requires some means of varying the exciter natural frequency in order that this coincides with the structure natural frequency, and condition (c) requires that the armature, and hence structural displacements, is zero.

To satisfy condition (a) a technique can be used which has been reported by Cox (11) and Taylor et al (3), whereby an additional current at quadrature phase relative to the excitation current, which is in phase with the oscillator reference voltage, is injected into the exciter to allow the phase angle of the excitation force to be modified, i.e. the effects of the exciter mass and stiffness can be compensated. The method of doing this is detailed in reference (3) and the effect of employing quadrature current is shown on Figure A.II.3, where the force vectors are drawn at resonance.

It can be seen from Figure A.II.3 that the addition of a current at quadrature to the reference current allows the effects of the exciter moving parts on the resultant force applied to the structure to be negated. It must be emphasised that the use of quadrature current techniques are only necessary when exciting lightly damped structures where the exciter effects are going to be significant and that in the general case of single point excitation methods where the actual input force (from a transducer) to the structure is used as the reference no exciter compensation is required, although mass,compensation due to the effective mass of the transducers may be necessary if this is significant (6).

If the force available from a force transducer attached to the structure at the excitation point is used as the reference then a 90^{o} phase angle between the output displacement and the input force defines the resonant condition.

It is important to realise the implications of the above

statements in that for each case, namely using current or force, it is a Transfer Function which is being used to establish the conditions for resonance, i.e. the phase angle between the output response and the input to the system and their appropriate magnitudes. If just the output response was measured and used, for example, assuming resonance to occur when the output resonse was a maximum, this would lead to erroneous results due to the exciter mass, stiffness and damping modifying the original structure (4).

This has been shown in Appendix II.2 by considering the forced response of a single degree-of-freedom system with a typical electro-dynamic vibration exciter.

The resulting displacement of the actual system which comprises both the test structure and the vibration exciter is given in Appendix II.2 by equation A.II.18 as:

$$|x| = \frac{|F/k_1|}{\left\{\left((1+k')-(1+m')\frac{\omega^2}{\omega_1^2}\right)^2 + \left(2\zeta_1\frac{\omega}{\omega_1}+2\zeta_2\frac{\omega}{\omega_2}k'\right)^2\right\}^{\frac{1}{2}}} \qquad (25)$$

The maximum response is given by equation A.II.20 as:

$$|x_{max}| = \frac{|F/k_1|}{2C\omega_1\left\{\frac{\omega_1^2C^2(m'-1) + (1+k')}{(1+m')}\right\}^{\frac{1}{2}}} \qquad (26)$$

where $C = \frac{\zeta_1}{\omega_1} + \frac{\zeta_2 k'}{\omega_2}$

Thus it can be seen from equation (26) that by merely using the output response of the system under test to indicate the resonant condition then large errors may be incurred.

The true resonant condition is given by replacing F in

equation (25) with that given by equation (15) and then differentiating the result for a turning point. This will then result in the familiar equation for a single degree-of-freedom system resonant amplitude as:

$$|x_{max}| = \frac{|F/k_1|}{2\zeta_1(1-\zeta_1^2)^{\frac{1}{2}}} \quad (27)$$

The above effects were verified during the constant current tests of Section 2.3 when both the output response and the ratio of the output response to the input force (measured with a piezoelectric force gauge) were plotted as a function of frequency. Figure 6 shows these effects quite alarmingly.

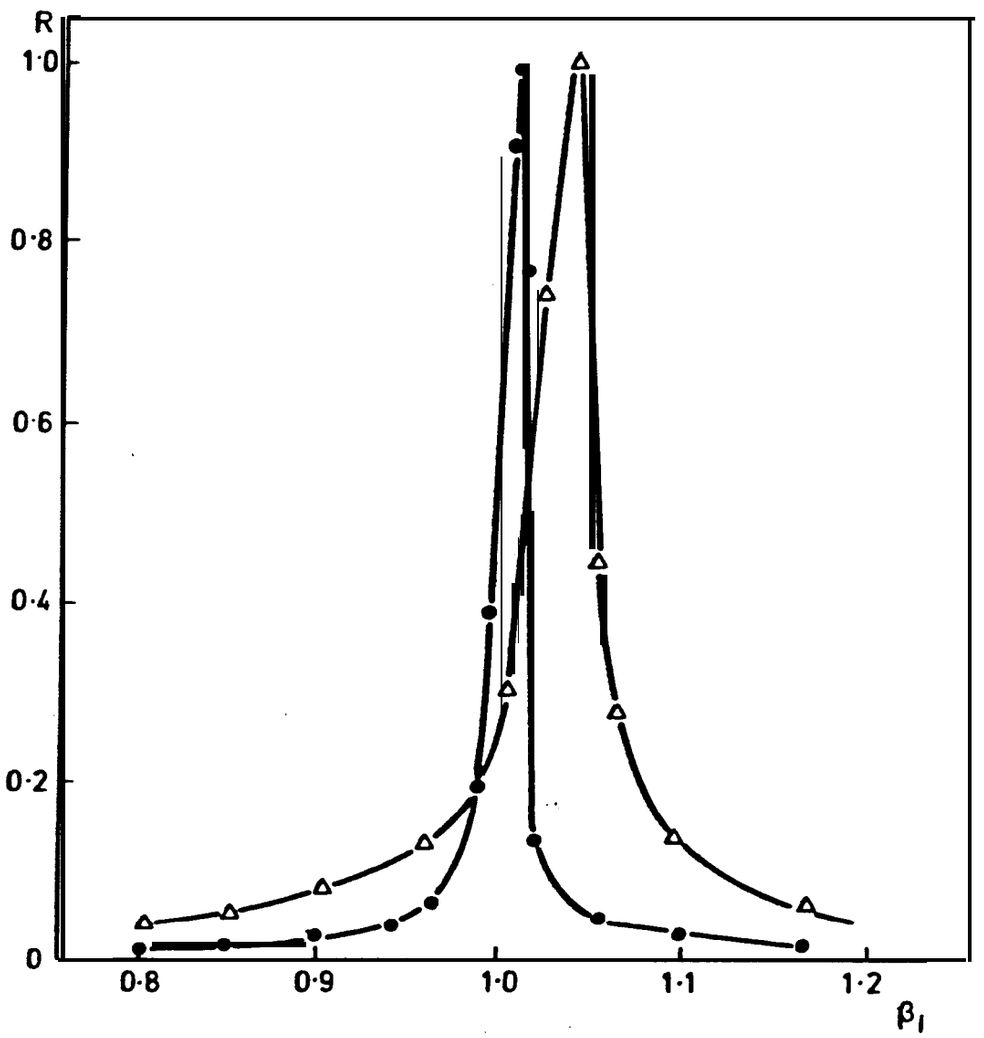

FIGURE 6

EXPERIMENTAL RESULTS OF CONSTANT INPUT CURRENT TESTS.

A OUTPUT RESPONSE ONLY
• RATIO OF OUTPUT RESPONSE TO INPUT FORCE (INERTIANCE)
R IS THE MEASURED QUANTITY NORMALISED **TO THE MAXIMUM VALUE**
β_1 **IS THE FREQUENCY RATIO.**

2. EXPERIMENTAL TESTS TO DETERMINE THE FORCE INPUT BEHAVIOUR AT A SYSTEM RESONANCE

2.1 INTRODUCTION

The predicted variation in the level of the input force and accompanying harmonic distortion detailed in Chapter 1 was investigated by carrying out a series of controlled experimental tests on a lightly damped structure.

The object of these tests was to examine the force injected into the structure under the structural resonant conditions with the input current to the exciter being held constant and then with the structural displacement being maintained constant. At the same time, the levels of harmonic distortion present in the force signal were also monitored.

To simplify the experimental procedures, to allow a comparison to be made with the theoretical predictions of Chapter 1, an effective single degree-of-freedom rig was used which was simply a uniform steel cantilever beam, with the frequency range of interest being restricted to the region of the fundamental resonant frequency.

2.2 EXPERIMENTAL ARRANGEMENT

The steel cantilever beam was excited at its tip by an electro-dynamic vibration exciter whose maximum peak force available was 24N. The exciter armature was connected to the tip of the cantilever beam using a push-rod (this is a device which has a high axial stiffness and does not otherwise restrict the movement of the structure (12)) and piezoelectric force transducer assembly (see Appendix VI), the force gauge being attached to the cantilever tip with a nylon stud. The response of the cantilever was monitored (at the excitation point) with a piezoelectric accelerometer which was also rigidly attached to the cantilever

with a nylon stud. The purpose of the nylon studs was to eliminate any noise which may have been generated by different earthing loops between the transducers and the test structure. The exciter was fed with a current from a d.c. coupled power amplifier which was controlled by the oscillator voltage source from a Solartron Frequency Response Analyser (FRA). The outputs of both the force and acceleration transducers were fed via charge amplifiers into the FRA which allowed either the individual properties of the acceleration or force to be recorded in their in-phase and quadrature components or in polar form. Alternatively the transfer function of output acceleration to input force in the same modes of measurement could be obtained.

Figure 7 shows a diagrammatic sketch of the experimental layout. Before any experimental tests were carried out the harmonic distortion levels on the outputs of both the FRA and the power amplifier were checked on a harmonic analyser. These quantities were found to be insignificant, the largest harmonic distortion, expressed as a percentage of the fundamental harmonic, was on the output of the power amplifier and was measured as 2% for the second harmonic and 0.7% for the third harmonic. Other researchers have noted similar characteristics where low power levels (as in this case) are used, but in the case of the output power of the amplifier being greater than 80% of the maximum, third harmonic distortion has been recorded as high as 20% (13).

2.3 CONSTANT INPUT CURRENT TESTS

The input current to the vibration exciter was monitored by measuring the voltage drop across a 0.1Ω resistor which was connected in series between the power amplifier and the vibration exciter.

For a constant input current of 0.1 amps, the excitation

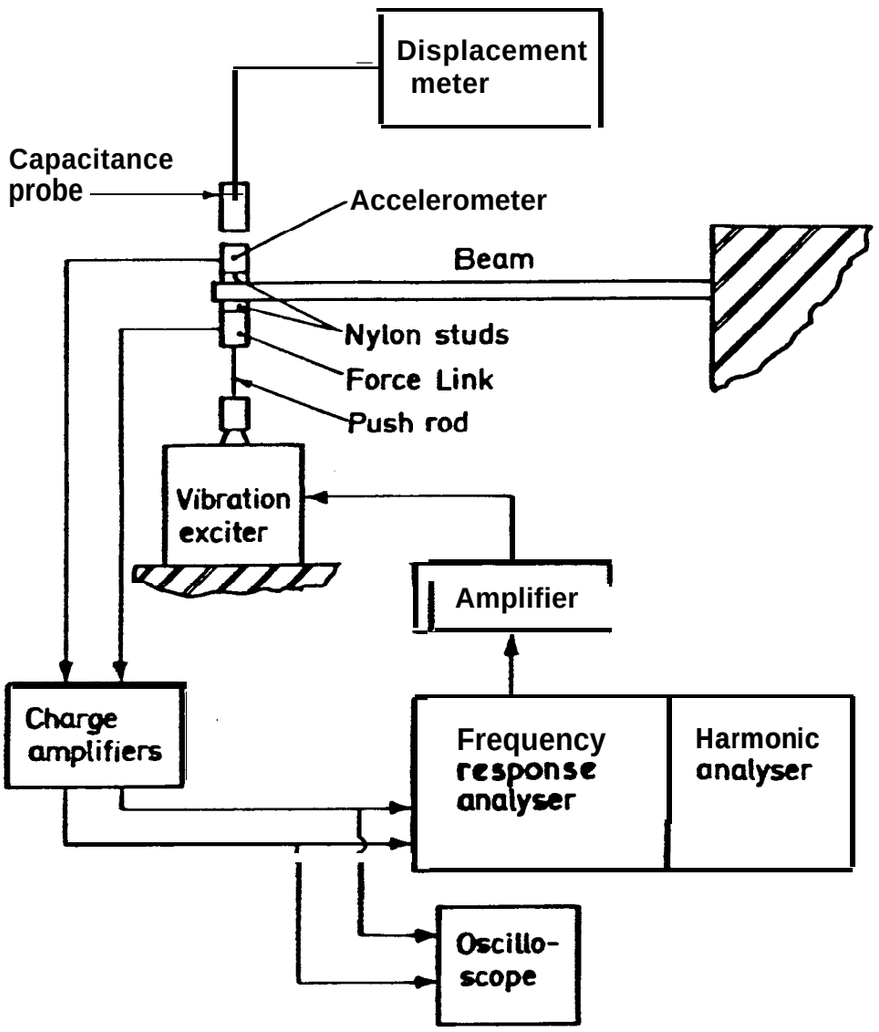

FIGURE 7

DIAGRAMMATIC SKETCH OF EXPERIMENTAL ARRANGEMENT FOR CANTILEVER BEAM TESTS.

frequency was varied over the fundamental resonant frequency range of the cantilever beam and the resultant input force level was measured together with the inertiance (ratio of output acceleration to resultant input force).

Figure 8 shows the pattern of behaviour of these quantities as the frequency is varied and it can be seen that there is a large variation in the force input components at or near the resonant condition. The most striking feature of Figure 8 is the rapid reduction in the resultant force at the resonant condition, followed by a rapid increase in the force just after resonance and the gradual reduction of the force to a level approaching its initial value.

For this test, the exciter natural frequency was greater than the beam resonant frequency, thus this condition was reversed by changing the length of the cantilever beam in order to make its fundamental resonant frequency greater than the exciter, natural frequency and the test was repeated.

Figure 8 also shows the results of this test and it can be seen that the pattern of force behaviour is inverted.

If the resultant force results of Figure 8 are compared with the theoretical results of Figure 5, it can be seen that there is excellent agreement between the theoretical and experimental results.

During the above tests, the harmonic content of the resultant applied force was also measured using the harmonic analyser unit on the FRA. This unit recorded the rms voltage levels of the harmonics up to the tenth harmonic. Figure 9 shows the second and third harmonics; expressed as a ratio of the fundamental harmonic, as the excitation frequency was varied over the resonant frequency and the predominent distortion can be seen to be due to the second harmonic components. The input current to the exciter,

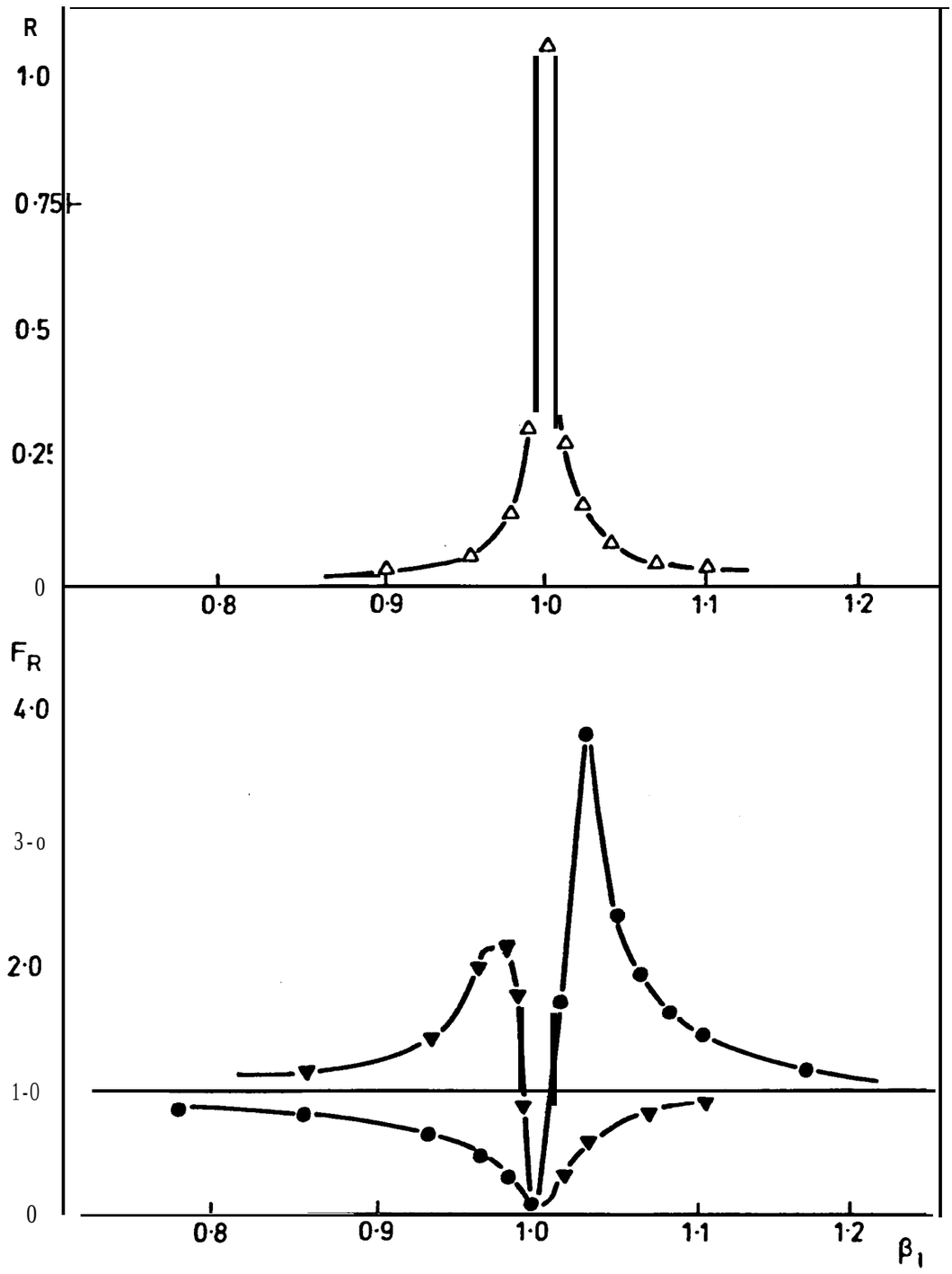

FIGURE 8

EXPERIMENTAL RESULTS FROM CONSTANT INPUT CURRENT TESTS

● **NORMALISED RESULTANT INPUT FORCE WITH** $\omega_1 < \omega_2$
▼ NORMALISED **RESULTANT INPUT FORCE WITH** $\omega_1 > \omega_2$
A NORMALISED **INERTIANCE WITH** $\omega_1 < \omega_2$
F_R **IS THE MAGNITUDE OF THE** RESULTANT **FORCE**
R **IS THE MAGNITUDE OF THE NORMALISED INERTIANCE**

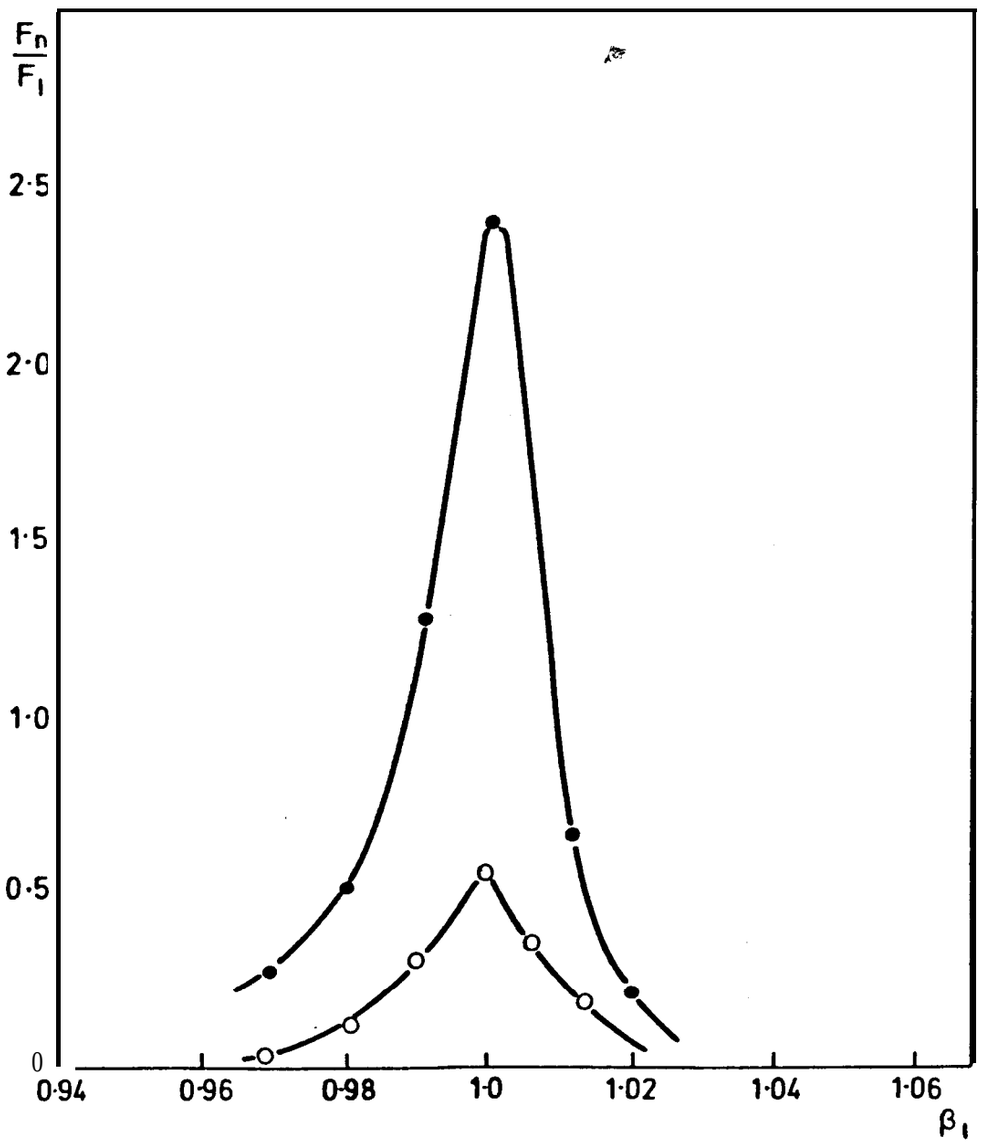

FIGURE 9

EXPERIMENTAL **RESULTS OF HARMONIC DISTORTION TESTS WITH CONSTANT INPUT CURRENT**

- ● **RATIO OF SECOND HARMONIC TO FUNDAMENTAL** $(\frac{F_2}{F_1})$
- o **RATIO OF THIRD HARMONIC TO FUNDAMENTAL** $(\frac{F_3}{F_1})$

which was observed throughout the tests, displayed no harmonic distortion.

2.4 CONSTANT DISPLACEMENT TESTS

In order to carry out constant displacement tests a non-contact capacitance probe was used to monitor the displacement of the beam since the signal from the accelerometer was continuously used for evaluating the inertiance as in the previous test.

The procedure for this test was the same as that of the constant current tests except that the output displacement was held constant as the frequency was varied. Figure 10 shows the variation in the resultant force input component and in this case it can be seen that there is a linear relationship between the resultant force and the frequency with a minimumagain occurring at the resonant frequency. These characteristics support the fact that the variation in input force to the structure is modified by the inertia and stiffness effects of the exciter since in the tests carried out the exciter's flexural stiffness was the predominant factor (inertia forces being much smaller due to the low acceleration) and when the displacement was maintained constant the resulting variations in the input force to the structure were minimised.

The harmonic content of the resultant force applied to the structure was also measured, the procedure employed being the same as that described in the constant input current tests. The trend of the results for the second and third harmonics, expressed as a percentage of the fundamental harmonic, were very similar to the results shown on Figure 9.

2.5 HARMONIC DISTORTION AS A FUNCTION OF DISPLACEMENT

Since the greatest harmonic force distortion occurred at

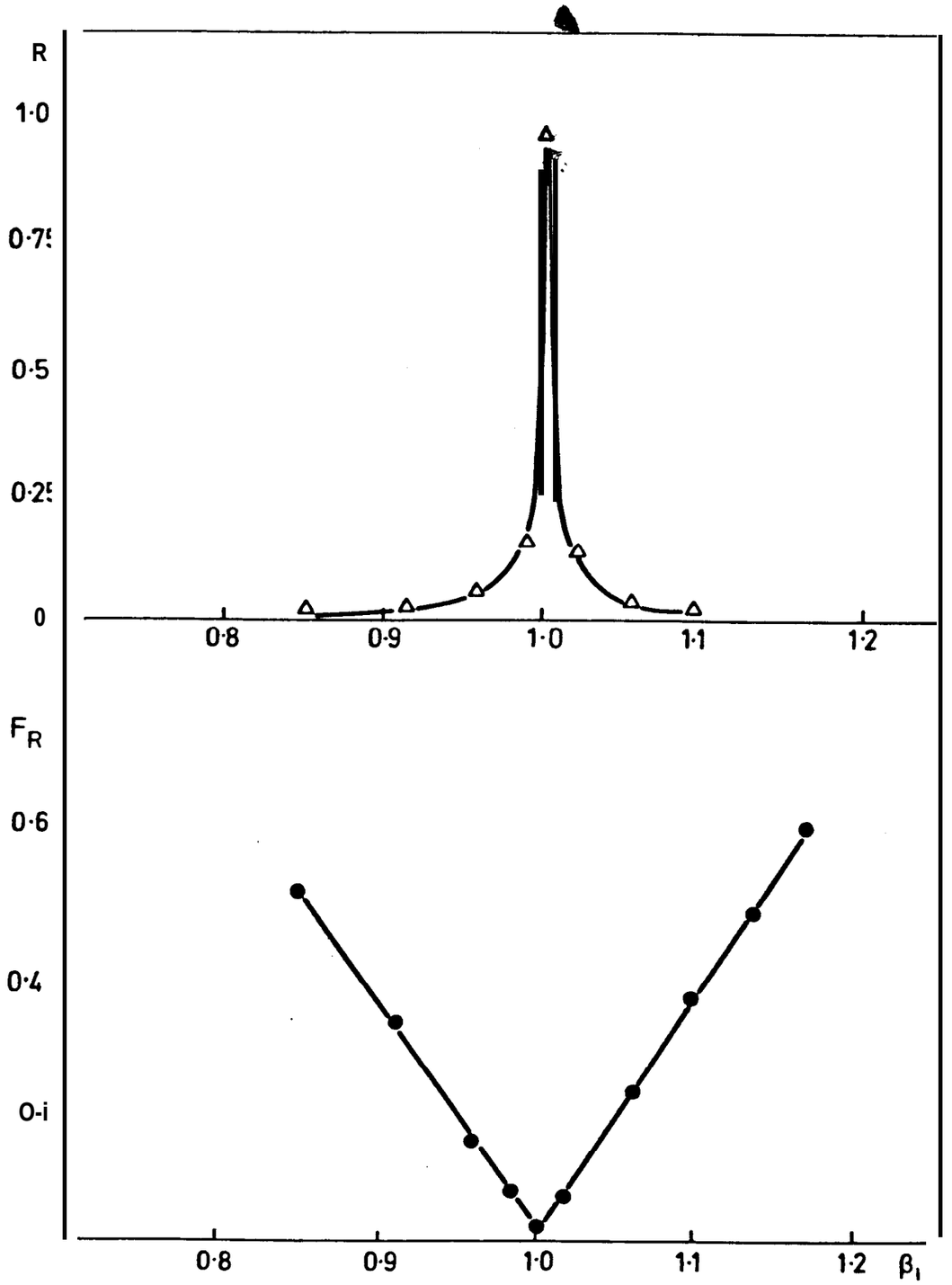

FIGURE 10

EXPERIMENTAL RESULTS FROM CONSTANT DISPLACEMENT TESTS

● **RESULTANT INPUT FORCE WITH** $\omega_1 < \omega_2$
A NORMALISED INERTIANCE WITH $\omega_1 < \omega_2$
F_R **IS THE MAGNITUDE OF THE RESULTANT FORCE**
R **IS THE MAGNITUDE OF THE NORMALISED INERTIANCE**

the resonance condition, a series of constant displacement tests were carried out on the cantilever beam with the beam in a resonant condition. The procedure employed was to monitor the displacement with the non-contact capacitance probe and maintain this at a pre-selected value at the fundamental resonant frequency of the cantilever beam, whilst the fundamental, second and third harmonics were measured on the harmonic analyser. This was repeated for a range of constant armature peak-to-peak displacement values.

The resulting harmonics were normalised to the harmonic levels obtained from the minimum displacement tests (i.e. the initial starting value). Figure 11 shows the results obtained at the resonant frequency as a function of armature displacement. It can be seen that the fundamental force component is directly proportional to the armature displacement, but the second and third harmonic components display a non-linear relationship. This supported the prediction of equation 21 that large amplitudes of vibration (i.e. flexible structures) produce significant harmonic force distortion.

Due to the fact that the tests had been carried out on a cantilever beam, at the higher amplitudes of vibration a significant amount of rotation accompanied the translation at the cantilever beam tip where the excitation was applied, with the possible result that the misalignment of the armature due to the rotational movement could be affecting the harmonic force distortion levels. In order to minimise these effects the same series of tests as detailed above were carried out on an encastré beam. Excitation was applied at the mid-point of the beam whereby only translational motion of the armature occurred and the harmonic content of the force input signal for a range of constant displacement values was measured.

The trend of the results was very similar to those obtained

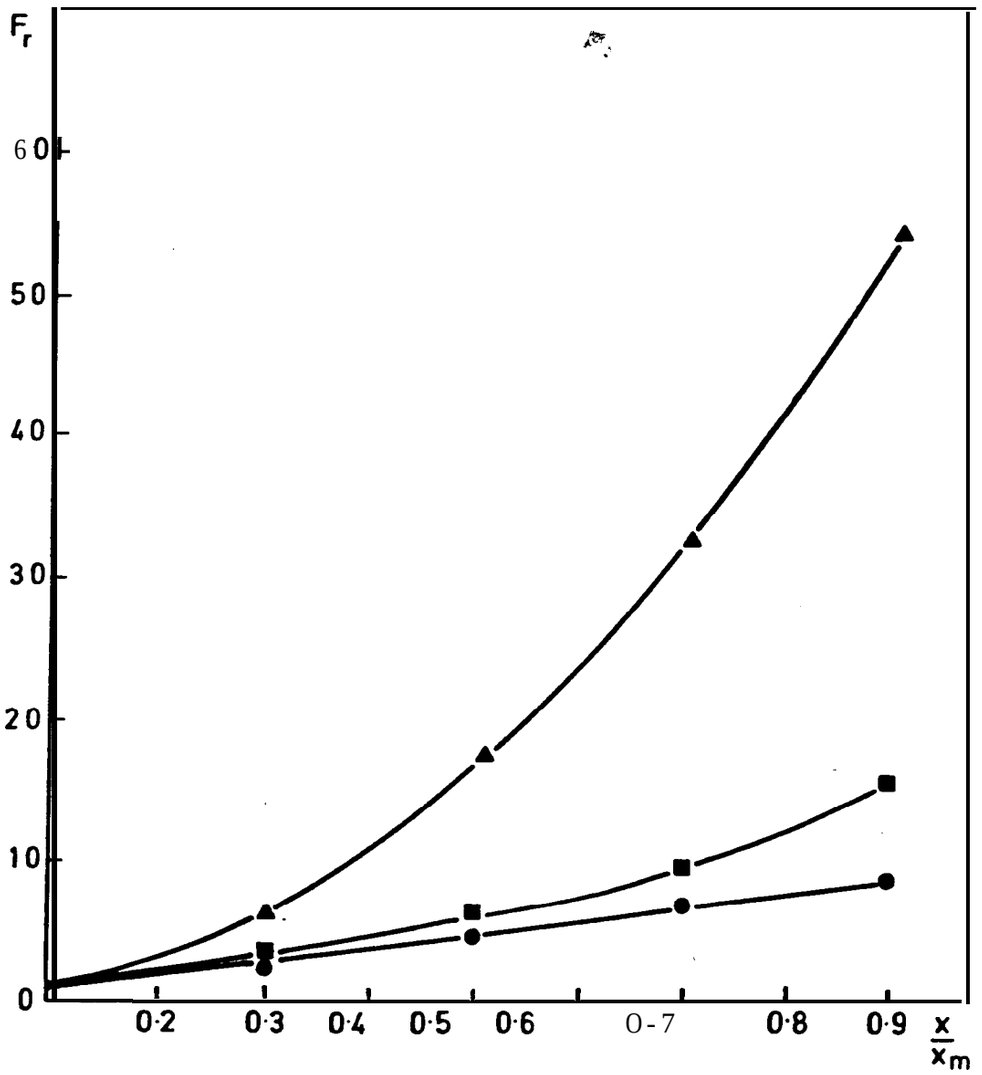

FIGURE 11

EXPERIMENTAL RESULTS SHOWING HARMONIC DISTORTION AS A FUNCTION OF DISPLACEMENT

● **FIRST (OR** FUNDAMENTAL**) HARMONIC,** ▲ **SECOND HARMONIC,** ■ **THIRD HARMONIC**

$\frac{x}{x_m}$ **IS THE RATIO OF ARMATURE DISPLACEMENT TO MAXIMUM RATED ARMATURE DISPLACEMENT** (x_m **– 2.5 mm peak)**

F_n **IS THE NORMALISED LEVEL OF** HARMONIC **DISTORTION**

from the constant displacement tests on the cantilever beam which indicated that the rotational effects from the cantilever experiments did not produce any significant harmonic force distortion.

The above tests had confirmed the theoretical predictions regarding the variation in the magnitude of the input force around the resonance region of a lightly damped structure and that the harmonic distortion present was predominantly second harmonic.

In order to minimise these effects, equation (21) showed that by keeping the value of k' (the ratio of the vibration exciter stiffness to the structural stiffness) to a minimum, then this should prevent severe harmonic force distortion.

In order to examine the validity of this equation a further set of tests were carried out on the cantilever beam. The tests allowed the stiffness ratio k' to be varied by changing the flexural stiffness'of a standard electro-dynamic vibration exciter. This method of varying k' was used in preference to simply changing the beam length in order to alter the value of k' since this had more practical significance, and also the mass ratio m' was constant. During the tests the beam was excited over its fundamental frequency range with a constant displacement and the first and second harmonic components of the input force signal were measured on the harmonic analyser. In order to provide a variation in k', the stiffness of the exciter was modified by removing one of the fibre flexure supports. This reduced the stiffness of the exciter by approximately 50%. As a result of this modification the lateral stiffness of the exciter was reduced to such an extent that a linear ball-race guide had to be used to provide lateral support and hence prevent side-stressing (armature rubbing on the centre pole magnet) of the exciter coil (81). Plate 2 shows the

experimental set-up for these tests. The linear ball-race obviously increased the exciter frictional damping but transient results indicated that this was minimal for steady state vibrations. The results of the harmonic distortion tests are shown on Figure 12 together with the theoretical curve from equation (14).

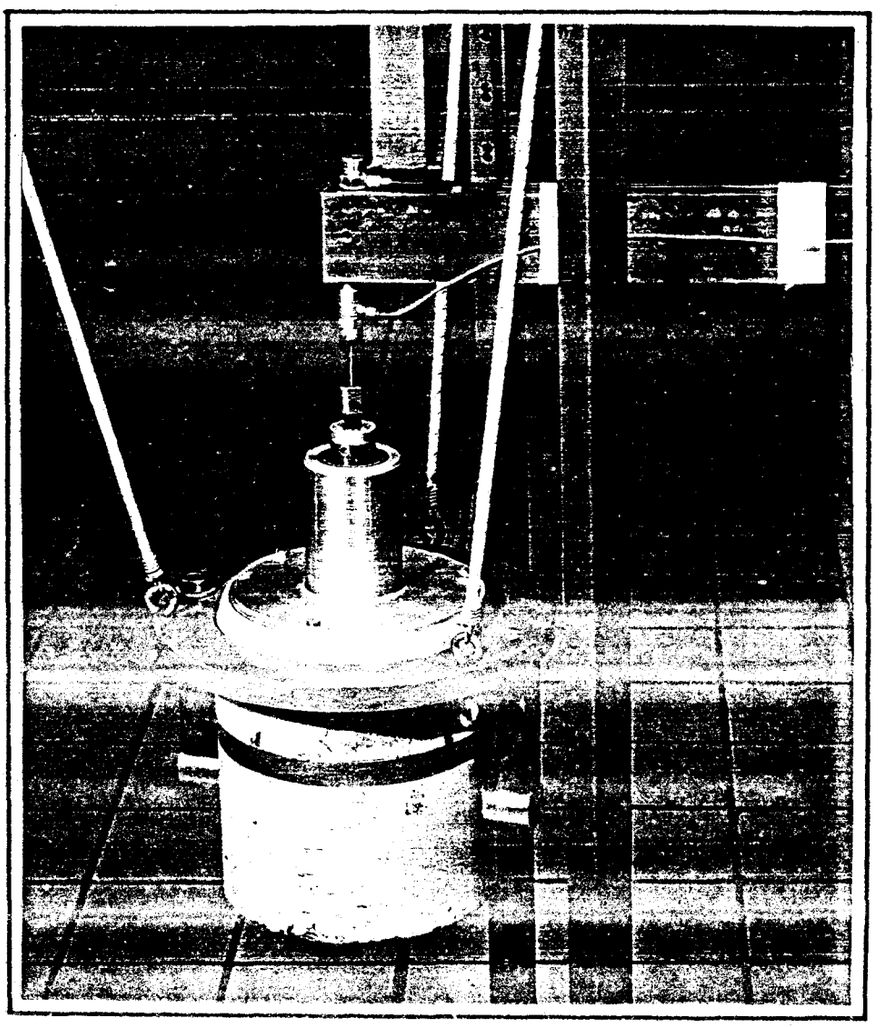

PLATE 2

FORCED VIBRATION TESTS WITH MODIFIED VIBRATION EXCITER SHOWING LINEAR BALL RACE GUIDE.

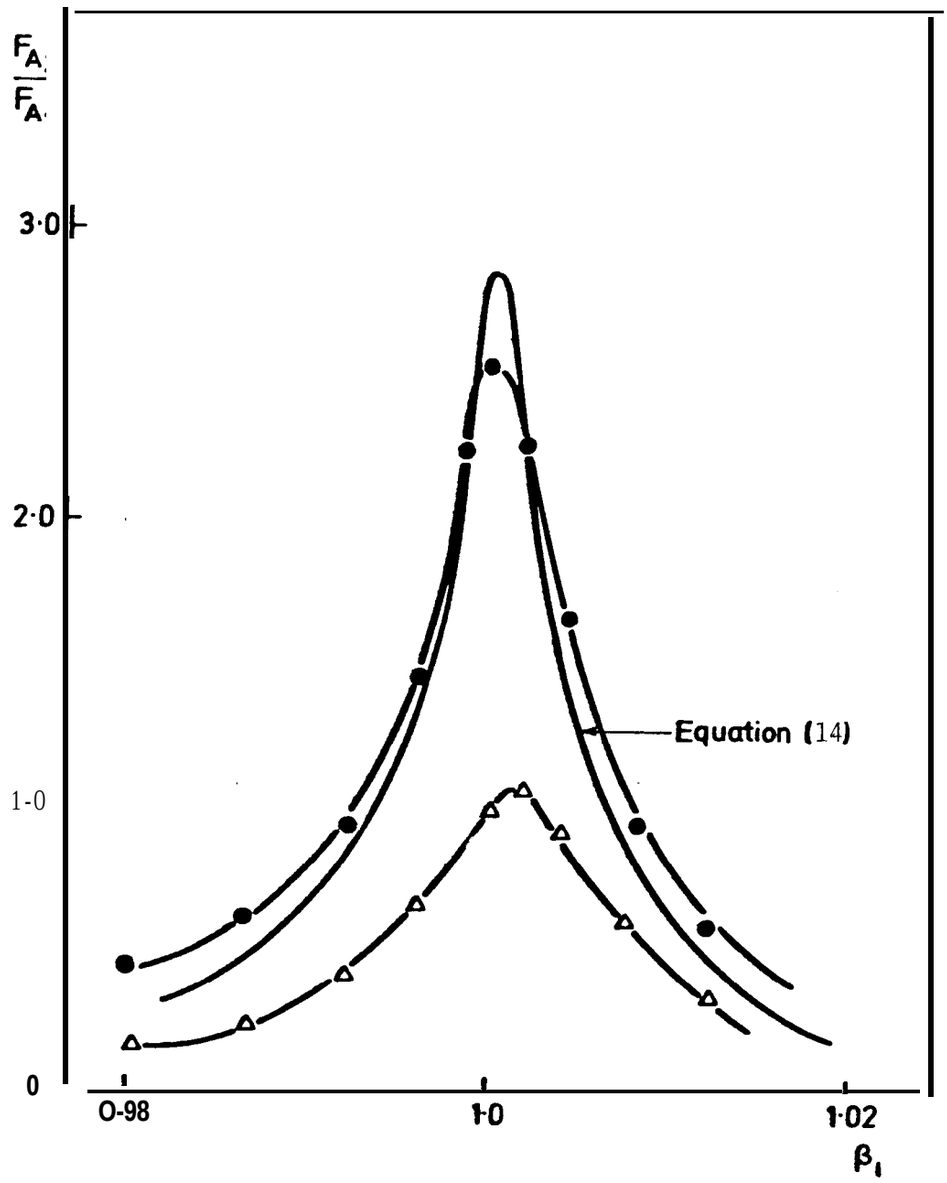

FIGURE 12

EFFECT ON SECOND HARMONIC FORCE DISTORTION LEVELS OF REDUCING EXCITER STIFFNESS.

● STANDARD EXCITER WITH $k' = 0.06$, $\zeta_1 = 0.01$, $m' = 0.005$
A MODIFIED EXCITER WITH $k' = 0.026$, $\zeta_1 = 0.01$, $m' = 0.005$

2.6 DISCUSSION AND CONCLUSIONS

1. It has been shown that harmonic distortion of the input force signal at a system resonance is primarily due to the non-linear characteristics of the electro-dynamic vibration exciter. These non-linearities, which characterise the magnetic field strength of the exciter, are basically square-law in nature which results in the force distortion being predom-inantly second harmonic. Higher harmonics will be present in the force signal due to the fact that distortions of the square-law characteristic will occur during testing from such aspects as armature misalingment, higher order terms in the magnetic field strength characteristics and variations in characteristics of one vibrator to another.

2. It is also shown that the damping factor in the system under test is a very important aspect and in order to minimise the harmonic force distortion occurring at resonance this must be significantly greater than the ratio of the vibration exciter stiffness to the test structure stiffness. If the amplitudes of vibration are small, e.g. as a result of exciting higher modes, the harmonic distortion is reduced as a result of two factors. The first is that small amplitudes of vibration restrict the armature movement in the non-linear magnetic field, and hence the non-linearities are minimised. The second factor is that higher modes of vibration tend to produce larger damping forces which result in an increase in the fundamental force component, whereas the second and higher order components remain approx-imately constant, consequently the effects of the harmonic distortion are less noticeable.

3. It has been further shown that regardless of whether or not a high output impedance amplifier is used to

supply a constant current source, large variations in the magnitude and phase of the input force can occur when testing lightly damped systems. This has been confirmed to be due to the forces arising from the mass and stiffness characteristics of the vibration exciter which modify the resultant force applied to the system at the system resonance.

4. If the natural frequency of the vibration exciter is the same as that of the system under test then a constant force would be applied to the system since the vibration exciter effects would be self-compensating.

5. If a constant current source is used as a reference force condition, then in the case of a lightly damped single degree-of-freedom system, a ninety degree phase shift between the input current and the output displacement (or acceleration) does not necessarily indicate a natural frequency. Only if the input force, measured at the point of application on the test system, and the corresponding response are used can this criterion be applied.

6. In terms of the harmonic force distortion levels at resonance, some improvement would be achieved by employing a constant current source since the magnitude of the non-linear term would be a function of the force current constant only as opposed to a combination of this and the back e.m.f. constant which would be the case with a voltage source.

SECTION 2

THE EFFECTS OF MODAL COUPLING IN LIGHTLY DAMPED STRUCTURES

3. THE INFLUENCE OF MODAL COUPLING IN LIGHTLY DAMPED STRUCTURES

3.1 INTRODUCTION

The following Chapters are concerned with the influence of damping on the modal properties of lightly damped structures. Of particular interest is the ability to generate real normal modes of vibration in structures where the damping matrix cannot be diagonalised by a transformation matrix (commonly called non-proportional damping (14)), since this is of fundamental importance in structural identification programmes.

It is worthwhile to consider initially the type of damping with which one should be concerned, e.g. should the model used to represent the damping mechanism be considered as a viscous property or should one assume a hysteretic damping model, or, if the system can be considered as lightly damped, are both these models really the same?

3.2 THE DAMPING MODEL

The subject of dynamic structural damping in relation to the vibrational characteristics of complex structures (in this context 'complex' being used to define structures which may have close natural frequencies and/or non-linear characteristics) is still a problem area and is continually receiving attention (15) with over 3,000 publications appearing on the subject of damping since the year 1900 (16). A review of the mathematical models and experimental techniques for measuring the damping behaviour of solid materials was given in a paper by Bert (17) who compared the mathematical models developed to describe rheological systems. One of the most common techniques used to represent the behaviour of viscoelastic solids is the two-parameter model of a spring in parallel with a dashpot, called the Kelvin-Voigt model (16). Although this model has some deficiencies

as a complex quantity when subjected to sinusoidal vibration. The common single degree-of-freedom model, namely the mass-spring-damper system, is actually a point mass rigidly attached to a Kelvin-Voigt element with the resulting linear differential equation of motion:

$$m\ddot{x} + c\dot{x} + kx = Fe^{j\omega t} \quad .. \quad .. \quad .. \quad .. \quad .. \quad (28)$$

where x is the displacement response.

By replacing the Kelvin-Voigt coefficients k and jwc with a single complex stiffness:

$$\hat{k} = k + j\omega c \quad . \quad . \quad . \quad . \quad . \quad . \quad . \quad . \quad . \quad . \quad . \quad . \quad (29)$$

equation (28) can be represented as:

$$m\ddot{x} + \hat{k}x = Fe^{j\omega t} \quad .. \quad .. \quad .. \quad .. \quad .. \quad .. \quad (30)$$

The energy dissipated during one cycle by a dashpot element subjected to an external sinusoidal force is:

$$U = \oint F.dx = \int_0^{2\pi/\omega} F\,\dot{x}\,dt \quad . \quad . \quad . \quad . \quad . \quad . \quad . \quad . \quad . \quad . \quad (31)$$

where F = dashpot force = $c\dot{x}$.

Now the response x is a complex quantity, which for steady state motion is:

$$x = ue^{j\omega t} \quad .. \quad .. \quad .. \quad .. \quad .. \quad .. \quad .. \quad (32)$$

where $|u|$ is the displacement amplitude, thus equation (31) gives:

$$U = \pi e\omega|u|^2 \quad . \quad . \quad . \quad . \quad ..... \quad (33)$$

Equation (33) shows that the energy loss due to a dashpot is dependent on the exciting frequency ω but it was observed by Kimball and Love11 (18) that in the case of many engineering materials, the energy losses were independent of ω and that the energy loss per cycle was governed by an equation of the type:

$$U = \hat{c}|u|^2 \quad \ldots\ldots\ldots\ldots\ldots\ldots \quad (34)$$

and this was later confirmed by other workers in this field (16) although contradictions to this exist (19). By combining equations (33) and (34) one finds that:

$$c = \frac{\hat{c}}{\pi\omega} \quad \ldots\ldots\ldots\ldots\ldots\ldots \quad (35)$$

This quantity is often termed the 'equivalent viscous damping' for structural damping models and the damping force is then given by:

$$F = \frac{d}{\omega}\dot{x} \quad \ldots\ldots\ldots\ldots\ldots\ldots \quad (36)$$

where $d = \frac{\hat{c}}{\pi}$

which is sometimes referred to as 'frequency-dependent damping' since the normal dashpot coefficient c has been replaced by $\frac{d}{\omega}$.

For structural damping mechanisms, the equations of motion include the constant d by combining it with the spring stiffness constant to give the Kimball-Love11 complex stiffness expression (20)

$$k^* = k + jd \quad \ldots\ldots\ldots\ldots\ldots\ldots \quad (37)$$

which results in an equation of motion in free vibration

of the form:

$$m\ddot{x} + (k + jd)x = 0 \qquad (38)$$

Other alternatives to equation (37) have been proposed (21, 22) but in all cases criticisms have been raised as to their validity and ease of application. The major concern over the use of an equation of motion of the form given in equation (38) is that the resulting solutions are complex exponential (23) and are physically unrealisable (24). Nevertheless, the use of equation (38) in connection with sinusoidally steady state forced vibration of structures is very common, although its main drawback in this context is that at zero frequency the conventionally defined magnification factor is not equal to unity, but this can be accounted for by defining the equivalent static deflection as:

$$u_s = \frac{F}{k_e} \text{ , where } k_e = (k^2 + d^2)^{\frac{1}{2}}$$

which results in a magnification factor for a single degree-of-freedom system as:

$$M' = (k^2 + d^2)^{\frac{1}{2}} / \left\{(k - mw^2)^2 + d^2\right\}^{\frac{1}{2}} \qquad (39)$$

$$\text{i.e. } M' = (1 + \delta^2)^{\frac{1}{2}} / \left\{(1 - (\frac{\omega}{\omega_n})^2) + \delta^2\right\}^{\frac{1}{2}} \qquad (40)$$

where δ is the structural damping factor or loss factor.

If one makes a comparison between a Kelvin-Voigt viscously damped single degree-of-freedom system and a mass-spring system where the spring is considered to behave as a Kimball-Lovell material (complex-modulus) then using the standard definitions for natural frequency, critical damping and damping ratio, e.g.

$$\omega_n^2 = \frac{k}{m}, \quad c_c = 2\sqrt{mk}, \quad \zeta = \frac{c}{c_c}$$

one finds that the conventionally defined magnification factor is (17)

$$M = \left\{\left(1 - \left(\frac{\omega}{\omega_n}\right)^2\right)^2 + 4\zeta^2\right\}^{-\frac{1}{2}} \quad .. \quad .. \quad .. \quad .. \quad (41)$$

for the Kimball-Love11 system, but for the Kelvin-Voigt viscously damped system this is:

$$M = \left\{\left(1 - \left(\frac{\omega}{\omega_n}\right)^2\right)^2 + 4\zeta^2\left(\frac{\omega}{\omega_n}\right)^2\right\}^{-\frac{1}{2}} \quad .. \quad .. \quad .. \quad (42)$$

Both equations give the same magnification factor when $\omega = \omega_n$, but the magnification factors at resonance (i.e. when M is a maximum) are different, although in the case of lightly damped structures ($\zeta < 0.2$) the difference between the results of equations (41) and (42) is very small and is generally ignored. If one considers the equations of motion for both systems subjected to a sinusoidal exciting force,

$$m\ddot{x} + c\dot{x} + kx = Fej^{\omega t} = m\ddot{x} + k(1 + j\delta)x \quad . \quad . \quad .. \quad (43)$$

and assuming harmonic motion, i.e. $x = uej^{\omega t}$,

$$(\omega_n^2 - \omega^2)u + j2\zeta\omega_n\omega u = (\omega_n^2 - \omega^2)u + j\omega_n^2\delta u \quad (44)$$

When the exciting frequency corresponds to the natural frequency (in the case of lightly damped systems this would be the resonant frequency), then equation (44) gives the useful expression:

$$\delta = 2\zeta \quad . \quad . \quad . \quad . \quad . \quad . \quad . \quad . \quad . \quad . \quad . \quad . \quad . \quad . \quad . \quad (45)$$

This can also be derived considering the energies dissipated in the dashpot and the spring (17).

Thus the question as to whether one should use a dashpot model or a spring with complex stiffness to represent the dissipation mechanism seems only to lie with the theoreticians, since in practical structural dynamic analysis, where the damping is normally low, particularly in the aerospace industry (25), then either model will suffice for steady state forced vibration analyses and this is borne out by the fact that both are widely used to represent the same physical systems subjected to forced sinusoidal vibration.

One aspect which may influence the choice of the damping model is that it is not possible to model hysteretic damping on an analogue computer (22), a tool which has seen extensive use in the study and behaviour of lumped parameter models of structural systems (26). In the case of finite element analyses, damping is generally introduced in terms of modal damping (as opposed to local dampers), i.e. some fraction (or percentage) of critical damping is introduced for a particular natural mode of structural vibration and thus the damping model can be of either form.

The next question one must ask has far reaching consequences both in terms of single and multi-point vibration testing methods and in relation to a widely used identification method, namely the Kennedy and Pancu vector plot (27). It is related to the interference of one mode of vibration with another as a result of the damping coupling and is simply "if a system is governed by a modal damping matrix in which the off-diagonal elements are non-zero and comparable in magnitude to the leading diagonal elements, is it possible to excite the normal modes of the system?"

3.3 NORMAL MODES OF VIBRATION IN DAMPED LINEAR SYSTEMS

The ability to analyse structural systems in terms of their classical normal or principal mode's (28) has been of great benefit to dynamicists, particularly in the aerospace industry (29). The existence of classical normal modes in undamped systems produces real mode shapes, (eigenvectors) with real natural frequencies (eigenvalues). However, when damping (either hysteretic or viscous damping) is introduced into the equations of motion, the resulting analysis is governed by certain constraints related to the distribution of the localised dampers in the structure, which may result in complex eigenvalues and eigenvectors (40)

One of these constraints was first pointed out by Rayleigh (30) who showed that if the damping matrix is a linear combination of the stiffness and mass matrices, the damped system will exhibit classical normal modes. Later, Foss (31) in 1956 published a general treatment of damped structures which utilised special co-ordinates to uncouple the equations of motion. The first analysis of the conditions which allow a damped linear system to possess classical normal modes was given by Caughey (28) in 1960 who showed that a necessary and sufficient condition for the existence of classical normal modes is that the damping matrix can be transformed to a diagonal matrix using the same transformation which results in the classical normal modes for the undamped system. In mathematical terms this can be expressed by firstly considering an n degree-of-freedom, undamped linear system which is represented as a set of n coupled equations in matrix form as,

$$\underset{\sim}{A}\ddot{u} + \underset{\sim}{K}u = 0 \quad \ldots\ldots\ldots\ldots \quad (46)$$

where A and K are n x n matrices representing the mass and stiffness properties respectively, which are symmetrical and positive-definite and u is a column vector of generalised co-ordinates. Equation (46) has n eigenvalues and

corresponding eigenvectors, namely wl, ω_2 . . . ω_n associated with $\Phi_1, \Phi_2 \ldots \Phi_n$. These eigenvalues and their corresponding eigenvectors unique&y define the modal properties of the system, unless there are repeated natural frequencies, and the eigenvectors also satisfy the orthogonality condition for i ≠ j, i.e.

$$\underset{\sim}{\Phi}_i^t \underset{\sim}{A} \underset{\sim}{\Phi}_j = 0 = \underset{\sim}{\Phi}_i^t \underset{\sim}{K} \underset{\sim}{\Phi}_j, \quad (j = 1, 2 \ldots n) \qquad (47)$$

If the modal matrix is given as:

$$\underset{\sim}{\Phi} = \left[\Phi_1 \Phi_2 \ldots \Phi_n\right] \qquad (48)$$

then equation (47) can be represented as:

$$\underset{\sim}{\Phi}^t \underset{\sim}{A} \underset{\sim}{\Phi} = \bar{A} \qquad (49)$$

$$\underset{\sim}{\Phi}^t \underset{\sim}{K} \underset{\sim}{\Phi} = \bar{K} \qquad (50)$$

where $\bar{A}$ and $\bar{K}$ are diagonal matrices of order n.

If we apply a co-ordinate transformation such that

$$u = \underset{\sim}{\Phi} Z \qquad (51)$$

then substitution of (51) into (46) and pre-multiplication by Φ^t gives:

$$\underset{\sim}{\Phi}^t \underset{\sim}{A} \underset{\sim}{\Phi} \ddot{Z} + \underset{\sim}{\Phi}^t \underset{\sim}{K} \underset{\sim}{\Phi} Z = 0 \qquad (52)$$

which, according to equations (49) and (50), can be represented by a set of n uncoupled equations of motion:

$$\bar{A}\ddot{Z} + \bar{K}Z = 0 \qquad (53)$$

where the vector Z is the principal or normal mode co-ordinate vector of the system. If equation (46) is now

modified to include viscous damping i.e.

$$\underset{\sim}{\bar{A}}\ddot{u} + \underset{\sim}{B}\dot{u} + \underset{\sim}{K}u = 0 \quad .. \quad .. \quad .. \quad .. \quad .. \quad .. \quad (54)$$

then the transformation of equation (51), according to Caughey, must also uncouple equation (53) if the system is to possess classical normal modes. The condition specified by Rayleigh, namely that:

$$\underset{\sim}{B} = sA + tK \quad . . . . . \quad (55)$$

where s and t are constants, obviously meets this condition and is known as proportional damping. Caughey et al (32) went on to show that if equation (54) is represented in the form:

$$\underset{\sim}{\hat{I}}\ddot{q} + \underset{\sim}{\hat{B}}\dot{q} + \underset{\sim}{\hat{K}}q = 0 \quad .. \quad .. \quad .. \quad .. \quad .. \quad .. \quad (56)$$

where the A matrix has been transformed to an identity matrix of order n, $\hat{B}$ and $\hat{K}$ are still symmetrical and positive definite, and q is the vector of transformed co-ordinates i.e.

$$u = \underset{\sim}{\Psi}\,\underset{\sim}{q} \quad . . . . . \quad (57)$$

where Ψ is a known transformation matrix, then systems governed by equation (56) possess classical normal modes if $\hat{B}$ and $\hat{K}$ commute i.e. if:

$$\underset{\sim}{\hat{B}}\underset{\sim}{\hat{K}} = \underset{\sim}{\hat{K}}\underset{\sim}{\hat{B}} \quad . . . . . \quad (58)$$

This results in a general expression for the form of the damping matrix given as (34):

$$\underset{\sim}{A}^{-1}\underset{\sim}{B} = \sum_{j=0}^{n-1} a_j (\underset{\sim}{A}^{-1}\underset{\sim}{K})^j \quad . . . . . \quad (59)$$

where a_j = constant.

A number of conditions which arise as a result of equations (58) and (59) are quoted by various authors. Bahar (33), showed an application of equation (59) to a three degree-of-freedom system, and a special form of equation (59) namely,

$$\underset{\sim}{B}\ \underset{\sim}{A}^{-1}\ K = \underset{\sim}{K}\ \underset{\sim}{A}^{-1}\ B \quad . \quad . \quad . \quad . \quad . \quad . \quad . \quad . \quad . \quad . \quad . \quad . \quad . \quad (60)$$

was applied to the same example by Fawzy (34). Fawzy also pointed out that an obvious solution of equation (58) was:

$$\hat{B} = \hat{K}^{-1} \quad . \quad . \quad . \quad . \quad . \quad . \quad . \quad . \quad . \quad . \quad . \quad . \quad . \quad . \quad . \quad (61)$$

Thus there are a number of conditions regarding the form of the damping matrix which allow classical normal modes to exist in damped structures other than the standard cases of the undamped and proportionally damped ones, although these seem to have eluded some authors (35)(36). The physical interpretation of the conditions given by equations (58) to (60) have not been considered by their authors, probably due to the fact that in practice the mass and stiffness matrix elements are generally know, or can be obtained directly, whereas the form of the damping matrix is a much more complex problem and cannot be obtained a priori.

3.4 FORCED NORMAL MODES OF VIBRATION

In real structures, it is unlikely that any of the above conditions which allow the equations of motion to be transformed to normal mode co-ordinates apply in general, and in practice the damping matrix will have leading and off-diagonal terms.

The question then arises as to whether or not it is possible to excite the normal modes of a structure whose modal damping matrix has off-diagonal elements, (the author feels it misleading to refer to this condition as non-proportional damping as have some past authors, since this is often used

to imply that the equations of motion cannot be transformed to uncoupled equations although this is not always the case as has been shown above in Section 3.3), even though the off-diagonal elements are not small compared to those of the leading diagonal.

The technique of exciting normal modes has its main applications in the aerospace industry where ground resonance tests attempt to isolate the normal modes of a structure within a given frequency range. Thus it would be useful to consider the question in the context of normal mode excitation as applied to a complex structure such as an aircraft.

The basic dynamic equations of motion of an unrestrained aeroelastic structure in terms of the normal modes are derived by Kiichemann et al (37) and a revision of these is given below. The equations of motion in generalised form are:

$$M_{ss}\ddot{q}_s(t) + M_{ss}\omega_s^2 q_s(t) + \sum_{r=1}^{\infty} D_{rs}\dot{q}_r(t) = Q_s(t) \quad .. \quad (62)$$

where,

$$M_{ss} = \sum_i \iiint_V m(P)\left\{u_{is}(P)\right\}^2 dP \quad . \quad . \quad . \quad . \quad . \quad . \quad . \quad . \quad (63)$$

$i = 1, 2, 3$; $\iiint_V$ = integration with respect to the volume

is the generalised mass of the s^{th} normal mode of vibration of the aerostructure in a vacuum:

(P is any point in the structure i.e. $P = (x_1, x_2, x_3)$
u_{is} are the normal mode functions of the undamped structure)

now, $M_{ss}\omega_s^2 = K_{ss} = \sum_i \sum_{k-v} \iiint_v \iiint S_{ik}(P,P')u_{is}(P)u_{ks}(P')dPdP'$

. . . . . (64)

($S_{ik}(P,P')$ being second order stiffness influence functions),

thus, K_{ss} is the generalised stiffness of the s^{th} normal mode.

$$D_{rs} = \sum_i \sum_k \iiint_v \iiint_v w_{ik}(P,P')f_{is}(P)f_{kr}(P')dPdP' \quad (65)$$

where w_{ik} are the damping influence functions, f_{is}, f_{kr} are mode functions which satisfy the boundary condtions and $Q_s(t)$ are the generalised surface forces given by:

$$Q(t) = \sum_i \iint_\sigma Q_i(P,t)u_{is}(P)d\sigma \quad . . . . . \quad (66)$$

σ denoting a surface integral.

$Q_i(P,t)$ is an arbitrary pressure function which generates displacement functions $u_i(P,t)$. Now $Q_i(P,t)$ can be expressed as:

$$Q_i(P,t) = \sum_{r=1}^{\infty} Q_{ir}(P)q_r(t) \quad . . . . . \quad (67)$$

If we assume that Q_{ir} is a harmonic exciting force with a normal mode frequency ω_s i.e.

$$q_s(t) = q_s e^{j\omega_s t} \quad . . . . . \quad (68)$$

then combining equations (62),(66), (67) and (68) gives:

$$\sum_{r=1}^{\infty} (j\omega_s D_{rs}) q_r = \sum_{r=1}^{\infty} \left\{ \sum_i \iint_\sigma Q_{ir}(P) u_{is}(P) \, d\sigma \right\} q_r \qquad (69)$$

Equation (69) shows that for equilibrium the external forces must balance the internal energy dissipation when the structure is vibrating in a normal mode.

In terms of experimental testing, it is impossible to excite the structure at an infinite number of points and thus equation (69) is realised as:

$$D_{rs} = \frac{1}{\omega_s} \sum_n \sum_i F_{ir}(P_n) u_{is}(P_n) \quad . \quad . \quad . \quad . \quad . \quad . \qquad (70)$$

$i = 1, 2, 3; \quad n = 1, 2 \ldots\ldots N$

Thus we have N discrete exciting force amplitudes $F_{ir}(P_n)$ at the N points (P_n). Equation (66) is satisfied when:

$$I_m(Q_{ir}(P)) = 0 \text{ and } R_e(u_{is}(P)) = 0 \qquad .. \quad .. \qquad (71)$$

Equation (71) forms the basis of the classical Phase-Resonance Criterion (7) which is commonly used to experimentally define a normal mode condition whereby the response is in-phase (or anti-phase) and at quadrature to the real input forces which are also in-phase (or anti-phase).

Thus it has been shown that regardless of the form of the damping matrix it is theoretically possible to excite the normal modes of a damped structure. The limitations of this are purely practical which results in the modified form of equation (69), namely equation (70).

These limitations result in one of the remaining controversial questions in the use of multi-point excitation methods for inducing pure normal modes of real structures,

"if the damping matrix is of such a form that it cannot be diagonalised according to any of the conditions given in Section 3.2, is it possible to excite a normal mode with a finite number of vibration exciters?". This has been examined for the simple case of a two degree-of-freedom model by Sloane et al (35) who showed that the natural frequencies for such a system differ from those of the undamped system and that the resulting eigenvectors are complex. He further showed that if the input forces are in-phase and at quadrature to the in-phase response (phase-resonance criterion) then the frequencies of excitation coincide with the natural frequencies of the undamped system; which are not equal to the natural frequencies of the system in question, and that the response at the excitation frequencies gives eigenvectors of the undamped system as opposed to the eigenvectors of the actual system.

To overcome this he proposed the use of an input excitation which is a complex frequency excitation. This would take the form of a damped sinusoid, pumped periodically into the structure to maintain sufficient energy to overcome any low-level non-linearities.

Unfortunately, no application of this method has been reported (at least to the author's knowledge) and the apparent added complexity of the method raises doubts as to its practicality and advantages over the existing methods unless the damping distribution is such that the existing tests cannot satisfactorily excite a normal mode.

In order to provide some guidance as to the problem of modal interaction resulting from the closeness of adjacent natural frequencies and/or damping distributions, an analysis was undertaken to examine the relationship between these.

3.5 MODAL INTERACTION CRITERIA

In order to obtain some guidelines relating the natural frequencies and damping of a structure to the effects that these have on the ability to excite real normal modes, a theoretical analysis has been carried out on a system represented by equations of motion in which the damping matrix does not necessarily satisfy any of the conditions of Section 3.2, i.e.:

$$\underset{\sim}{m}\ddot{x} + \underset{\sim}{d}\dot{x} + \underset{\sim}{k}x = fe^{j\omega t} \quad \ldots\ldots\ldots\ldots \quad (72)$$

where x represents a vector of discrete co-ordinates, f is a force vector, ω is the excitation frequency and $\underset{\sim}{m}$, $\underset{\sim}{d}$ and k are the square symmetric mass, damping and stiffness matrices respectively. Using the standard transformation matrix to represent equation (72) in terms of the normal mode co-ordinates:

$$x = \underset{\sim}{\Phi}\, q \quad \ldots\ldots\ldots\ldots\ldots\ldots\ldots \quad (73)$$

equation (72) becomes:

$$\underset{\sim}{M}\ddot{q} + \underset{\sim}{D}\dot{q} + Kq = F \quad \ldots\ldots\ldots \quad (74)$$

where M and K are square diagonal matrices, but D is non-diagonal. If the system is linear the response will have the form $q = \hat{q}ej^{\omega t}$ and equation (74) can be written as:

$$-\underset{\sim}{I}\omega^2\hat{q} + \underset{\sim}{\omega}_r^2\hat{q} + j\xi\hat{q} = \underset{\sim}{M}^{-1}F \quad \ldots\ldots\ldots\ldots \quad (75)$$

where $\underset{\sim}{I}$ = unity matrix

$\underset{\sim}{\omega}_r^2$ = diagonal matrix where each element is given by

$$\omega_{rr}^2 = \frac{K_{rr}}{M_{rr}}$$

ξ = non-diagonal matrix of modal damping coefficients.

Following the technique of Hasselman (23), the matrix ξ can be considered as:

$$\underset{\sim}{\xi} = \underset{\sim}{\xi}_d + \underset{\sim}{\xi}_n \quad \ldots\ldots\ldots\ldots \quad (76)$$

where $\underset{\sim}{\xi}_d$ is a square diagonal matrix, each element taking the form $\xi_{rr} = 2\zeta_r\omega_r$, and $\underset{\sim}{\xi}_n$ is a square symmetric matrix which represents the coupling terms between the normal modes whose leading diagonal is zero. This results in equation (75) being written as:

$$(\underset{\sim}{z}_d + \underset{\sim}{z}_n)\hat{q} = \underset{\sim}{M}^{-1}\underset{\sim}{F} \quad \ldots\ldots\ldots\ldots \quad (77)$$

where z_d is a diagonal matrix whose elements take the form:

$$\underset{\sim}{z}_{d_{rr}} = \omega_r^2 - \omega^2 + j2\zeta_r\omega_r \quad \ldots\ldots\ldots\ldots \quad (78)$$

and $z_n = j\xi_n$, a non-diagonal matrix whose leading diagonal elements are zero.

In order to be able to have a meaningful relationship between the elements of z_d and z_n it is useful to apply a transformation to diagonalise z_d to a unity matrix i.e. consider the transformation from the $\hat{q}$ co-ordinate system to the y co-ordinates:

$$\underset{\sim}{\hat{q}} = \underset{\sim}{\Psi}\,\underset{\sim}{\gamma} \quad \ldots\ldots\ldots\ldots \quad (79)$$

where the transformation matrix Ψ is-given by $\Psi = z_d^{-\frac{1}{2}}$. Thus equation (77) becomes:

$$(I + z_{n\gamma})\gamma = z_d^{-\frac{1}{2}t}\underset{\sim}{M}^{-1}\underset{\sim}{F} \quad \ldots\ldots\ldots\ldots \quad (80)$$

where I is the unity matrix and $z_{n\gamma} = z_d^{-\frac{1}{2}t}\underset{\sim}{z}_n z_d^{-\frac{1}{2}}$. For simplicity consider two adjacent modes of vibration whose natural frequencies and modal damping coefficients are given respectively as:

ω_j, ξ_{jj} and ω_k, ξ_{kk} where $\xi_{jj} = 2\zeta_j\omega_j$ and

$\xi_{kk} = 2\zeta_k\omega_k$.

Then we can write equation (77) as:

$$\left[\begin{pmatrix} \omega_j^2-\omega^2+j\omega\xi_{jj} & 0 \\ 0 & \omega_k{}^2-\omega^2+j\omega\xi_{kk} \end{pmatrix} + \begin{pmatrix} 0 & j\omega\xi_{jk} \\ j\omega\xi_{kj} & 0 \end{pmatrix}\right]\begin{bmatrix} \hat{q}_j \\ \hat{q}_k \end{bmatrix}$$

$$= \begin{bmatrix} M_{jj}^{-1}F_j \\ M_{kk}^{-1}F_k \end{bmatrix} \quad .. \quad .. \quad .. \quad .. \quad .. \quad .. \quad .. \quad (81)$$

and applying the transformation of equation (79) to equation (81) leads to:

$$\left[\begin{pmatrix} 1 & 0 \\ 0 & 1 \end{pmatrix} + \begin{pmatrix} 0 & \mathcal{Z}n\gamma \\ \mathcal{Z}n\gamma & 0 \end{pmatrix}\right]\begin{Vmatrix} \gamma_{jj} \\ \gamma_{kk} \end{Vmatrix} = \begin{bmatrix} \mathcal{Z}d_{jj}\, M_{jj}\, F_j \\ \mathcal{Z}d_{kk}\, M_{kk}\, F_k \end{bmatrix} \quad (82)$$

where,

$$\mathcal{Z}n\gamma = \frac{j\omega\xi_{ik}}{(\omega_j^2 - \omega^2 + j\omega\xi_{jj})^{\frac{1}{2}}(\omega_k^2 - \omega^2 + j\omega\xi_{kk})^{\frac{1}{2}}} \quad .. \quad (83)$$

If $\omega = \omega_j < \omega_k$, then equation (83) becomes:

$$\mathcal{Z}n\gamma = \frac{j\omega_j\xi_{jk}}{(j2\zeta_j\omega_j{}^2)^{\frac{1}{2}}((\omega_k{}^2 - \omega_j{}^2)\, j2\zeta_k\omega_k\omega_j)^{\frac{1}{2}}} \quad . \quad (84)$$

$$\mathcal{Z}n\gamma = \frac{\xi_{jk}(j2\zeta_j\omega_j)^{\frac{1}{2}}}{2\zeta_j\omega_j((\omega_k{}^2 - \omega_j{}^2)\quad j2\zeta_k\omega_k\omega_j)^{\frac{1}{2}}} \quad .. \quad .. \quad (85)$$

and,

$$|\text{Znγ}| = \left\{ \frac{2\zeta_j \omega_j \left(\frac{\omega_k}{\omega_j}\right)^2}{\left(\left(\omega_k^2 - \omega_j^2\right)^2 + 4\zeta_k \omega_k \omega_j\right)^2} \right\}^{\frac{1}{2}} \left| \frac{\xi_{jk}}{\xi_{jj}} \right| \quad \text{(86)}$$

where $\xi_{jj} = 2\zeta_j \omega_j$.

Equation (86) represents the interaction between the two adjacent modes of vibration and if the off-diagonal elements of the damping matrix, ξ_{jk}, are assumed equal to the diagonal elements, ξ_{jj}, then equation (86) becomes:

$$|\text{Znγ}| = \frac{(2\zeta_j)^{\frac{1}{2}}}{\left(\left(\beta^2 - 1\right)^2 + 4\zeta_k^2 \beta^2\right)^{\frac{1}{4}}} \quad \text{(87)}$$

where $\beta = \omega_k / \omega_j$

Equation (87) shows that the modal interaction is dependent upon the closeness of the natural frequencies and the relative damping in each mode.

This has also been shown by Marples (39) who derived an interference boundary showing the relation between modal damping and natural frequency ratios. However, he was concerned with the errors invoked in estimating modal characteristics from the vector plots as a result of modal interaction and no reference was made to the form of the system damping matrices.

In order to show a graphical representation of the interaction mechanism, a carpet plot of equation (87) is shown on Figure 13. The plot is in terms of the frequency ratio, ω_k/ω_j and the damping ratios ζ_j/ζ_k as a function of the parameter $|\text{Znγ}|$, which represents the modal coupling terms.

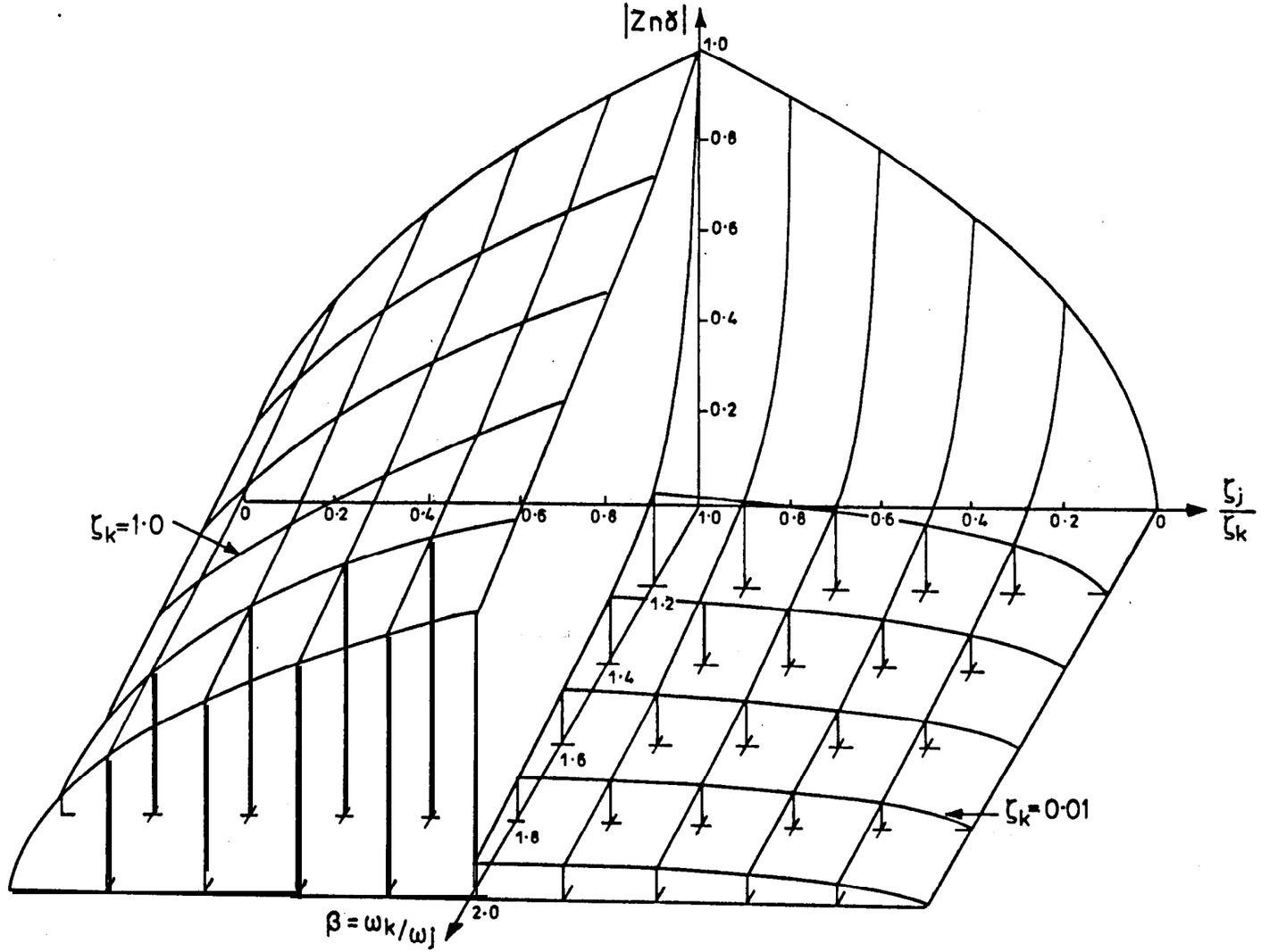

FIGURE 13 INTERACTION BETWEEN ADJACENT MODES OF VIBRATION FOR A SYSTEM WITH A FULL MODAL DAMPING MATRIX

Inspection of Figure 13 shows that the worst condition for modal interaction (which is almost intuitive) is when the natural frequencies and damping ratios in the two adjacent modes of vibration are equal in magnitude, (point $|\mathbb{Z}_{n\gamma}| = 1.0$).

As the separation between either the damping ratios or the natural frequencies increases, the magnitude of $|\mathbb{Z}_{n\gamma}|$ reduces and hence the effect of the off-diagonal damping terms is reduced. It can be seen that the most sensitive factor is that of the natural frequency ratio, indicating that complex structures which have natural frequency clusters will have severe modal interaction, regardless of the level of damping, unless of course the relative damping of a pair of adjacent modes is significantly different i.e. $\zeta_j/\zeta_k << 1$.

One may ask what significance equation (87) really has since it does not offer any guidelines as to when modal interaction is going to become a problem. Unfortunately, this is a question of how small is small, since in the above case one is comparing the off-diagonal modal coupling terms with unity. The important point which must be borne in mind is that we have assumed that the off-diagonal modal damping coefficients (ξ_{jk}) are equal in magnitude to the diagonal terms, yet if the natural frequencies of the two modes are well separated, modal interaction becomes negligible.

In order to apply equation (87) and establish its credibility in terms of what level of magnitude the off-diagonal elements can take with respect to the leading diagonal elements, before serious errors are incurred in the identification process, a simulation exercise was carried out on a digital computer of a two degre-of-freedom system. The aim of the exercise was to explore the effects of close natural frequencies and damping ratios on the ability to excite normal modes using multi-point excitation methods.

3.6 DIGITAL SIMULATION OF NORMAL MODES IN DAMPED LINEAR SYSTEMS

The model chosen for this analysis was a simple two degree-of-freedom system, since whatever applies to this system must apply to an n degree-of-freedom system. Figure 14 shows a diagrammatic sketch of the physical model used for the simulation exercise.

Two fundamental areas were considered in the analysis, both being related to the form of the damping matrix. The first area of interest was related to the analysis carried out in Section 3.4 and here the equations governing the physical model were transformed to their modal co-ordinates in order that the magnitude of the off-diagonal elements of the damping matrix could be chosen in relation to the magnitude of the leading diagonal elements and the effect of close modal natural frequencies and damping separation on the normal modes could be investigated.

The second area was concerned with an investigation into how sensitive were changes in the normal modes to deviations in the force input magnitudes and phases from those required to classically excite the normal modes when the damping matrix was proportional to the stiffness matrix.

3.6.1 THE MATHEMATICAL MODEL

The equations of motion of the physical model in terms of the co-ordinates x_1 and x_2 of Figure (14) are:

$$\underset{\sim\sim}{m}\ddot{\underset{\sim\sim}{x}} + \underset{\sim\sim}{k}\underset{\sim\sim}{x} + j\underset{\sim\sim}{d}\underset{\sim\sim}{x} = fe^{j\omega t} \qquad .. \quad .. \quad .. \quad .. \quad .. \quad (88)$$

where the mass matrix m is:

$$\begin{bmatrix} \frac{m}{4} + \frac{J}{L^2} & \frac{m}{4} - \frac{J}{L^2} \\ \frac{m}{4} - \frac{J}{L^2} & \frac{m}{4} + \frac{J}{L^2} \end{bmatrix} \qquad .. \quad .. \quad .. \quad .. \quad .. \quad (89)$$

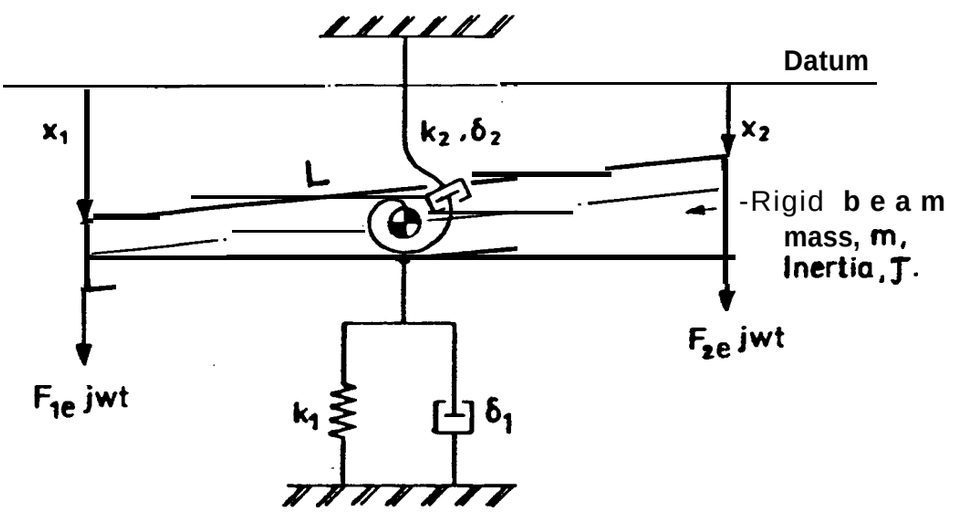

FIGURE 14

TWO DEGREE-OF-FREEDOM.PHYSICAL MODEL EMPLOYED IN THE SIMULATION EXERCISE.

k_1, δ_1 RESPRESENT **THE STIFFNESS AND HYSTERETIC DAMPING IN THE TRANSVERSE MODE.**

k_2, δ_2 **REPRESENT THE STIFFNESS AND HYSTERETIC DAMPING IN THE TORSIONAL MODE.**

the stiffness matrix k:

$$\begin{bmatrix} \frac{k_1}{4} + \frac{k_2}{L^2} & \frac{k_1}{4} - \frac{k_2}{L^2} \\ \frac{k_1}{4} - \frac{k_2}{L^2} & \frac{k_1}{4} + \frac{k_2}{L^2} \end{bmatrix} \quad \text{(90)}$$

and the hysteretic damping matrix d is:

$$\begin{bmatrix} d_{11} & d_{12} \\ d_{21} & d_{22} \end{bmatrix} \quad \text{(91)}$$

where the elements d_{ij} of the damping matrix are given by:

$$d_{ij} = \delta k_{ij} \text{ for } i = j,\ i, j = 1, 2 \ldots n \quad \text{(92)}$$

$$= c_i \delta k_{ij} \text{ for } i \neq j,\ i, j = 1, 2 \ldots n \quad \text{(93)}$$

k_{ij} being the elements of the stiffness matrix
δ being the hysteretic damping factor or loss factor
c is a constant which is greater than zero.

In the special case of a stiffness proportionally damped system,

$$d_{ij} = \delta k_{ij} \text{ for } i, j = j, 2 \ldots n \quad \text{(94)}$$

The force vector f is simply:

$$\begin{bmatrix} f_1 \\ f_2 \end{bmatrix} \quad \text{(95)}$$

The modal matrix for this system, derived from the eigenvalue

problem is obtained as:

$$\underset{\sim}{\Phi} = \begin{bmatrix} 1.0 & 1.0 \\ 1.0 & -1.0 \end{bmatrix} \quad \ldots\ldots\ldots\ldots\ldots\ldots \quad (96)$$

and the eigenvalue matrix is:

$$\underset{\sim}{\omega}^2 = \begin{bmatrix} \omega_b^2 & 0 \\ 0 & \omega_t^2 \end{bmatrix} \quad \ldots\ldots\ldots\ldots\ldots\ldots \quad (97)$$

where, ω_b is termed the transverse normal mode frequency of vibration

ω_t is termed the torsional normal mode frequency of vibration, and

$$\underset{\sim}{f} = \begin{bmatrix} f_1 \\ f_2 \end{bmatrix} \quad \ldots\ldots\ldots\ldots\ldots\ldots \quad (98)$$

If equation (88) is expressed in terms of the modal co-ordinates, $\hat{q}$, the resulting equation for the model is:

$$(\underset{\sim}{\omega}_r^2 - \underset{\sim}{I}\omega^2 + j\underset{\sim}{\zeta})\hat{\underset{\sim}{q}} = \underset{\sim}{M}^{-1}\underset{\sim}{F} = Q \quad \ldots\ldots\ldots\ldots\ldots\ldots \quad (99)$$

where $\omega_{rr}^2 = K_{rr}/M_{rr}$,

and
$$\left.\begin{aligned} \underset{\sim}{K} &= \underset{\sim}{\Phi}^t \underset{\sim}{k} \underset{\sim}{\Phi} \\ \underset{\sim}{M} &= \underset{\sim}{\Phi}^t \underset{\sim}{m} \underset{\sim}{\Phi} \\ \underset{\sim}{\zeta} &= \underset{\sim}{M}^{-1} \underset{\sim}{\Phi}^t \underset{\sim}{d} \underset{\sim}{\Phi} \\ F &= \underset{\sim}{\Phi}^t \underset{\sim}{f} \end{aligned}\right\} \quad \ldots\ldots\ldots\ldots\ldots\ldots \quad (100)$$

3.7 COMPUTER PROGRAMS

In order to be able to investigate efficiently the large number of input conditions on the normal mode response of the two degree-of-freedom system and to have a standard

method of calculating such factors as modal damping ratios and normal mode frequencies, two computer programs were developed.

The programs are listed in Appendix III and a brief description of their use will be given in this section.

The first program, (program ZTHA), is a general purpose program for hysteretically damped multi degree-of-freedom systems. This program reads in the mass, stiffness and damping matrices together with the appropriate frequency parameters and in particular, the input forces in their real and imaginary parts. Thus, any combination of input force conditions in terms of their relative magnitude and phase could be used.

This allowed the effect of any arbitrary force distribution on the theoretical normal modes to be observed, whilst varying the closeness of the normal mode frequencies and modal damping.

Further, by presenting the data in terms of the modal mass, stiffness and damping matrices the effect on the normal modes of varying the magnitudes of the off-diagonal elements of the modal damping matrix could be observed when the correct input force distributions were used. This again could be carried out for a wide range of normal mode frequencies and modal damping ratio conditions.

The second computer program, (program CFIT), was written to allow the data generated by the first program to be presented graphically, on-line, in terms of a vector plot. This program was based on the theory of the Kennedy and Pancu vector plots in which the response of a lightly damped system traces out the locus of a circle in the resonant region (27). To do this, a curve fitting procedure which produced a 'best-fit' circular arc within the resonant region of the computed response data was developed.

This 'circle of best-fit' was plotted by the computer and the modal damping ratio and resonant frequency were evaluated from this.

3.8 EXCITATION OF THE NORMAL MODES IN A SYSTEM WITH A FULL MODAL DAMPING MATRIX

The theoretical analysis of Section 3.4 showed that modal interaction was minimised when there was sufficient separation between the natural frequencies of any two adjacent modes of vibration, or when the damping in one of the modes was very small compared to that in the adjacent mode, even when the modal damping matrix was 'full' (14).

In order to investigate the limits on the closeness of the modal natural frequencies, in terms of errors arising from the determination of the individual modal damping ratios and natural frequencies of the computed responses, a series of tests were carried out using computer program ZTHA.

Obviously, there can be no hard and fast criterion which establishes the amount of error one can expect in the calculated values of natural frequency and modal damping for a given frequency separation of adjacent modes, since these are dependent upon the level of damping in the individual modes. Thus, the simulation tests were carried out for a level of structural damping typical of aircraft structures, namely 2% critical damping. The individual modal damping ratios were maintained at a constant value and the closeness of the two natural frequencies was adjusted by varying the torsional mode natural frequency, the transverse mode natural frequency being held constant.

The values assigned to the physical parameters of equations (89) to (95) were based upon the values of the experimental rig described in Chapter 4. These are listed below:

$m = 16$ kg; $J = 1.0$ kgm^2; $L = 1$m;

$k_1 = 400$ kN/m; k_2(initial) $= 56 k \frac{Nm}{rad}$;

$\delta = 0.04$; $f1 = f_2 = 4$N.

The above quantities were used in equations (89) through to (100) to give the transformed modal matrices:

$$\underset{\sim}{\omega}^2 = \begin{bmatrix} \omega_b^2 & 0 \\ 0 & \omega_t^2 \end{bmatrix} = \begin{bmatrix} 0.25 & 0 \\ 0 & 0.56 \end{bmatrix} 10^5 \left(\frac{rad}{s}\right)^2 \quad .. \quad (101)$$

$$\underset{\sim}{\xi} = \begin{bmatrix} \xi_{11} & \xi_{12} \\ \xi_{21} & \xi_{22} \end{bmatrix} = \begin{bmatrix} \omega_b{}^2 g & \xi_{12} \\ \xi_{21} & \omega_t{}^2 g \end{bmatrix} \left(\frac{rad}{s}\right)^2 \quad .. \quad .. \quad (102)$$

$$\underset{\sim}{Q} = \begin{bmatrix} 0.5 \\ 0 \end{bmatrix} N; \quad \underset{\sim}{\hat{q}} = \begin{bmatrix} \underset{\sim}{\hat{q}}_1 \\ \underset{\sim}{\hat{q}}_2 \end{bmatrix} \quad .. \quad .. \quad (103)$$

The off-diagonal elements, ($\xi_{12} = \xi_{21}$) of equation (102) were chosen to be equal to the value of ξ_{11} throughout the analysis.

The value of 0.56×10^5 $(rad/s)^2$ for the torsional mode natural frequency was incrementally reduced until the difference between the frequencies of vibration was only 2%, i.e. $\omega_t/\omega_b = 1.02$; the modal damping matrix at this condition being given as:

$$\underset{\sim}{\xi} = \begin{bmatrix} 0.1 & 0.1 \\ 0.1 & 0.104 \end{bmatrix} 10^4 \left(\frac{rad}{s}\right)^2$$

For each frequency ratio increment the modal co-ordinates were automatically plotted on a vector plot and the modal damping ratio and normal mode frequencies evaluated.

3.9 RESULTS OF COMPUTER SIMULATION

3.9.1 THE EFFECT OF CLOSE NATURAL FREQUENCIES

Figures 15 to 20 show the effect of varying the closeness of the natural frequencies of the simulated two degree-of-freedom system in terms of the vector plots for the transverse normal mode response. It can be seen that as the separation between the two frequencies increases (i.e. β increases) and approaches a value of 1.25, the response approaches that of a pure normal mode.

The effect of the off-diagonal terms of the damping matrix on the vector plot response, due to the closeness of the natural frequencies, is to cause a rotation and a displacement of the pure normal mode response. This is evident from Figures 15 to 20, where these effects can be clearly seen as the frequency ratio β approaches 1.0.

These effects have been reported by other workers in the field (40) (41), but if one extends the analysis and extracts the modal information from these results then it is possible to identify the errors in derived modal properties which arise due to the above effects.

Figure 21 shows the deviation from a pure normal mode response due to the closeness of the modal natural frequencies. This figure was obtained by determining the ratio of the real to imaginary parts of the response at the true transverse normal mode frequency of vibration. It can be seen from Figure 21 that when the frequency separation of the two modes of vibration is greater than 1.25, only a small improvement in the normal mode response is obtained since the curve becomes asymptotic to the zero condition, which is the required value.

From each of the responses shown on Figures 15 to 20 the modal damping factors and normal mode frequencies were

computed. Table 3.1 shows these quantities expressed as percentage errors of the true values. The errors in the results are, in the case of the modal damping factors, very large whereas the errors in the normal mode frequencies are considerably lower and again, as the frequency separation approaches 1.25 the errors in both these quantities reduces considerably.

These results, which are based on a modal damping matrix whose coupling (off-diagonal) elements are comparable in magnitude to the leading diagonal elements indicate that, for the level of structural damping used in the analysis, if the frequency separation of any two adjacent modes is greater than 1.25, then it is possible to excite a normal mode within normal experimental error bounds, and the modal damping and natural frequencies of vibration determined from this response will be within acceptable limits.

If, however, the modal damping levels are changed then the value of 1.25 for the frequency ratio separation will no longer be an accurate criterion for the minimal modal interaction.

Table 3.2 shows this effect by giving similar information as in Table 3.1 except that the results are for a damping level of 4% critical, i.e. $\delta = 0.08$.

It can be seen that for the same frequency separation factor the errors in the estimated modal damping factors and normal mode frequencies have increased.

3.10 PROPORTIONALLY DAMPED SYSTEMS

With proportionally damped systems the equations of motion can be transformed into individual uncoupled equations which leads to a number of interesting results when such systems are subject to multi-point excitation.

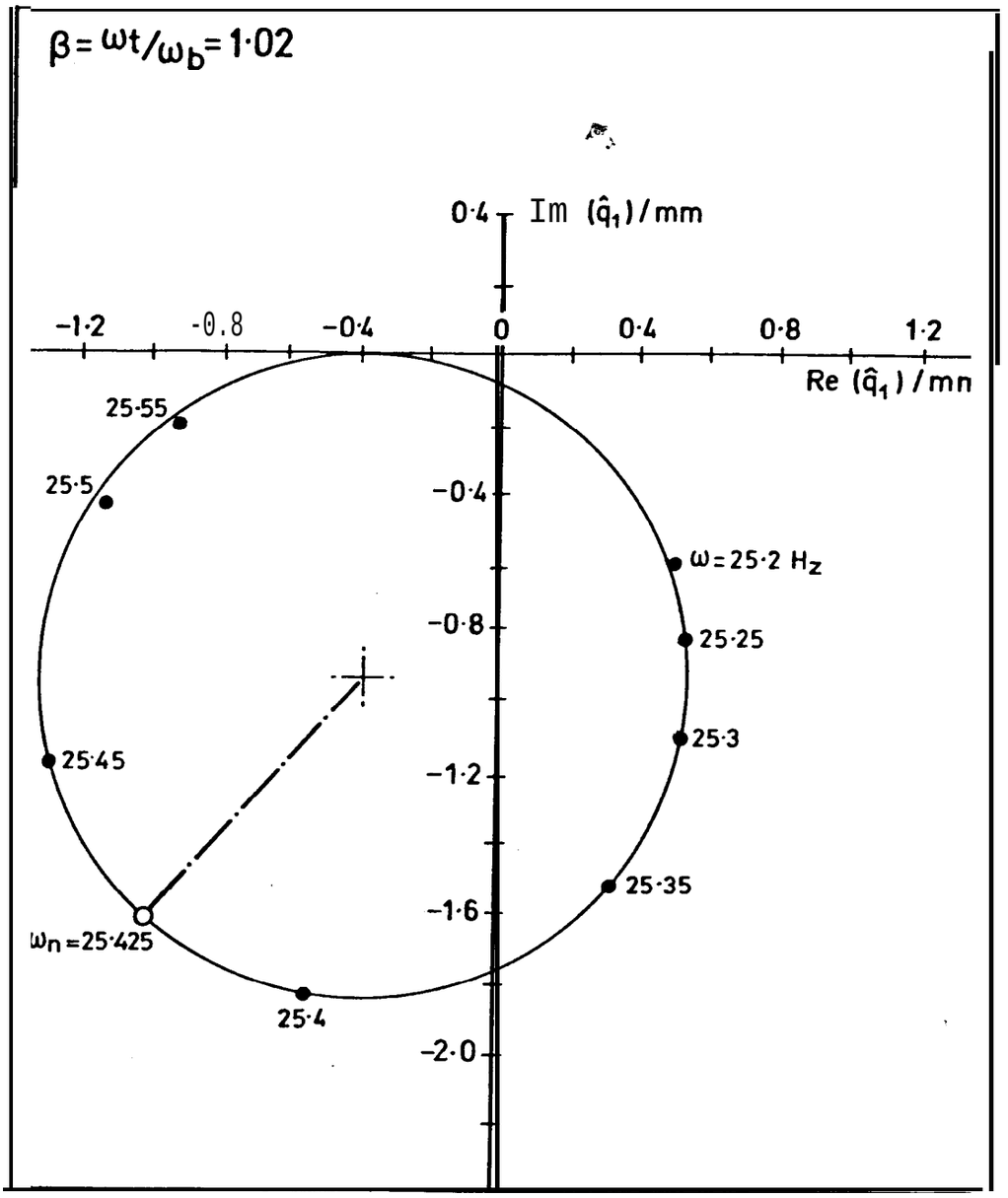

FIGURE 15

VECTOR PLOT OF THE MODAL RESPONSE $\hat{q}_1$ IN THE TRANSVERSE MODE.

FREQUENCY SEPARATION BETWEEN THE TRANSVERSE (ω_b) AND THE TORSIONAL MODE (ω_t) IS 2%.

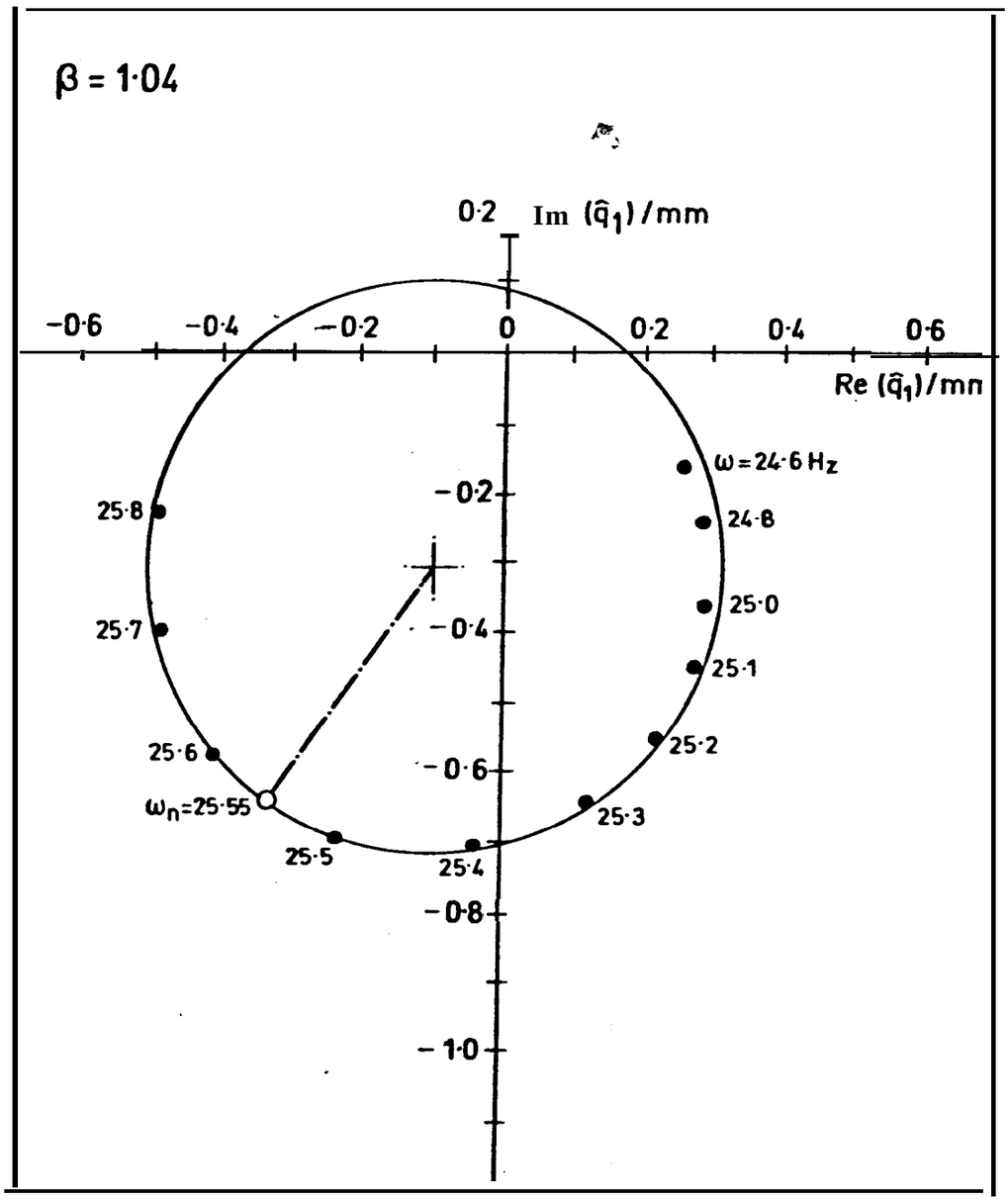

FIGURE 16

VECTOR PLOT OF $\hat{q}_1$. FREQUENCY SEPARATION BETWEEN THE TRANSVERSE (ω_b) AND TORSIONAL MODE (ω_t) IS 4%.

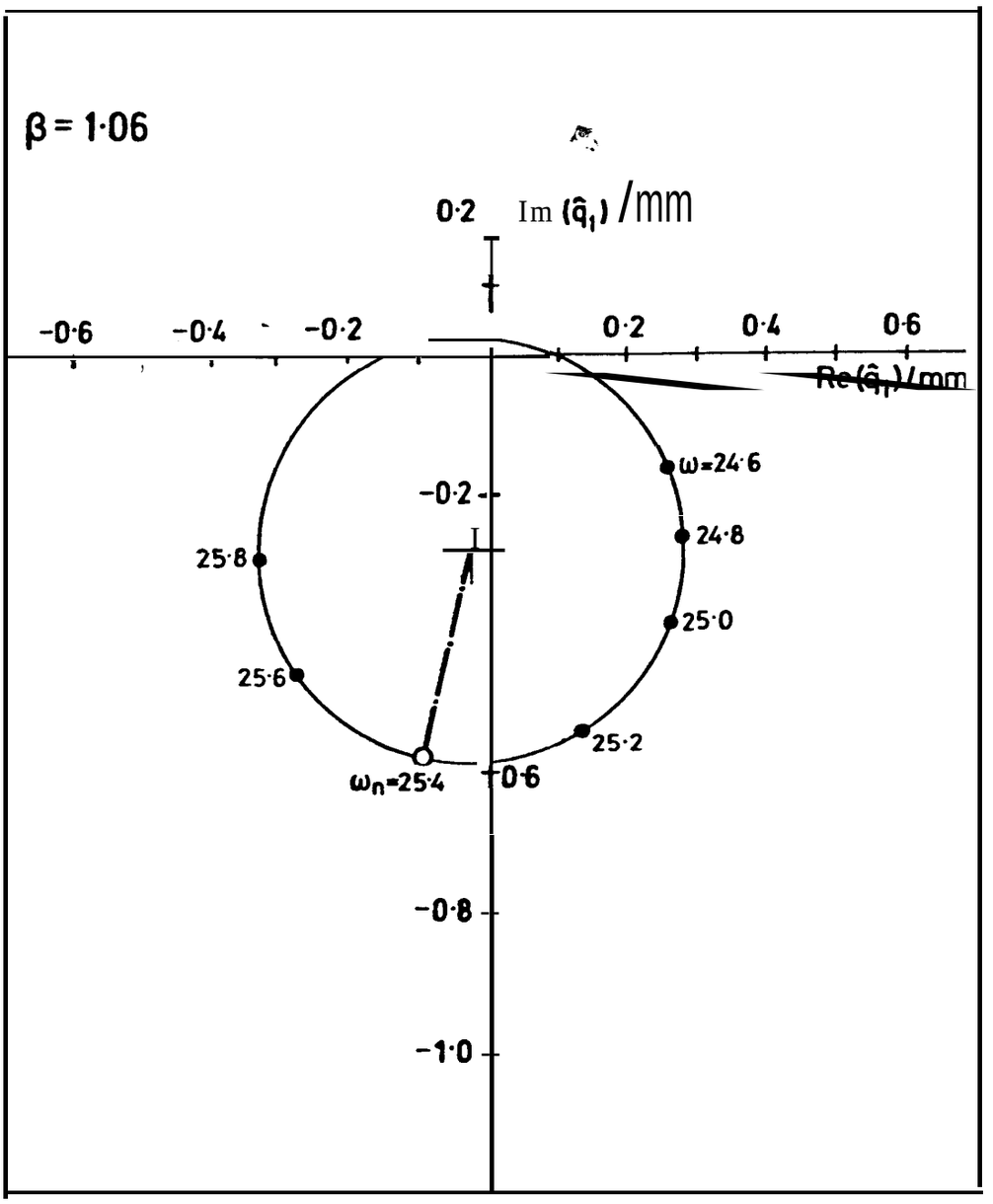

FIGURE 17

VECTOR PLOT OF $\hat{q}_1$. **NATURAL FREQUENCY SEPARATION BETWEEN MODES IS 6%.**

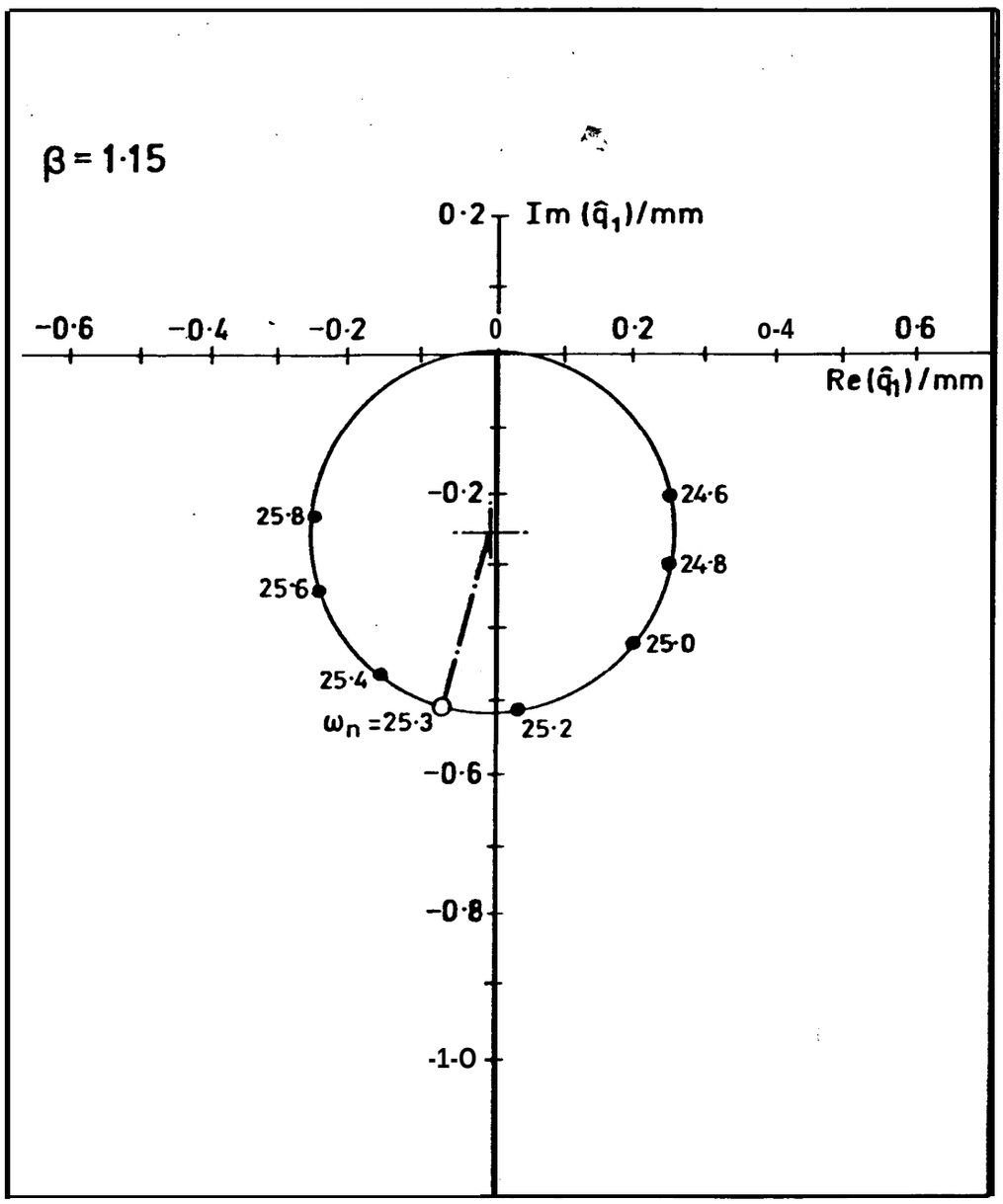

FIGURE 18

VECTOR PLOT OF $\hat{q}_1$. NATURAL FREQUENCY SEPARATION BETWEEN MODES IS 15%.

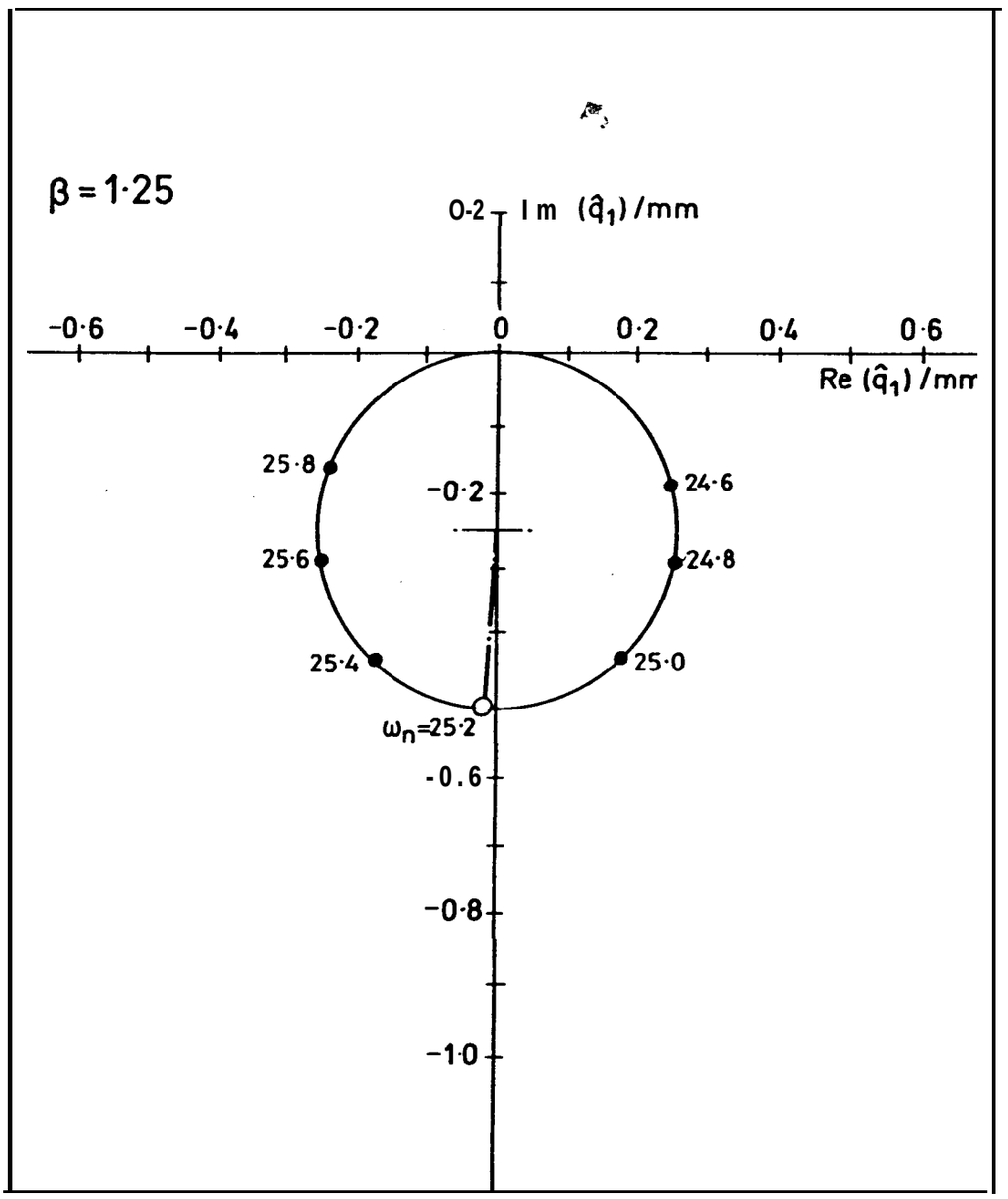

FIGURE 19

VECTOR PLOT OF $\hat{q}_1$. NATURAL FREQUENCY SEPARATION BETWEEN MODES IS 25%.

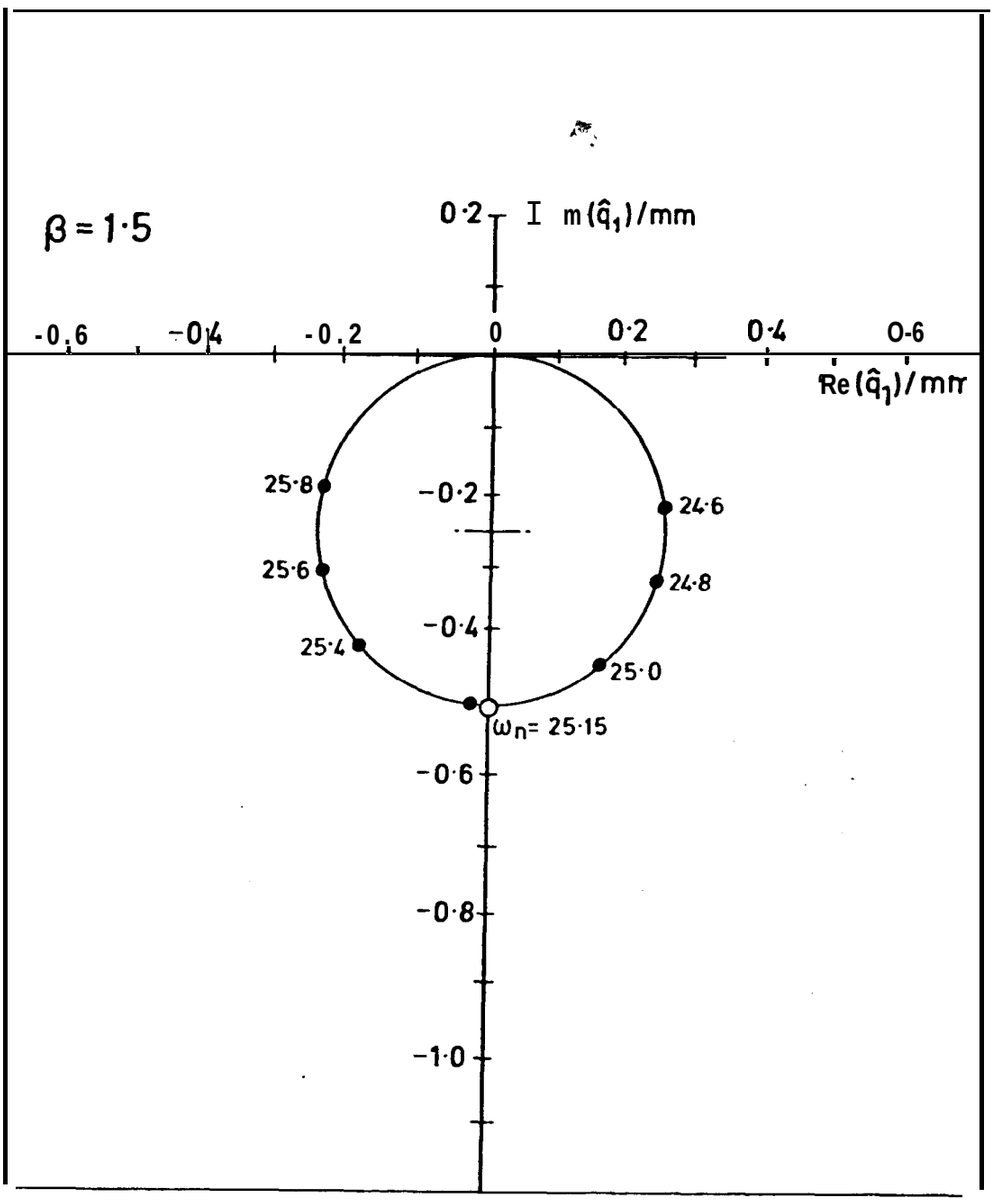

FIGURE 20

VECTOR PLOT OF $\hat{q}_1$. NATURAL FREQUENCY SEPARATION BETWEEN MODES IS 50%

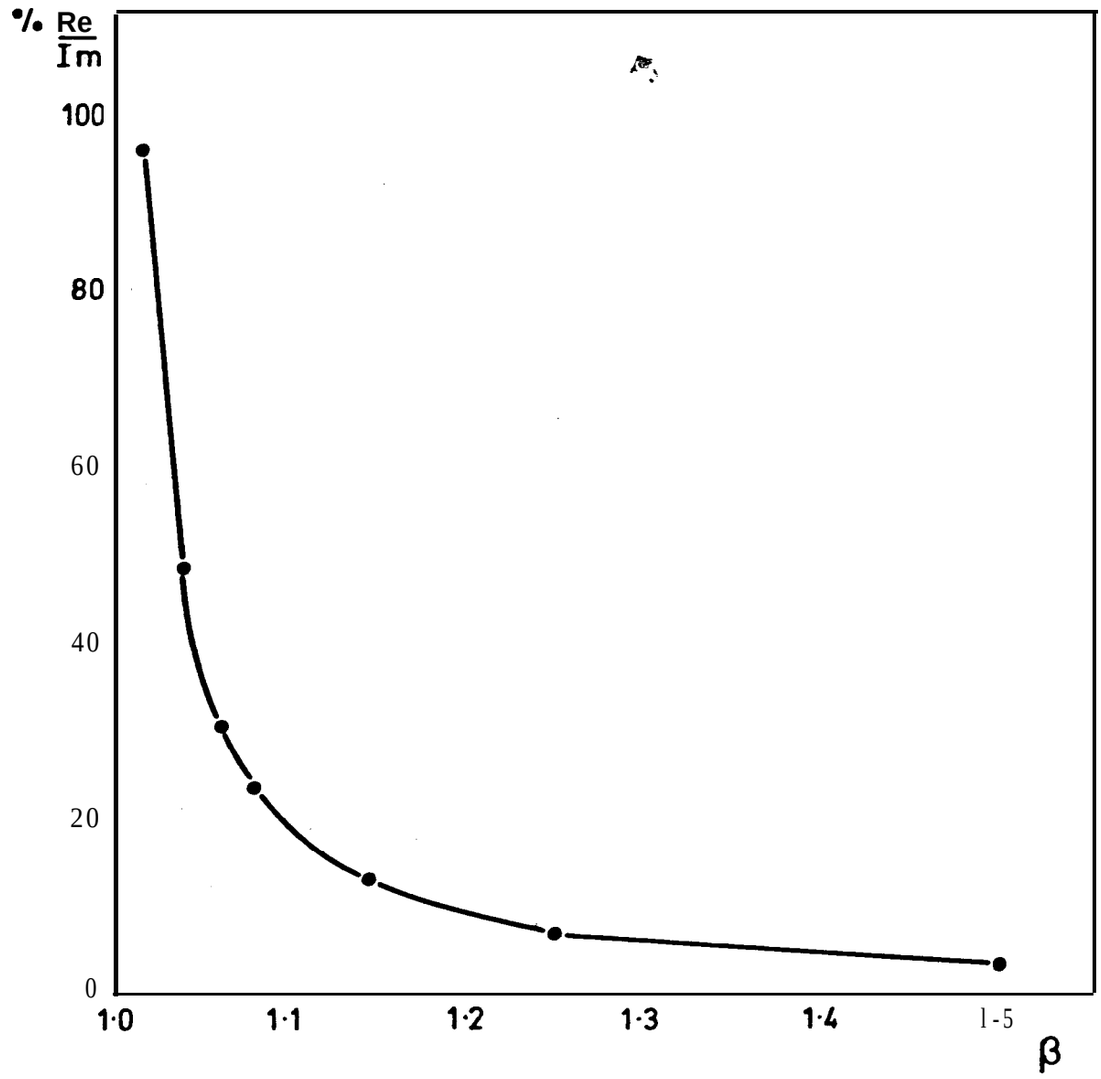

FIGURE 21

THE EFFECT OF CLOSE NATURAL FREQUENCIES ON THE ABILITY TO EXCITE A PURE NORMAL MODE

$\%\frac{R_e}{I_m}$ **REPRESENTS THE PERCENTAGE OF REAL TO IMAGINARY PART OF THE MODAL RESPONSE** $\hat{q}_1$ **AT THE TRUE TRANSVERSE NORMAL MODE FREQUENCY,** ω_b **= 25.165 Hz**

TABLE 3.1 $\delta = 0.04$, $\omega_b = 158.1 \frac{rad}{s}$ (25.165 Hz)

Frequency Separation Ratio $\beta=\omega_k/\omega_b$	ε_δ	ε_ω
1.02	84	1.5
1.04	30	1.3
1.06	2	0.9
1.15	1.8	0.54
1.25	1.1	0.14
1.5	0.01	0.06

TABLE 3.2 $\delta = 0.08$, $\omega_b = 158.1 \frac{rad}{s}$

Frequency Separation Ratio $\beta=\omega_k/\omega_b$	ε_δ	ε_ω
1.02	95	1.0
1.15	14	0.8
1.5	10	0.14

In the above Tables, the parameters ε_δ and ε_ω represent the percentage errors in the modal damping factor and the normal mode frequency of the transverse mode, i.e.

$$\varepsilon_\delta = \left| \frac{\delta - \delta \text{ calculated}}{\delta} \times 100 \right|$$

$$\varepsilon_\omega = \left| \frac{\omega_b - \omega \text{ calculated}}{\omega_b} \times 100 \right|$$

3.10.1 NORMAL MODES OF PROPORTIONALLY DAMPED SYSTEMS

The mathematical model used in the simulation studies of the previous sections was again used except that the damping matrix was proportional to the stiffness matrix, i.e.

$$d = \delta k \quad . \quad . \quad . \quad . \quad . \quad . \quad . \quad . \quad . \quad . \quad . \quad . \quad . \quad . \quad . \quad . \quad . \quad (104)$$

and the equations were solved in terms of the discrete co-ordinates x_1 and x_2, not the modal co-ordinates $\hat{q}_1$ and $\hat{q}_2$.

The force vector given by $[4.0, \ 4.0]^t_N$ was used to excite the transverse normal mode of vibration and the results of this test are shown in terms of the output response xl and x_2 in Table 3.3. This table shows the real, quadrature and corresponding polar output responses as the frequency is varied over both the normal mode frequencies of vibration. The interesting result of this table is that the mode shape remains unchanged for any excitation frequency. The responses in this case are of course equal in magnitude due to the symmetry of the system, but even if the model had not had symmetrical properties and the correct excitation vector was used, the only difference in the results would have been a change in the individual magnitudes, but the ratio of these would have remained unchanged and equal to the mode shape.

Since there are no coupling terms in the transformed equations of motion, the closeness of the natural frequencies have no effect upon the modal responses of the system. This leads to a further interesting result which is related to estimating the natural frequencies and damping ratios of multi-degree-of-freedom systems with proportional damping.

Excitation Frequency (Hz)	x (mm)	Real (x) (mm)	Quadrature (x) (mm)	Polar (x) R(mm)	θ(deg)
24.6	x_1	0.249	-0.224	0.335	41.97
	x_2	0.249	-0.224	0.335	41.97
25.0	x_1	0.147	-0.452	0.475	71.98
	x_2	0.147	-0.452	0.475	71.98
25.165	x_1	0.0	-0.5	0.5	90.0
	x_2	0.0	-0.5	0.5	90.0
25.6	x_1	-0.248	-0.284	0.377	131.1
	x_2	-0.248	-0.284	0.377	131.1
26.0	x_1	-0.219	-0.13	0.255	149.0
	x_2	-0.219	-0.13	0.255	149.0

TABLE 3.3

Proportionally Damped System Response
Showing that the Mode Shape (x_1/x_2)
Remains Unchanged with Excitation Frequency

ω_b = 25.165 Hz
ω_t = 25.6 Hz

3.10.2 THE EFFECT OF AN INCORRECT FORCE INPUT VECTOR ON THE ESTIMATED MODAL DAMPING RATIOS AND NATURAL FREQUENCIES

The fact that systems which have off-diagonal terms in the modal damping matrix are sensitive to an incorrect (based on the requirement of normal mode excitation) force vector leads one to investigate the effect of this on a system with proportional damping.

This was done by arbitrarily changing the input force vector of the transverse mode so that the elements of the vector were in-phase but incorrect in magnitude, relative to the true transverse normal mode excitation vector.

The results of these simulations are shown on Figure 22 where the response, in terms of the modal co-ordinate for the transverse mode are plotted on a vector plot. The constant frequency lines are also drawn on these plots and it can be seen that the effect of an incorrect input force vector is to merely increase (or decrease) the radius of the response circle along a given constant frequency line. Thus the damping ratio determined from these plots is unchanged and the natural frequency is always given by the point at which the real part of the response is zero.

These results are obvious when one considers that the transformed equations of motion remain unchanged except that the modal input forces are changed in magnitude. This is readily shown by the following simple analysis.

Let the equations of motion of a system, in terms of the discrete co-ordinates, be given as:

$$\begin{bmatrix} m_1 & 0 \\ 0 & m_2 \end{bmatrix} \begin{bmatrix} \ddot{x}_1 \\ \ddot{x}_2 \end{bmatrix} + (1+j\delta) \begin{bmatrix} k_1+k_2 & -k_2 \\ -k_2 & k_2 \end{bmatrix} \begin{bmatrix} x_1 \\ x_2 \end{bmatrix} = \begin{bmatrix} f_1 \\ f_2 \end{bmatrix} e^{j\omega t} \qquad (105)$$

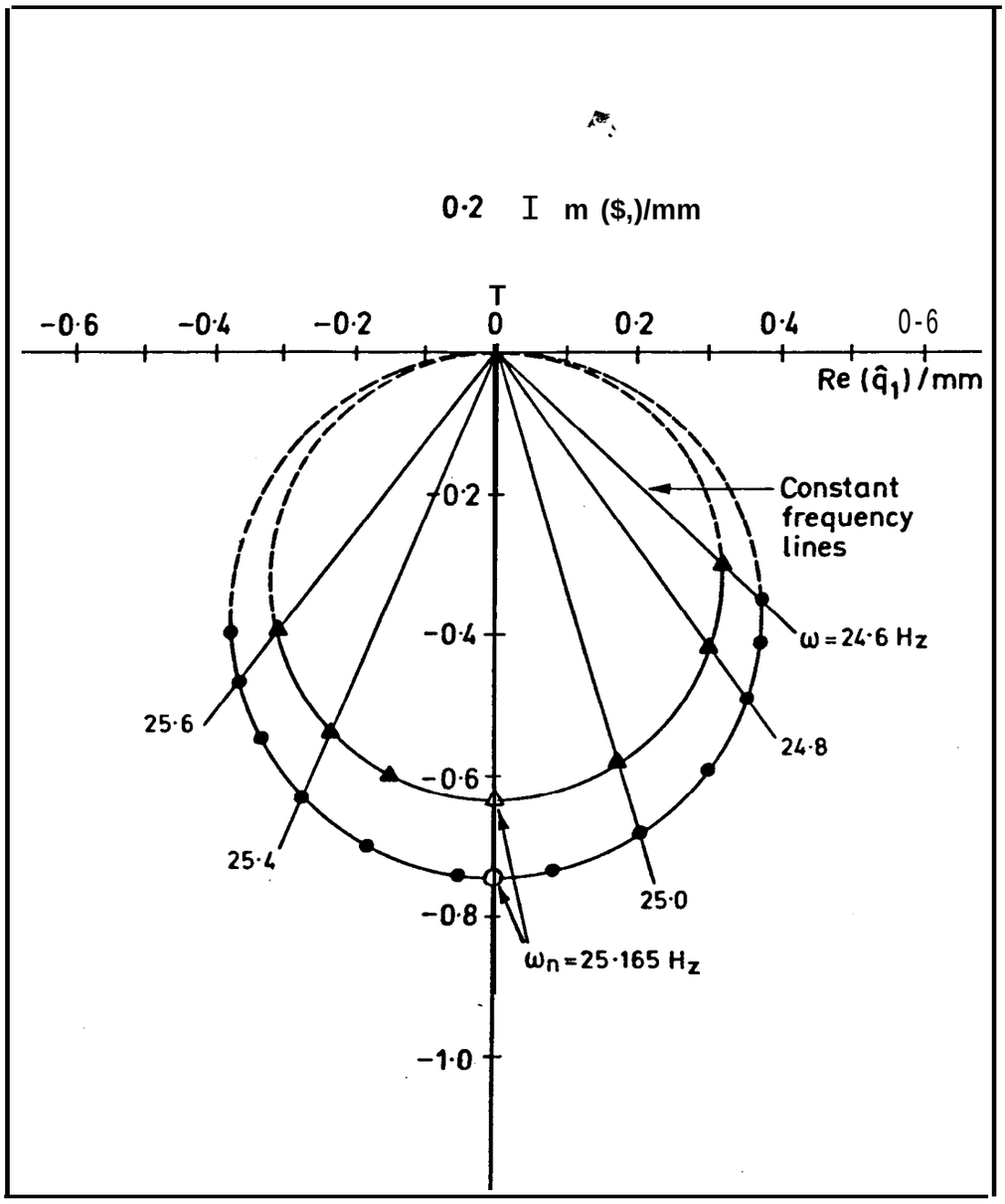

PROPORTIONALLY DAMPED SYSTEM VECTOR PLOTS SHOWING EFFECT OF AN ARBITRARY INPUT FORCE VECTOR

A INPUT FORCE VECTOR: $\begin{bmatrix} F_1 \\ F_2 \end{bmatrix} = \begin{bmatrix} 4.0 \\ 1.0 \end{bmatrix}$

- **INPUT FORCE VECTOR:** $\begin{bmatrix} F_1 \\ F_2 \end{bmatrix} = \begin{bmatrix} 4.0 \\ 2.0 \end{bmatrix}$

If a solution of the form $x = ue^{j\omega t}$ is assumed, then by solving the characteristic equation,

$$([k] - [m]\omega^2)\underset{\sim}{u} = 0 \qquad \ldots\ldots\ldots\ldots \quad (106)$$

the general expressions for the undamped normal mode vectors, assuming the last component u_2 is unity, are:

$$u^{(1)} = \begin{bmatrix} 1 - \frac{m_2}{k_2}\omega_1^2 \\ 1 \end{bmatrix} \qquad \ldots\ldots\ldots \quad (107)$$

$$u^{(2)} = \begin{bmatrix} 1 - \frac{m_2}{k_2}\omega_2^2 m_2 \\ 1 \end{bmatrix} \qquad \ldots\ldots\ldots \quad (108)$$

where $\omega_1^2, 2 = \frac{1}{2}\left\{\left(\frac{k_1}{m_1} + \frac{k_2}{m_2}(1 + \frac{m_2}{m_1})\right) \mp \left(\left(\frac{k_1}{m_1} + \frac{k_2}{m_2}(1 + \frac{m_2}{m_1})\right)^2 - 4\,\frac{k_1 k_2}{m_1 m_2}\right)\right\}$ $\qquad \ldots\ldots\ldots \quad (109)$

If equation (105) is transformed into modal co-ordinates, the mass, stiffness and damping matrices become diagonal and the transformed force vector is given by:

$$\underset{\sim}{Q} = \begin{vmatrix} f_1(l)(l - \$12) + f_2^{(1)} \\ f_1^{(2)}(1 - \frac{m_2}{k_2}\omega_2^2) + f_2^{(2)} \end{vmatrix} \qquad \ldots\ldots \quad (110)$$

In order for a normal mode of this system to be excited,

$f_1^{(1)}$, $f_2^{(1)}$ and $f_1^{(2)}$, $f_2^{(2)}$, which denote the magnitudes of the individual elements of the real force vectors in the first and second normal modes of vibration, will be unique, i.e. if $f_2^{(1)} = f_2^{(2)} = 1$, these are given by:

$$f_1^{(1)} = -1 - \left(\frac{k_1 - m_1\omega_2^2}{k_2}\right) \quad .. \quad .. \quad .. \quad .. \quad (111)$$

$$f_1^{(2)} = -1 - \left(\frac{k_1 - m_1\omega_1^2}{k_2}\right) \quad . \; . \; . \; . \; . \; . \; . \; . \; . \quad (112)$$

However, when these force vectors are not normal mode vectors then this merely means that the response amplitude is changed by a scalar quantity, i.e.:

$$f_1^{(1)'} = af_1^{(1)} \quad . \; . \; . \; . \; . \; . \quad .. \quad .. \quad .. \quad (113)$$

$$f_2^{(1)'} = bf_2^{(1)} \quad . \; . \; . \; . \; . \; . \quad .. \quad .. \quad .. \quad (114)$$

$$\text{and } Q = \begin{vmatrix} f_1^{(1)'}\left(1 - \frac{m_2}{k_2}\omega_1^2\right) + f_2^{(1)'} \\ \\ f_1^{(2)'}\left(1 - \frac{m_2}{k_2}\omega_2^2\right) + f_2^{(2)'} \end{vmatrix} \quad .. \quad .. \quad (115)$$

where a and b represent the scalar changes in the magnitudes of the forces.

The implications of this are that the mode shape changes with frequency and only satisfies the normal mode condition when the excitation frequency corresponds to the normal mode frequency, but the modal damping and normal mode frequency remain unchanged. Thus, if it was possible to know a priori that the damping was proportional, then it

would not be necessary to obtain the actual force distribution required to excite a normal mode if all one was interested in obtaining was the modal damping and natural frequency, since an approximation to the normal mode excitation vector,maintained in that appropriation, as the excitation frequency was varied would enable vector plots to be obtained which would provide accurate values for the natural frequency and modal damping ratio.

3.11 DISCUSSION AND CONCLUSIONS

The work detailed in this section was concerned with the effect of modal interaction in complex systems. The following points are the conclusions that have been drawn from this work.

1. The main factor contributing toward modal interaction is the closeness of the natural frequencies of adjacent modes, and that in all practical terms the modes of structurally damped systems can be considered uncoupled if the frequency ratio of adjacent modes is greater than 1.5, even if the off-diagonal terms of the damping matrix are comparable to the leading diagonal terms. The factor of 1.5 is, of course, only a guide and is based upon a maximum structural damping factor of 0.08.

2. In the case of proportionally damped systems the normal mode conditions are independent of the excitation frequency.

3. If an input force vector, which does not correspond to a normal mode excitation vector, is used to excite a multi degree-of-freedom system which can be classified as proportionally damped then the mode shape changes with frequency. However, the vector plot of the modal responses merely increases in magnitude along the constant frequency lines. As a result of

this the modal damping ratios and normal mode frequencies determined from these plots remain unchanged.

The implications of this are that for systems where modal interaction is minimal then it would appear that it is not necessary to set up an accurate normal mode excitation vector if all one is interested in is the modal damping ratio and normal mode frequency.

4. EXPERIMENTAL PROGRAMME

The aim of the experimental work was to design an experimental rig on which multi-point excitation tests could be carried out in order that normal mode excitation methods of complex structures could be investigated. Since the techniques involved in exciting normal modes of complex structures required some practice, (the author had spent some time during the research period at British Aerospace, Warton, Preston, on multi-point excitation tests of military aircraft and found the procedures involved somewhat lengthy), it was decided that the initial experimental programme should be used to 'practice' the techniques which had been observed in the ground resonance testing of aircraft at British Aerospace.

4.1 INITIAL NORMAL MODE INVESTIGATIONS

4.1.1 INTRODUCTION

The preceeding Chapters have shown that there are important criteria which must be satisfied in order that normal modes can be experimentally produced when exciting complex structures. In order to design a rig which could be used to experimentally investigate the effect of non-linearities and which incorporated multiple shakers to excite the normal modes, the information obtained from the experimental and analysis work of the preceeding Chapters had to be considered.

The fact that modal interaction can be minimised by choosing a suitable natural frequency separation between adjacent modes of vibration, and that this can be further enhanced by employing the same principle with the consecutive damping ratios (with the levels of damping being small), poses somewhat of a paradox. The work which was carried out on harmonic force distortion and detailed in Chapters 1 and 2 showed that for lightly damped structures the force levels

at resonance are very small and harmonic distortion of the input force can be very severe.

In the case of multi-point excitation methods, this aspect can be particularly important since the input forces (both in magnitude and phase) are used as part of the criterion for establishing the normal modes and, if the levels are very small (bearing in mind that one is merely overcoming the local structural damping at the input points when the structure is vibrating in a normal mode) then problems with phase coherence could be critical.

Thus the paradox is that although one would prefer a structure with very light damping to minimise damping coupling, the force levels at resonance are so small (and resulting amplitudes relatively high) that vibration exciter and distortion effects may become a problem.

Since the ultimate aim of the experimental work was to investigate the use of normal modes in identifying the modal properties of complex structures, it was felt necessary to initially establish what levels of modal stiffness (based on purely hysteretic damping) would allow the generation of normal modes without severe force distortion occurring and without having to compensate for the vibration exciter characteristics. This would then allow a rig to be designed with modal stiffnesses which would require exciting forces that were not so small in magnitude to prevent satisfactory normal modes being excited.

The techniques employed for exciting the normal modes together with the instrumentation used in this preliminary experimental work are discussed in detail in Sections 4.6 to 4.8 together with details of the transducer calibrations.

4.2 DESCRIPTION OF EXPERIMENTAL PROCEDURES

A simple rig was designed which utilised two-point excitation

to excite the normal modes. The rig was designed to have two principal modes of vibration, a transverse (or bending mode) and a torsional mode. The rig basically consisted of a rectangular solid steel beam, pinned at one end and encastré at the other which supported a hollow steel cross-tube. Figure 23 shows a diagrammatic sketch of the rig, together with the positions of the measuring transducers and the vibration exciters. The rig was designed to be symmetrical so that the mode shapes and corresponding input force ratios were simple to produce experimentally, e.g. the transverse normal mode was to be identified when the accelerometers on each end of the cross-tube were equal in magnitude and phase and at quadrature to the input forces, which were also equal in magnitude and phase and the torsional mode when the responses were in anti-phase with the input forces in-phase and at quadrature to the response.

The aim of the tests was to determine the modal stiffness which would allow the transverse normal mode to be excited with the input force ratio $F_2/F_1 = 1.0$. This was to be done by varying the position of the cross-tube along the beam and at each position exciting the transverse normal mode of vibration.

The effect of varying the position of the cross-tube was to change the mass and stiffness distribution of the rig and thus for each re-location (within the constraints of the rig) it was necessary to determine the modal stiffness as well as excite the 'new' normal mode of vibration. It was found that with the cross-beam in a position which approximated to half-way along the beam (i.e. the most flexible position) difficulty was encountered in obtaining an input force ratio which resembled the required ratio i.e. $F_2/F_1 = 1$) to excite the normal modes. Hence it was found necessary to obtain a check on the modal stiffness by exciting the transverse mode with one exciter acting at the centre of the cross-tube (the nodal point of the

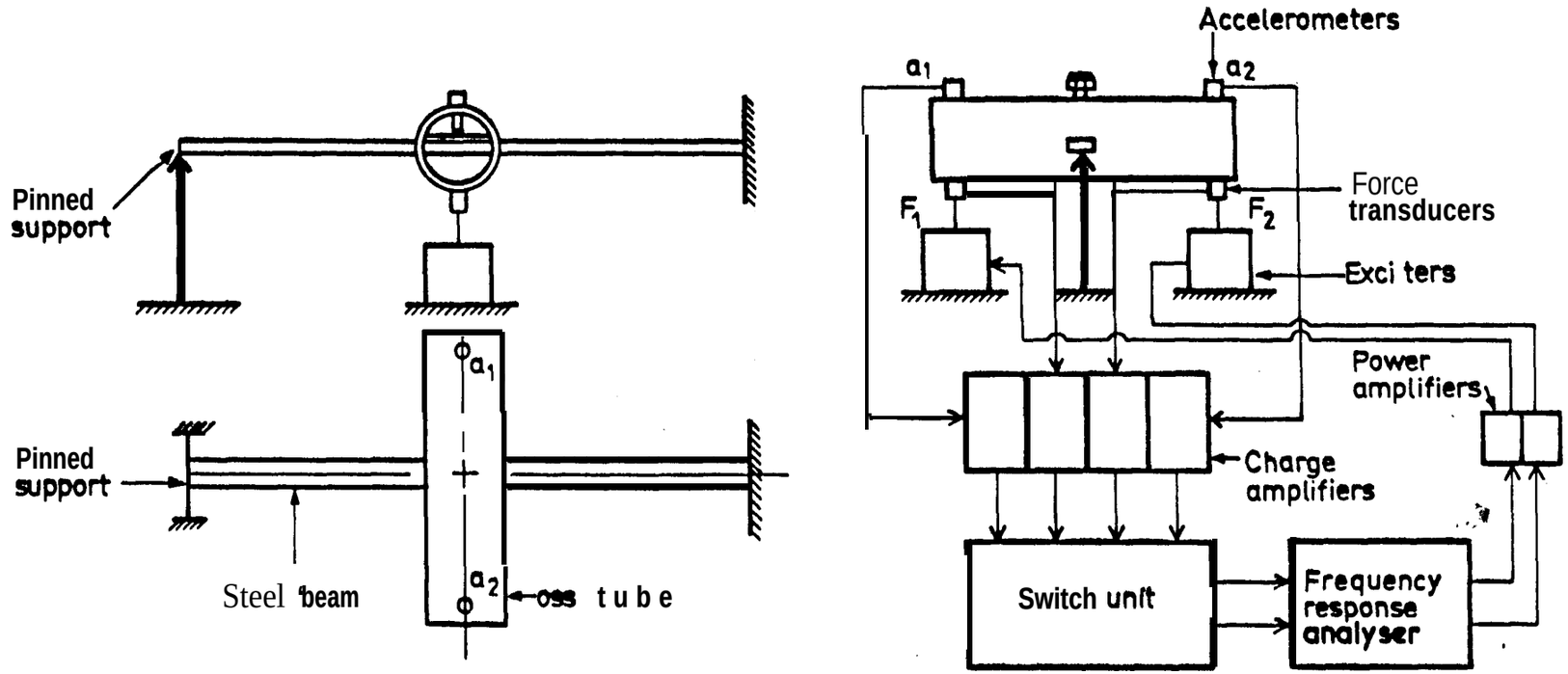

FIGURE 23

DIAGRAMMATIC SKETCH OF THE INITIAL TWO DEGREE-OF-FREEDOM EXPERIMENTAL RIG.

torsional mode) and this was carried out for each re-location of the cross-tube. As a further check on the stiffness properties, occasional static tests were carried out. These comprised loading the rig at the centre of the cross-tube and measuring the resulting static deflections under the applied load.

4.3 SINGLE POINT EXCITATION TESTS

The results of these tests were obtained in the form of the inertiance i.e. output acceleration divided by input force (this being kept constant). This quantity was measured with the frequency response analyser and was recorded in the form of the real and quadrature components in order that the results could be presented in the form of the Kennedy and Pancu vector plots. This mode of presentation allowed the modal stiffness and damping to be readily evaluated and also allowed the use of the computer programs, developed in the previous Section, to obtain accurate curve fits to the experimental data.

The initial single point excitation tests were concerned with establishing the 'damping symmetry' of the experimental rig. These were carried out by exciting the cross-beam at points symmetrical about the centre line of the rig (with the same exciter) and measuring the inertiance as the frequency was varied over the transverse mode natural frequency. The resulting vector plots of these tests are shown on Figure 24.

It can be seen from Figure 24 that the vector plots differ very slightly, with the result that the calculated damping factors are different, indicating damping asymmetry.

Figure 25 shows a typical vector plot of the transverse mode from which the modal stiffness was evaluated for that particular configuration and Figure 27 shows the results of the static stiffness tests which provided a check on

the modal stiffnesses.

The results of the static and single point excitation tests are given in Table 4.1.

4.4 TWO-POINT EXCITATION TESTS

For each of the cross-tube positions employed in the single point excitation tests, a multi-point excitation test was carried out with the intention of exciting the transverse normal mode. As mentioned earlier, difficulties were encountered in satisfying the normal mode criterion, and it was decided that a normal mode was excited when the resulting responses were in-phase and at quadrature (within a phase tolerance of $\pm 5^{o}$) to the in-phase input forces. The results of these tests are detailed in Table 4.1 which shows the input force ratios as a function of the modal stiffness and the associated modal damping.

A typical vector plot from these tests is shown on Figure 26 with the input force ratio satisfying almost exactly the theoretical ratio of 1.0.

4.5 DISCUSSION OF RESULTS

The aim of these tests was to establish a suitable modal stiffness whereby it was possible to excite a structure, in its normal mode, such that the individual input forces used to overcome the structural damping and maintain the normal mode condition were not affected by significant harmonic distortion.

Since the input force levels at a normal mode frequency are merely overcoming the modal structural damping, then the stiffer the structure, the larger will be the levels of input force for a given displacement and structural damping factor. This in turn means that the effects of exciter and harmonic distortion characteristics are

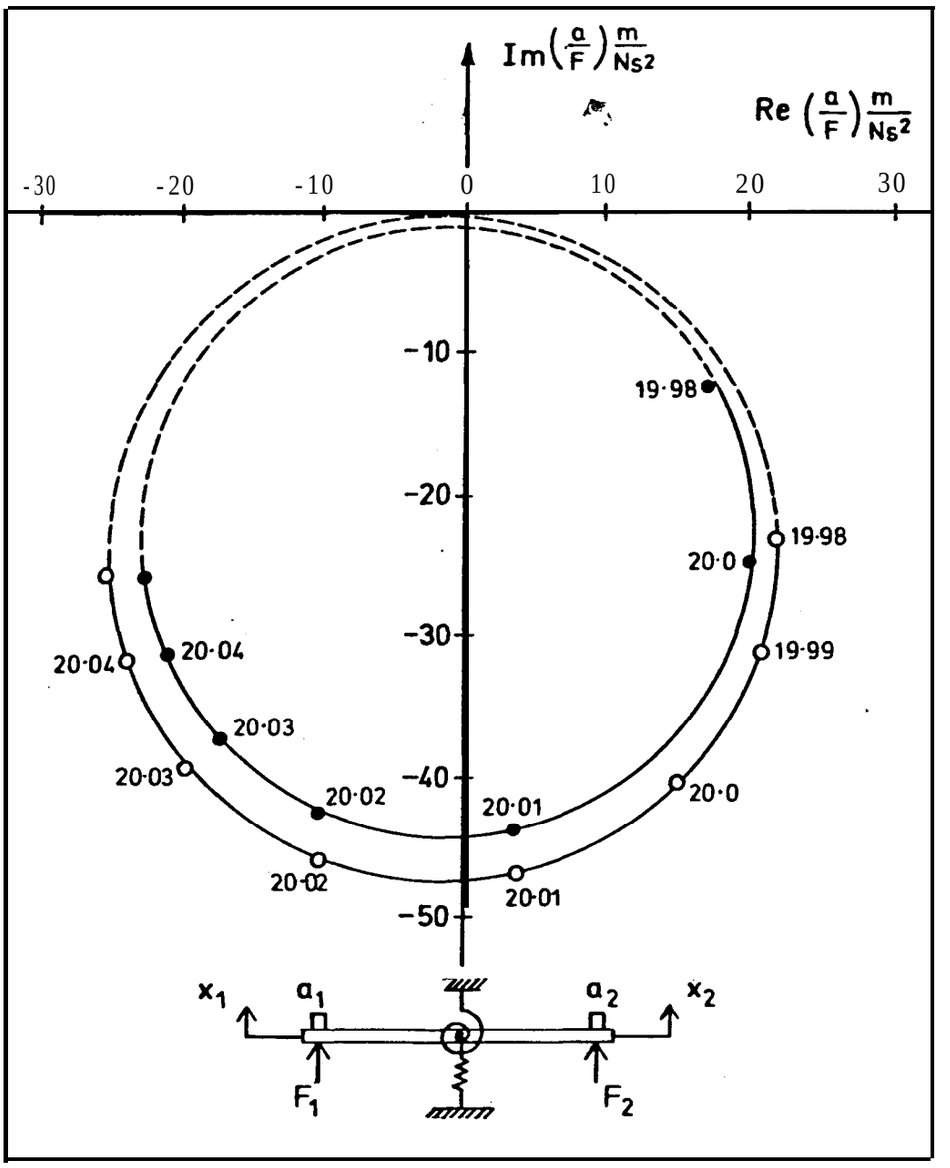

FIGURE 24

SINGLE POINT EXCITATION TESTS:
INVESTIGATION OF DAMPING SYMMETRY FOR THE TRANSVERSE MODE OF VIBRATION

- **RESPONSE OF** a_1 **WITH ONLY** F_1 **ACTING** $(\ddot{x}_1/F_1)$
- **RESPONSE OF** a_2 **WITH ONLY** F_2 **ACTING** $(\ddot{x}_2/F_2)$
- **CALCULATED DAMPING FACTOR** δ_1 = 0.0034
- **CALCULATED DAMPING FACTOR** δ_2 = 0.0024

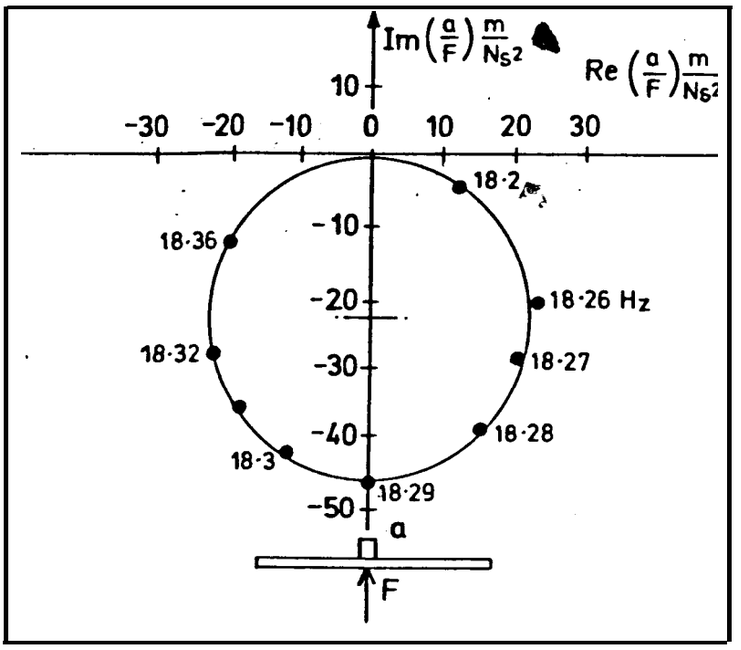

FIGURE 25

VECTOR PLOT FROM TYPICAL SINGLE POINT EXCITATION TEST AT CENTRE OF BEAM

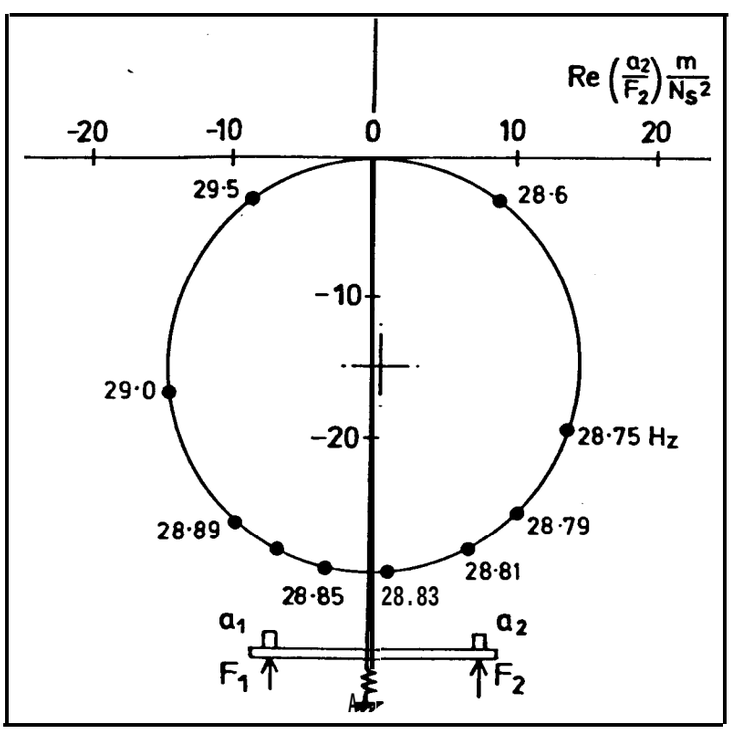

FIGURE 26

VECTOR PLOT FROM TWO-POINT EXCITATION TEST WITH F_2/F_1 = 0.975

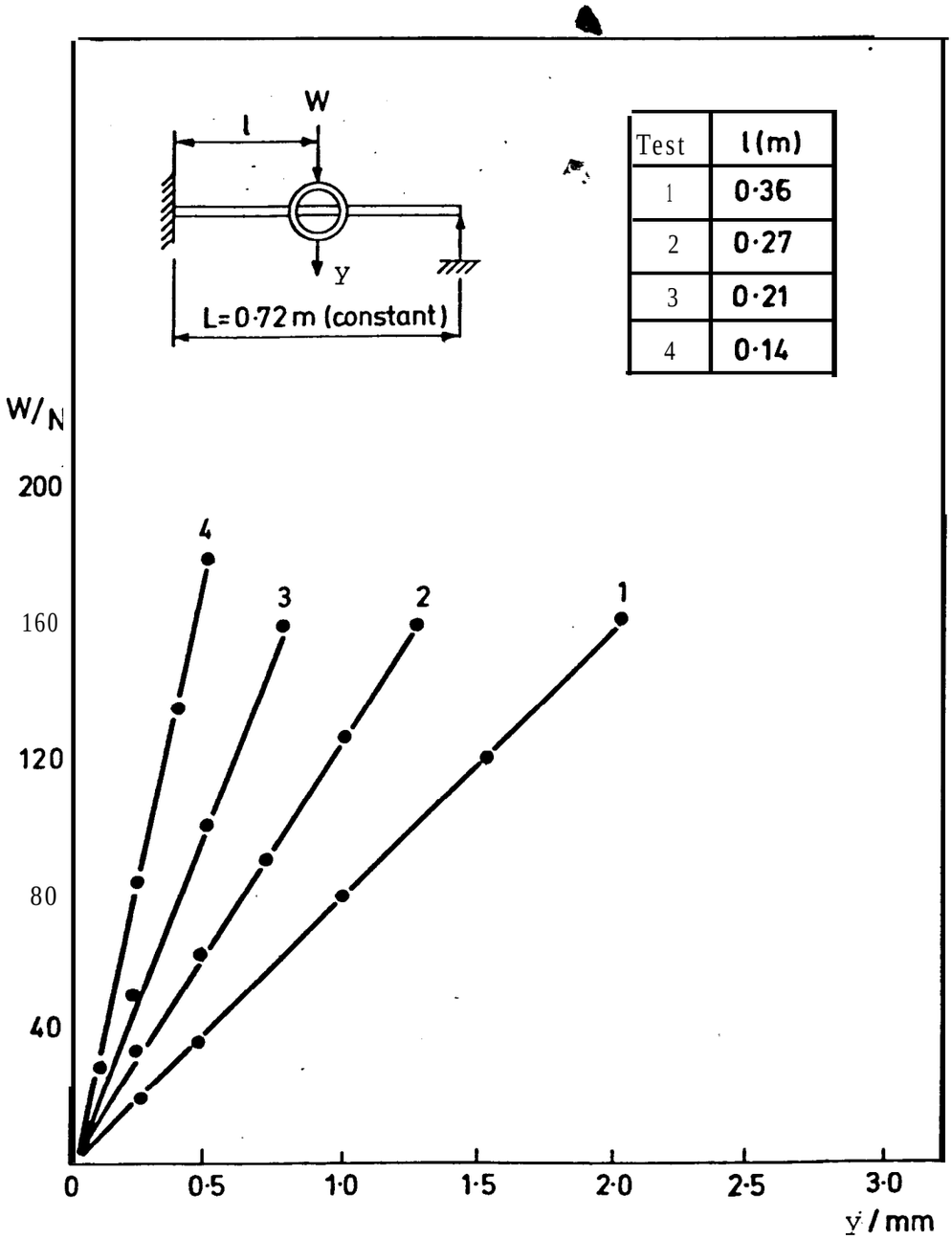

FIGURE 27

STATIC LOAD DEFLECTION CURVES TO DETERMINE EFFECTIVE STATIC STIFFNESSES.

W IS THE APPLIED LOAD, y THE RESULTING DEFLECTION UNDER THE APPLIED LOAD.

Test	Normal Mode Frequency (Hz)	Static Stiffness (kN/m)	Modal Stiffness From Single Point Tests (kN/m)	Modal Damping Factor 'δ'	Force Ratio F_2/F_1 From Multi-point Tests	Theoretical Force Ratio
1	18.29	79.5	74.7	0.008	0.20	1.0
2	21.72	130.0	144.0	0.010	0.26	1.0
3	26.8	200.0	190.0	0.013	0.87	1.0
4	34.7	350.0	321.0	0.015	0.97	1.0

TABLE 4.1

Normal Mode Excitation Force Ratios
as a Function of Modal Stiffness for the Transverse Mode

also reduced.

This is borne out by examining the results detailed in Table 4.1. When the modal stiffness of the rig was low it was not possible to achieve a force ratio which corresponded to the theoretical force input ratio of 1.0. Nevertheless, the vector plot response indicated an almost pure single mode response when this force ratio was maintained constant as the frequency was varied over the natural frequency range and the vector plot measured.

An explanation of why the ratio of the force input of one side of the rig to the other (F_2/F_1) should always be less than 1.0 can be explained by the results obtained from Figure 24. These results indicated that the damping distribution was asymmetrical and that the damping ratio calculated from tests carried out using F_2 as the input source was lower than that at the other side of the rig, namely input source Fl. Since the damping level is small, the resulting force levels are also small and hence the input force at the point where the damping was the greatest became the predominant exciting force.

As the modal stiffnesses were increased, the individual force levels increased and the input force ratio approached the theoretical ratio of 1.0 as shown by Table 4.1. The resulting modal stiffness which gave this condition was then the required minimum design stiffness in order that suitable force levels would be available to excite the normal mode.

4.6 TEST INSTRUMENTATION

. The instrumentation used to excite, measure and record the normal mode results is shown on Plates 3 and 4. The method of exciting the normal modes required that the various phases and magnitudes of the input and output responses be monitored almost instantaneously. This was

achieved during the experimental tests by designing a switching unit which allowed both of the input forces, the output accelerations and the individual input forces and output accelerations to be observed by a simple series of switching operations.

The output of the transducers was fed via this unit to the frequency response analyser (F.R.A.).

The F.R.A. had a dual role. The response of the system was measured on the F.R.A. (this was displayed in digital form) in either the real and quadrature components or in polar form. The F.R.A. had two input channels which allowed either a comparison between the two input signals (i.e. a transfer function) or simply each individual channel could be observed.

The other role of this instrument was as the master frequency control. An output voltage from the F.R.A. was fed to two individual amplifiers which in turn were connected to the vibration exciters. The frequency of the excitation voltage (and hence current) fed to the vibration exciters was thus controlled by the internal oscillator unit of the F.R.A., thus all the frequency information supplied as inputs to the F.R.A. were referenced to its own internal oscillator. This allowed the instrument to correlate the input frequencies with its reference frequency and thus reject high levels of harmonic distortion.

The vibration exciters used were electro-dynamic models with a peak force rating of 25N. These were connected to the test rig (the cross-beam) via the push-rod and force link assemblies, the output current of each exciter being controlled by its own amplifier which allowed the force levels to be adjusted independently.

The two input forces were measured with piezoelectric force transducers and the two output responses, monitored

at the same points were measured with piezoelectric accelerometers. The outputs of these transducers were fed to a bank of four charge amplifiers which in turn were connected to the switching unit in order that the various configurations of responses could be recorded on the F.R.A.

Throughout the tests, the output accelerations and input forces were continuously monitored on oscilloscopes in order to give both a visual picture of the phase orientations of the responses (i.e. for identifying in-phase or anti-phase conditions) and to observe the quality of the input forces to check for such aspects as misalignment or bottoming of the armature in the vibration exciters, both of which produce a distorted force input waveform (81).

A second switch was incorporated between each vibration exciter and its corresponding amplifier in order that transient tests could be carried out. This switch allowed the exciters to be simultaneously open-circuited and hence virtually uncoupled (electrically) from the excitation system. The actual location of this switch is very important in order that the free-vibration response of the rig is not to be affected by the electrical damping characteristics of the vibration exciters. These effects are due to the back emf generated during free vibration and unless the amplifier unit feeding the exciter has a very high output impedance (which in the case of the exciter input being open-circuited produces the effect of an amplifier with an infinite output impedance) this results in a finite current in the coil of the exciter armature which produces a force opposing the motion of the armature and effectively damps the free vibration. These back emf effects have been recorded by other researchers (4) and are particularly important in the case of lightly damped structures.

4.6.1 CALIBRATION OF TRANSDUCERS

In order that a common reference sensitivity could be applied to each of the piezoelectric transducers and also to act as a check on the manufacturer's calibrations, each of the transducerswere--calibrated using a non-contact technique.

The calibration technique used had previously been employed to calibrate force transducers (13) and relied upon a solid steel prism with grids of 0.127 mm (0.005") and 0.254 mm (0.010") etched onto one face which was highly polished. The transducer to be calibrated was securely located on the steel prism which was then vibrated at a given frequency. By adjusting the amplitude of vibration at this frequency and observing the grids with a microscope, synchronisation of the lines indicated peak-to-peak amplitudes of vibration in steps of 0.127 mm or 0.254 mm.

The output from the transducer was fed to its corresponding charge amplifier and the voltage from the cha-rge amplifier was recorded on a digital voltmeter. By repeating this procedure for a range of frequencies (this technique was found satisfactory over the frequency range 5 to 400 Hz) a calibration graph of output voltage against acceleration (derived from the product of $\omega^2 x$ displacement) for an accelerometer and its charge amplifier was obtained.

In the case of the piezoelectric force links, the procedure was modified slightly in that a body of known mass was rigidly mounted on a force link and the same procedure applied as with the accelerometers,except that in this case the resulting calibration curves were in terms of output voltage against force (this being determined from the product of the known mass and the acceleration). Throughout the tests the responses of the transducers were observed on an oscilloscope to ensure that simple harmonic motion was occurring, otherwise the calibration curves would have

been invalid. Appendix VII gives the results of the calibration tests and resulting sensitivities.

4.7 DESIGN OF A TWO DEGREE-OF-FREEDOM TEST RIG WITH TUNABLE FREQUENCIES

The final experimental rig design had to incorporate the information obtained from the earlier tests on the lightly damped simple beam rig described in Section 4.2 where it was shown that difficulties in setting up the normal modes were experienced with lightly damped structures. It was established from these tests that if the modal stiffness was sufficiently high then the resulting excitation forces at resonance would be of a sufficient magnitude to satisfactorily excite the normal modes of the test rig. Thus the two modes of vibration of the experimental rig had to satisfy these conditions.

Plate 3 shows a photograph of the experimental rig and test instrumentation. The rig basically consists of a steel rectangular tube encastré at one end and on a support at the other end which allows axial movement to occur but restricts torsional and vertical movement (simple-support). The rectangular steel tube supports a solid square steel cross-beam which is located on the tube by allowing the tube to pass through the steel cross-beam. The cross-beam is securely fastened to the rectangular steel tube by bolts acting on a brass slipper pad to prevent local deformation of the steel tube;

The cross-beam had additional masses secured symmetrically which were adjustable in position in order to vary the mass moment of inertia, and hence vary the torsional natural frequency of vibration without changing the transverse natural frequency of vibration. This provided tunable natural frequencies.

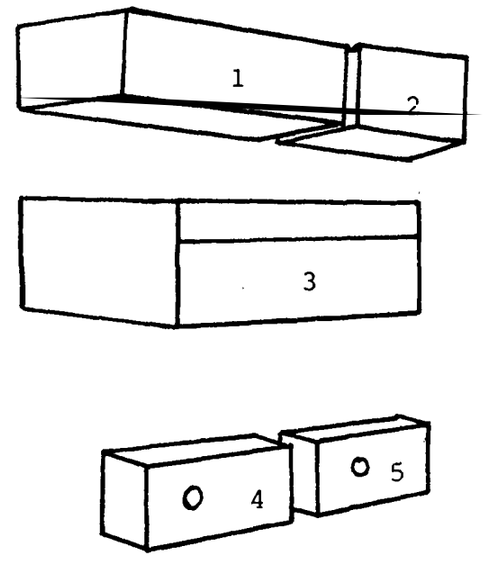

1. Digital Phasemeter
2. Switch Unit for F.R.A.
3. Frequency Response Analyser (F.R.A.)
4,5. Amplifiers
6. Charge Amplifiers
7. Oscilloscopes
8. Vibration Exciters
9. Switch Unit for Open-circuiting exciters

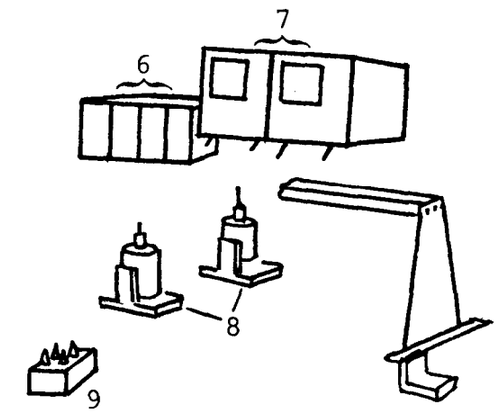

KEY FOR PLATE 3 OVERLEAF

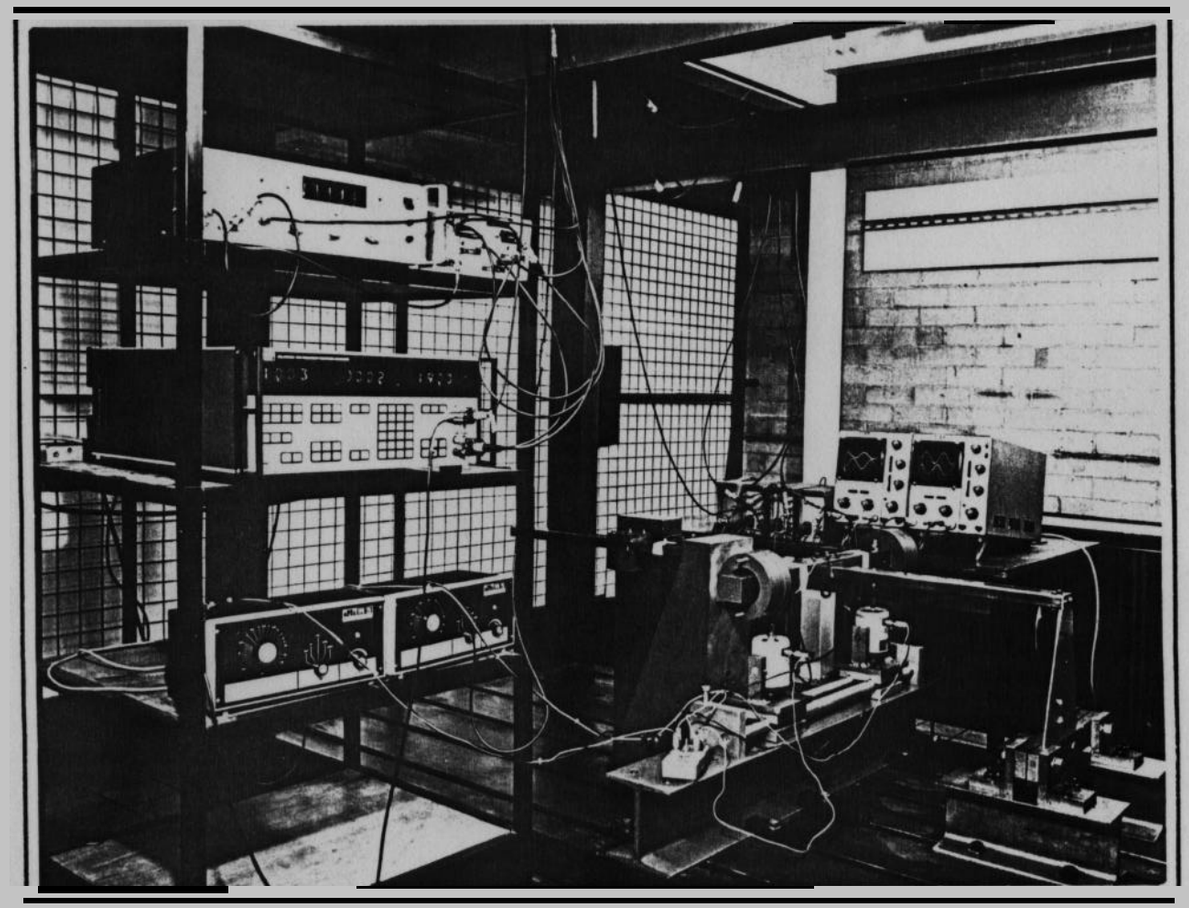

PLATE 3

EXPERIMENTAL RIG AND TEST INSTRUMENTATION.

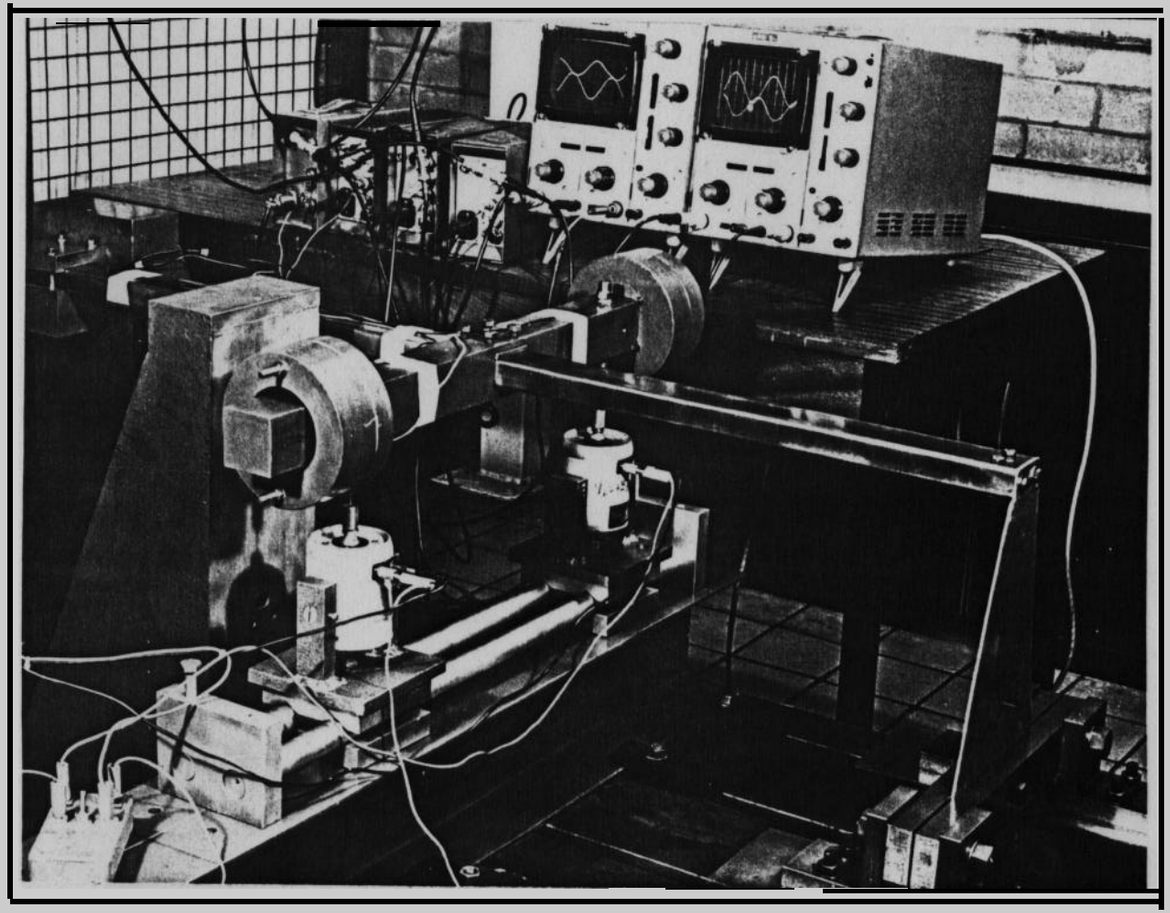

PLATE 4

EXPERIMENTAL RIG SHOWING VIBRATION EXCITERS LOCATED ON GUIDE-RAILS.

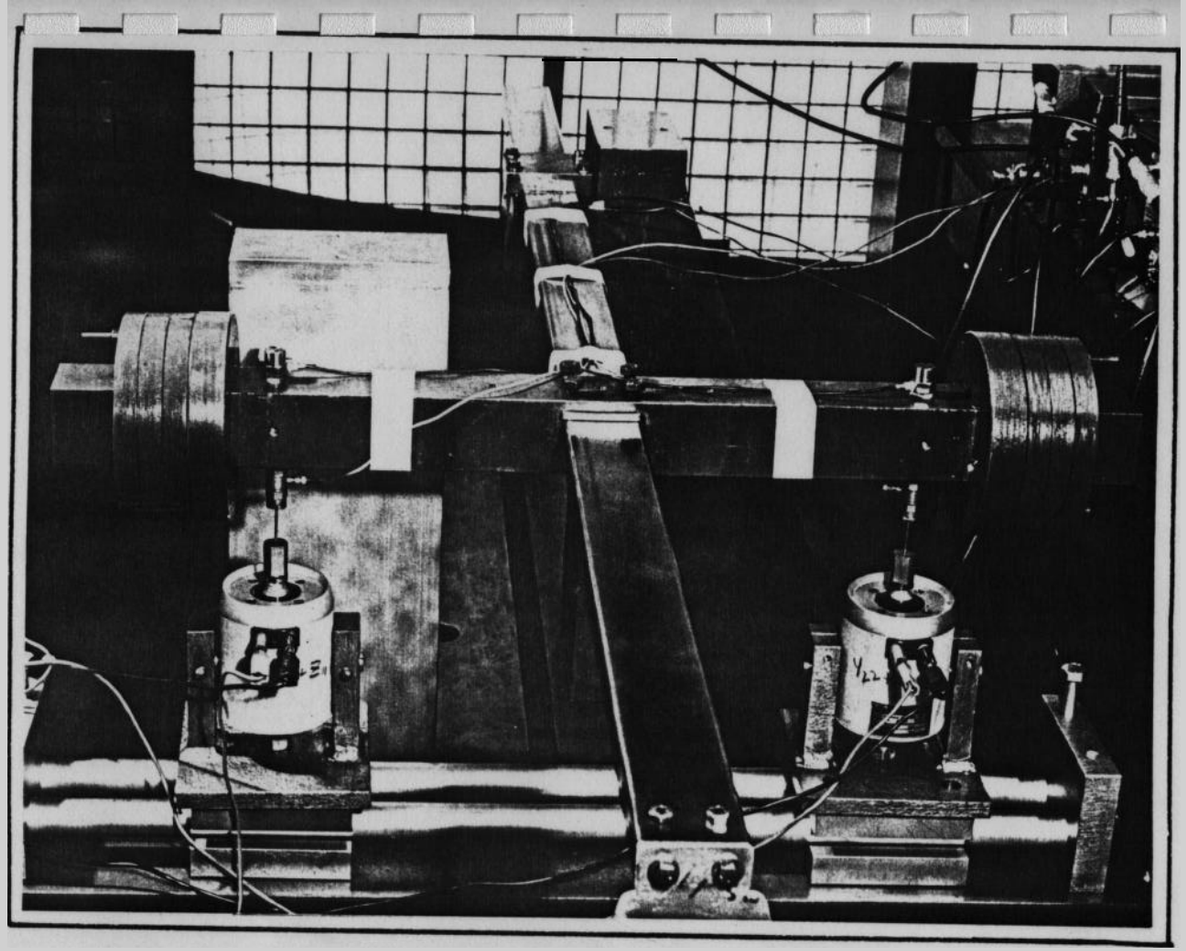

PLATE 5

EXPERIMENTAL RIG SHOWING TRANSDUCER POSITIONS AND PUSH-ROD ASSEMBLIES.

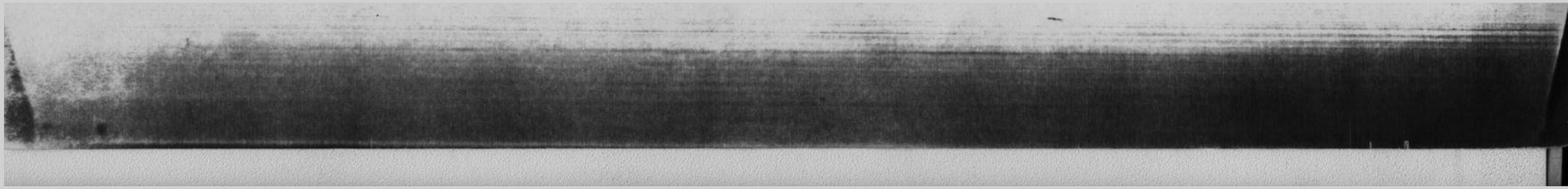

The use of a rectangular steel tube to provide the transverse and torsional spring effects arose from the fact that in order to have a high modal stiffness in both modes of vibration it was necessary to increase the polar and second moments of area without increasing significantly the mass of the elastic member. The fundamental natural frequencies of vibration for the two modes were chosen to be in the frequency range 15 - 30 Hz, this range being a typical frequency range which is encountered during aircraft ground vibration tests.

Facilities were available for attaching electro-dynamic vibration exciters to the bottom of the cross-beam. These allowed the exciters to be situated at any position along the cross-beam by having them mounted on trunnions running on guide-rails, Plate 4 shows these aspects.

The exciters were connected to the cross-beam via push-rod and force link assemblies as shown on Plate 5. The push-rod assemblies allowed the vibration exciters to be easily positioned and in particular alignment and set-up of the exciters, so that when the rig was in its static equilibrium position the armatures of the exciters were not pre-loaded; and due to their lateral and torsional flexibility they did not restrict the motion of the system.

The entire rig was mounted on massive cast-iron bed plates in a fabricated rolled-steel-joist framework whose natural frequencies were well above those used throughout the tests. The design calculations for the experimental rig are given in Appendix VI.

4.8 NORMAL MODE TESTING PROCEDURES

In order to assess the quality of the rig in terms of exciting real normal modes of vibration and to determine the normal mode frequencies of vibration, a series of transient and forced vibration tests were carried out on the rig. Before these are discussed in detail, it is felt that an introduction to normal mode experimental procedures would be worthwhile.

The techniques employed in experimentally exciting normal modes of vibration employ the phase-resonance criterion and are based on an iterative process since little information is known *a priori* regarding the mode shapes (and hence appropriate force distributions). The usual procedure, for example, in a ground vibration test on an aircraft is to initially excite the structure by using two vibration exciters (usually placedsymmetrically, one on each wing), and to sweep a given frequency range and record the transducer (accelerometer) responses over the structure. This is done for in-phase and anti-phase excitation conditions.

From the resulting responses, guidance as to the symmetric and anti-symmetric mode shapes and resonant frequencies of vibration is obtained. Using this information, vibration exciters are located in positions which will (hopefully) excite only a particular single mode of vibration, i.e. the effects of adjacent modes are eliminated. The input forces are then adjusted, one at a time, until the response of the structure is approaching an in-phase (or anti-phase) condition. If this cannot be achieved, the frequency is adjusted until the responses converge to this condition. The force magnitude distribution is then adjusted until an in-phase condition, which is at quadrature with the response, is obtained. This may also require a frequency adjustment as well as employing exciter compensation methods to satisfy the required criterion.

If it is still found that it is not possible to obtain a set of conditions which reasonably conform to the above, it may be necessary to adjust the location of the exciters, in which case the whole procedure has to be repeated.

Once the phase resonance criteria have been satisfied, the frequency can be varied around the normal mode frequency (with the force appropriation held constant in magnitude and phase) in order that vector plots or complex power plots can be obtained from which such aspects as the modal damping can be calculated. Techniques for improving this tedious iterative method are being continuously investigated and reference to (42 → 49) providesan overall view of these.

In the case of the author's experimental rig, the theoretical mode shapes were simple and known *a priori* and thus the experimental procedure was greatly simplified. Nevertheless, the process of setting-up the normal modes accurately was extremely time consuming since the force levels and frequency adjustments were all manually controlled, whereas most industrial tests are fully automated.

The procedure employed for exciting the normal modes on the test rig was to set the excitation frequency at the natural frequency indicated by a transient test and to adjust the two force levels until the two responses were in-phase (or anti-phase). The phase angle between one of the forces and the corresponding output response (acceleration) at that point was then checked for a 90^{o} phase difference. If this was in error by more than plus or minus two degrees, the frequency of excitation was changed until this condition was achieved. The phase of the output responses was again checked and if this was not within the phase margin of plus or minus two degrees the other excitation force magnitude was adjusted until this condition was satisfied. The phase angles between the two input forces were then checked for an in-phase condition

and if this was within the phase margin of two degrees it was then assumed that the frequency of excitation was at the normal mode frequency.

Under these conditions the rig was vibrating as a single degree-of-freedom with the output response in-phase (or anti-phase) and at quadrature to the input forces which were also in-phase (or anti-phase). Once the normal mode conditions were established, the purity of the normal mode was checked by carrying out a transient test. This was done by switching off the excitation to the vibration exciters (switching the exciters to open-circuit) and recording the response on an ultra-violet recorder.

4.9 NORMAL MODE EXPERIMENTAL TEST RESULTS

A typical set of experimental results, for an arbitrary level of input force at the normal mode frequencies, are shown in Tables 4.2 and 4.3 for the transverse and torsional modes respectively.

It can be seen from both Tables 4.2 and 4.3 that the input forces are predominantly real and that the output accelerations are almost purely imaginary. The phase angle margins of $\pm 2^{o}$ are satisfied and the input forces are at quadrature to the output. Thus the conditions satisfy (within the set experimental bounds) the classical phase-resonance criterion.

Figures 28 and 29 show the transient response for the transverse and torsional modes when the exciters were switched to open-circuit with the rig vibrating under the conditions specified by Tables 4.2 and 4.3.

The modal purity from observation of the transient traces is obvious since, had the excitation configuration not been correct,beating would have been evident in the transient responses. Thus it was established that the normal

Measured Quantity	a_1 (volts)	a_2 (volts)	F_1 (volts)	F_2 (volts)	a_1/F_1	a_2/F_2
Real	0.03	0.032	1.65	1.64		
Imaginary	-0.7	-0.71	0.04	0.05		
Polar	0.701/-87.5	0.71/-87.4	1.65/1.39	1.64/1.75	0.425/88.9	0.427/89.2

TABLE 4.2

Transverse Normal Mode Excitation Conditions

ω_B = 23.3 Hz

Measured Quantity	a_1 volts)	a_2 (volts)	F_1 (volts	F_2 (volts)	a_1/F_1	a_2/F_2
Real	0.02	-0.02	-1.0	1.02	-	-
Imaginary	0.8	-0.78	-0.02	+0.03	-	-
Polar	0.8/88.6	0.78/-88.5	1/181.1	1.02/1.7	0.8/89.9	0.78/-9°.2

TABLE 4.3

Torsional Normal Mode Excitat on Conditions

ω_t = 22 Hz

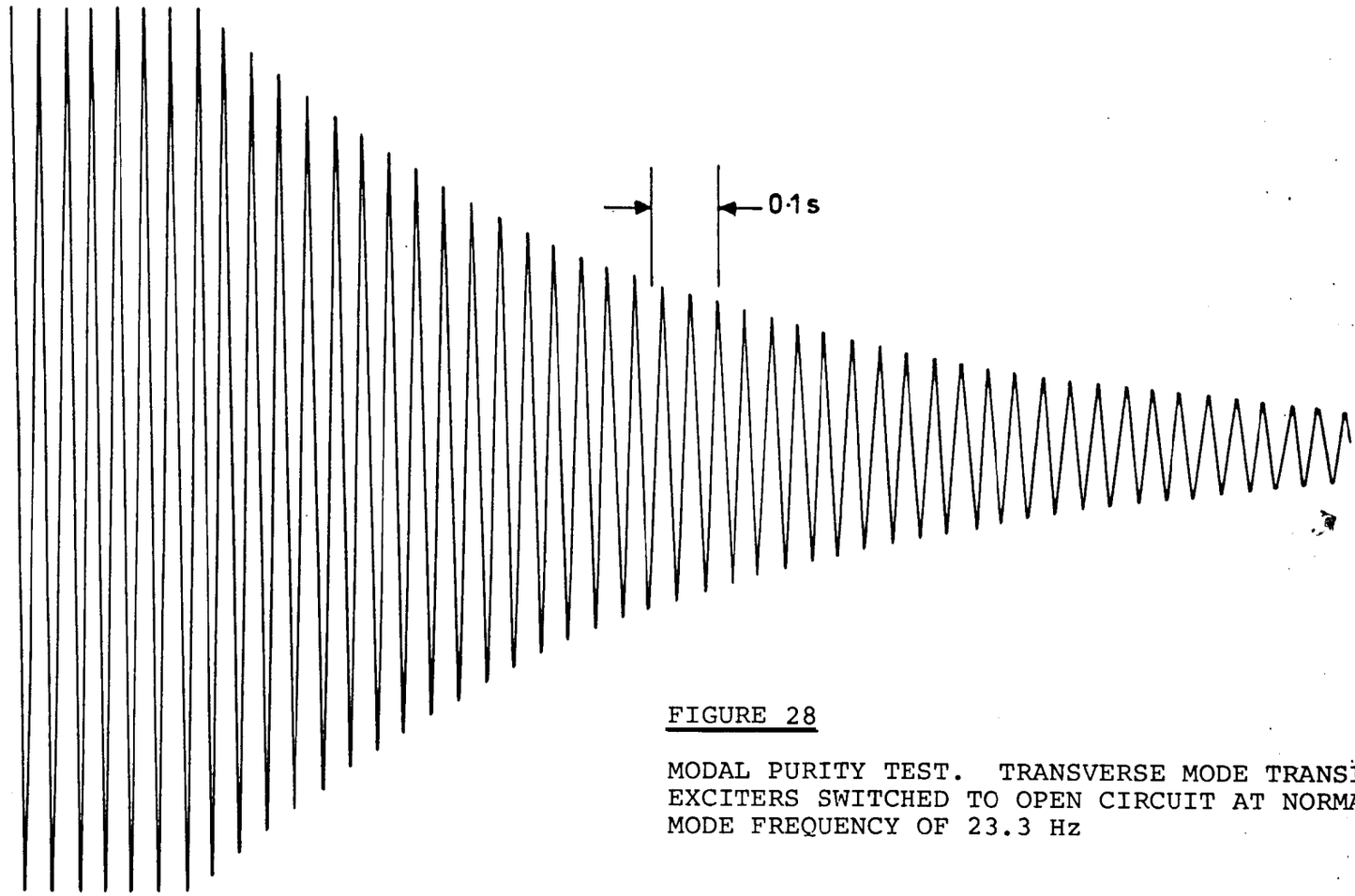

FIGURE 28

MODAL PURITY TEST. TRANSVERSE MODE TRANSIENT. EXCITERS SWITCHED TO OPEN CIRCUIT AT NORMAL MODE FREQUENCY OF 23.3 Hz

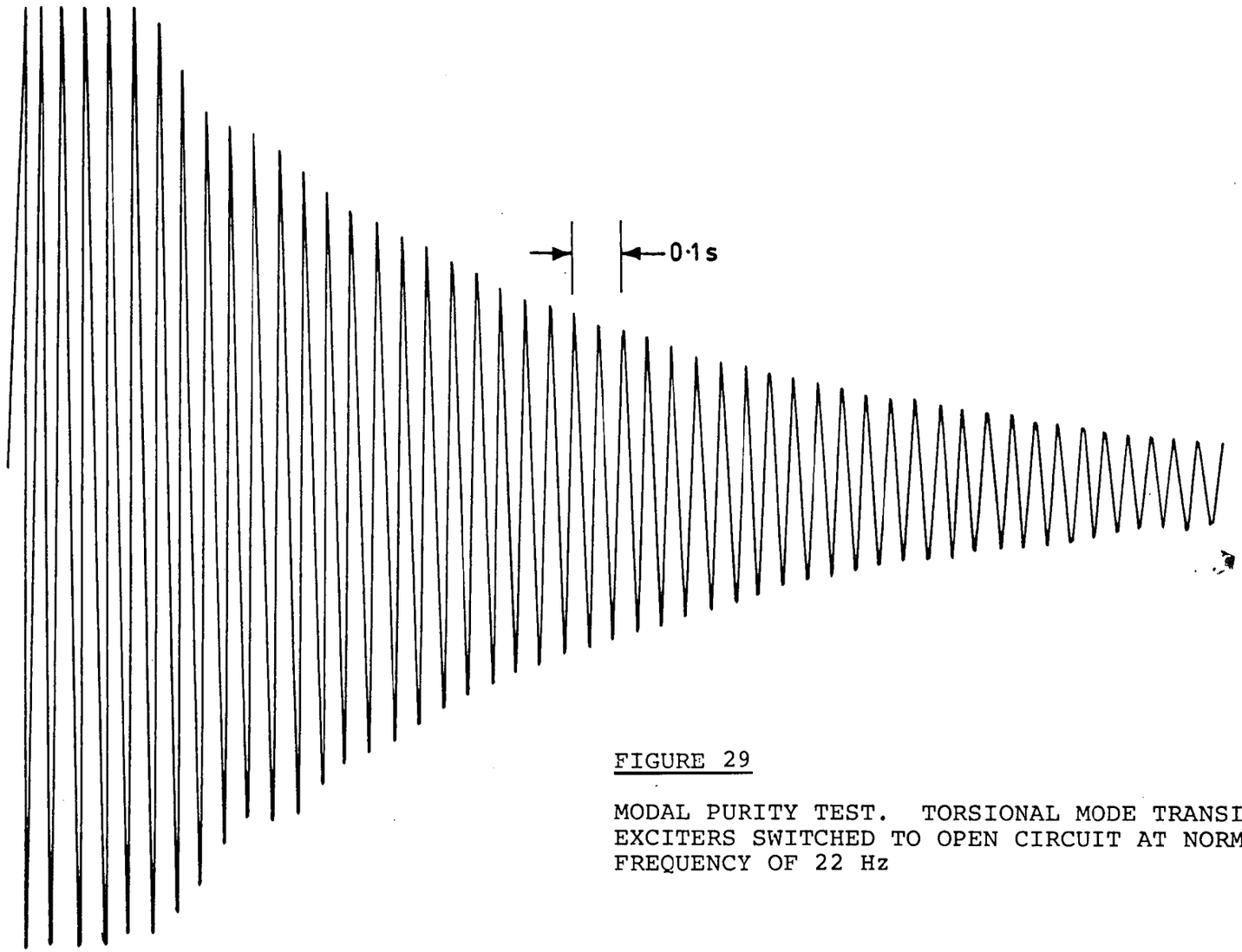

FIGURE 29

MODAL PURITY TEST. TORSIONAL MODE TRANSIENT. EXCITERS SWITCHED TO OPEN CIRCUIT AT NORMAL MODE FREQUENCY OF 22 Hz

modes of vibration of the rig could be excited and confidence placed in the measured results.

4.10 DISCUSSION

The experimental work described has shown that problems can arise in obtaining satisfactory normal mode excitation vectors of flexible (i.e. lightly damped) structures.

These problems are due to the fact that the internal damping of flexible structures is very low at resonance and consequently the excitation force levels are small. As a result of this, the force signals become non-linear. with significant harmonic distortion (see Section 1). It has been shown that by choosing a suitable combination of modal stiffness, and hence damping levels, that these problems can be overcome and accurate normal mode investigations using multi-point excitation methods can be carried out under controlled conditions.

The final section of the dissertation concerned the investigation of the effects of non-linearities, particularly the non-linear effects caused by dry surfaces in contact moving relative to each other - Coulomb friction - using the above experimental rig.

SECTION 3

ANALYSIS OF STRUCTURES WITH COMMON NON-LINEARITIES

5. IDENTIFICATION OF STRUCTURES WITH NON-LINEAR CHARACTERISTICS

5.1 INTRODUCTION

Non-linearities represent one of the major stumbling blocks in the field of dynamic modelling and frequency response testing methods. In the field of structural dynamics the most common type of non-linearities encountered are those due to Coulomb friction (SO), and non-linear stiffness characteristics (51).

Another very common non-linearity, is that due to 'backlash' (52), although this type of non-linearity causes problems mainly in mechanisms and control systems and thus no emphasis is placed on the analysis of structural systems with backlash in this dissertation, although reference may be made to its effects in the following Chapters.

The main non-linearity which is investigated is that of Coulomb friction as a result of the author's involvement with ground resonance testing of aircraft where this type of non-linearity is very common (38)(53)(54). A section of the work is also devoted to analysing systems with non-linear stiffness characteristics, since in regard to aircraft flutter analyses these structurally caused non-linearities can have serious consequences (51).

The analytical techniques available for analysing systems governed by non-linear differential equations of motion are numerous, the basic mathematical ideas and techniques being developed by Poincaré (55). The study of the basic physical problems (which is the author's prime concern) was attributed to Rayleigh (31), Van Der Pol (56) and Duffing (57). Van Der Pol's and Duffing's well-known equations continuously form the basis for investigations of non-linear systems, and the analysis techniques of

Kryloff and Bugoliuboff (58) and numerous others (59) have contributed to a better understanding of the various phenomena which occur in the field of non-linear systems.

The effects of the non-linear elements under consideration, namely stiffness and friction effects, are analysed by linearising these elements using the method of Harmonic Balance (or Harmonic Linearisation) (60). This is often termed the 'Describing Function Method' and its origins lie in the analysis of non-linear control systems (61).

This method has found extensive use in the field of non-linear dynamics, particularly in the aerospace field (51, 53), and the linearised equivalent elements for such characteristics as non-linear stiffness and Coulomb friction are readily available in the cited literature (60, 62).

Unfortunately, few of these areas of analysis make any progress toward identifying real structures. For example, methods have been proposed for the forced vibration analysis of systems with Coulomb friction (50) (63) (64), various types of non-linear damping (65) (66) and stiffness characteristics (67), but in each case little experimental evidence is available to establish the validity or direct application of these methods.

The work detailed in the following chapters describes a technique, based upon the work by Bonneau (68) and Baticle (69), which considers the complex power input to systems at resonance that allows multi degree-of-freedom systems with non-linear stiffness and Coulomb friction elements to be identified employing normal-mode multi-point excitation methods.

5.2 THE COMPLEX POWER SUPPLIED AT RESONANCE

In order to express the basic principles involved in the

Kryloff and Bugoliuboff (58) and numerous others (59) have contributed to a better understanding of the various phenomena which occur in the field of non-linear systems.

The effects of the non-linear elements under consideration, namely stiffness and friction effects, are analysed by linearising these elements using the method of Harmonic Balance (or Harmonic Linearisation) (60). This is often termed the 'Describing Function Method' and its origins lie in the analysis of non-linear control systems (61).

This method has found extensive use in the field of non-linear dynamics, particularly in the aerospace field (51, 53), and the linearised equivalent elements for such characteristics as non-linear stiffness and Coulomb friction are readily available in the cited literature (60, 62).

Unfortunately, few of these areas of analysis make any progress toward identifying real structures. For example, methods have been proposed for the forced vibration analysis of systems with Coulomb friction (50) (63) (64), various types of non-linear damping (65) (66) and stiffness characteristics (67), but in each case little experimental evidence is available to establish the validity or direct application of these methods.

The work detailed in the following chapters describes a technique, based upon the work by Bonneau (68) and Baticle (69), which considers the complex power input to systems at resonance that allows multi degree-of-freedom systems with non-linear stiffness and Coulomb friction elements to be identified employing normal-mode multi-point excitation methods.

5.2 THE COMPLEX POWER SUPPLIED AT RESONANCE

In order to express the basic principles involved in the

use of the complex power method, the important relationships which arise as a result of the method will be given in this section, the derivation of these quantities being given in Appendix IV.

If one considers a viscously damped, linear single degree-of-freedom system subject to forced vibration, the response of the system in terms of the in-phase and quadrature components can be expressed as:

$$u = u' + ju'' \quad . \quad . \quad . \quad . \quad . \quad . \quad . \quad . \quad . \quad . \quad . \quad . \quad . \quad (117)$$

where u' represents the in-phase displacement
u'' represents the quadrature displacement.

If the total input power at a given frequency of excitation is W, this must be composed of the quantities:

$$W = W' + jW'' \quad . \quad . \quad . \quad . \quad . \quad . \quad . \quad . \quad . \quad . \quad . \quad . \quad . \quad (118)$$

where W' the in-phase power $= -F\omega u''$
W'' the quadrature power $= jF\omega u'$
and F is the magnitude of the input force.

Appendix V shows that when the excitation frequency equals the natural frequency of the single degree-of-freedom system, the following conditions apply:

$$W''\Big|_{\omega=\omega_n} = \frac{dW'}{d\omega}\Big|_{\omega=\omega_n} = 0 \quad . \quad . \quad . \quad . \quad . \quad . \quad . \quad . \quad . \quad . \quad (119)$$

and

$$\frac{dW''}{d\omega}\Big|_{\omega=\omega_n} = \text{a maximum} \quad . \quad . \quad . \quad . \quad . \quad . \quad . \quad . \quad .. \quad (120)$$

These conditions can be shown (Appendix V) to give the damping ratio as:

$$\zeta = \frac{1}{\omega_n} \cdot \left. \frac{W'}{dW''/d\omega} \right|_{\omega=\omega_n} \qquad (121)$$

The in-phase and quadrature power components are given by equations A.V.5 and A.V.6 as:

$$W' = \frac{2\zeta \frac{F^2}{k} \omega\Omega}{(1 - \Omega^2)^2 + 4\zeta^2\Omega^2} \qquad (122)$$

$$W'' = \frac{\frac{F^2\omega}{k}(1 - \Omega^2)}{(1 - \Omega^2)^2 + 4\zeta^2\Omega^2} \qquad (123)$$

where $\Omega = \omega/\omega_n$

If equations (122) and (123) are plotted as a function of the excitation frequency ω, then the characteristics appear as shown on Figure 30 and from these the various quantities necessary to determine the damping ratio, given in equation (121), can be obtained.

5.3 "ANALYSIS OF A SINGLE DEGREE-OF-FREEDOM SYSTEM WITH NON-LINEAR STIFFNESS PROPERTIES USING COMPLEX POWER METHODS

Non-linear structural stiffnesses usually arise as a result of movements in joints (51)(70), guideways (71), and elastic elements such as plates and beams subject to large deflections (72).

In all cases, the non-linear terms usually represent a hardening or a softening spring characteristic (73) which results in an equation of motion for a hysteretically damped single degree-of-freedom system subjected to an external harmonic excitation force of constant magnitude as:

$$m\ddot{x} + k(1 + j\delta)x + c'x^3 = Fe^{j\omega t} \qquad (124)$$

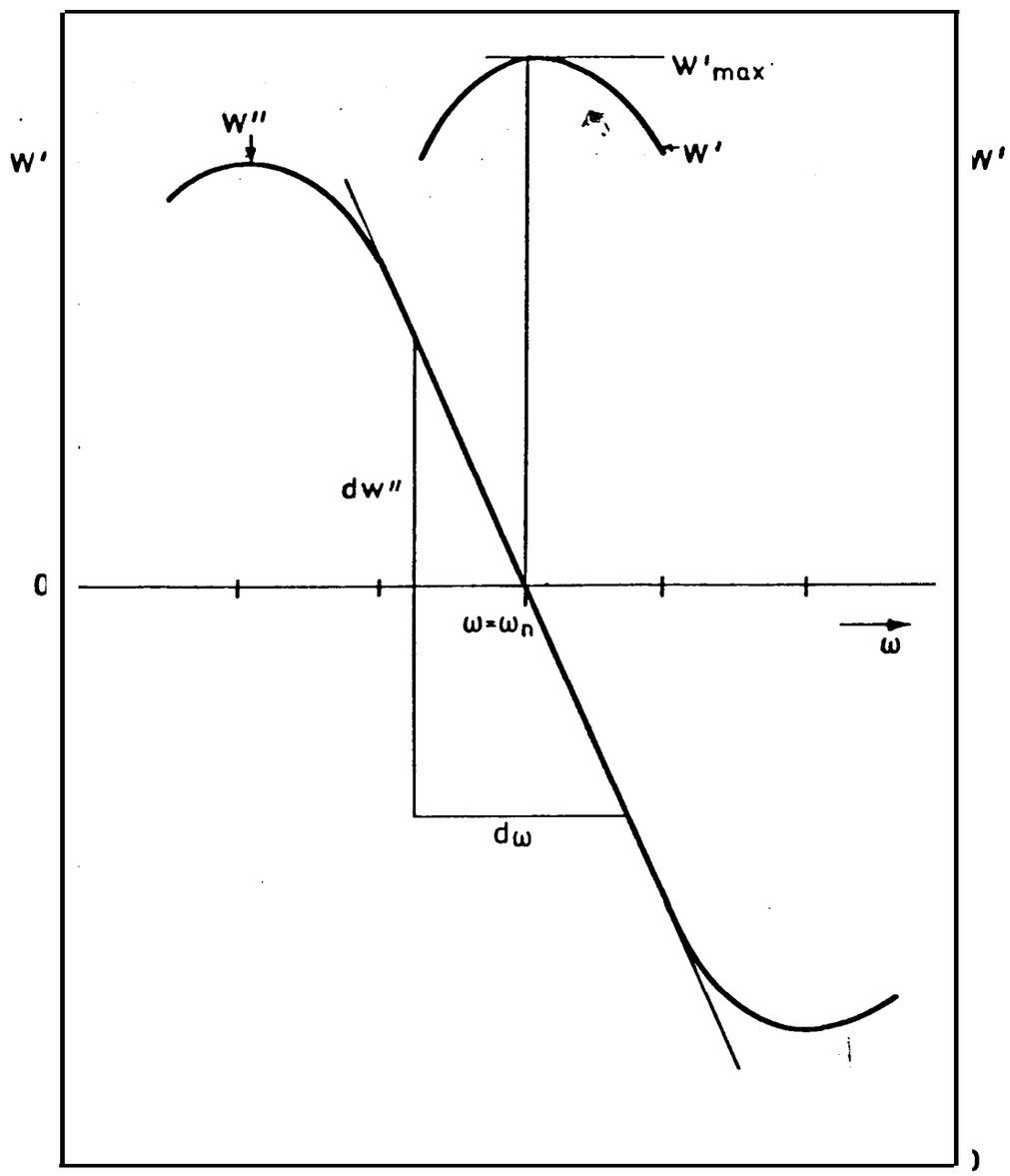

FIGURE 30

IN-PHASE (W') AND QUADRATURE (W") COMPLEX POWER COMPONENT CHARACTERISTICS AS A FUNCTION OF THE EXCITATION FREQUENCY FOR A SINGLE DEGREE-OF-FREEDOM SYSTEM

where c' is a constant coefficient.

By employing the principle of harmonic balance, equation (124) becomes:

$$m\ddot{x} + k(1 + j\delta)x + k^*x = Fe^{j\omega t} \quad .. \quad .. \quad .. \quad (125)$$

where $k^* = \frac{3}{4}c'A^2$, A being the amplitude of vibration of the non-linear element.

Assuming a steady state solution of the form

$$x = ue^{j\omega t}, \text{ where } |u| = A$$

we obtain the solution of equation (125) as:

$$u = \frac{F}{(k - m\omega^2 + k^*) + jk\delta} \quad .. \quad .. \quad .. \quad .. \quad (126)$$

$$\text{i.e. } u = \frac{u_s}{(D_A^2 - \Omega^2) + j\delta} \quad .. \quad .. \quad .. \quad .. \quad .. \quad (127)$$

where $D_A^2 = 1 + \nu(\frac{k^*}{c'})$; $\nu = \frac{c'}{k}$

$\Omega = \omega/\omega_n$

$u_s = F/k$

Now $A = |u|$, thus

$$A = \frac{|u_s|}{((D_A^2 - \Omega^2)^2 + \delta^2)^{\frac{1}{2}}} \quad .. \quad .. \quad .. \quad (128)$$

. The solution of equation (128) for Ω^2 is:

$$\Omega^2 = D_A^2 \pm ((\frac{u_s}{A})^2 - \delta^2)^{\frac{1}{2}} \quad .. \quad .. \quad .. \quad .. \quad (129)$$

The maximum value of A occurs at a frequency given by:

$\Omega^2 = D_A{}^2$ i.e. when,

$$A = \frac{|u_s|}{\delta} \quad \ldots\ldots\ldots\ldots\ldots \quad (130)$$

and $$\Omega^2 = 1 + \nu\left(\frac{\overset{*}{k}}{C'}\right) \quad \ldots\ldots\ldots\ldots\ldots \quad (131)$$

The interesting point about equation (131) is that the point at which the excitation frequency equals the system natural frequency (i.e. $\Omega = 1$) does not coincide with a 90^o phase angle between the displacement response A and the excitation force unless $v = 0$, i.e. there are no non-linear terms in the equation of motion. This has been observed by a number of researchers who showed that the effect of the non-linear stiffness terms is to curve the constant frequency lines on the vector plot (72) (73).

A second effect occurs on the vector plot which renders a criterion, invaluable in the analysis of linear systems, ineffective in this case. This is the criterion whereby the maximum rate of change of arc length per unit frequency (d_s/d_ω), denotes the natural frequency condition (74). This was analysed in some detail by White (72) who showed that as the non-linear effects increase, the frequency at which the value of d_s/d_ω is a maximum corresponds to values well above those of the true natural frequency. The values of the system damping ratios, derived from vector plots using the half-power point method (75) and the method due to Mead (78), were also in error which reduces the vector plot approach for a system with a non-linear stiffness quite ineffedtive,as one would expect.

If one considers equation (126) in terms of its real and quadrature parts, the expression becomes:

$$u = \frac{u_s (D_A^2 - \Omega^2)}{(D_A^2 - \Omega^2)^2 + \delta^2} - j\frac{u_s \delta}{(D_A^2 - \Omega^2) + \delta^2} \qquad (132)$$

Equation (132) can be expressed in terms of its in-phase and quadrature power components as:

$$W = W' + jW'' \qquad (133)$$

where,

$$\text{In-phase power } W' = \frac{Fu_s (D_A^2 - \Omega^2)}{(D_A^2 - \Omega^2)^2 + \delta^2} \qquad (134)$$

$$\text{Quadrature power } W'' = \frac{Fu_s \omega \delta}{(D_A^2 - \Omega^2)^2 + \delta^2} \qquad (135)$$

Expressing equations (134) and (135) as:

$$\frac{W'}{\omega_n} = \frac{Fu_s \delta \Omega}{(D_A^2 - \Omega^2)^2 + \delta^2} \qquad (136)$$

$$\frac{W''}{\omega_n} = \frac{Fu_s (D_A^2 - \Omega^2)\Omega}{(D_A^2 - \Omega^2)^2 + \delta^2} \qquad (137)$$

allows the individual power components to be plotted as a function of Ω for given values of F, u_s and 6. Figure 31 shows a plot of the expressions (136) and (137) for constant values of F, u_s and δ with different values of the non-linear stiffness coefficient v. From Figure 31 the damping ratios and natural frequencies are determined using the expressions:

$$\zeta = \frac{W'/\omega_n \Big|_{max}}{\Omega \frac{d}{d\Omega}(W''/\omega_n)\Big|_{W'' = 0}} \quad .. \quad .. \quad .. \quad .. \quad .. \quad (138)$$

where $\frac{d}{d\Omega}(W'/\omega_n) = -\frac{2\Omega^2}{\delta^2}$ at $W'' = 0$ .. .. (139)

The values of the non-linear stiffness coefficient v used in the above analysis are the same as those used by White (72), (White's notation for the non-linear stiffness coefficient was α). Thus it is possible to make a direct comparison between the resonant frequencies and damping ratios obtained from the vector plots by White with those obtained from the above complex power expressions.

Table 5.1 shows the results for three values of v, (the largest value of v being just below that which would produce the jump phenomena) and it can be clearly seen that the most consistent and accurate results are those obtained from the complex power expressions.

White attempted to apply the vector plot approach to a set of experimental results, however his results at the highest force levels produced distortion of the vector plots which prevented any analysis being carried out.

However, his experimental results are somewhat dubious in that use was made of the current in the exciter coil as a force reference, and since the system was being driven into large amplitudes of vibration at resonance, the actual magnitude and phase of the force input to the structure would almost certainly be different to that in the exciter coil, as was shown by the results of Chapter 1.

The concept of resonance in a system with a non-linear stiffness element (in this context, resonance is defined as the frequency at which the maximum response is obtained for a constant input force) has been discussed by Tondl

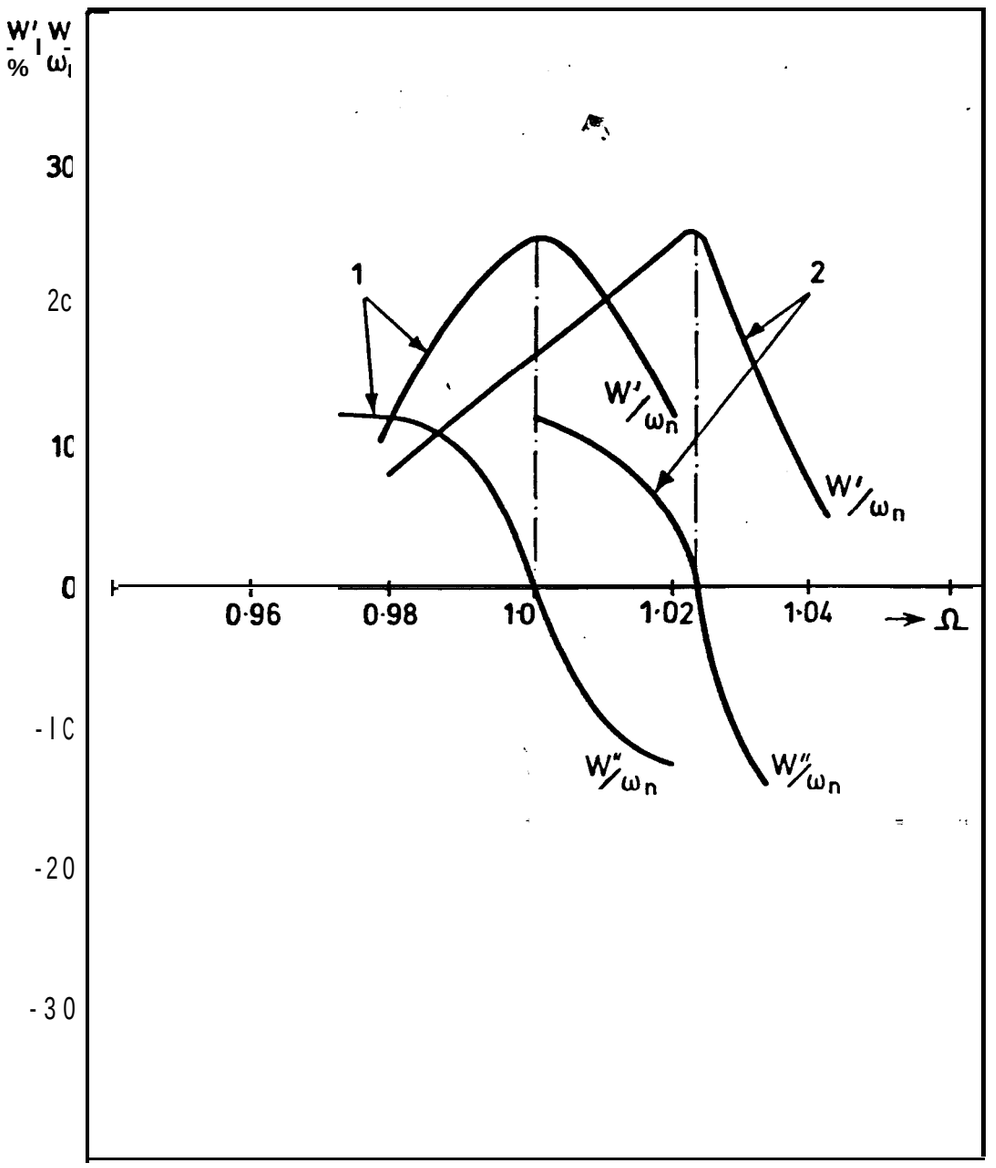

FIGURE 31

COMPLEX POWER PLOTS FOR A SINGLE DEGREE-OF-FREEDOM SYSTEM WITH A HARDENING SPRING CHARACTERISTIC GOVERNED BY EQUATIONS (136) AND (137) WITH:

1. $\nu = 0$; 2. $\nu = 1 \times 10^{-4}$ } $\delta = 0.04$, $Fu_s = 1$

v	ζ_H*	ζ_p*	ζ_{c-p}
0	0.0200	0.0200	0.0200
0.5×10^{-4}	0.0205	0.0180	0.0200
1.0×10^{-4}	0.0210	0.0240	0.0191

TABLE 5.1

* from reference (72)

ζ_H = ζ measured from half power point method

ζ_p = ζ measured from phase difference method, reference (78)

ζ_{c-p} = ζ measured from complex power plot

v = non-linear stiffness coefficient

(76) who points out that due to the fact that a non-linear system resonance may have no typical single-peak character, it would be sensible only to acknowledge the existence of a resonance within a given excitation frequency range.

It is interesting to note that the frequency at which the complex power components denote a natural frequency is when the real part of the response (or the quadrature power) is zero, which is the same condition that defines a natural frequency in a linear single degree-of-freedom system.

This may not be a very useful guide in practical systems when single point excitation methods are used, due to the fact that damping coupling between adjacent modes can cause modal interaction as discussed in Chapter 3, but in the case of multi-point excitation methods where a single mode response is excited, or when the adjacent modal natural frequencies satisfy the criteria of Section 3.8.1, then the concept of zero quadrature power could be used to identify the natural frequency of a non-linear system.

5.4 ANALYSIS OF A SINGLE DEGREE-OF-FREEDOM SYSTEM WITH COULOMB FRICTION USING COMPLEX POWER METHODS

5.4.1 THE EFFECT OF COULOMB FRICTION ON THE VECTOR PLOT

The previous section has shown that the use of complex power methods in analysing simple single degree-of-freedom systems with non-linear stiffnesses offers advantages over the vector plot approach. The approach used in the previous section can be applied to non-linear damping characteristics since the non-linear element can readily be represented by an equivalent linearised element using the method of harmonic balance.

Following the approach used in the previous section, a non-linear Coulomb damping element is represented as an

equivalent hysteretic damping constant h*,

$$\text{where } h^* = \frac{4q}{\pi |u|} \qquad \ldots \qquad (140)$$

and q represents the level of the frictional force, which for Coulomb type damping is governed by the system relations:

$$f(\dot{x}) = q \text{ for } \dot{x} > 0 \qquad \ldots \qquad (141)$$

$$f(G) = -q \text{ for } \dot{x} < 0, \ \dot{x} = \text{velocity}$$

and $|u|$ is the peak displacement.

The equivalent hysteretic damping constant given by equation (140) can be combined with the elastic dissipative properties of a structure to give an element whose complex stiffness is given as:

$$k + jh^* = k'(1 + j\delta^*) \qquad \ldots \qquad (142)$$

where k = elastic stiffness component

$\delta^* = \delta + h^*/k'$, δ being the structural damping factor.

Thus a single degree-of-freedom system can now be represented as a body of mass m supported by an element with a complex stiffness given by equation (142). Thus the equation of motion of this single degree-of-freedom system subjected to a harmonic force $Fe^{j\omega t}$ becomes:

$$m\ddot{x} + k'(1 + j\delta^*)x = Fe^{j\omega t} \qquad \ldots \qquad (143)$$

The solution of this equation is simply:

$$x = ue^{j\omega t}, \text{ where } u = |u|e^{j\phi}$$

Thus $|u| = \dfrac{\frac{F}{k'}}{((1 - \Omega^2)^2 + \delta^{*2})^{\frac{1}{2}}}$ . . . . . (144)

and $\phi = \tan^{-1}(\delta^*/1 - \Omega^2)$, $\Omega = \omega\sqrt{m/k'}$

From equation (144),

$$|u|^2\{(1 - \Omega^2)^2 + \delta^{*2}\} - (\frac{F}{k'})^2 = 0 \quad . . \quad . . \quad . . \quad (145)$$

substituting $\delta^* = \delta + \frac{h^*}{k'} = \delta + \frac{r}{|u|}$, where $r = \frac{4q}{\pi k}$ in equation (145) and solving for $|u|$ gives:

$$|u| = \frac{-\delta r + \left\{(\frac{F}{k'})^2((1-\Omega^2)^2+\delta^2) - r^2(1-\Omega^2)^2\right\}^{\frac{1}{2}}}{(1 - \Omega^2)^2 + \delta^2} \quad . . \quad (146)$$

and $\tan\phi = \dfrac{\delta + (\frac{r}{|u|})}{1 - \Omega^2}$ . . . . . (147)

Inspection of equation: (146) shows that a solution for $|u|$ is only possible if the following condition is satisfied:

$$r < \frac{F}{k'}$$

The practical significance of this is that the magnitude of the applied force F must be greater than the magnitude of the friction force q in order for any motion to exist, which is usually the case in practice (62).

By plotting equations (146) and (147) in terms of their real and quadrature components the vector plot for a single degree-of-freedom system with Coulomb damping is obtained. Figure 32 shows the typical loci obtained for various

values of r, which for a given elastic stiffness is directly proportional to the frictional force level q.

Clearly, the effect of the Coulomb- friction is to distort the normal circular locus in such a manner that the quadrature axis components become elongated, resulting in an almost elliptical shape as the frictional forces increase.

Although it is quite obvious from Figure 32 that errors will be incurred if any attempt is made to extract damping ratios using the normal techniques of half-power point or reduced angle formulae, it appears that the natural frequency still occurs at the point where the rate-of-change of arc length per equal frequency increment is a maximum, as in the case of linear systems.

This can be investigated by obtaining an expression in terms of an arc length denoted by s, the phase angle ϕ, and the frequency ratio Ω.

Let ds = small arc at a radius $|u|$, then

$$ds = |u|.d\phi \quad \ldots\ldots\ldots \quad (148)$$

$$\therefore \quad \frac{ds}{d\Omega} = |u|\frac{d\phi}{d\Omega} \quad \ldots\ldots\ldots \quad (149)$$

$$= |u|\frac{d\phi}{dy}.\frac{dy}{d\Omega} \quad \ldots\ldots\ldots \quad (150)$$

$$\text{where } y = \text{cotan } \phi = \frac{1 - \Omega^2}{\delta + r\ u} \quad \ldots\ldots\ldots \quad (151)$$

$$\therefore \quad \frac{ds}{d\Omega} = \frac{2|u|\Omega}{(1 + y^2)(\delta + r/|u|)} \quad \ldots\ldots\ldots \quad (152)$$

Equation (152) is shown plotted on Figure 33 as a function of the frequency ratio, and it can be seen that $\frac{ds}{d\Omega}$ is a

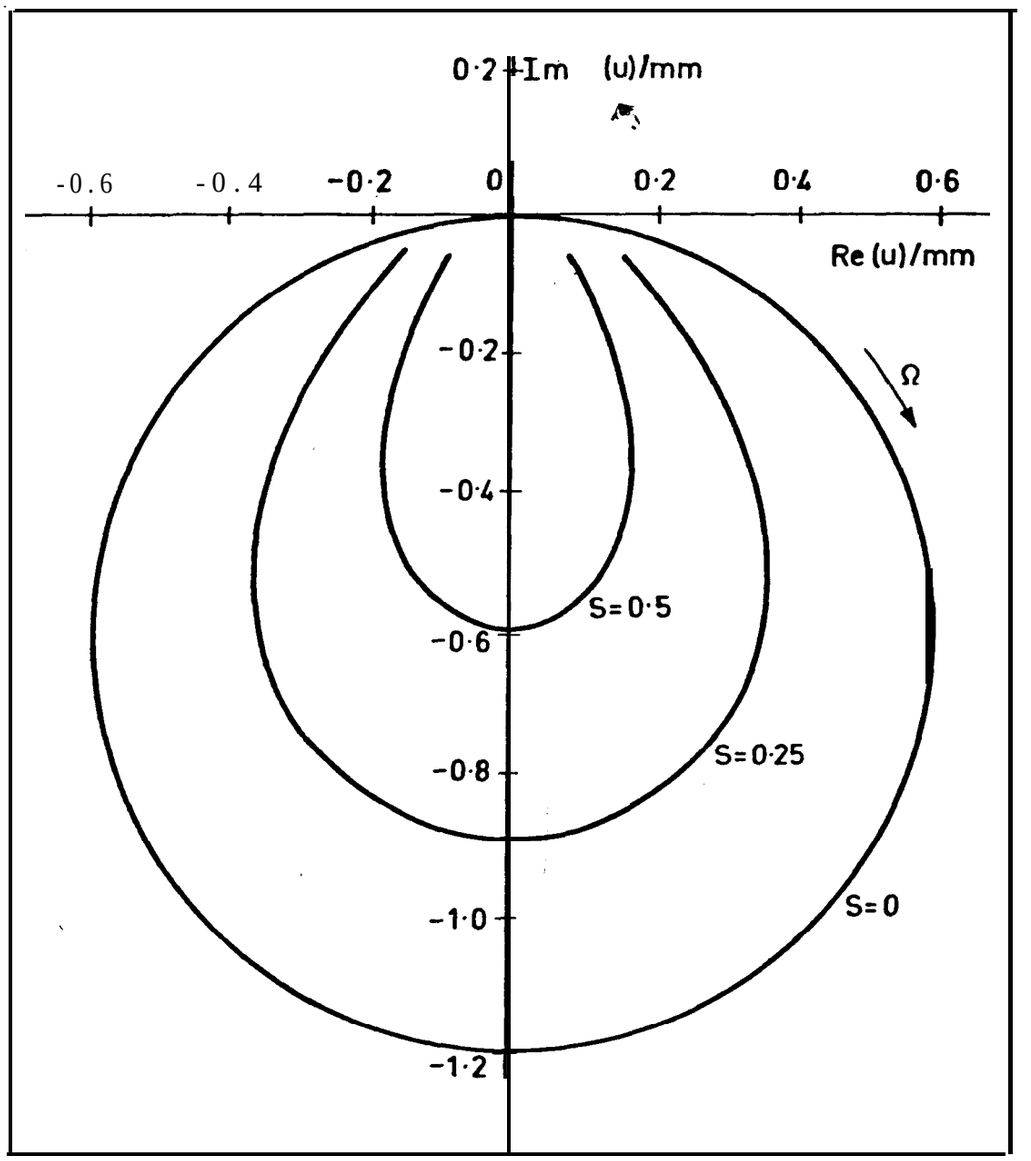

FIGURE 32

VECTOR PLOTS FOR A SINGLE DEGREE-OF-FREEDOM SYSTEM WITH COULOMB DAMPING

$S = \frac{rk'}{F} = \frac{4}{\pi} \cdot \frac{q}{F}$

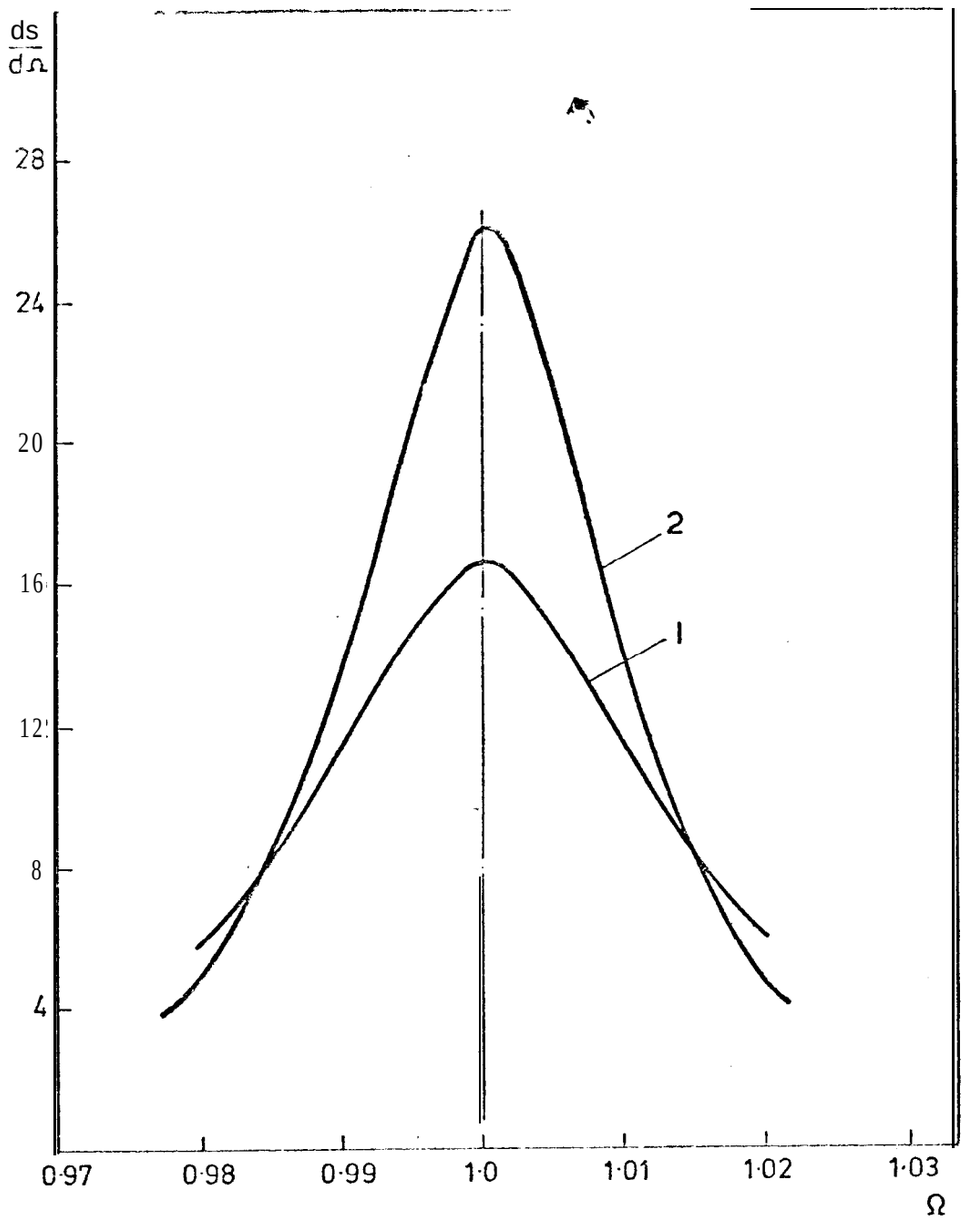

FIGURE 33

RATE-OF-CHANGE 0" ARC LENGTH PER UNIT FREQUENCY ds/dΩ AGAINST Ω FOR A SINGLE DEGREE-OF-FREEDOM SYSTEM WITH COULOMB FRICTION.

1. $\delta = 0.015$ } $F = 5N$, $q = 2.5N$
2. $\delta = 0.012$ } $k' = 350$ N/m

maximum when $\Omega = 1$ for the conditions given. Hence in the case of a system with a non-linear Coulomb type friction element, it would appear that it is still possible to identify the natural frequency condition as that frequency which gives a maximum rate-of-change of arc length with frequency.

5.4.2 THE RESPONSE IN TERMS OF THE COMPLEX POWER COMPONENTS

The response in terms of the in-phase and quadrature power components is given as:

$$W = W' + jW''$$

$$\text{i.e.} \quad W = \frac{\frac{F^2}{k'}\omega\delta^*}{(1 - \Omega^2)^2 + \delta^{*2}} + j\frac{\frac{F^2}{k'}\omega(1 - \Omega^2)}{(1 - \Omega^2)^2 + \delta^{*2}} \quad \ldots \quad (153)$$

$$\therefore \quad \frac{W}{\omega_n} = \frac{\frac{F^2}{k'}\Omega\delta^*}{(1 - \Omega^2)^2 + \delta^{*2}} + j\frac{\frac{F^2}{k'}(1 - \Omega^2)\Omega}{(1 - \Omega^2)^2 + \delta^{*2}} \quad \ldots \quad (154)$$

The similarity between equation (153) and equations (122 and 123), which depicts the complex power components for a linear hysteretically damped system at resonance, allows the same analytical approach which results in the system damping and natural frequency being obtained from the graphical characteristics of the complex power components. This can be best illustrated by an example.

Consider a single degree-of-freedom system with a linear elastic spring element and a linearised Coulomb friction element, the equation of motion of the system being the same as that of equation (143) i.e.

$$m\ddot{x} + k'(1 + j\delta^*)x = Fe^{j\omega t} \quad \ldots \quad (155)$$

where $\delta^* = \delta + \frac{4q}{\pi k' |u|}$

and $|u|$ is given by equation (146). Let the system physical parameters be:

$$\delta = 0.015; \quad q = 2.5N; \quad F = 5N; \quad k' = 350N/mm:$$

The i-n-phase and quadrature power components are given by equation (154) and these are shown plotted on Figure 34. It can be seen that the in-phase power is a maximum and that the quadrature power is zero at the natural frequency of the system.

The total damping is calculated from the expression:

$$\delta^* = \left. \frac{2W'/\omega_n}{\Omega \frac{dW''/\omega_n}{d\Omega}} \right|_{\Omega=1} \qquad \text{(156)}$$

which gives from Figure 34:

$$\delta^* = \frac{2 \times 1.735}{1 \times 83.3} = 0.0416$$

This compares with the exact value of $\delta^* = 0.0412$.

Unfortunately this approach does not offer any information relating to the individual (i.e. linear and non-linear) damping factors. In order to obtain expressions for both the linear damping factor and that due to the Coulomb damping, it is necessary to consider the power input to the system at resonance.

At resonance, the in-phase power input to the system (the quadrature power is zero) is obtained from equation (154) as:

$$W'\Big|_{\Omega=1} = \frac{F^2\omega_n}{k'\delta^*} \quad .. \quad .. \quad .. \quad .. \quad .. \quad .. \quad .. \quad (157)$$

$$= \omega_n k'(\delta|u|^2 + r|u|) \quad .. \quad .. \quad .. \quad .. \quad (158)$$

which can be expressed as:

$$\frac{W'}{\omega_n|u|}\Big|_{\Omega=1} = k'\delta|u| + k'r \quad .. \quad .. \quad .. \quad .. \quad (159)$$

Equation (159) represents a straight line of slope $k'\delta$ and intercepts $k'r$. Hence by plotting $W'/\omega_n|u|$ as a function of $|u|$ at resonance, the individual damping factors and the non-linear Coulomb friction force level can be obtained since $k'r = 4q/\pi$.

5.5 APPLICATION OF THE COMPLEX POWER METHOD TO SYSTEMS WITH SEVERAL DEGREES-OF-FREEDOM

It has been shown that for systems which can be described by a single degree-of-freedom that if the non-linearity has either a stiffness or a Coulomb friction characteristic then it is possible to define the modal properties of the system. There are two rather important factors which arise as a result of the single degree-of-freedom analysis which may not apply when the techniques used in the above analysis are applied to non-linear systems with more than one degree-of-freedom.

The first factor is related to the location of the non-linear element in the previous analyses. In these analyses it was assumed that the non-linear element was connected between the defined co-ordinate position and ground i.e. the instantaneous displacement of the non-linear element was absolute. In the case of systems with several degrees-of-freedom it may well be that the non-linear element (or

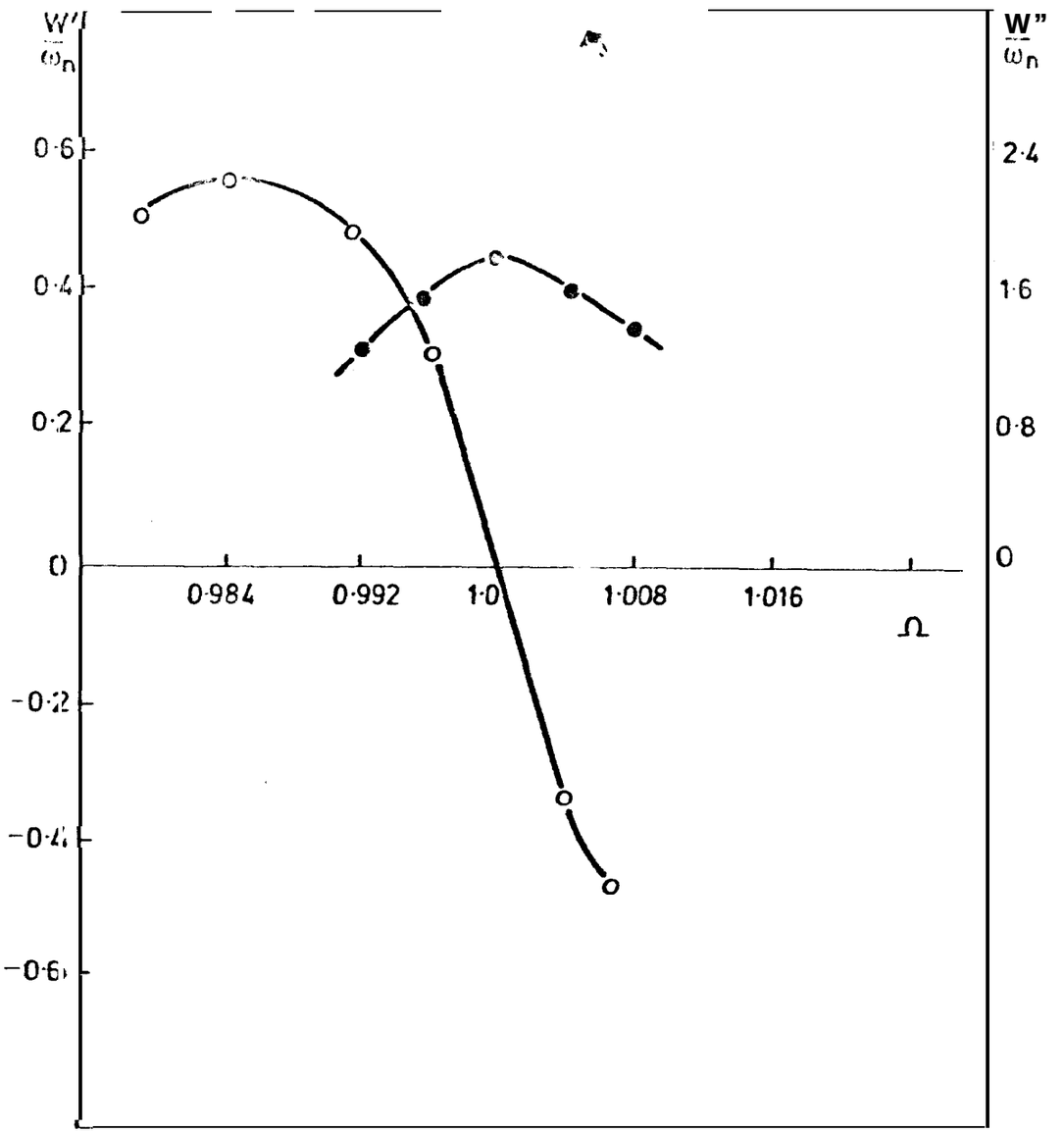

FIGURE 34

COMPLEX POWER CHARACTERISTICS FOR A SINGLE DEGREE-OF-**FREEDOM SYSTEM WITH COULOMB FRICTION GOVERNED BY EQUATION (155).**

. W''/ω_n

0 W'/ω_n

elements) is situated between two co ordinates, say the r^{th} and the s^{th} (which need not necessarily be adjacent). The effect of this is to couple these points in the structure which places restrictions on the previously simple analysis.

The second factor is only relevant to multi degree-of-freedom systems where the non-linearity is a hard or soft spring characteristic. In these cases, the normal mode shape and frequency may change with input force level, the deviation in the mode shapes also being dependent upon the location of the non-linearity.

This factor restricts the amount of information which can be obtained from a system which has a non-linear stiffness characteristic since it is not possible to determine the form of the non-linearity due to the fact that any variation in the input power at a given normal mode frequency will change the mode shape, which is not the case with the Coulomb friction elements. However, assuming that it is possible using multi-point excitation methods to excite a 'given normal mode', i.e. satisfy the normal mode criterion for a given input force level and distribution of a system with several degrees-of-freedom, then the 'given normal mode' frequency and the system damping can be estimated as detailed in Section 6.3.

5.6 THE EFFECT OF COULOMB FRICTION Oh' SYSTEMS HAVING SEVERAL DEGREES-OF-FREEDOM

In order to analyse systems with several degrees-of-freedom it is necessary to represent the system by a lumped-parameter modal with n degrees-of-freedom. If the system is assumed to be linear with a harmonic solution $x = ue^{jwt}$, the resulting equations of motion are given as:

$$-\omega^2 \underset{\sim}{M}\underset{\sim}{u} + \underset{\sim}{K}\underset{\sim}{u} + j\underset{\sim}{H}\underset{\sim}{u} = p \quad . . . . . \quad (160)$$

where $\underset{\sim}{M}$, $\underset{\sim}{k}$ and H are the symmetrical mass, stiffness and

damping matrices.

If the system is excited at its i^{th} normal mode frequency ω_1 by an appropriate force distribution p_i, equation (160) gives:

$$j\underset{\sim}{H}\underset{\sim}{u}_i = \underset{\sim}{p}_i \quad \ldots\ldots\ldots\ldots\ldots \quad (161)$$

since $\omega^2_i \underset{\sim}{M}\underset{\sim}{u}_i = \underset{\sim}{K}\underset{\sim}{u}_i$ and $\underset{\sim}{u}_i$ represents the peak displacements.

In terms of the i^{th} normalised mode shape, equation (162) can be written as:

$$j\lambda\underset{\sim}{H}\underset{\sim}{v}_i = \underset{\sim}{p}_i \quad \ldots\ldots\ldots\ldots\ldots \quad (163)$$

where $\underset{\sim}{v}_1$ represents the normalised mode shape and λ is a constant.

Equation (163) shows that if the vector of input forces is real, all the displacements will be in phase with each other and at quadrature to the input forces, this condition satisfying the classical phase-resonance criterion.

Since we are concerned with both Coulomb and hysteretic damping it will be necessary to consider the way in which these separate quantities will contribute to the response of the system.

The non-linear Coulomb friction elements which are linearised by the method of harmonic linearisation take the general form:

$$f_i = \frac{b_i}{|u|} \quad \ldots\ldots\ldots\ldots\ldots \quad (164)$$

where bi is a constant which depends upon the level of the Coulomb friction force and $|u|$ is the peak amplitude of vibration of the non-linear element.

Since we are dealing with n degrees-oi-freedom, the elements given by equation (164) can be represented by a frictional damping matrix. If this damping matrix is definedas F, its elements may be expressed in terms of the displacements as:

$$f_{kl} = \sum \frac{b_{kl}}{g_{kl}(u_1, u_2 \ldots u_n)} \quad .. \quad .. \quad .. \quad .. \quad (165)$$

where f_{kl} is an element in the k^{th} row and i^{th} column
b_{kl} is a constant
g_{kl} is a linear function of amplitudes $u_1 \ldots\ldots u_n$.

A physical representation of equation (165) can be shown by considering the lumped parameter three degree-of-freedom system with linearised Coulomb friction elements situated as shown in Figure 35.

The linearised elements are given from equation (164) as:

$$f_1 = \frac{b_1}{|u_1|}, \quad f_2 = \frac{b_2}{|u_2 - u_1|}, \quad f_3 = \frac{b_3}{|u_3 - u_1|} \quad .. \quad (166)$$

The frictional damping matrix for this system is:

$$F = \begin{vmatrix} f_1+f_2+f_3 & -f_2 & -f_3 \\ -f_2 & f_2 & 0 \\ -f_3 & 0 & f_3 \end{vmatrix} \quad .. \quad .. \quad .. \quad (167)$$

and thus from equation (165):

$$f_{11} = \frac{b_1}{\begin{bmatrix} 1 & 0 & 0 \end{bmatrix}\begin{bmatrix} u_1 \\ u_2 \\ u_3 \end{bmatrix}} + \frac{b_2}{\begin{bmatrix} -1 & 1 & 0 \end{bmatrix}\begin{bmatrix} u_1 \\ u_2 \\ u_3 \end{bmatrix}} + \frac{b_3}{\begin{bmatrix} -1 & 0 & 1 \end{bmatrix}\begin{bmatrix} u_1 \\ u_2 \\ u_3 \end{bmatrix}} \quad (168)$$

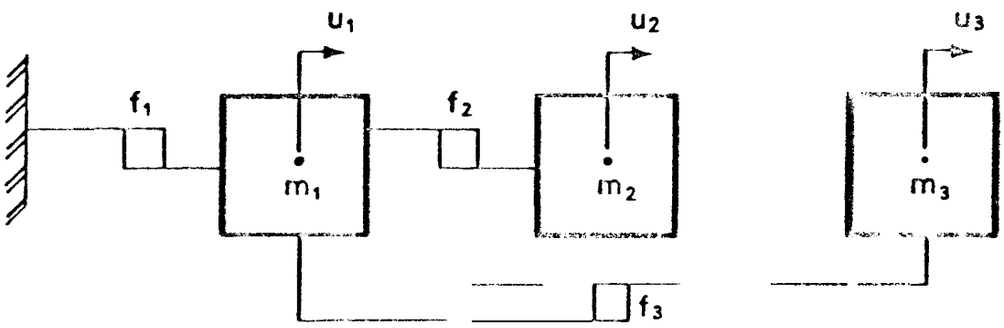

FIGURE 35

LUMPED PARAMETER SYSTEM WITH COULOMB FRICTION ELEMENTS (f_1, f_2, f_3) **ONLY.**

$$f_{22} = \frac{-b_2}{\begin{bmatrix}-1 & 1 & 0\end{bmatrix}\begin{bmatrix}u_1\\u_2\\u_3\end{bmatrix}} \quad \text{etc.}$$

If the system is excited at its i^{th} natural frequency, equation (168) can be represented in terms of the normalised mode shape as:

$$f_{kl} = \sum \frac{b_{kl}}{\lambda g_{kl}^{t} v_i} \quad .. \quad .. \quad .. \quad .. \quad .. \quad .. \quad (169)$$

The frictional damping matrix can now be expressed in the form:

$$F = (\frac{1}{\lambda}) F_i \quad .. \quad .. \quad .. \quad .. \quad .. \quad .. \quad .. \quad (170)$$

where the elements of F_i are independent of the amplitude of vibration and take the form:

$$F_i = \frac{b_{kl}}{g_{kl}^{t} v_i} \quad .. \quad .. \quad .. \quad .. \quad .. \quad .. \quad .. \quad (171)$$

If the hysteretic damping matrix, which represents the damping in the linear system, is denoted by S, then the system damping matrix may be derived from equations (171) and (163) as:

$$H = \lambda S + F_i \quad . \quad . \quad . \quad \cdots \quad .. \quad .. \quad .. \quad .. \quad (172)$$

thus, equation (163) becomes:

$$j(\lambda S + F_i) v_i = p_i \quad . \quad . \quad . \quad . \quad . \quad . \quad . \quad . \quad . \quad . \quad . \quad (173)$$

The complex power components when the system is vibrating

at its i^{th} normal mode frequency are obtained with the aid of equation (173). The power dissipated at this frequency is given by:

$$W_i = -\underset{\sim}{u}_i^t \underset{\sim}{p}_i = -j\omega_i \underset{\sim}{v}_i^t \underset{\sim}{p}_i \quad .. \quad .. \quad .. \quad .. \quad (174)$$

which represents the quadrature input power components, the in-phase power components being zero.

It. follows from equations (173) and (174) that:

$$W_i = \omega_1 \cdot \underset{\sim}{v}_i^t (\lambda^2 S + \lambda \underset{\sim}{F}_i) \underset{\sim}{v}_i \quad . \quad . \quad . \quad . \quad . \quad . \quad . \quad . \quad (175)$$

and

$$\frac{W_i}{\lambda \omega_i} = \lambda \underset{\sim}{v}_i^t \underset{\sim}{S} \underset{\sim}{v}_i + \underset{\sim}{v}_i^t \underset{\sim}{F}_i \underset{\sim}{v}_i \quad .. \quad .. \quad .. \quad .. \quad (176)$$

Equation (176) represents the total input power to the system at the normal mode frequency ω_i and shows that it is possible to evaluate n values of $\underset{\sim}{v}_i^t \underset{\sim}{F}_i \underset{\sim}{v}_i$ corresponding to n modes of vibration. Unfortunately, in order to define the form of the Coulomb damping matrix and identify individual friction force levels this information is not sufficient to completely define the Coulomb damping matrix $\underset{\sim}{F}_i$.

If one bears in mind that the off-diagonal terms of the matrix $\underset{\sim}{F}_i$ are related to co-ordinates coupled by Coulomb damping elements, then if it is known a priori that all the Coulomb damping elements are grounded then the $\underset{\sim}{F}_i$ matrix must be diagonal and a unique solution can be obtained to give the values of the corresponding hysteretic damping constants.

However, the author has not been successful in deriving such a general unique solution when the system also posesses Coulomb frictional devices which couple one co-ordinate to

another.

Nevertheless, a technique has been developed which allows the locations and, in the case of a single non-linear element, the characteristics of the Coulomb friction elements to be identified.

Consider a lumped parameter system and let the power input to each co-ordinate be W_{ir}, i.e. individual power input in the i^{th} mode at the r^{th} co-ordinate = W_{ir}. Consider the r^{th} co-ordinate of equation (176):

$$\frac{W_{ir}}{\lambda\omega_i} = \lambda \underset{\sim}{v}_i^t \underset{\sim}{S}_r v_{ir} + \underset{\sim}{v}_i^t \underset{\sim}{F}_{ir} v_{ir} \quad .. \quad .. \quad .. \quad (177)$$

where $\underset{\sim}{S}_r$ is the r^{th} column of the S matrix
v_{ir} is the r^{th} element of the vector $\underset{\sim}{v}_i$
$\underset{\sim}{F}_{ir}$ is the r^{th} column of the $\underset{\sim}{F}_i$ matrix

Equation (177) is now of the same form as equation (159). Thus equation (177) can be used in the same way as equation (159) to identify the location and characteristics of the non-linearity.

For example, if the left-hand-side of equation (177) is plotted as a function of λ, a non-zero $\underset{\sim}{v}_i^t \underset{\sim}{F}_{ir} v_{ir}$ intercept indicates that a frictional device is coupled to the r^{th} co-ordinate. Thus it is possible, by measuring the power input at each co-ordinate, to determine the locations of the Coulomb damping elements.

Further, if only a single Coulomb damping element coupling say the r^{th} and s^{th} co-ordinates in the system is present, then the only non-zero intercepts would be those associated with the r^{th} and s^{th} co-ordinates and hence the magnitude q of the Coulomb damping elements could be evaluated directly, since:

$$F_{i_{rr}} = F_{i_{ss}} = -F_{i_{rs}} = -F_{i_{sr}} = \frac{4q}{\pi(v_r - v_s)} \quad \ldots \quad (178)$$

In order to examine the mechanism of applying equations (174) through to (178), two worked examples are given in Appendix V. The first example deals with grounded Coulomb damping elements and the second example considers a system with a coupled Coulomb element.

A programme of experimental work was carried out on the rig discussed in Section 4.7, which included a controlled non-linear device that provided a characteristic closely resembling that of Coulomb friction, and the techniques described above were applied with the aim of establishing the level of the Coulomb damping force.

6. EXPERIMENTAL TESTS ON A TWO-DEGREE-OF-FREEDOM SYSTEM WITH A COULOMB FRICTION ELEMENT

6.1 DESIGN OF THE COULOMB FRICTION ELEMENT

The Coulomb friction element consisted of two items, the body which housed an adjustable highly polished steel disc and spring assembly, and an aluminium pad coated with Teflon. Appendix VI shows the construction of the element and Plate 6 shows the actual element which was located at one end of the cross-beam of the main rig described in Chapter 4. The location of the non-linear device was not altered throughout the series of tests.

The body of the Coulomb friction element was securely located to a rigid support which in turn was rigidly connected to the massive cast-iron base supporting the entire rig. Thus this part of the friction element was not physically connected to the vibration elements of the rig, i.e. it was grounded. The disc assembly was permanently pre-loaded by a spring, which could be adjusted by a calibrated screw mechanism in order to increase or reduce this pre-load and hence retract or extend the disc assembly from a given position.

The disc assembly was aligned horizontally and normal to an aluminium pad which was secured to the cross-beam of the main rig, i.e. this formed the vibrating element. This aluminium pad was evenly coated with Teflon to prevent scuffing arising from a metal-to-metal interface.

Initially the pad was not in contact with the steel disc, but by adjusting the screw mechanism it was possible to bring the disc into contact with the pad, hence creating a 'Coulomb' friction force between the vibrating cross-beam of the rig and ground, the interface pressure and hence the level of the frictionforce between the vibrating Teflon coated pad and the stationary hardened steel disc being

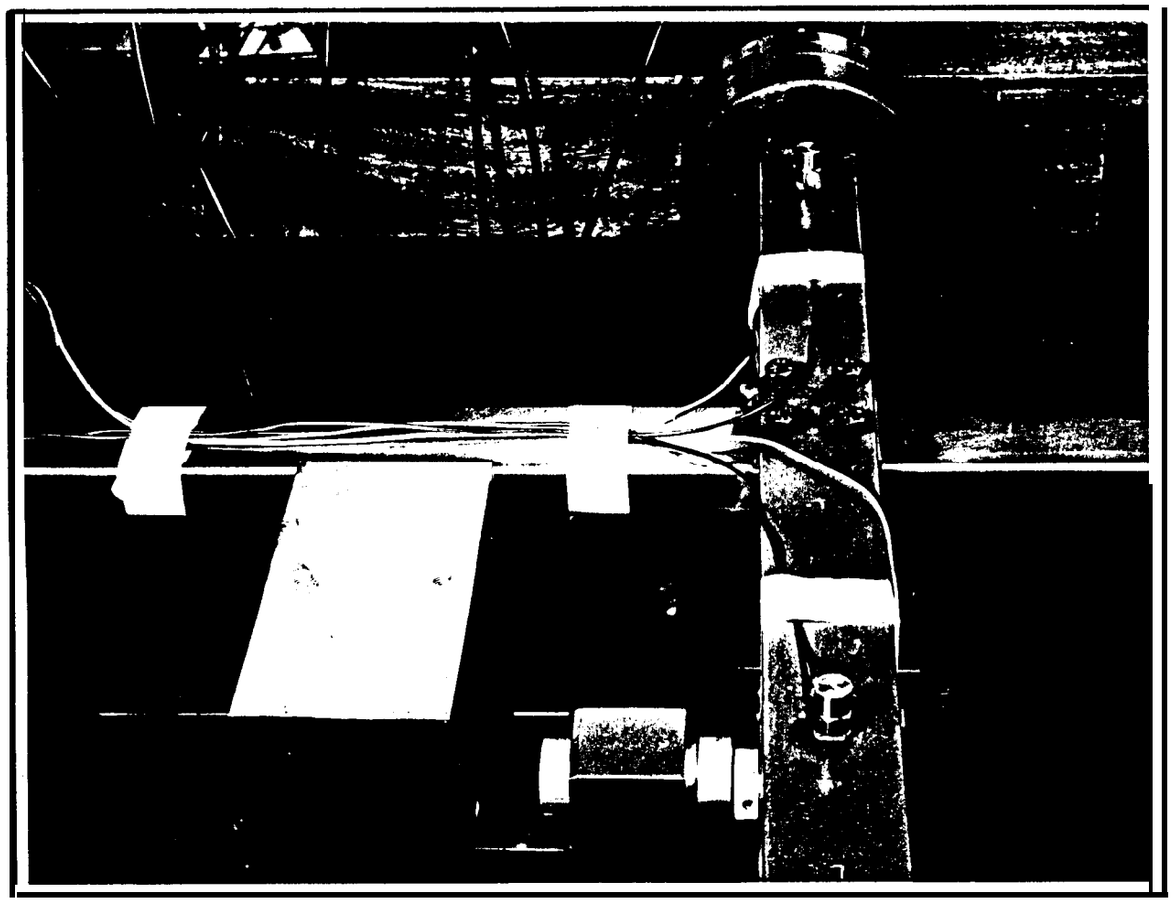

PLATE 6

EXPERIMENTAL RIG SHOWING THE LOCATION OF THE COULOMB FRICTION ELEMENT. THE ALUMINIUM PAD IS SITUATED DIRECTLY BELOW THE ACCELEROMETER:

adjustable by merely varying the pre-load on the spring.

6.2 CALIBRATION TESTS OF THE COULOMB FRICTION ELEMENT

In order to examine the characteristics of the Coulomb friction element it was necessary to carry out tests which would allow the actual friction force levels to be measured. It was felt also that if the hysteresis characteristics for the Coulomb friction elements could be obtained at the same time, then a visual comparison between the actual behaviour of the device and the theoretical characteristics of a Coulomb friction element would be possible which would indicate the effectiveness of the device in its role as a Coulomb damper.

This was achieved by carrying out a set of quasi-static tests. These consisted of exciting the system at a very low frequency and measuring the input force and the corresponding system displacement.

6.2.1 QUASI-STATIC VIBRATION TESTS

Figure 36 shows a diagrammatic sketch of the rig and the instrumentation used in these tests. With the steel disc retracted so that no contact was made with the Teflon coated pad, i.e. no Coulomb friction was present, the cross-beam was excited at symmetrical points with the input forces equal in magnitude. The output displacement was measured at the position of the Coulomb friction element using a non-contact displacement transducer, which had been previously calibrated so as to provide a known output voltage for a known displacement, and this was fed into the 'X' axis channel of an X-Y recorder.

The voltage representing the force input at the position nearest to the Coulomb friction element was fed into the 'Y' axis of the X-Y recorder. Since both the vibration exciters were controlled from the Frequency Response

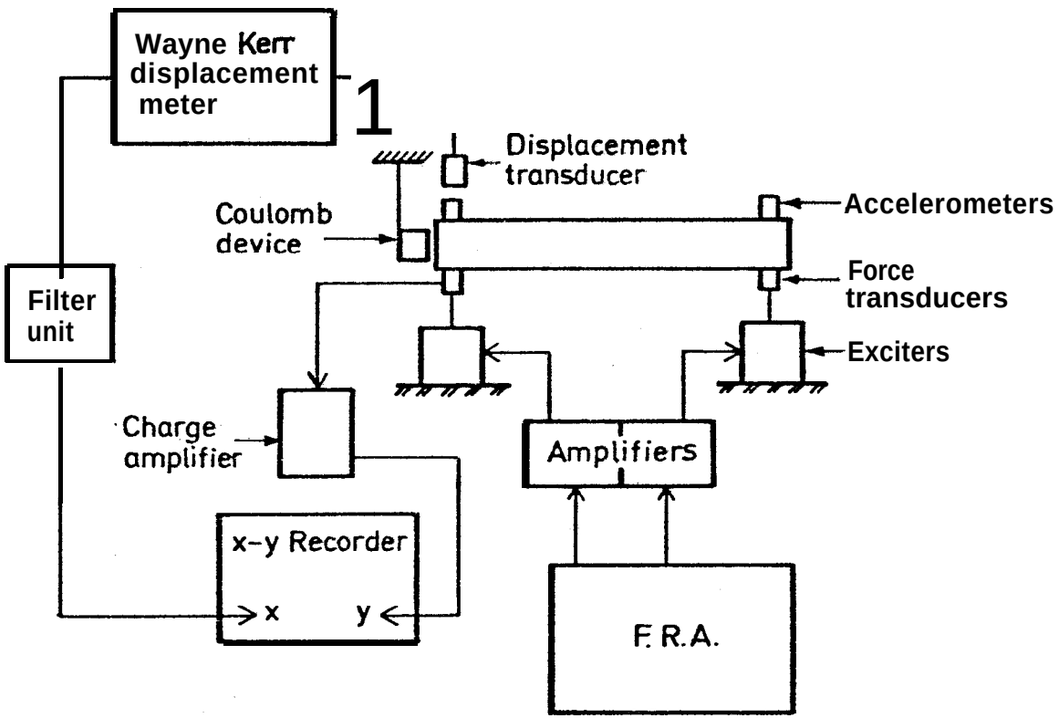

FIGURE 36

DIAGRAMMATIC SKETCH OF EXPERIMENTAL SET-UP FOR QUASI-STATIC TESTS.

Analyser via their individual matched amplifiers, no problems were encountered with the phase or frequency control of the two input forces. By choosing a very low excitation frequency (hence the title of the tests) of 20mHz, the X-Y plotter could record directly the cyclic load deflection characteristics of the system. It must be mentioned here that in order to produce satisfactory results the instrumentation, and in particular the charge amplifiers, must have low drift characteristics otherwise the low frequencies of operation required cannot be used in conjunction with the piezoelectric force links.

6.2.2 RESULTS OF THE QUASI-STATIC TESTS

Figure 37 shows the hysteresis loop obtained from the first test when there was no contact between the Teflon coated pad and the steel disc. The mean slope of this characteristic represents the static stiffness of the rig in the transverse mode, the small area enclosed by the curve being due, of course, to the cyclic strain energy absorbed by the rig. The actual stiffness in this mode, determined from the mean slope was 380 kN/m, which compares well with the results of a static stiffness test of 370 kN/m.

Figure 38 shows the hysteresis loops obtained with the disc and pad in contact for increasing values of the Coulomb friction force. The behaviour of the device as a Coulomb friction element is excellent, as demonstrated by the measured hysteresis curves compared to a theoretical hysteresis loop for a Coulomb friction element (62). The slopes of these curves again represent the stiffness of the transverse mode of vibration and the linearity and repeatability of these endorse the behaviour of the device.

At the higher friction force levels stiction became a problem. This is indicated on Figure 38 where this effect is plainly seen on curve 3, and as a consequence of this all steady state forced vibration tests were carried out at

friction force levels below those at which stiction was apparent. The cause of the stiction effect was attributed to the fact that the face of the hardened steel disc was not exactly parallel to the Teflon coated face of the aluminium pad, and when the force between these reached a certain level, the misalignment caused the steel disc to 'score' the Teflon coating.

6.2.3 STEADY STATE VIBRATION CHARACTERISTICS WITH COULOMB FRICTION

Plate 7 shows a comparison between the output acceleration, velocity and displacement in the transverse mode with and without the Coulomb damper in operation.

It is interesting to note from these that the assumptions used in the analysis regarding the method of harmonic balance are justified and that the velocity profile with Coulomb friction closely resembles the theoretical case.

6.3 EXPERIMENTAL DETERMINATION OF THE COULOMB FRICTION FORCE LEVEL BY THE METHOD OF COMPLEX POWER

In order to be able to determine the characteristics of the non-linearity, equation (177) showed that it was necessary to obtain the power input to a normal mode as a function of some reference amplitude of the normal mode, This requires that within a given frequency range all the normal modes are excited (this being done by multi-point excitation methods) and at each normal mode frequency the force levels are varied and the corresponding change in the levels of the mode shape measured. These results provide the power input to the mode and can then be plotted as described in Section 6.6 to obtain the level of the Coulomb friction forces.

Since the responses throughout the tests were measured in terms of acceleration levels it is worthwhile considering

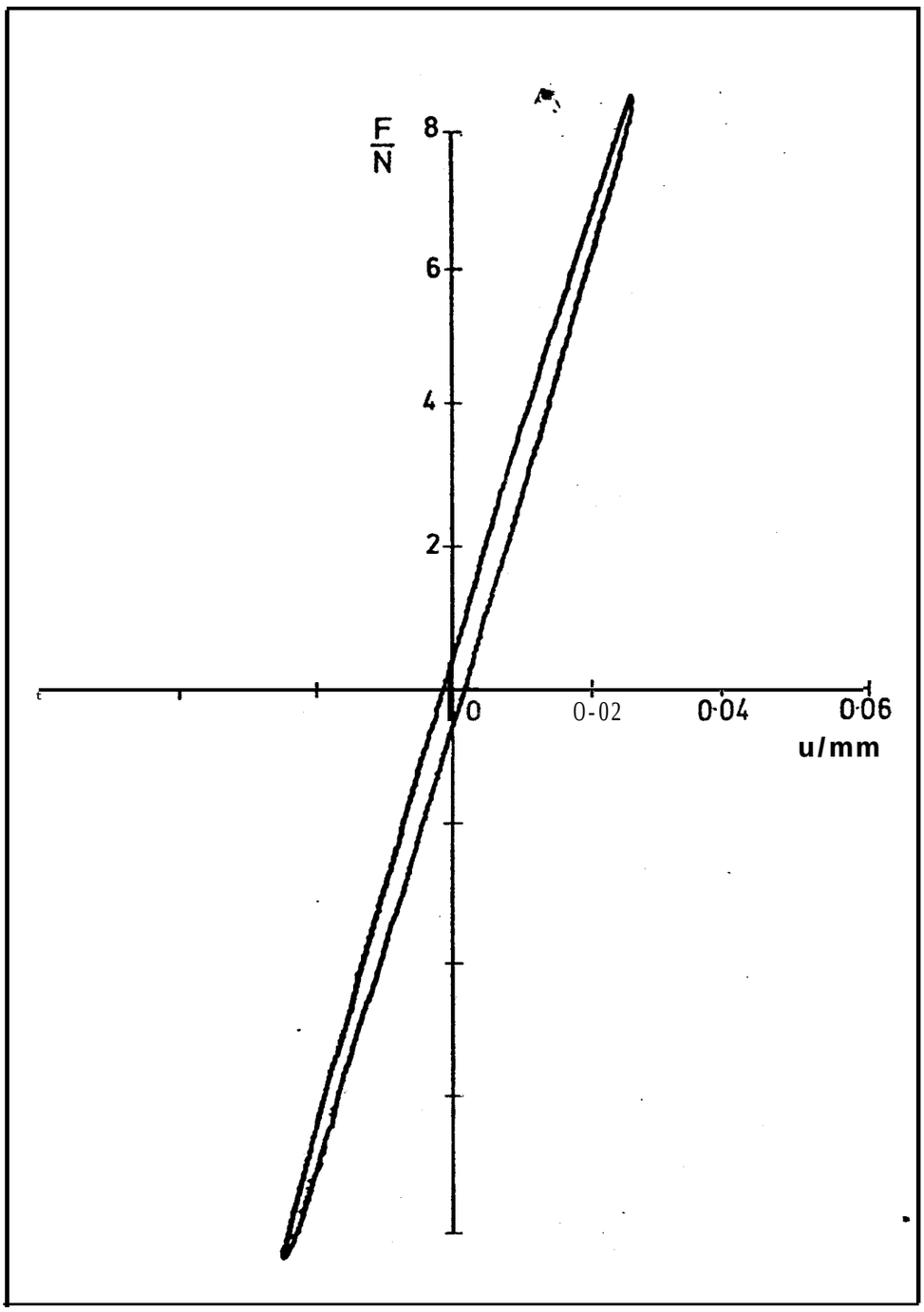

FIGURE 37

QUASI-STATIC TEST WITH COULOMB FRICTION REMOVED. HYSTERESIS LOOP OF EXCITATION FORCE (F) AGAINST RESULTING DISPLACEMENT (u). EXCITATION FREQUENCY 2OmHz.

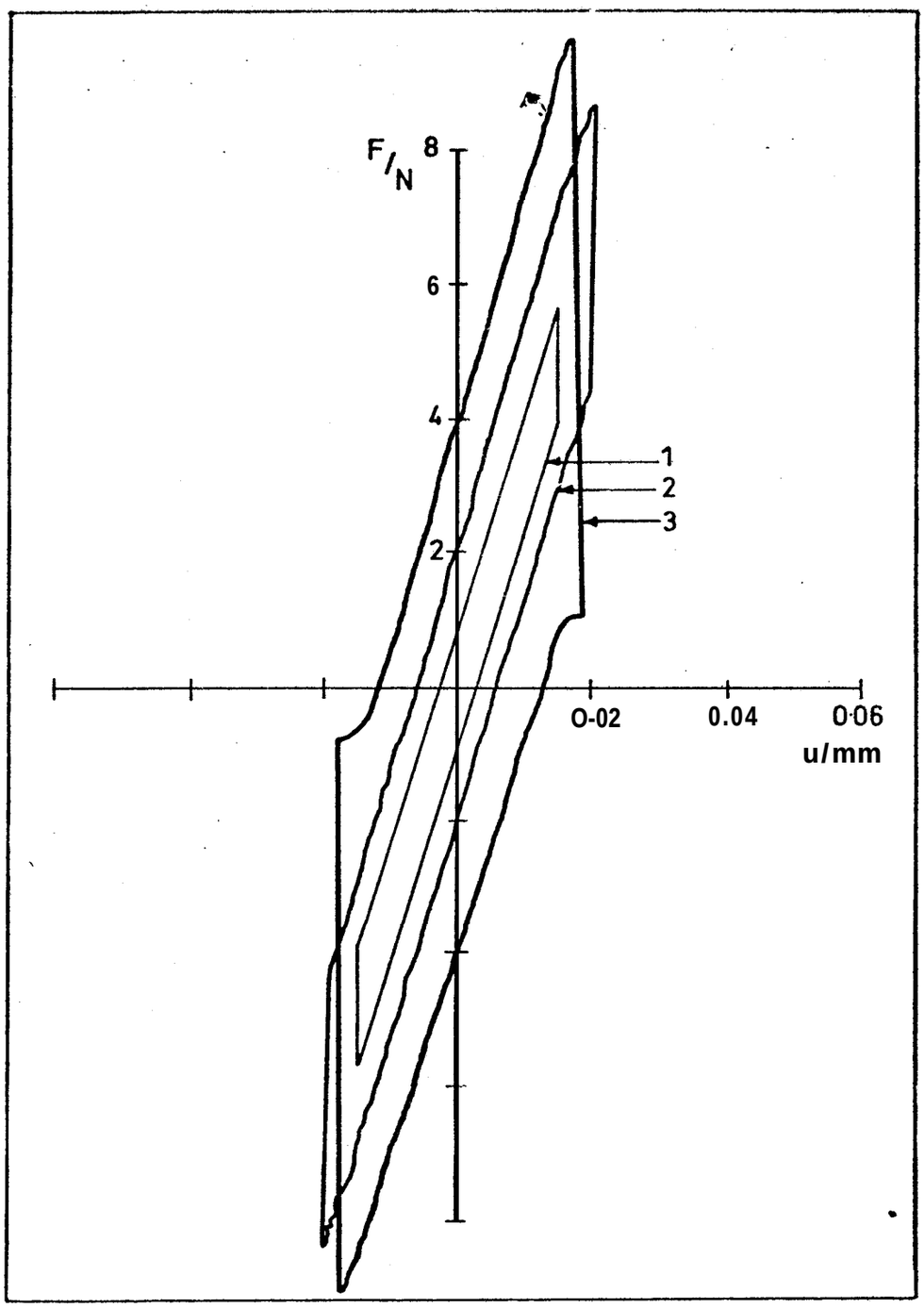

FIGURE 38

HYSTERESIS CURVES FROM QUASI-STATIC TESTS FOR VARIOUS LEVELS OF COULOMB FRICTION FORCE:

1 – **FRICTION FORCE PEAK-TO-PEAK LEVEL** = 1.75N
2 – **FRICTION FORCE PEAK-TO-PEAK LEVEL** = 4.5N
3 – **FRICTION FORCE PEAK-TO-PEAK LEVEL** = 8.5N

} **EXCITATION FREQUENCY 20mHz**

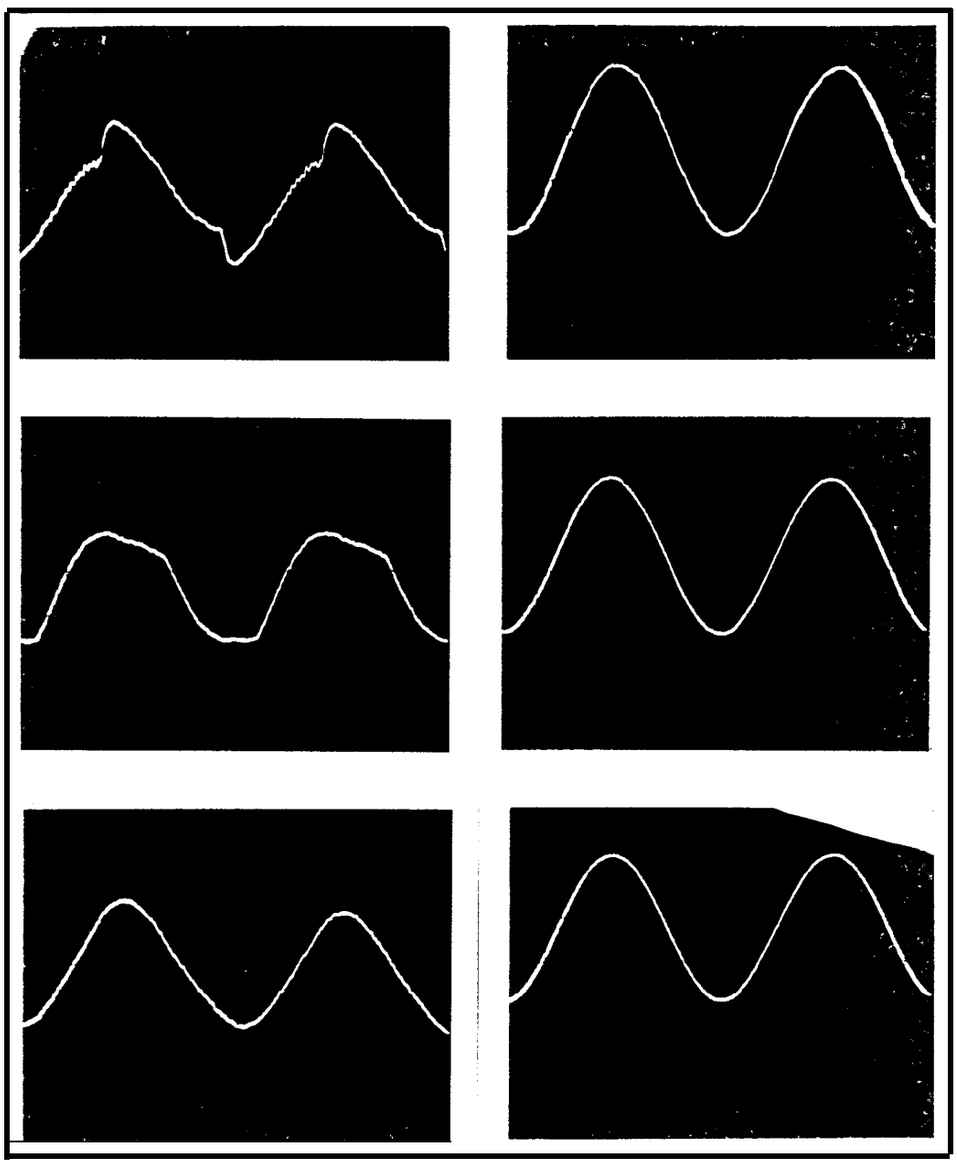

RESPONSE WITH COULOMB FRICTION

RESPONSE WITHOUT COULOMB FRICTION

PLATE 7

EXPERIMENTAL RESULTS SHOWING THE OUTPUT RESPONSE IN THE TRANSVERSE MODE WITH AND WITHOUT THE COULOMB FRICTION ELEMENT IN OPERATION.

A - ACCELERATION
V - VELOCITY
D - DISPLACEMENT

the complex power expressions in terms of the acceleration response.

6.3.1 COMPLEX POWER INPUT USING ACCELERATION RESPONSES

The total power input to a given mode of vibration is given by:

$$W = \sum_{i=1}^{N} F_i \dot{u}_i \quad \ldots \quad (179)$$

where F_i = Force input level at station i
$\dot{u}_i$ = Velocity level at station i
N = Number of exciters

If the excitation frequency is changed by only a small amount around the normal mode frequency, then the force vector will be predominantly real and:

$$W = W' + jW'' \quad \ldots \quad (180)$$

where $W' = F_i \dot{u}_i'$, $\dot{u}_i'$ = in-phase velocity
$W'' = F_i \dot{u}_i''$, $\dot{u}_i''$ = quadrature velocity

In the case of the response being in terms of acceleration units:

$$W' = F_i \ddot{u}_i''/\omega_r \quad \ldots \quad (181)$$

$$W'' = F_i \ddot{u}_i'/\omega_r \quad \ldots \quad (182)$$

where W_r = normal mode frequency
$\ddot{u}_i''$ = quadrature acceleration
$\ddot{u}_i'$ = in-phase acceleration

Thus the in-phase power is given as the product of the force

and quadrature acceleration, and the quadrature power as the product of force and in-phase acceleration component.

In terms of the experimental rig requirements, where there were two input forces and two responses, this meant:

$$W_1 = W_1' + jW_1'' = \frac{F_1}{\omega_r}(\ddot{u}_1'' + j\ddot{u}_1') \quad \ldots \quad (183)$$

$$W_2 = W_2' + jW_2'' = \frac{F_2}{\omega_r}(\ddot{u}_2'' + j\ddot{u}_2') \quad \ldots \quad (184)$$

Now since the normal mode shapes were $\underset{\sim}{v}_1^t = \lfloor 1.0,\ 1.0 \rfloor$ $\underset{\sim}{v}_2^t = \lfloor 1.0,\ -1.0 \rfloor$ then the acceleration components at the symmetrical points on the rig should be equal at the normal mode frequency, and the in-phase and quadrature power components given as:

$$W' = W_1' + W_2' = \frac{\ddot{u}_1''}{\omega_r}(F_1 + F_2) \quad \ldots \quad (185)$$

$$W'' = W_1'' + W_2'' = \frac{\ddot{u}_1'}{\omega_r}(F_1 + F_2) \quad \ldots \quad (186)$$

Unfortunately the experimental values of the accelerations were not identical and as a result of this it was necessary to obtain a range of values of the in-phase and quadrature responses around the normal mode frequency of vibration which could then be plotted in terms of the in-phase and quadrature power inputs to the normal mode (equations (184) and (185)) and from these results the average power input to the mode could be derived at the normal mode frequency.

6.3.2 EXPERIMENTAL PROCEDURE FOR DETERMINING THE COMPLEX POWER INPUT TO A NORMAL MODE

The experimental procedure required to measure the in-phase

and quadrature power components is almost identical to that used for obtaining vector plots. The only differences are that the individual force and response measurements are required (vector plots can utilise the ratio of these) in order that the actual power can be evaluated and that this information is obtained from a much smaller frequency range than that required'for a vector plot.

Once a normal mode had been established, (by the procedure described in Section 4.8), the force distribution arising from this was maintained constant as the frequency of excitation was varied around the normal mode frequency, and the acceleration responses, in terms of the in-phase and quadrature components, were recorded at each frequency increment.

This procedure was repeated for a range of force input levels in the transverse and torsional normal modes in order that equation (177) could be applied. The in-phase and quadrature powers were obtained from equations (183) and (184).

6.4 RESULTS OF NORMAL MODE TESTS

6.4.1 TRANSVERSE MODE

Figures 39 to 41 show typical in-phase and quadrature power inputs as a function of the excitation frequency around the normal mode frequency for a range of input powers. It can be seen from these figures that the maximum in-phase power does not always occur at the frequency where the quadrature power is zero, whereas the theoretical expressions show that the in-phase power is a maximum at the normal mode frequency and the quadrature power is zero. Thus to allow for experimental error the normal mode frequency was calculated from the expression:

$$\omega_n = \frac{\omega'\big|_{W'=\max} + \omega\big|_{W''=0}}{2} \qquad (187)$$

and this average value of ω_n was used to determine the conditions in the expression for the damping ratio,

$$\zeta = \frac{W'}{\omega \frac{dW''}{d\omega}}\Bigg|_{\omega=\omega_n} \qquad (188)$$

Figure 43 shows the normal mode frequency as a function of the input power levels. These results show that there is a slight reduction in the normal mode frequency with increasing input power.

These effects can be explained by the fact that the Coulomb friction non-linearity can be considered as an extreme case of a soft-spring characteristic (77) which produces a reduction in the resonant frequency for an increasing input excitation force level, these effects of course being the exact opposite of a system with a non-linear hardening spring characteristic. This observed reduction in the normal mode frequency of vibration with increasing input power was confirmed by simulation tests. The tests involved modelling a single degree-of-freedom system with viscous damping and an ideal Coulomb friction characteristic (i.e. a simple relay) on an analog results of this simulation, which confirm the practical results, are shown on Figure 44.

6.4.2 TORSIONAL MODE

The in-phase and quadrature power inputs for a similar set of input power levels are shown on Figures 45 to 47. Again the maximum in-phase power does not always occur at the same frequency where the quadrature power is zero, thus the same procedures as in 6.4.1 were used for establishing the normal mode frequency and damping ratios.

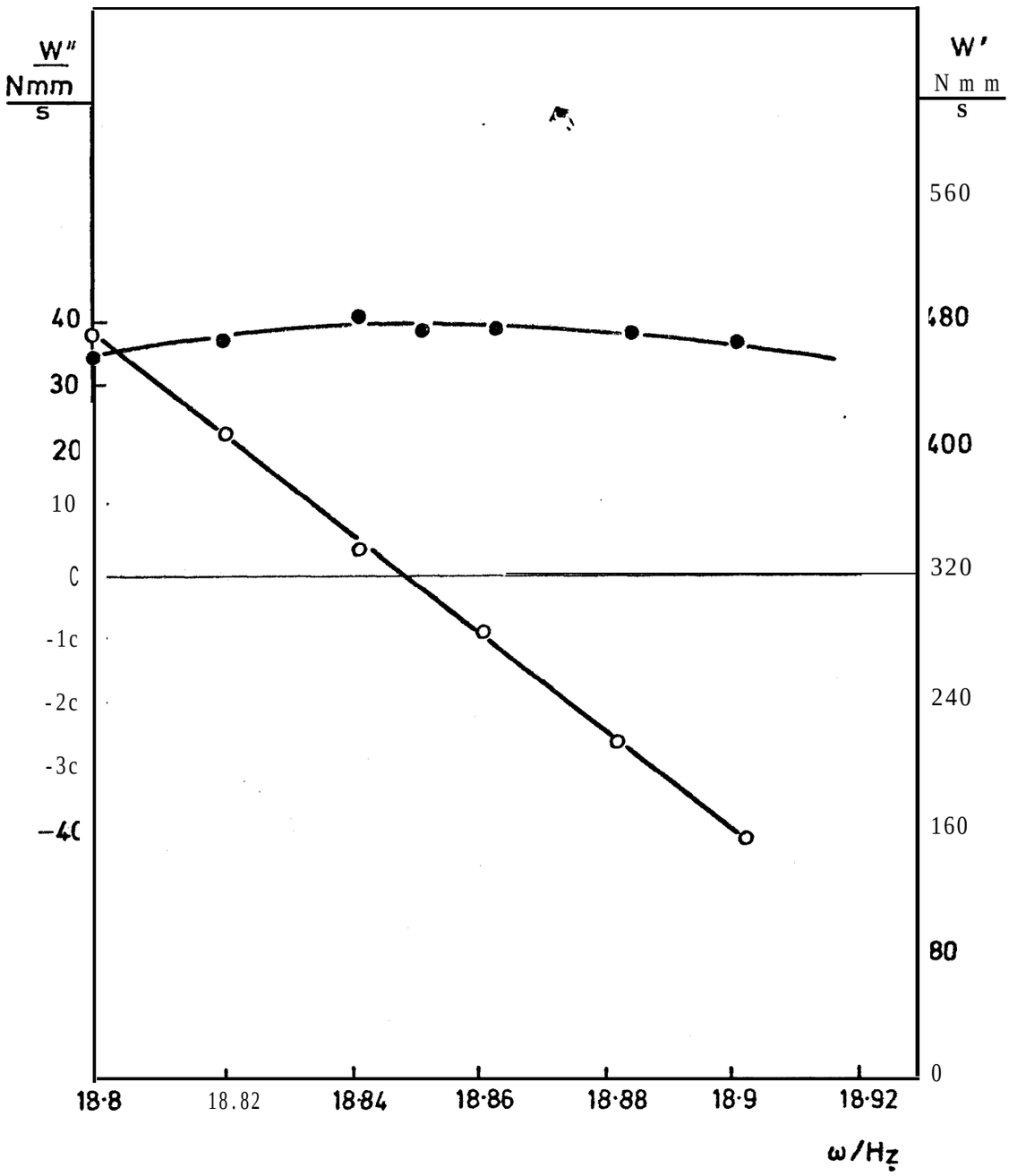

FIGURE 39

TRANSVERSE MODE COMPLEX POWER CHARACTERISTICS

● **IN-PHASE POWER** W'
o **QUADRATURE POWER** W"
NORMAL MODE RESPONSE VECTOR = 0.45 $\begin{bmatrix} 1.01 \\ 1.0 \end{bmatrix}$ mm AT A
NORMAL MODE FREQUENCY OF 18.85 **Hz.**

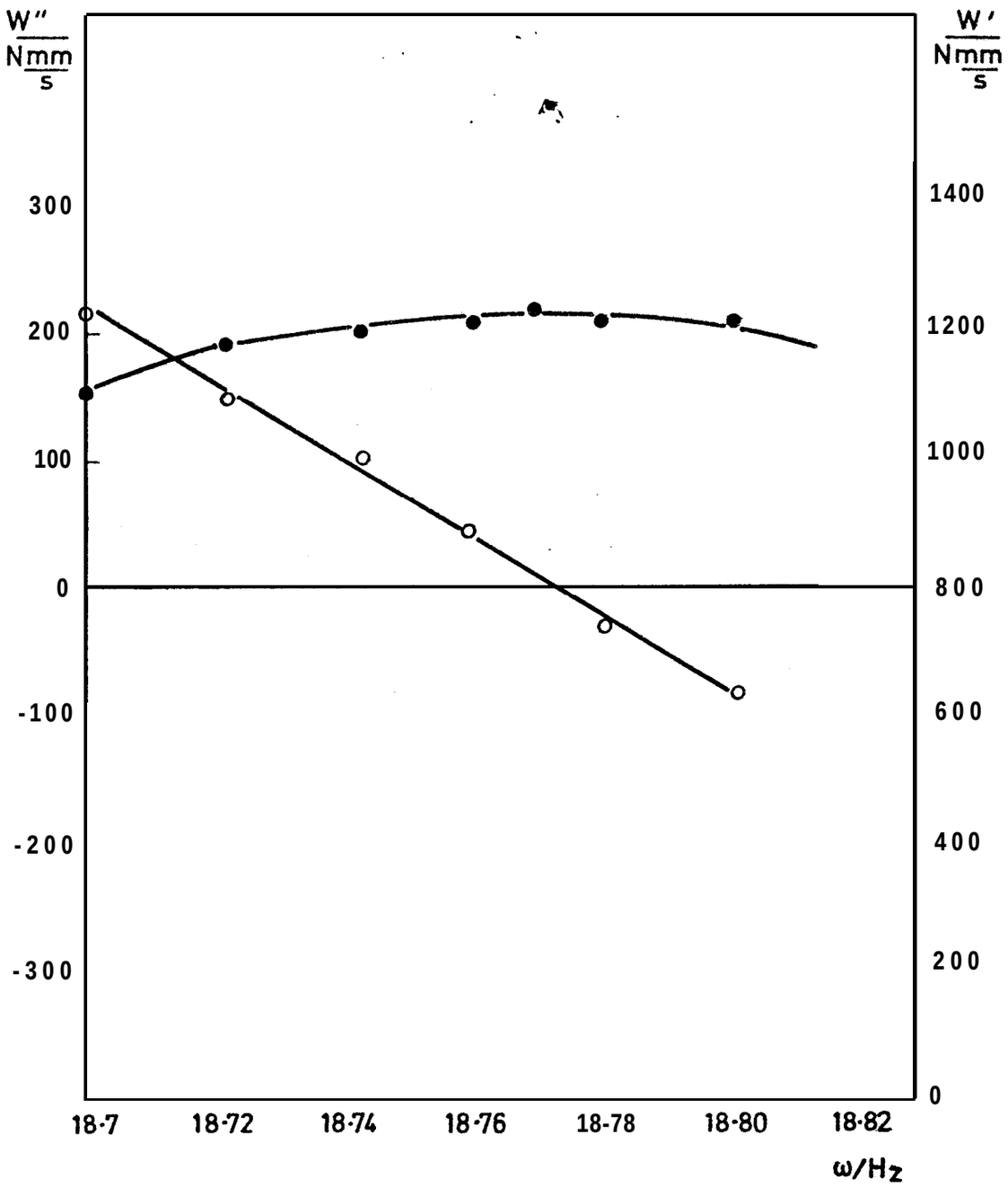

FIGURE 40

TRANSVERSE MODE COMPLEX POWER CHARACTERISTICS

● IN-PHASE POWER W'
o QUADRATURE POWER W"
NORMAL MODE RESPONSE VECTOR = 0.84 [1.0 1.0 1] mm AT A
NORMAL MODE FREQUENCY OF 18.77 Hz

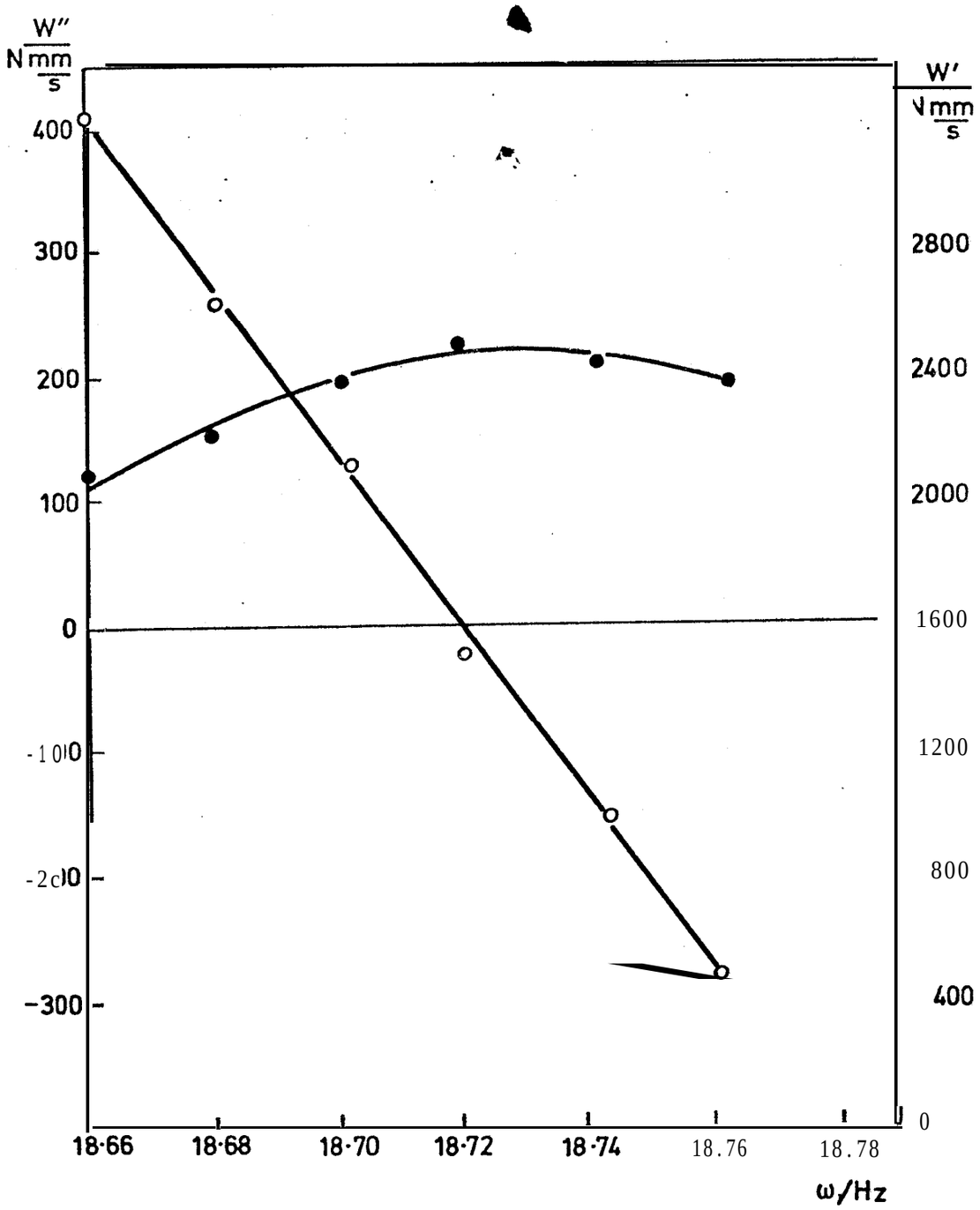

FIGURE 41

TRANSVERSE MODE COMPLEX POWER CHARACTERISTICS

● IN-PHASE POWER W'
o QUADRATURE POWER W"
NORMAL MODE RESPONSE VECTOR ≐ 1.32 $\begin{bmatrix} 1.61 \\ 1 \end{bmatrix}$ mm AT A NORMAL MODE FREQUENCY OF 18.72 Hz

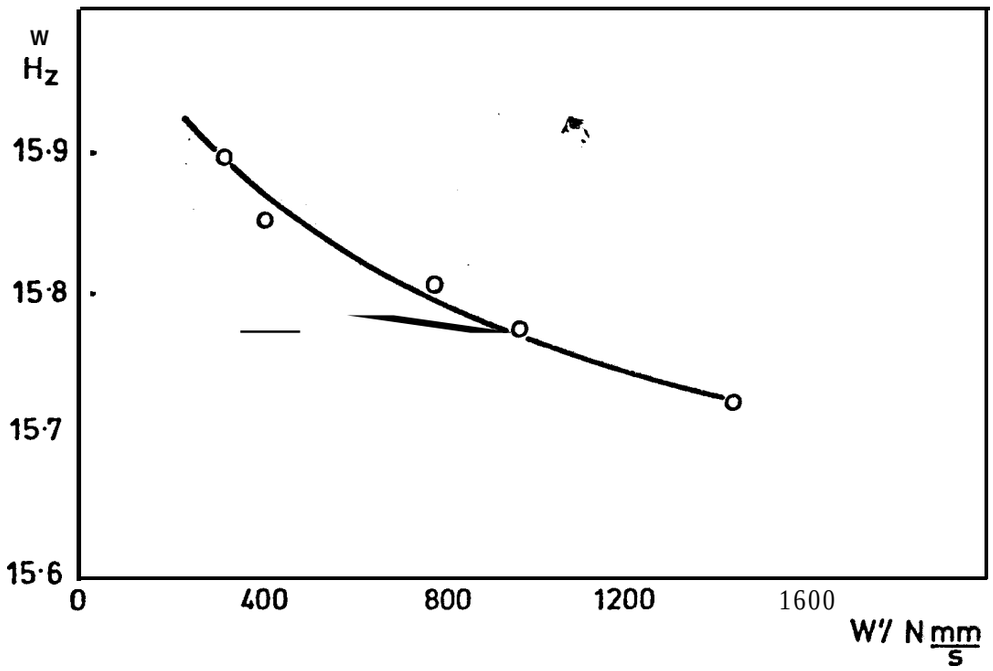

FIGURE: 42

REDUCTION IN TORSIONAL NORMAL MODE FREQUENCY WITH INCREASING POWER INPUT

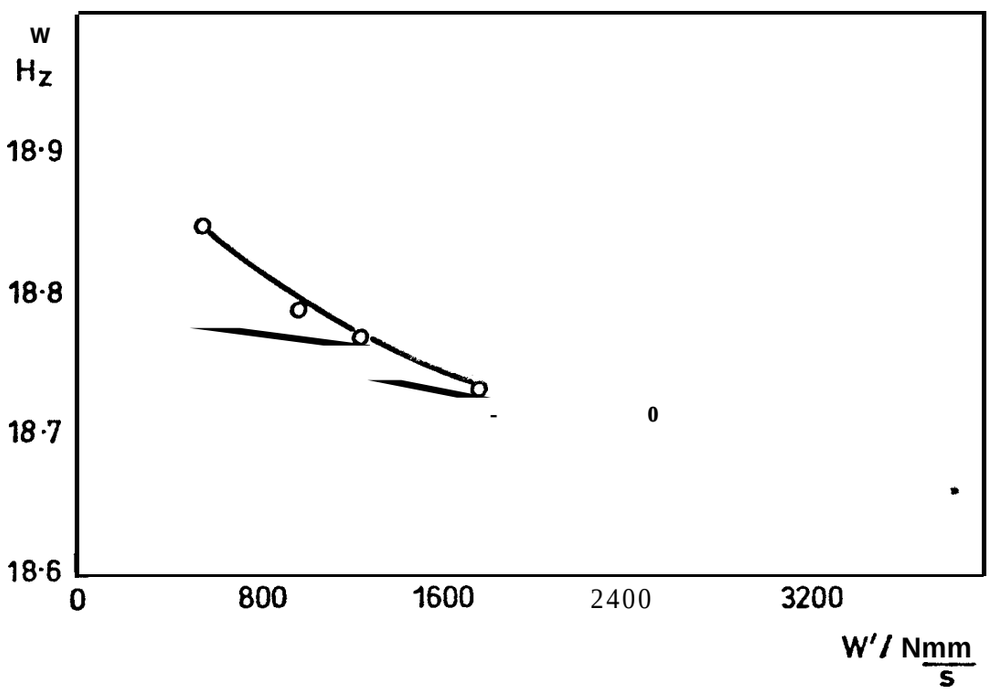

FIGURE 43

REDUCTION IN TRANSVERSE NORMAL MODE FREQUENCY WITH INCREASING POWER INPUT

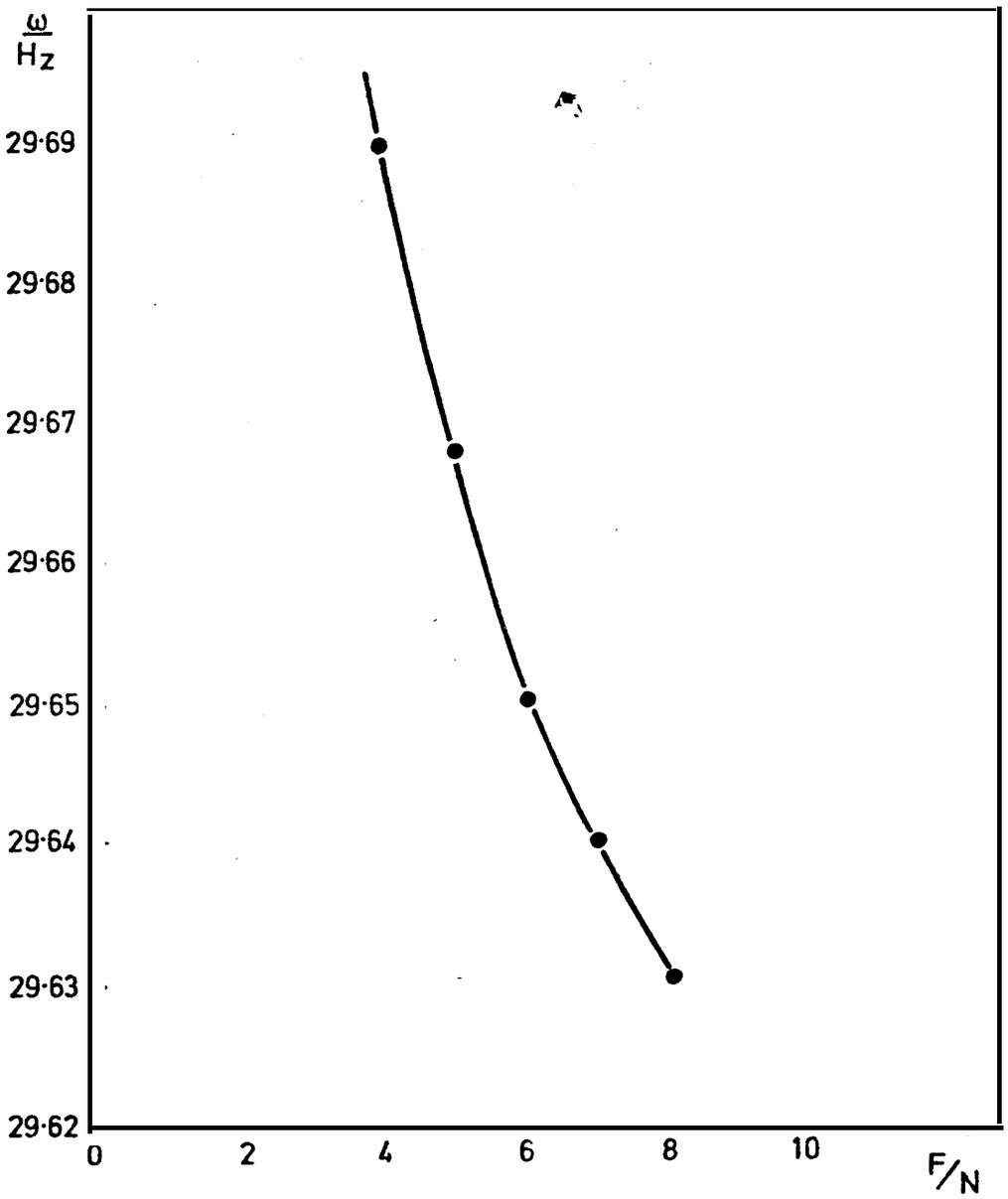

FIGURE 44

RESULTS OF ANALOG SIMULATION SHOWING REDUCTION IN THE NATURAL FREQUENCY OF A S.D.O.F. SYSTEM WITH COULOMB FRICTION FOR INCREASING INPUT FORCE.

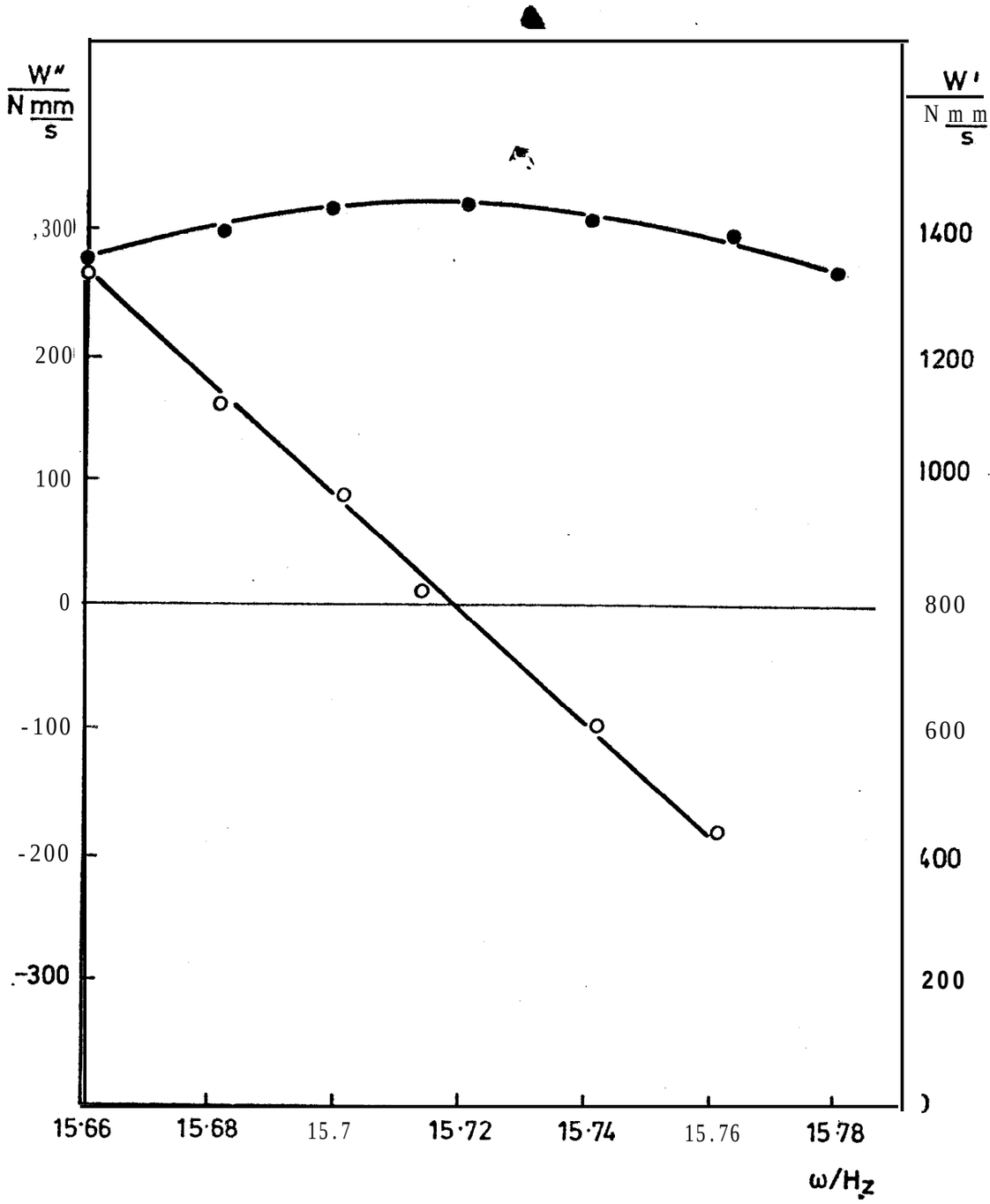

FIGURE 45

TORSIONAL MODE COMPLEX POWER CHARACTERISTICS AS A FUNCTION OF THE EXCITATION FREQUENCY

● IN-PHASE POWER W'
o QUADRATURE POWER W"
NORMAL MODE RESPONSE VECTOR = 1.44 $\begin{bmatrix} 1.01 \\ -1 \end{bmatrix}$ mm AT A NORMAL MODE FREQUENCY OF 15.72 Hz

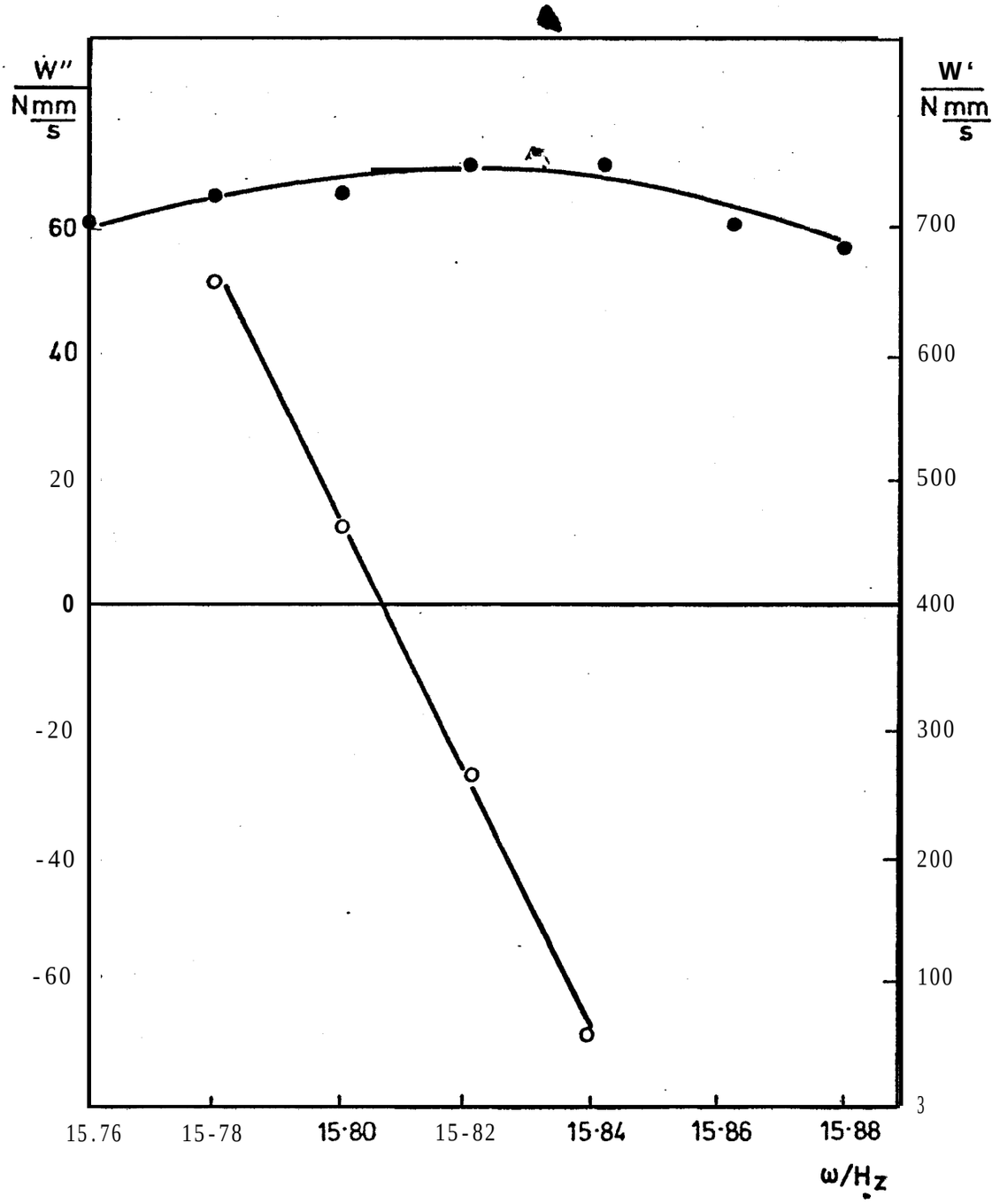

FIGURE 46

TORSIONAL MODE COMPLEX POWER CHARACTERISTICS

• IN-PHASE POWER W'
o QUADRATURE POWER W"
NORMAL MODE RESPONSE VECTOR = 0.88 $\begin{bmatrix} 1.04 \\ -1 \end{bmatrix}$ mm AT A
NORMAL MODE FREQUENCY OF 15.81 Hz

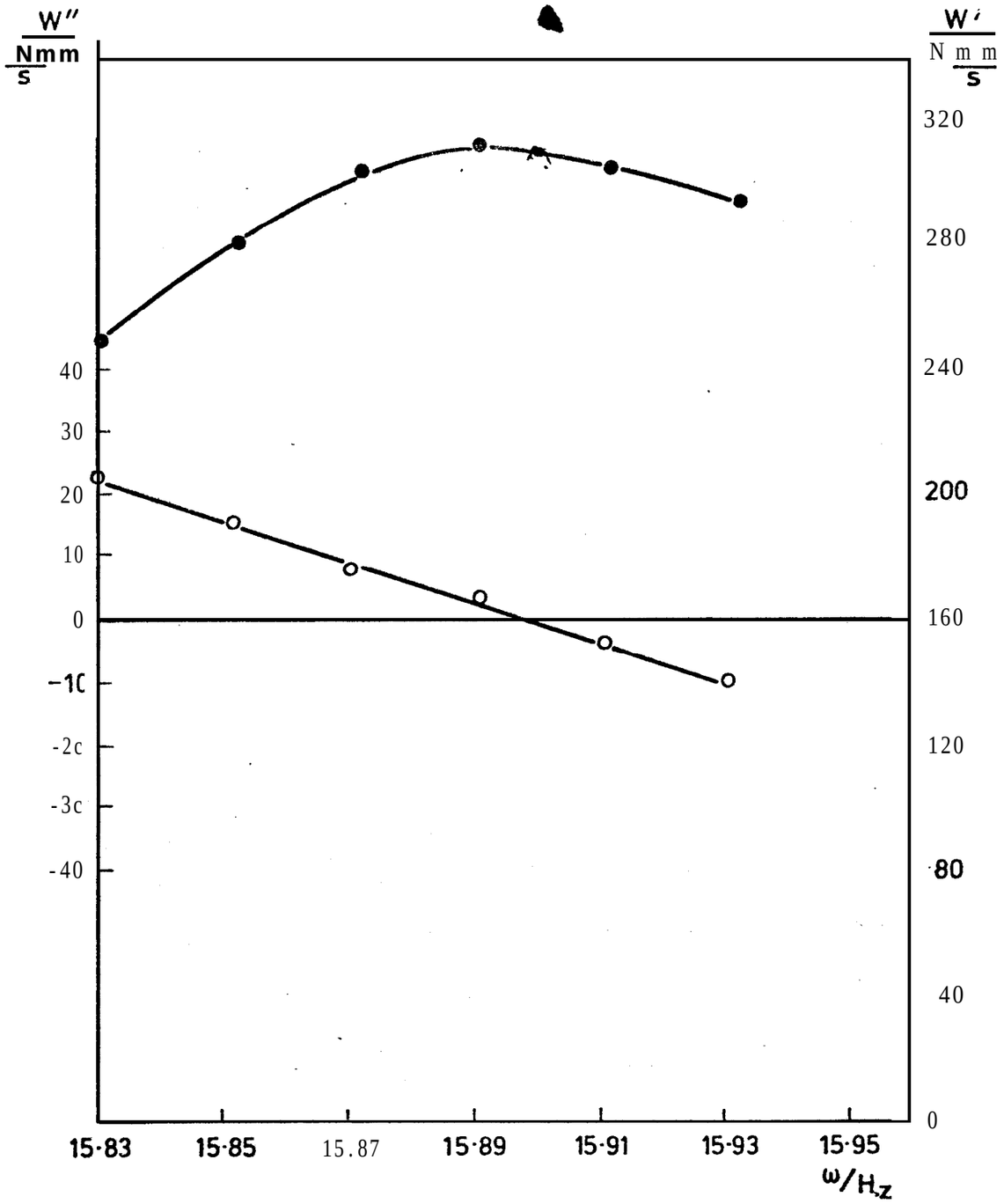

FIGURE 47

TORSIONAL MODE COMPLEX POWER CHARACTERISTICS

● IN-PHASE POWER W'
o QUADRATURE POWER W''
NORMAL MODE RESPONSE VECTOR = 0.45 $\begin{bmatrix} 1.0 \\ -1 \end{bmatrix}$ mm AT A
NORMAL MODE FREQUENCY OF 15.9 Hz

Figure 42 shows the same trend for the torsional normal mode frequency for increasing input power levels as those of the transverse mode of 6.4.1 which of course was expected.

6.5 VECTOR PLOTS WITH COULOMB FRICTION

In Section 6.4.1 of Chapter 6 the theoretical analysis of a single degree-of-freedom system with Coulomb friction shows that when the response is plotted as a vector plot the result no longer represents a circular locus (Figure 32).

Figure 48 shows the experimental results from one of the tests of Section 6.4.1 plotted as a vector plot together with the theoretical curve from equations (146) and (147).

The close similarity between these results confirms the theoretical predictions.

6.6 DETERMINATION OF THE COULOMB FRICTION FORCE LEVEL

From the experimental results of the normal mode shapes and the power absorbed at the normal mode frequency of each mode for various levels of input powers, equation (176) could be applied.

The in-phase power at the normal mode frequency was determined. This, together with the corresponding overall change in the level of the mode shape was plotted in the form of equation (176) and is shown on Figure 49.

The intercepts of the ordinate on Figure 49 represent the elements $\underset{\sim}{F}_i$ of the frictional damping matrix and the slopes represent the linear hysteretic damping factors of each mode of vibration.

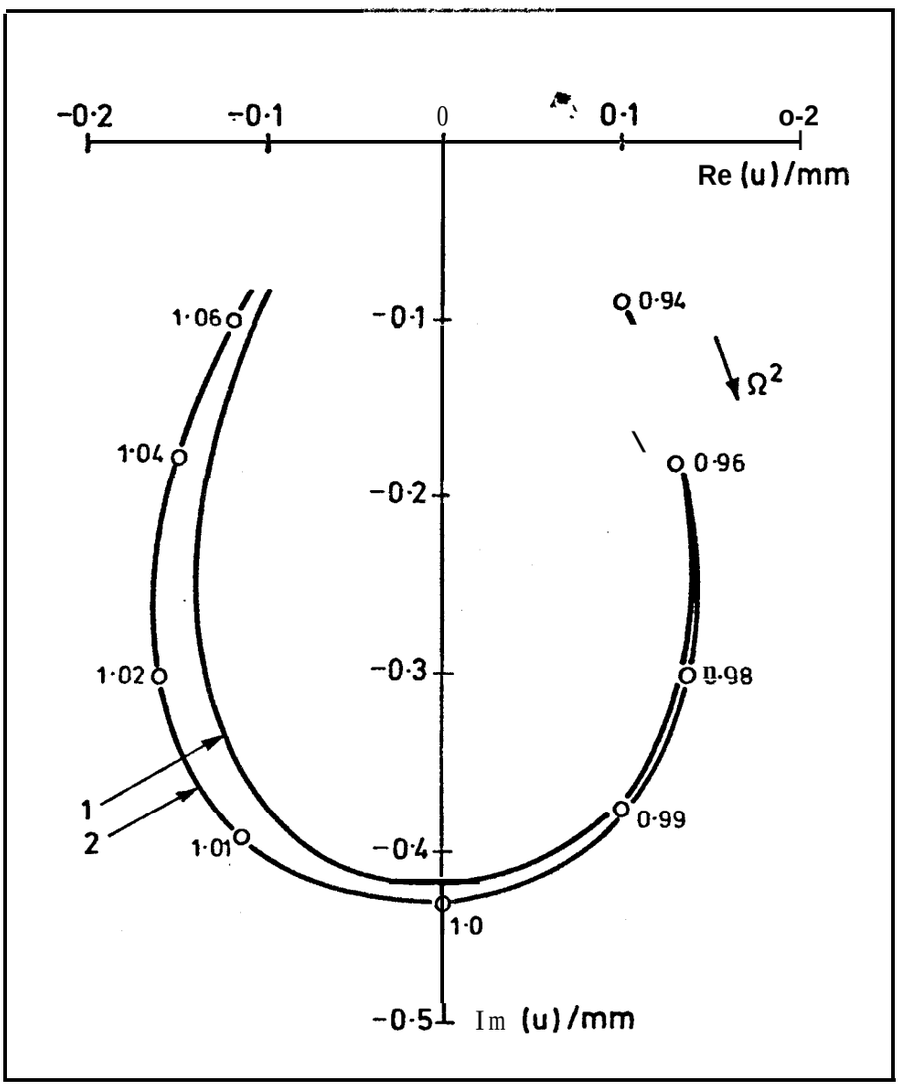

FIGURE 48

SINGLE DEGREE-OF-FREEDOM SYSTEM VECTOR PLOT WITH COULOMB FRICTION

CURVE 1 IS PLOTTED FROM EQUATIONS (146) **AND (147) WITH** 6, r and **F/k OBTAINED FROM THE EXPERIMENTAL RESULTS OF CURVE 2.**

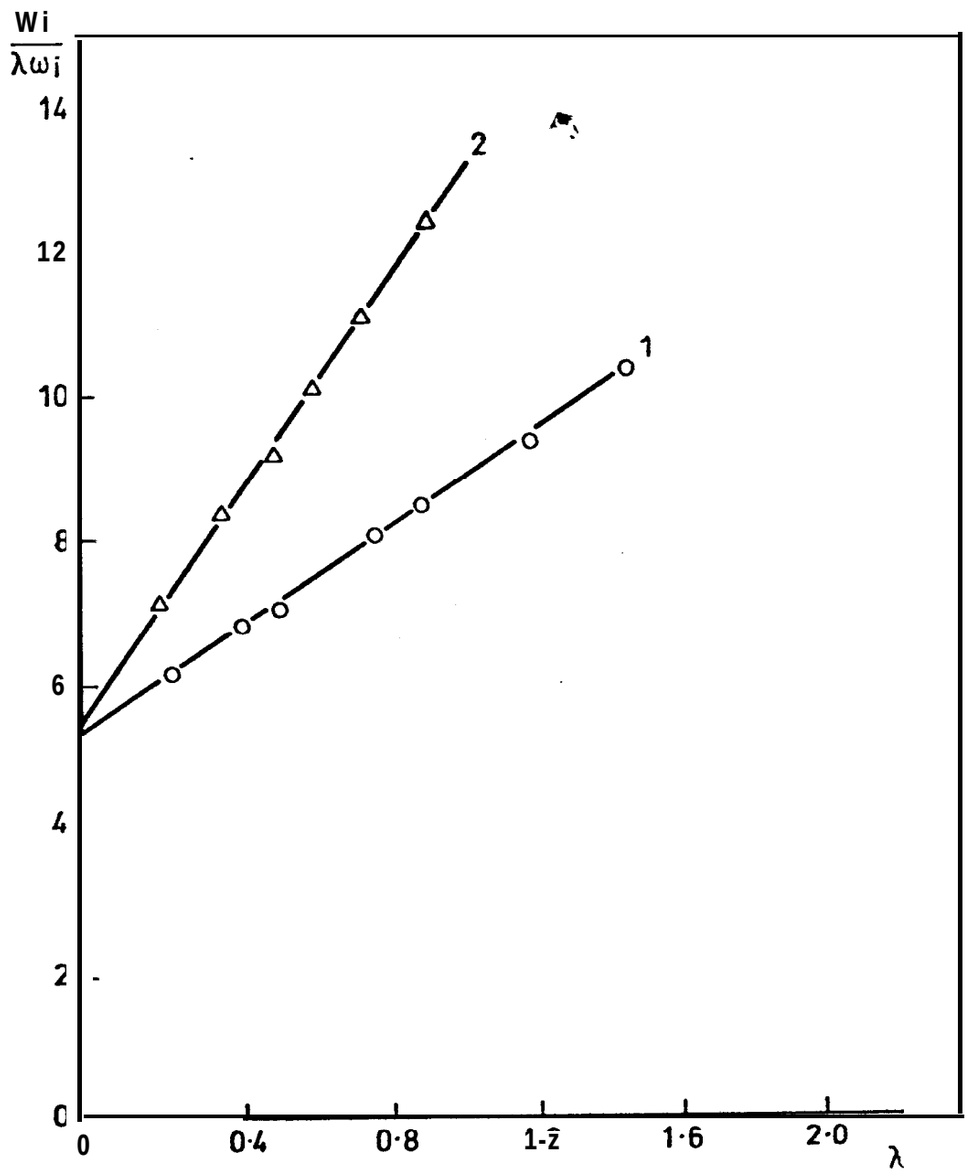

FIGURE 49

EXPERIMENTAL MODAL INPUT POWERS PLOTTED ACCORDING TO EQUATION (176) AS A FUNCTION OF THE SCALAR CHANGE IN THE MODE SHAPE

1 – **TORSIONAL MODE**
2 – **TRANSVERSE MODE**

The magnitude of the Coulomb friction force is readily obtained from either value of the intercepts with the aid of equation (178) since the normalised mode shapes were:

$$\underset{\sim}{v}_1{}^t = [1.0, 1.0], \quad \underset{\sim}{v}_2{}^t = [1.0, -1.01$$

and hence from equation (178):

$$F_i = \frac{4q}{\pi} \quad \ldots\ldots\ldots\ldots\ldots \quad (189)$$

since the Coulomb element was grounded and thus q can be evaluated directly.

Table 6.1 shows the values of the magnitude of the Coulomb friction force determined from the intercepts and equation (189) for each mode together with the actual friction force level determined from the quasi-static tests.

6.7 TRANSIENT TEST RESULTS WITH COULOMB FRICTION

During the normal mode tests a series of transient tests were carried out to investigate the purity of the normal modes and the behaviour of the transient response of a system with Coulomb friction.

Figures 50 and 51 show the transient response in the transverse and torsional modes respectively when the exciters were switched to open circuit.

The quality of the normal mode excitation can be observed by the fact that very little beating is apparent in either response. The linear decay of each trace represents the Coulomb friction and the remaining exponential type decay represents the damping, which continues when relative vibration occurs as a result of the motion at the location of the Coulomb friction element being zero. Striking

examples of similar effects are given in the paper by Haidl (53), who carried out tests on a model of a torsional system with Coulomb friction.

Method of Evaluation		Coulomb Friction Force Level (N peak-to-peak)
Normal Mode Power Curve (Fig. 57)	Transverse Mode	4.4
	Torsional Mode	4.16
Quasi-Static Tests		4.5

TABLE 6.1

Coulomb Friction Force Levels Obtained from the Power Input to a Mode Compared to the Actual Friction Force Level Measured Directly from Quasi-static Tests

Method of Evaluation		Coulomb Friction Force Level (N peak-to-peak)
Normal Mode Power Curve (Fig. 57)	Transverse Mode	4.4
	Torsional Mode	4.16
Quasi-Static Tests		4.5

TABLE 6.1

Coulomb Friction Force Levels Obtained from the Power Input to a Mode Compared to the Actual Friction Force Level Measured Directly from Quasi-static Tests

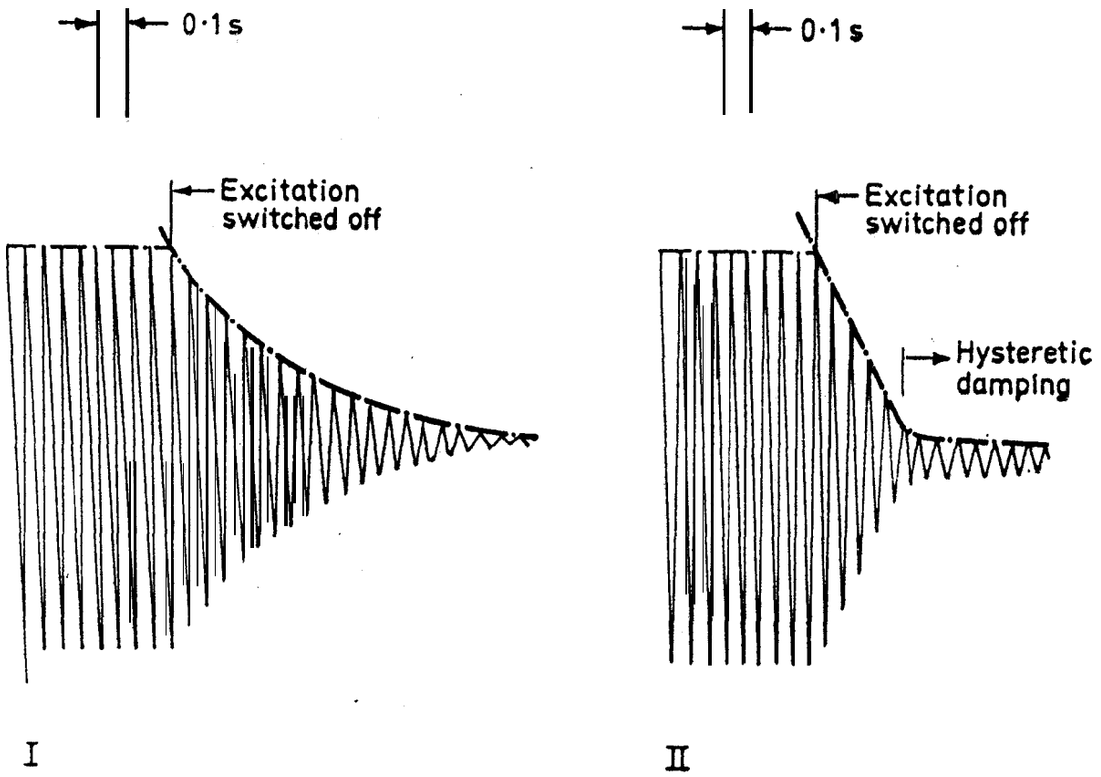

FIGURE 50

TRANSVERSE MODE TRANSIENT RESPONSES (EXCITERS SWITCHED TO OPEN-CIRCUIT)

= WITH NO COULOMB FRICTION (HYSTERETIC DAMPING ONLY)
=I WITH COULOMB FRICTION (FRICTIONAL + HYSTERETIC DAMPING)

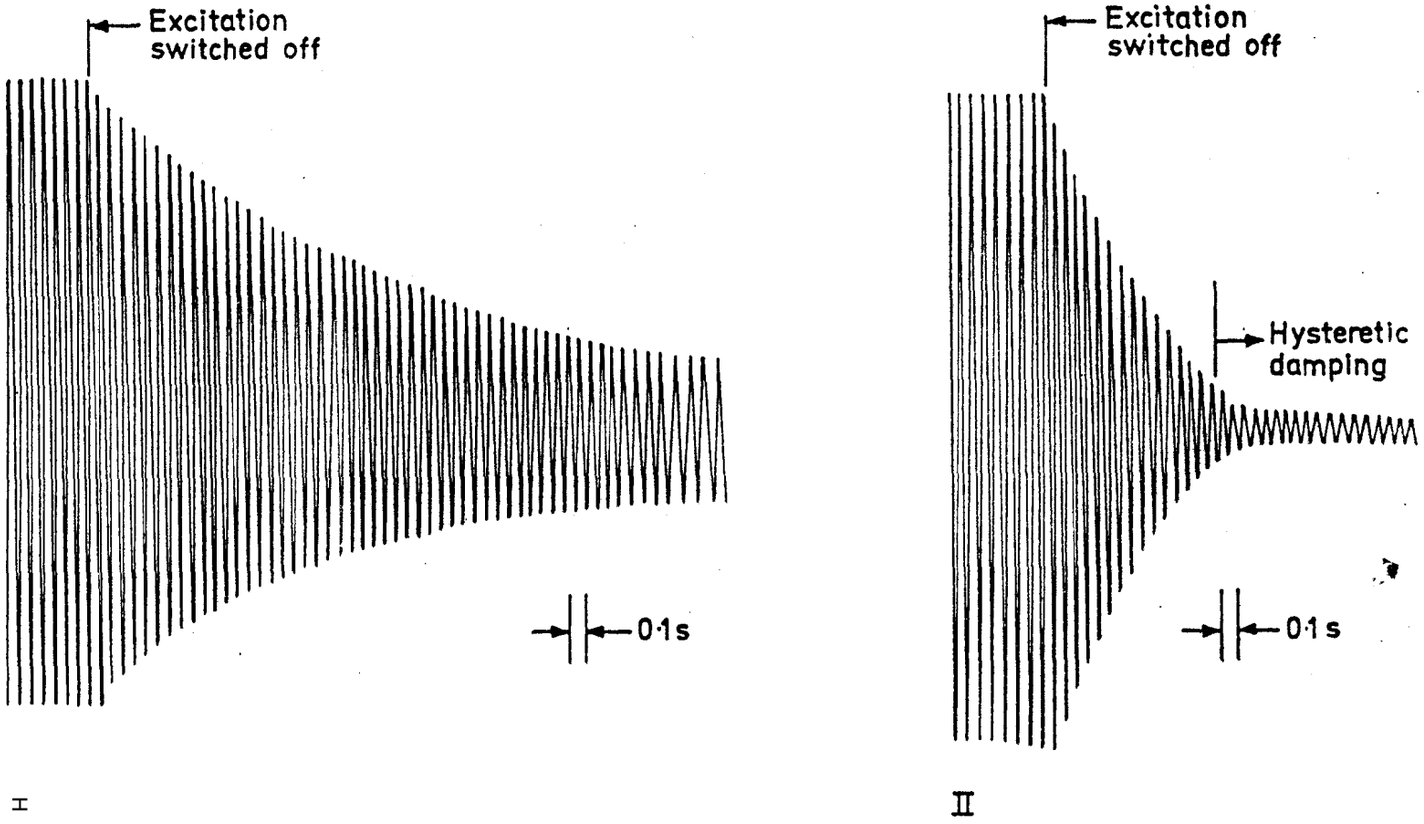

FIGURE 51

TORSIONAL MODE TRANSIENT RESPONSES (EXCITERS SWITCHED TO OPEN-CIRCUIT)

I WITH NO COULOMB FRICTION (HYSTERETIC DAMPING ONLY)
II WITH COULOMB FRICTION (FRICTIONAL + HYSTERETIC DAMPING)

6.8 DISCUSSION AND CONCLUSIONS

1. The work described in this section has shown that it is possible to identify systems which include either Coulomb friction non-linearities or non-linear stiffness characteristics on the understanding that the system can be excited in a normal mode, i.e. the response of the system is that of a single degree-of-freedom system.

2. In the case of a system with hysteretic damping and a non-linear stiffness characteristic, it has been shown that the 'normal mode frequency' and modal damping ratio can be accurately determined as long as no discontinuities (i.e. the jump phenomena) occur in the excitation frequency range. Further, the natural frequency for a given excitation level is denoted as the condition at which the quadrature power input is zero and this provides a useful criterion in experimental testing methods.

   Although the model analysed was a single degree-of-freedom system it is obvious that the techniques employed are applicable to multi degree-of-freedom systems which can be excited in their normal modes using multi-point excitation methods.

3. For a non-linear system which has only a single Coulomb friction element and hysteretic damping it has been shown that not only can the magnitude of the frictional force be evaluated, the actual location of the non-linear element within the system can be obtained.

   In the case of more than one Coulomb friction element, it is necessary to have a *priori* knowledge regarding the location of these non-linearities in order that their complete characteristics can be evaluated.

4. The application of complex power techniques to the frequency response testing of both linear and non-linear systems appears to offer considerable advantages over other established techniques such as the vector plot since no extra experimentation is required, it actually requires fewer frequency increments to produce the necessary plots, and errors in the derived modal properties due to non-linearities are minimised.

5. The techniques developed in this section apply only to systems where the damping, besides the Coulomb damping, is assumed to be linear and the elastic elements are assumed linear.

6. The results of the experimental programme gave very encouraging results and showed that, for the system tested, a high degree of accuracy is possible in the identification of systems with Coulomb friction non-linearities. Further, the use of multi-point excitation methods has allowed non-linear systems to be identified which would not have been possible using single-point modal testing methods.

SUMMARY OF CONCLUSIONS

The three sections of work described in this dissertation are summarised below. These are abridged conclusions taken from the detailed conclusions given at the end of each section.

1. The harmonic distortion of the input force signal to a lightly damped system is primarily due to the non-linear magnetic field characteristics of the electro-dynamic vibration exciter. These non-linearities are square-law in nature resulting in significant second harmonic distortion of the force input signal at the test structure resonance condition. It has been shown that harmonic distortion can be minimised if $k' << 2\zeta$, where k' is the ratio of the vibration exciter stiffness to the structure modal stiffness.

2. With lightly damped modal structures, there is a large variation in the magnitude of the input force in the region of the test structure resonance. This is due to the forces arising from the exciter mass and stiffness characteristics and is independent of the amplifier output impedance.

3. The main factor which contributes to modal interaction of complex structures is the closeness of the natural frequencies of adjacent modes. It has been shown that if the frequency ratio of adjacent modes is greater than 1.5, then in all practical terms the modes of structurally damped systems can be considered uncoupled, even if the magnitude of the off-diagonal terms of the damping matrix are comparable to the leading diagonal terms.

4. If a multi degree-of-freedom system can be classified as proportionally damped, then the excitation vector

does not have to conform to a normal mode excitation vector in order to determine the modal damping ratio and resonant frequency from a vector plot.

5. For non-linear lumped parameter multi degree-of-freedom systems which have only a single Coulomb friction element and hysteretic damping, the location of the element and the magnitude of the Coulomb frictional force can be evaluated by determining the power input to excite a normal mode of the system.

   For systems with more than one Coulomb friction element, *a priori* knowledge of their location is required in order to fully identify their characteristics.

6. In the case of systems with hysteretic damping and a non-linear stiffness characteristic, the measurement of the complex power required to excite a normal mode allows accurate determination of the resonant frequency and modal damping ratio, provided no discontinuities occur in the response of the system.

7. Although current trends in modal testing methods are emphasising post-measurement analysis techniques, the identification of non-linear structures has, until now, been very limited. The techniques presented for identifying non-linear structures employ the rather involved multi-point modal testing method. However, on-line computer control of these procedures is now reasonably well established (82) which reduces the intensive experimental work, and may well justify the continued use of multi-point testing methods for both complex linear and non-linear structures.

SUGGESTIONS FOR FURTHER WORK

The first section of the dissertation indicated that problems can be encountered during the forced vibration testing of lightly damped structures due to harmonic distortion. However, no attempt was made to establish where a structure should be excited in order that these effects would be minimised.

For example, if one were to excite a beam element at a position which offered low flexibility then the amplitudes of vibration for a given input force level would be smaller than if the excitation point were at a position adjacent to the most flexible region of the element, with the result that the harmonic force distortion would be reduced. This could be extended to plate and shell elements where the damping is small and where judicious choice of excitation positions could be beneficial.

The second section of work, which was concerned with the effects of modal interaction, was based upon a theoretical model and digital simulation, no experimental work was carried out to support the conclusions of this section. The author feels that this is a very important area which needs experimental justification. This would require a structure which would have controlled known levels of damping at pre-determined locations. Thus the damping distribution is known *a priori* and hence tests could be carried out to ascertain the effects of this on the ability to excite the normal modes of vibration.

Finally the remaining section of the work, which was concerned with the identification of non-linear structures, by measuring the power input to a normal mode, is only a beginning in this area. The method developed was applied to a very simple structure which was devoid of the complexities of, say, an aircraft wing. In order to fully establish the advantages, or disadvantages, of the proposed

method an experimental programme on a more complex non-linear structure should be carried out.

Further, to improve the efficiency of applying the method to a complex structure, an on-line identification method, based on measured data from single point frequency sweep tests, should be developed which would allow the appropriate force distributions necessary to excite the normal modes with a given frequency range to be more effectively obtained. This would greatly enhance the application of the complex power method and hence the identification procedures of complex linear and non-linear structures.

British Aerospace have expressed an interest in these latter proposals and these now form part of a further research contract which, it is hoped, will result in a more cost effective and satisfactory approach to the normal mode testing of military'aircraft,

REFERENCES

1. Bruel and Kjaer 1960
Technical Review, 3
Vibration Exciter Characteristics.

2. C M Harris and C E Crede 1961
McGraw-Hill Book Co., New York
Shock and Vibration Handbook.

3. G A Taylor, D R Gaukroger and C W Skingle 1967
R.A.E. Technical Report 67211
M.A.M.A.: A Semi-Automatic Technique for Exciting the Principal Modes of Vibration of Coupled Structures.

4. P J Holmes and R G White 1972
Journal of Sound and Vibration 25, 217-243
Data Analysis Criteria and Instrumentation Requirements for the Transient Measurement of Mechanical Impedance.

5. L R Burrow 1964
Test Engineering 16-19
Tracking Filters Standardise Sinusoidal Vibration Tests.

6. D J Ewins 1966
Ph.D. Dissertation, University of Cambridge
The Effects of Detuning upon the Vibration of Bladed Discs.

7. R C Lewis and D L Wrisley 1950
Journal of Aeronautical Sciences, 17 -11, 705-722.
A System for the Excitation of Pure Natural Modes of Complex Structures.

8. M G Say 1971
Pitman Press, first edition
Introduction to the Unified Theory of Electro-magnetic Machines.

9. G W Asher 1958

Institute of Aeronautical Science Proceedings, Specialists Meeting on Dynamics and Aeroelasticity, Fort Worth, 69-76

A Method of Normal Mode Excitation Utilizing Admittance Measurements.

10. H G Natke 1969

V.F.W. Report EV-B 11

Description of a Vibration Test Unit and Its Use for the Third Stage of Europa 1.

11, J Cox 1972

British Aircraft Corporation Internal Report No. TN.3207

Development of the Ground Resonance Test Equipment for the Measurement of Generalised Inertias.

12. D J Ewins 1975-76

Journal of the Society of Environmental Engineers 14 -4 December 1975: 15 -1 March 1976: 15 -2 June 197%

Measurement and Application of Mechanical-Impedance Data Part I: Introduction and Ground Rules 3-12, Part II: Measurement Techniques 13-21, Part III: Interpretation and Application of Measured Data 22-32.

13. J H Hibbert 1972

Ph.D. Dissertation, University of Salford

The Dynamics and Design of Shear-Film Auxiliary Mass Dampers.

14. T K Hasselman 1972

A.I.A.A. Journal 10 -4, 526-527

Method for Constructing a Full Modal Damping Matrix from Experimental Measurements.

15. P Santini, A Castellani and A Nappi 1977

A.G.A.R.D. Report No. 663

An Introduction to the Problem of Dynamic Structural Damping.

16. B J Lazan 1968
Oxford Pergamon Press
Damping of Materials and Members in Structural Mechanics.

17. C W Bert 1973
Journal of Sound and Vibration 29, 129-153
Material Damping: An Introductory Review of Mathematical Models, Measures and Experimental Techniques.

18. A L Kimball and D E Love11 1927
Physical Review Series 2, 30, 948-959
Internal Friction in Solids

19. G K Hobbs 1971
AIAA/ASME 12th Structures, Structural Dynamics and Materials Conference, Anaheim, California, Paper 71-349
Methods of Treating Damping in Structures.

20. W W Soroka 1949
Journal of Aeronautical Sciences 16, 409-410
Note on the Relations Between Viscous and Structural Damping Coefficients.

21. N 0 Myklestad 1952
Journal of Applied Mechanics 19, 284-286
The Concept of Complex Damping.

22. T J Reid 1956
Journal of the Royal Aeronautical Society 60, 283
Free Vibration and Hysteretic Damping.

23. T K Hasselman 1974
AIAA/ASME/SAE 15th Structures, Structural Dynamics and Materials Conference, Las Vegas, Nevada, Paper 74, 387
Damping Synthesis from Substructure Tests.

24. P Lancaster 1960
Journal of the Royal Aeronautical Society 64, 229
Free Vibration and Hysteretic Damping.

25. Fokker-VFW Space Division Report No. ESRO CR(P)-539
Survey of Data on Damping in Spacecraft Structures.

26. A Craggs and M R North 1966
M.I.R.A Report No. 1966/6
A Study of the Frequency Response Curves of a System with Close Natural Frequencies by Means of an Analog Computer.

27. C C Kennedy and C D P Pancu 1947
Journal of Aeronautical Sciences 14, 603-625
Use of Vectors in Vibration Measurement and Analysis.

28. T K Caughey 1960
Journal of Applied Mechanics, Transactions of the A.S.M.E. 60, 269-271
Classical Normal Modes in Damped Linear Dynamic Systems.

29. Modal Survey 1976
Lectures and Discussions held at E.S.T.C.E., Noordwijk, The Netherlands.

30. Lord Rayleigh 1945
Dover Publications, New York.
Theory of Sound, Volume 1.

31. K A Foss 1956
Massachusetts Institute of Technology Report No. 25-30
Co-ordinates which Uncouple the Equations of Motion of Damped Linear Systems.

32. T K Caughey and M E J O'Kelly 1965
Journal of Applied Mechanics, Transactions of the A.S.M.E. 32, 583-588
Classical Normal Modes in Damped Linear Dynamic Systems.

33. L Y Bahar 1978

Journal of Applied Mechanics, Transactions of the A.S.M.E. 45, 225-226

Discussion on "A Theorem on the Free Vibration of Damped Systems."

34. I Fawzy 1977

Journal of Applied mechanics, Transactions of the A.S.M.E. 44, 132-134

A Theorem on the Free Vibration of Damped Systems.

35. E Sloane and B McKeever 1975

Society of Automotive Engineers, National Aerospace Engineering and Manufacturing Meeting, Los Angeles, Paper ho. 751067

Modal Survey Techniques and Theory.

36. A Klosterman and R Zimmerman 1975

Society of Automotive Engineers, National Aerospace Engineering and Manufacturing Meeting, Los Angeles, Paper No. 751068

Modal Survey Activity via Frequency Response Functions.

37. D Küchemann et al

Pergamon Press, New York

Progress in Aerospace Sciences, 4.

38. E Breitbach 1973

Proceedings E.S.R.O. Testing Symposion, E.S.R.O. SP-99, 519-528

A Semi-Automatic Modal Survey Test Technique for Complex Aircraft and Spacecraft.

39. V Marples 1973

Journal of Sound and Vibration 31 -1, 105-117

The Derivation of Modal Damping Ratios from Complex-Plane Response Plots.

40. A L Klosterman 1971

Ph.D. Dissertation, University of Cincinnati

On the Experimental Determination and Use of Modal Representations of Dynamic Characteristics.

41. D J Ewins 1978
Imperial College, London, Internal Report No. 78005
Whys and Wherefores of Modal Testing.

42. G de Vries 1964
Recherche Aerospatiale 102, 43-49
The Problem of Appropriation of the Excitation Forces in Vibration Testing. N.A.S.A. Translation No. TTF-348.

43. R C Stroud, S Smith and G A Hamma 1976
Shock and Vibration Bulletin 5 -46, 153-175
Modal Test and Analysis.

44. G A Hamma, S Smith and R C Stroud 1976
Society of Automotive Engineers, Paper No. 760872
An Evaluation of Excitation and Analysis Methods for Modal Testing.

45. E L Leppert, S H Lee, F D Day et al 1976
Society of Automotive Engineers, Paper No. 760879.
Comparison of Modal Test Results: Multi-point Sine Versus Single-point Random.

46. M Richardson and J Kniskern 1976
Society of Automotive Engineers, Paper No. 760875
Identifying Modes of Large Structures from Multiple Input and Response Measurements.

47. R W Mustain 1976
Society of Automotive Engineers, Paper No. 760870
Survey of Modal Vibration Test/Analysis Techniques.

48. R Dat 1975
O.N.E.R.A. Technical Report No. 493
Structural Vibration Test Methods Implemented at O.N.E.R.A.

49. P Ibáñez 1976
Society of Automotive Engineers, Paper No. 760873
Force Appropriation by Extended Asher's Method.

50. J P Den Hartog 1931
Transactions of the American Society Mechanical Engineers, 53, 107-115
Forced Vibrations with Combined Coulomb and Viscous Friction.

51. E Breitbach 1974
D.F.V.L.R. Technical Report No. DLP-FB73-30 E.S.R.O. Translation No. TT-121
Aircraft Flutter Simulation by Means of an Analog Computer with Special Regard to Structural Non-linearities.

52. J J D'Azzo and C H Houpis 1966
McGraw-Hill Book Company, 2nd Edition
Feedback Control System Analysis and Synthesis.

53. G Haidl 1976
43rd Meeting of the Messerschmitt-Bolkow-Blohm (M.B.B.) Report No. UFE 1273(0), Structures and Materials Panel of A.G.A.R.D., London
Non-linear Effects in Aircraft Ground and Flight Vibration Tests.

54. R Dat, R Tretout and J M Lafont 1975
Recherche Aerospatiale 3 -166, 169-174
Vibration Test of a Structure with Dry Friction.

55. H Poincaré 1957
Dover Publications Inc., New York.
Reprint of: Les Methodes Nouvelles de la Mecanique Celeste.

56. B Van Der Pol 1927
Philosophical Magazine
Forced Oscillations in a System with Non-linear Resistance.

57. G Duffing, 1918
F. Vieweg u. Sohn
Erzqungene Schwingungen bei Veranderlicher Eigen Frequenz.

58. N Kryloff and N Bogoliuboff 1947
Translation from the Russion by S. Lefschetz, Annals of Mathematical Studies 11
Introduction to Non-linear Mechanics.

59. B N Agrawal 1975
Shock and Vibration Digest 7 -8, 77-87
Non-stationary and Non-linear Vibration Analysis and Its Application.

60. F S Tse, I Morse and R Hinkle 1978
Allyn and Bacon, London, 2nd Edition
Mechanical Vibrations, Theory and Applications.

61. H D Grief 1953
Transactions of the American Institute of Electrical Engineers, 2, 243-248
Describing Function Method.of Servomechanism Analysis Applied to Most Commonly Encountered Non-linearities.

62. S R Timoshenko, D H Young and W Weaver Jr. 1974
John Wiley and Sons, 4th Edition
Vibration Problems in Engineering.

63. G C K Yeh 1966
Journal of the Acoustical Society of America 39, 14-24
Forced Vibrations of a Two Degree-of-Freedom System with Combined Coulomb and Viscous Damping.

64. V G Podolskii 1975
Mechanics of Solids 10 -3, 16-22
Qualitative Theory of Forced Periodic Vibrations of Structures with Account for Dry Friction.

65. L Pust 1971

Proceedings of the Third World Congress for the Theory of Machines and Mechanisms, Kupari, Yugoslavia. Volume A, Paper A-15, 169-182.

The Influence of Non-linear Damping on the Non-symmetry of the Dynamic Compliance Matrix of Vibration Systems.

66. A Tondl 1973

Acta Technica C.S.A.V. 18 -2, 166-179

Some Properties of Non-linear System Characteristics and Their Application to Damping Identification.

67. L Pust 1974

Proceedings of the Fourth World Congress for the Theory of Machines and Mechanisms, Yugoslavia, 16-24

Properties of the Dynamic Compliance Matrix.

68. E Bonneau 1969

La Recherche Aerospatiale 130, 45-51

Determination of the Vibratory Characteristics of a Structure from the Expression of the Complex Power Supplied.

69. J Baticle 1971

Proceedings of the Third World Congress for the Theory of Machines and Mechanisms, Kupari, Yugoslavia. Volume A, Paper A-4, 27-32

Measuring Processes of Vibratory Characteristics of Mechanical Structures.

70. Z M Levina 1967

Proceedings of the Eight International M.T.D.R. Conference 737-755

Research on the Static Stiffness of Joints in Machine Tools.

71. M Polacek and Z Vavra 1967

Proceedings of the Eight International M.T.D.R. Conference 1127-1138

The Influence of Different Types of Guideway on the Static and Dynamic Behaviour of Feed Drives.

72. R G White 1971

Journal of Sound and Vibration 16 -2, 255-267

Effects of Non-linearity Due to Large Deflections in the Resonance Testing of Structures.

73. N H Hanna and S A Tobias 1969

International Journal of Machine Tool Design and Research, 9, 293-307

The Non-linear Dynamic Behaviour of a Machine Tool Structure.

74. R E D Bishop and G M L Gladwell 1963

Philosophical Transactions of the Royal Society Series A, 255, 241-280.

An Investigation into the Theory of Resonance Testing.

75. M Rades 1976

Shock and Vibration Digest 8 -2, 73-88

Methods for the Analysis of Structural Frequency Response Measurement Data.

76. A Tondl 1971

Journal of Sound and Vibration 17 -3, 429-436

Letters to the Editor on 'Effects of Non-linearity Due to Large Delfections in the Resonance Testing of Structures'.

77. J C West 1960

English Universities Press Limited

Analytical Techniques for Non-linear Control Systems.

78. D J Mead 1958

A.R.C. Rep. 19870

The Internal Damping Due to Structural Joints and Techniques for General Damping Measurement.

79. E J Roark 1965

McGraw-Hill Book Company, New York, Fourth Edition

Formulas for Stress and Strain.

80. J Case and A H Chilver 1971
Edward Arnold Publishing Company
Mechanics of Solids

81. G R Tomlinson 1979
Journal of Sound and Vibration 63 -3, 1 - 14
Force Distortion in Resonance Testing of Structures with Electra-dynamic Vibration Exciters.

82. J T Matthews and B Gabri 1979
SEECO Conference, London
Normal Mode Testing using Multiple Exciters under Digital Control.

APPENDIX I

The physical model of an electro-dynamic exciter can be considered simply as a resistor rkpresenting the coil with an additional voltage drop due to the velocity of the coil moving through the magnetic field of the permanent magnet. The mechanical sub-system is merely a mass and a spring driven by a force proportional to the current, damping effects due to the flexure stiffness hysteresis and the rubber dust cap being ignored. The basic equations of motion are:

$$m\ddot{x} + kx = k_F i \qquad \text{(A.I.l)}$$

$$Ri + k_B\dot{x} = v\cos\omega t \qquad \text{(A.I.2)}$$

where m = effective armature mass
k = flexure stiffness
k_F = force current constant
k_B = back emf constant
i = armature current
v = applied voltage at frequency ω
R = exciter coil resistance plus drive amplifier output resistance
x = armature displacement

Thus the equation of motion of the armature from A.I.l and A.I.2 is:

$$\ddot{x} + \frac{kx}{m} + \frac{k_F k_B}{mR}\dot{x} = \frac{k_F}{mR} v\cos\omega t \qquad \text{(A.I.3)}$$

Assuming that the electrical power developed in the armature is equal to the mechanical power absorbed, then:

$$k_B\dot{x}i = k_F\dot{x}i, \text{ i.e. } k_B = k_F \qquad \text{(A.I.4)}$$

and equation (A.I.3) is:

$$\ddot{x} + \frac{kx}{m} + \frac{K}{mR}\dot{x} = \frac{k_F}{mR} v\cos\omega t \qquad \text{(A.I.5)}$$

where $K = k_F k_B$

APPENDIX II

THE EFFECTS OF AN ELECTRO-DYNAMIC EXCITER ON A VIBRATING STRUCTURE

II.1 THE USE OF INPUT CURRENT AS A REFERENCE FORCE

The force necessary to vibrate a structure is produced by the current through the exciter coil. The moving elements of the exciter, namely the armature and some fraction of the flexure mass and the push-rod assembly (which incorporates the force gauge), are rigidly attached to the structure under test and as a result some of the force is used to accelerate these additional masses. If the structure under test is at resonance then the displacement of the excitation point is at quadrature to the exciting force. The additional masses of the moving elements of the exciter are in-phase with the structure but the acceleration forces of these additional masses oppose the forces arising from the effect of the flexure stiffness of the exciter. This results in the oscillator current vector not being at quadrature to the displacement of the structure at resonance. This can be explained by considering a single degree-of-freedom system excited by an electro-dynamic exciter. The model of the system under analysis is shown on Figure 3, Chapter 1.

The resultant R force applied to the structure is:

$$R = Fe^{j\omega t} - m_2\ddot{x}_2 - c_2\dot{x}_2 - k_2x_2 \quad .. \quad .. \quad (A.II.1)$$

where F is the force delivered to the moving parts of the exciter as a result of the oscillator current (which is held constant in magnitude and phase with the oscillator reference voltage). If the stiffness of the force transducer is considered to be infinite compared to the exciter and test structure stiffness the displacements within the

system are common, i.e.

$$x_2 = x_1 = x \quad .. \quad .. \quad .. \quad .. \quad .. \quad .. \quad \text{(A.II.2)}$$

The displacement of the armature (and structure) is related to the oscillator reference current by:

$$x = Xe^{j(\omega t + \psi)} \quad .. \quad .. \quad .. \quad .. \quad .. \quad \text{(A.II.3)}$$

where ψ is the phase angle between the oscillator reference current and the displacement
X is the peak amplitude of the displacement
ω is the angular frequency.

Equations (A.II.1) and (A.II.3) are expressed on a vector diagram on Figure A.II.1 and the resultant force applied to the structure is obtained as:

$$R = F\cos\omega t + m_2\omega^2 X\cos(\omega t-\psi) - k_2 X\cos(\omega t-\psi) + c_2\omega X\sin(\omega t-\psi) \quad .. \quad .. \quad .. \quad .. \quad .. \quad \text{(A.II.4)}$$

The reaction force of the structure, which will be equal and opposite to R, will be:

$$R_F = -R = m_1\omega^2 X\cos(\omega t-\psi) - k_1 X\cos(\omega t-\psi) + c_1\omega X\sin(\omega t-\psi) \quad .. \quad \text{(A.II.5)}$$

If the forces are expressed relative to the oscillator reference then at a given frequency there will be a phase angle between the force delivered from the exciter and the resultant force as a result of equation (A.II.4). Thus the vector diagram can now be drawn as shown on Figure A.II.2.

From Figure A.II.2, the resultant force applied to the structure expressed relative to the oscillator reference

is:

$$R\sin\phi = m_2\omega^2 X\sin\psi - k_2 X\sin\psi + c_2 X\omega\cos\psi \quad .. \quad (A.II.6)$$

$$R\cos\phi = m_2\omega^2 X\cos\psi + k_2 X\cos\psi - c_2\omega X\sin\psi + F \quad (A.II.7)$$

For a lightly damped single degree-of-freedom system resonance occurs when the phase angle between the resulting displacement and the applied force is 90^o, i.e. when:

$$\phi + \psi = 90^o \quad .. \quad .. \quad .. \quad .. \quad .. \quad .. \quad (A.II.8)$$

Substituting $\psi = 90 - \phi$ in equations (A.II.6) and (A.II.7) gives:

$$R\sin\phi = (m_2\omega^2 - k_2)X\cos\phi - c_2 X\sin\phi \quad .. \quad (A.II.9)$$

$$R\cos\phi = (m_2\omega^2 - k_2)X\sin\phi - c_2 X\cos\phi + F \quad .. \quad (A.II.10)$$

Multiplying equation (A.II.9) by $\cos\phi$ and equation (A.II.10) by $\sin\phi$ and rearranging gives:

$$(m_2\omega^2 - k_2)X = F\sin\phi \quad .. \quad .. \quad .. \quad .. \quad (A.II.11)$$

Denoting the exciter and structure natural frequency respectively by:

$$\omega_2^2 = \frac{k_2}{m_2}, \qquad \omega_1^2 = \frac{k_1}{m_1} \quad .. \quad .. \quad .. \quad .. \quad (A.II.12)$$

equation (A.II.11) can be written as:

$$k_2 X\left(\left(\frac{\omega_1}{\omega_2}\right)^2 - 1\right) = F\sin\phi \quad .. \quad .. \quad .. \quad .. \quad (A.II.13)$$

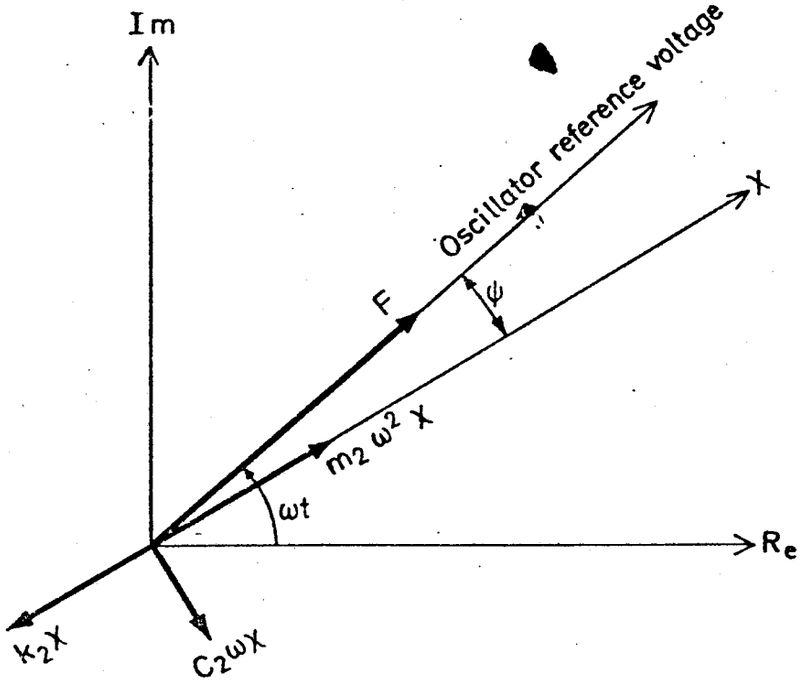

FIGURE A.II.1

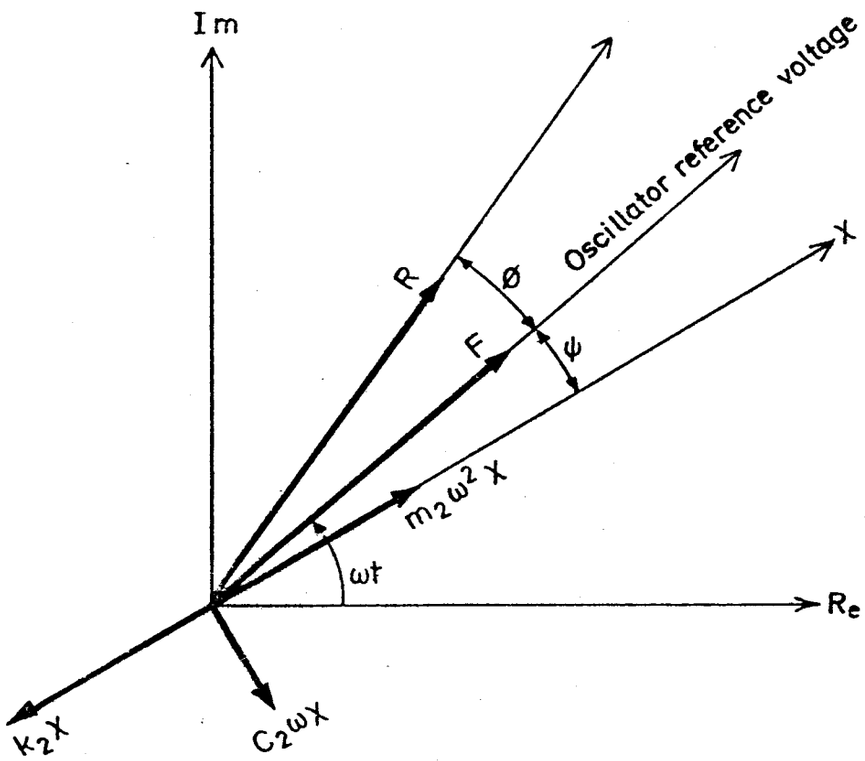

FIGURE A.II.2

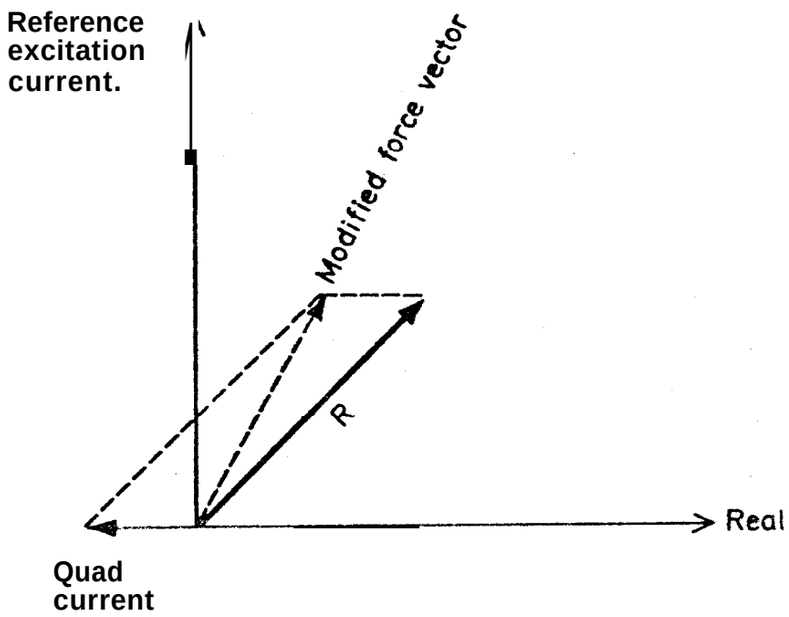
Reference
excitation
current.
Modified force vector
R
Real
Quad
current

FIGURE A.II.3

Thus the force which is applied to the structure is only in phase with the force delivered by the exciter when one or more of the following conditions arises:

(a) $\phi = 0$
(b) $\omega_1 = \omega_2$
(c) $X = 0$

Condition (a) is satisfied by adding a current at quadrature to the excitation current which modifies the force injected into the structure as shown by Figure A.II.3.

II.2 IDENTIFICATION OF A SYSTEM RESONANCE

The response of a single degree-of-freedom system with viscous damping to a single harmonic force input is given by:

$$|x| = \frac{F}{\{(k_1 - m_1\omega^2)^2 + (c_1\omega)^2\}^{\frac{1}{2}}} \quad \text{(A.II.14)}$$

where the input force F is assumed to have a constant magnitude as the frequency is varied.

Differentiating equation (A.II.14) and equating to zero for a turning point gives the frequency for maximum response as:

$$\omega^2 = \omega_n^2(1 - 2\zeta_1^2) \quad \text{(A.II.15)}$$

Substitution of (A.II.15) in (A.II.14) gives the maximum response as:

$$|x_{max}| = \frac{F/k_1}{2\zeta_1(1 - \zeta_1^2)^{\frac{1}{2}}} \quad \text{(A.II.16)}$$

If one now considers the actual system, comprising both the test system and the electro-dynamic vibration exciter, equation (A.II.14) is modified to give:

$$|x| = \frac{|F|}{\left\{\{(k_1+k_2) - (m_1+m_2)\omega^2\}^2 + (c_1+c_2)^2\omega^2\right\}^{\frac{1}{2}}} \quad \text{(A.II.17)}$$

$$\text{i.e. } |x| = \frac{|F/k_1|}{\left\{\{(1+k') - (1+m')\frac{\omega^2}{\omega_1^2}\}^2 + (2\zeta_1\frac{\omega}{\omega_1} + 2\zeta_2\frac{\omega}{\omega_2}k')^2\right\}^{\frac{1}{2}}} \quad \text{(A.II.18)}$$

The frequency at which the maximum response occurs is again given by:

$$\frac{d|x|}{d\omega} = 0$$

$$\text{i.e. } \omega^2 = \frac{\omega_n^2}{(1+m')}(1+k') - 2\omega_1^2\left(\frac{\zeta_1}{\omega_1} + \zeta_2\frac{k'}{\omega_2}\right)^2 \quad \text{(A.II.19)}$$

Putting A.II.19 in A.II.18 and simplifying gives the maximum response as:

$$|x_{max}| = \frac{|F/k_1|}{2C\omega_1\left\{\frac{\omega_1^2C^2(m'-1) + (1+k')}{(1+m')}\right\}^{\frac{1}{2}}} \quad \text{(A.II.20)}$$

$$\text{where } C = \frac{\zeta_1}{\omega_1} + \frac{\zeta_2 k'}{\omega_2} \quad \text{(A.II.21)}$$

Thus if one compares A.II.20 with A.II.16 it can be seen that by merely using the output response of the system large errors may be incurred, as the true resonant condition can only be obtained by replacing F in equation

A.II.18 with that given in equation (15), Chapter 1, and then differentiating for a turning point. This will then result in the same equation as A.II.16 which is the correct one.

The natural frequency of the combined system is given as:

$$\omega_n = \left\{\frac{k_1 + k_2}{m_1 + m_2}\right\}^{\frac{1}{2}} \quad .. \quad .. \quad .. \quad .. \quad .. \quad \text{(A.II.22)}$$

$$\therefore \quad \omega_1 = \frac{\frac{1}{m_1}(1 + k')}{\frac{1}{k_1}(1 + m')} \quad .. \quad .. \quad .. \quad .. \quad .. \quad \text{(A.II.23)}$$

If k' = m', i.e. the exciter natural frequency is the same as the natural frequency of the system under test, then equation (A.II.23) reverts to:

$$\omega_1 = \left\{\frac{k_1}{m_1}\right\}^{\frac{1}{2}}$$ which is the true system natural frequency.

APPENDIX III

A.III.l Listing of Program ZTHA
A.III.2 Listing of Program CFIT

A.IIX.l - Listing of Program ZTHA

```
      MASTER HYSYSTEMS                                                  HDS010
C---------PROGRAM FOR HARMONIC ANALYSIS OF HYSTERETICALLY-
          DAMPED SYSTEMS
C---------THE H MATRIX MAY NOT BE A SCALAR MULTIPLE OF THE
          K MATRIX
C---------G. TOMLINSON
      COMPLEX F,X,Z,FO,ZO,FV                                            HDS020
      REAL MASS,K                                                       HDS030
      DIMENSION F(10),FR(10),FI(10),FSC(10),X(10),FV(10)                HDS040
      DIMENSION MASS(10,10),K(10,10),Z(10,10),DAMP(10,10)               HDS050
      DATA STAR/4H****/,PI/3,1415926/,EPS/1.0E-5/,TEN3/                 HDS055
      1.0E3/IERR=0                                                      HDS060
      PI2=2.0*PI                                                        HDS065
C---------READ IN NUMBER OF PARAMETRIC SETS IN DATA GROUPS
1     READ(1,1005)NSETS                                                 HDS070
1005  FORMAT(10)                                                        HDS075
      IF (NSETS.EQ.0) STOP                                              HDS078
C---------MAIN LOOP FOR DATA GROUPS
      DO 250 NS=1,NSETS                                                 HDS080
C---------READ IN FUNDAMENTAL PARAMETERS
5     READ(1,1000)N,H,FMIN,FMAX,DF                                      HDS085
1000  FORMAT(10,4F0.0)                                                  HDS090
C---------CHECK DEGREES OF FREEDOM
      IF(N.GT.0.AND.N.LE.10) GOT0 10                                    HDS095
      WRITE(3,1990)STAR,STAR                                            HDS100
1990 FORMAT(1X,A4,29H ERROR IN DEGREES OF FREEDOM ,A4)                  HDS105
      IERR=1                                                            HDS110
C---------CHECK FOR +VE OR ZERO DAMPING FACTOR
10    IF (H.GE.0.0) GOT0 20                                             HDS120
      WRITE(3,1980)STAR,STAR                                            HDS130
1980 FORMAT(1X,A3,23H DAMPING FACTOR IS -VE ,A4)                        HDs135
C---------CHECK FOR +VE FREQUENCY PARAMETERS
20    IF (FMAX.GT.0.0.AND.FMIN.GT.0.0.AND.DT.GT.0.0) GOT0 30            HDS150
      WRITE(3,1970)STAR,STAR                                            HDS160
1970 FORMAT(1X,A4,31H A FREQUENCY PARAMETER NOT +VE ,A4)                HDS165
      IERR=1                                                            HDS170
      GOT0 50                                                           HDS175
C---------CHECK ORDER OF FREQUENCY LIMITS
30    IF (FMAX.GT.FMIN) GOT0 40                                         HDS180
      WRITE(3,1960)STAR, STAR                                           HDS190
1960 FORMAT(1X,A4,33H FREQUENCY LIMITS IN WRONG ORDER ,A4)              HDS195
      IERR=1                                                            HDS200
C---------CHECK FREQUENCY INCREMENT
40    FDIFF=FMAX-FMIN                                                   HDS210
      IF (DF.LE.ABS(FDIFF)) GOT0 50                                     HDS220
      WRITE(3,195))STAR,STAR                                            HDS230
1950 FORMAT(1X,A4,31H FREQUENCY INCREMENT TOO LARGE ,A4)                HDS235
      IERR=1                                                            HDS240
C---------STOP RUN IF ERRORS ON 1ST CARD
50    IF (IERR.EQ.l) STOP                                               HDS245
C---------OUTPUT PROGRAM TITLE AND DATA ON 1ST CARD
      WRITE(3,2000)                                                     HDS250
2000 FORMAT(51H1HARMONIC ANALYSIS OF HYSTERETICALLY
      DAMPED SYSTEMS)                                                   HDS260
      IF (H.EQ.0.0) WRITE (3,2005)N,FMAX,FMIN,DF                        HDS265
```

```
2005 FORMAT(34HONUMBER OF DEGREES OF FREEDOM N = ,12/                HDS270
     *       36H NO PROPORTIONAL DAMPING COEFFICIENT/                HDS271
     *       26H MAXIMUM FREQUENCY FMAX = ,F8.2,4H CPS/              HDS272
     *       26H MINIMUM FREQUENCY FMIN = ,F8.2,4H CPS/              HDS273
     *       26H FREQUENCY INCREMENT DF = ,F8.4,4H CPS/              HDS274
      IF (H.GT.O.O) WRITE(3,2010)N,H,FMAX,FMIN,DF                    HDS275
2010 FORMAT(34HONUMBER OF DEGREES OF FREEDOM N = ,12/                HDS280
     *       25H DAMPING COEFFICIENT H = ,F6.3/                      HDS281
     *       26H MAXIMUM FREQUENCY FMAX = ,F8.2,4H CPS/              HDS282
     *       26H MINIMUM FREQUENCY FMIN = ,F8.2,4H CPS/              HDS283
     *       26H FREQUENCY INCREMENT DF = ,F8.4,4H CPS)              HDS284

C---------CONVERT CYCLE-FREQUENCY INTO ANGULAR-FREQUENCY
      WMAX=P12*FMAX                                                  HDS290
      WMIN=P12*FMIN                                                  HDS295
      DW=P12*DF                                                      HDS300
      WMAX1=WMAX+O.5*DW                                              HDS305
      IF (NS.GT.L) GOT0 65                                           HDS308
C---------READ IN MASS MATRIX - 1 COMUMN ON EACH CARD
      DO 60 J=1,N                                                    HDS310
60    READ(1,1O1O)(MASS(I,J), I=1,N)                                 HDS320
1010  FORMAT(1OFO.O)                                                 HDS330
C---------NPRINT = NEAR OR AT MIDDLE OF MATRIX
      NPRINT=(N+1)/2                                                 HDS340
C---------OUTPUT MASS MATRIX BY ROWS
65    WRITE(3,2O2O)                                                  HDS350
2020 FORMAT(26HOORIGINAL MASS MATRIX(KG)/1X,25(1H-))                 HDS360
      DO 70 I=1,N                                                    HDS370
      WRITE(3,2O3O)(MASS(I,J),J=1,N)                                 HDS380
2030  FORMAT(7X,1O(F8.4,1X))                                         HDS390
      IF (I.EQ.NPRINT) WRITE(3,2O4O)                                 HDS395
2040 FORMAT(7H+M = )                                                 HDS400
70    CONTINUE                                                       HDS410
      IF (NS.GT.l) GOT0 80                                           HDS415
C---------READ IN STIFFNESS MATRIX - 1 COLUMN ON EACH CARD
      DO 75 J=1,N                                                    HDS420
75    READ(l,lOlO)(K(I,J),I=l,N)                                     HDS430
C---------OUTPUT STIFFNESS MATRIX BY ROWS
80    WRITE(3,2O5O)                                                  HDS440
2050 FORMAT(32HOORIGINAL STIFFNESS MATRIX (N/M)/1X,31(1H-))          HDS450
      DO 85 I=1,N                                                    HDS460
      WRITE(3,2O6O)(K(I,J),J=1,N)                                    HDS470
2060  FORMAT(7X,1O(E1O.4,1X))                                        HDS475
      IF (I.EQ.NPRINT) WRITE(3,2065)                                 HDS480
2065 FORMAT(7H+K = )                                                 HDS485
85    CONTINUE                                                       HDS490 .
C---------CHECK FOR ZERO DAMPING FACTOR
      IF (H.EQ.O.O) GOT0 92                                          HDS492
C---------DAMPING MATRIX = DAMPING FACTOR*STIFFNESS MATRIX
      DO 90 I=1,N                                                    HDS493
      DO 90 J=1,N                                                    HDS494
90    DAMP(I,J)=H*K(I,J)                                             HDs495
      GOT0 98                                                        HDS496
C---------READ IN DAMPING MATRIX - 1 COLUMN ON EACH CARD
      DO 95 J=1,N                                                    HDS500
95    READ(1,1O1O)(DAMP(I,J),I=1,N)                                  HDS502
C---------OUTPUT DAMF'ING MATRIX BY ROWS
```

```
98    WRITE(3,2055)                                                    HDS504
2055 FORMAT(3OHOORIGINAL DAMPING MATRIX (N/M)/iX,29(1H-))              HDS505
      DO 100 I=1,N                                                     HDS506
      WRITE(3,2060)(DAMP(I,J),J=1,N)                                   HDS508
      IF (I.EQ.NPRINT) WRITE(3,2075)                                   HDS509
2075 FORMAT(7H+H = )                                                   HDS510
100   CONTINUE                                                         HDS512
C---------READ IN SCALAR MULTIPLIERS AND FORCE VECTOR
      DO 105 I=1,N                                                     HDs515
105   READ(1,1020)FSC(I),FR(I),FI(I)                                   HDS518
1020 FORMAT(3F0.0)                                                     HDS520
C---------OUTPUT FORCE VECTOR BY ELEMENTS
      WRITE(3,2070)                                                    HDS530
2070 FORMAT(26HOORIGINAL FORCE VECTOR (N)/iX,25(1H-))                  HDS540
      DO 110 I=1,N                                                     HDS550
      WRITE(3,2080)FR(I),FI(I)                                         HDS560
2080  FORMAT(7X,2(F8.4.2X))                                            HDS570
      IF (I.EQ.NPRINT) WRITE(3,2090)                                   HDS575

2090 FORMAT (7H+F = )                                                  HDS580
110   CONTINUE                                                         HDS590
      LINE=1                                                           HDS600
C---------FORM THE COMPLEX VECTOR F
      DO 120 I=1,N                                                     HDS605
120   F(I),FV(I)=CMPLX(FR(I),FI(I))*FSC(I)                             HDS610
C---------MAIN LOOP OF PROGRAM - USING COMPLEX EQUATIONS
      CPS=FMIN                                                         HDS615
      w=WMIN                                                           HDS620
130   WW=W*W                                                           HDS625
c---------FORM THE COMPLEX MATRIX Z
      DO 140 I=1,N                                                     HDS630
      DO 140 J=1,N                                                     HDS640
140   Z(I,J)=CMPLX(K(I,J)-WW*MAXX(I,J),DAMP(I,J))                      HDS650
C---------COMPUTE DISPLACEMENT VECTOR X FROM EQUATIONS
      DO 200 I=k,N                                                     HDS660
      ZMAX=0.0                                                         HDS665
C---------FIND COLUMN ELEMENT WITH MAXIMUM MODULUS
      DO 150 L=I.N                                                     HDS670
      ZMOD=CABS(Z(L,I))                                                HDS680
      IF (ZMOD.LE.ZMAX) GOT0 150                                       HDS685
      ZMAX=ZMOD                                                        HDS690
      IND=L                                                            HDS695
150   CONTINUE                                                         HDS700
C---------CHECK FOR A SINGULAR MATRIX
      IF (ZMAX.GT.EPS) GOT0 155                                        HDS705
      WRITE(Z,1900)STAR,STAR                                           HDS708
1900 FORMAT(1H ,A4,33H ILL-BEHAVED SYSTEM OF EQUATIONS ,A4)            HDS710
      STOP                                                             HDS712
155   IF (I.EQ.N) GOT0 205                                             HDS715
      YMIN=1.0/ZMAX                                                    HDS718
      IF (IND.EQ.I) GOT0 165                                           HDS719
C---------TTANSPOSE ROWS IN EQUATIONS AND SCALE NEW ROW I
      DO 160 J=1,N                                                     HDS720
      ZO= Z(I.J)                                                       HDS730
      Z(IJ)=Z(IND,J)*YMIN                                              HDS735
160   Z(IND,J)=ZO                                                      HDS740
      FO=F(I)                                                          HDS750
      F(I)=F(IND)*YMIN                                                 HDS755
      F(IND)=FO                                                        HDS760
```

```
      GOTO 175                                                          HDS762
C---------SCALE ROW I
165   DO 170 J=1,N                                                      HDS764
170   Z(I.J)=Z(I.J)*YMIN                                                HDS766
                                                                        HDS768
      F(I)=F(I)*YMIN
C---------CONVERT MATRIX INTO TRIANGULAR FORM
175   DO 190 L=I+i,N                                                    HDS770
      IF(CABS(Z(L,I)) EQ.O) GOT0 190                                    HDS775
      F(L)=Z(I,I)*F(L)-Z(L,I)*D(I)                                      HDS780
      DO 180 J=I+1,N                                                    HDS790
180   Z(L,J)=Z(I,I)*Z(L,J)-Z(L,I)*Z(I,J)                                HDS800
190   CONTINUE                                                          HDS810
200   CONTINUE                                                          HDS820
C---------SOLVE EQUATIONS BY BACKWARD SUBSTITUTION
205   X(N)=F(N)/Z(N,N)                                                  HDS830
      F(N)=FV(N)                                                        HDS835
      DO 220 I=l,N-1                                                    HDS840
      L=N-I                                                             HDS845
      X(L)=F(L)                                                         HDS850
C---------RESTORE FORCE VECTOR
      F(L)=FV(L)                                                        HDS855
      DO 210 J=L+1,N                                                    HDS860
210   X(LO=X(L)-2(L,J)*X(L)                                             HDS865
220   X(L)=X(L)/2(L,L)                                                  HDS870

C---------CONVERT DISPLACEMENTS INTO MILLIMETRES
      DO 225 L=1,N                                                      HDS875
225   X(L)=X(L)*TEN3                                                    HDS880
C---------OUTPUT TABLE OF DISPLACEMEMTS IN COMPONENTS-FORM
      IF (LINE.EQ.l) WRITE(3,2100)CPS                                   HDS885
2100  FORMAT(22H1FREQUENCY IN CPS = ,F8.4)                              HDS890
      IF (LINE.GT.l) WRITE(3,2110)CPS                                   HDS895
2110  FORMAT(22HOFREQUENCY IN CPS = ,F8.4)                              HDS900
      WRITE(3,2120)                                                     HDS905
2120  FORMAT(23X,9HCARTESIAN,23X,5HPOLAR/                               HDS910
     *       6H X(MM),15X,4HREAL,6X,4HIMAG,14x,17HMODULUS
            ARG(DEG))                                                   HDS911
C---------CARTESIAN AND POLAR COMPONENTS OF DISPLACEMENTS
      DO 230 I=1,N                                                      HDS915
      XR=REAL(X(I))                                                     HDS920
      XI=AIMAG(X(I))                                                    HDS925
      XM=CABS(X(I))                                                     HDS930
      XA=PI2-ACOS(XR/XM)                                                HDS940
      IF (XI.LT.O.O) XA=PI2-XA                                          HDS945
C---------EXPRESS ANGLE IN DEGREES
      XA=180.O*XA/PI                                                    JDS950
230   WRITE(3,2130)I,XR,XI,XM,XA                                        HDS955
2130  FORMAT(2X,I2,1X,2(11X,F9,2,1X,F9,3))                              HDS960
C---------INCREMENT ANGULAR-FREQUENCY FOR NEXT TABLE
      CPS=CPS+DF                                                        HDS965
      W=W+DW                                                            HDS970
      IF (W.GT.WMAX1) GOT0 250                                          HDS975
C---------CHECK POSITION OF 1ST LINE IN TABLE
      LINE=LINE+N+4                                                     HDS980
      IF (LINE+N+2.GT.60) LINE=1                                        HDS985
```

```
C---------RETURN TO CALCULATE NEXT TABLE
      GOT0130                                                    HDS988
250   CONTINUE                                                   HDS990
      GOTO 1                                                     HDS992
      END                                                        HDS995

END OF SEGMENT, LENGTH 1320, NAME HDSYSTEMS
```

A.III.2 - Listing of Program CFIT

```
      MASTER CFIT                                                        CFP010
C-----PROGRAM TO FIND A CIRCLE OF BEST FIT-ERROR MARGIN POSSIBLE
C-----G.TOMLINSON
      DIMENSION FILE (1),XP(100),YP(100),AST(1),PL(1),TEST(1),SFCAP(11) CFP011
      DIMENSION XAX(1),YAX(1),FREQ(100),IRAD(11),SFC(2),SFS(1)          CFP012
      DATA  SFCAP(1)/32H10.0  8.0     6.25    5.0     /                 CFP014
      DATA SFCAP(5)/32H4.0     3.125  2.5     2.0     /                 CFP016
      DATA SFCAP(9)/24H1.6     1.25   1.0     /                         CFP018
      DATA IRAD/40,50,64,80,100,128,160,200,250,320,400/                CFP023
      DATA SF/10.0,8.0,6.25,5.0,4.0,3.125,2.5,2.0,1.6,1.25,1.0/         CFP024
      DATA FILE(1)/8HZTCFR2FZ/,STAR/4H****/,PREC/1.0E-6/                CFP025
      DATA AST(10/1H*/,PL(1)/1H*/,TEST(1)/8HTEST NO /                   CFP026
      DATA XAX(1)/4HREAD/,YAX(1)/4HIMAG/,SFC(1)/16H SCALE FACTOR = /    CFP027
C-----STATEMENT FUNCTION FOR DISTANCE
      DIST(XA,YA,XB,YB)=SQRT((XB=XA)**2+(YB-YA)**2)                     CFP028
      QPI=ATAN(1.0)                                                     CFP029
      NDATA,NPAGE=0                                                     CFP030
      HPI=2,0*QPI                                                       CFP031
C-----INITIALIZE GRAPH=PLOTTER PARAMETERS
      CALL HGPDISC(0,FILE,0)                                            CFP032
      CALL HGPLOT(0.0,0.0,16,1)                                         CFP035
      CALL  HGPIDENT(FILE)                                              CFP040
      CALL HGPLOT(0.0,3.0,0.4)                                          CFP045
      CALL DATE(DAY)                                                    CFP046
      IERR=0                                                            CFP04.8
C-----READ NUMBER OF POINTS, X,Y-ERROR MARGINS AND ANNOTATION
10    READ(1,1000)NP,ZERR,YERR,INOT                                     CFP050
1000  FORMAT(I0,2G0.0,I0)                                               CFP055
      IF (NP.EQ.0) GOT0 999                                             CFP060
C-----CHECK NUMBER OF POINTS GE 4 AND LE 100
      IF (NP.GE.4.AND.NO.LE.100) GOT0 20                                CFP065
      WRITE(3,1995)STAR,STAR                                            CFP070
1995  FORMAT(1X,A4.24H NUMBER OF POINTS WRONG, A4)                      CFP075
      IERR=1                                                            CFP078
C-----CHECK ERROR MARGINS ARE NOT -VE
20    IF (XERR,GT.-PREC) GOT0 25                                        CFP080
      WRITE(3,1990)STAR,STAR                                            CFP085
1990  FORMAT(1X,A4,20H -VE X-ERROR MARGIN ,A4)                          CFP090
      IERR=1                                                            CFP092
25    IF (YERR.GT.-PREC) GOT0 30                                        CFP095
      WRITE(3,1985)STAR,STAR                                            CFP100
1985  FORMAT(1X,A4.20H -VE Y-ERROR MARGIN ,A4)                          CFP105
      IERR=1                                                            CFP108
C-----READ IN CO-ORDINATES OF POINTS AND FREQUENCIES
30    DO 40 NN=1,NP                                                     CFP118
      READ(1,1010)FREQ(NN),XP(NN),YP(NN)                                CFP120
1010  FORMAT(3G0.0)                                                     CFP122
C-----CHECK FREQUENCY VALUE
      IF (FREQ(NN),GT.0.0.AND.FREQ(NN).LE.100.0) GOT0 38                CFP124.
      WRITE(3,1975)STAR,NN,STAR                                         CFP126
1975  FORMAT(1X,A4.32H WRONG FREQUENCY VALUE AT POINT ,I2,1X,A4)        CFP128
      IERR=1                                                            CFP129
C-----CHECK FOR Y CO-ORDINATE WITHIN RANGE
38    IF (YP(NN).GE.0.0.AND.YP(NN).LE.20.0) GOT0 40                     CFP130
      WRITE(3,1970)STAR,NN,STAR                                         CFP131
```

```
1970   FORMAT(1X,A4,32H Y-VALUE OUTSIDE RANGE AT POINT ,I2,1X,A4)          CFP132
       IERR=1                                                              CFP134
40     CONTINUE                                                            CFP135
C------FIND RANGE OF X CO-ORDINATE
       XMIN=1.OE7                                                          CFP136
       XMAX=-XMIN                                                          CFP137
       DO 45 NN=1,NP                                                       CFP138
       IF (XMIN.GT.XP(NN)) XMIN=XP(NN)                                     CFP140
       IF  (XMAX.LT.XP(NN))  XMAX=XP(NN)                                   CFP142
45     CONTINUE                                                            CFP144
C------CHECK POINTS ARE WITHIN RANGE
       XSPAN=XMAX=XMIN                                                     CFP145
       IF (XSPAN.LE.20.0) GOT0 48                                          CFP146
       WRITE)3,1965)STAR,STAR                                              CFP148
1965   FORMAT(1X,A4.28H CO-ORDINATES OUTSIDE RANGE ,A6)                    CFP149
       IERR=1                                                              CFP150
48     IF (IERR.EQ.O) GOT0 49
C------STOP RUN FOR ERRORS IN INPUT DATA
       WRITE(3,196O)STAR,STAR                                              CFP151
1960   FORMAT(1X,A4.28H RUN STOPPED THROUGH ERRORS ,A4)                    CFP154
       GOT0 999
C------FIND CENTROID OF CIRCLE-CENTRES
49     XBAR,YBAR,RMAX=O.O                                                  CFP155
       NC=O                                                                CFP156
       DO 60 Nl=l,NP-2                                                     CFP158
       DO 55 N2=N1+1,NP-1                                                  CFP160
       DO 50 N3=N2+1,NP                                                    CFP162
       X21=XP(N2)-XP(N1)                                                   CFP164
       Y21=YP(N2)-YP(N1)                                                   CFP166
       X31=XP(N3)-XP(N1)                                                   CFP168
       Y31=YP(N3)-YP(N1)                                                   CFP170.
       DEL=X21*Y31-X31*Y21                                                 CFP172
       IF (ABS(DEL).LT.PREC) GOT0 50                                       CFP174
       NC=NC+1                                                             CFP176
       RR21=X21*(XP(N2)+XP(N1))+Y21*(YP(N2)+YP(N1))                        CFP178
       RR31=X31*(XP(N3)+XP(N1))+Y31*(YP(N3)+YP(N1))                        CFP180
       REC=O.5/DEL                                                         CFP182
       XBAR=REC*(RR21*Y31-RR31*Y21)+XBAR                                   CFP184
       YBAR=REC*(RR31*X21-RR21*X31)+YBAR                                   CFP185
50     CONTINUE                                                            CFP186
55     CONTINUE                                                            CFP188
60     CONTINUE                                                            CFP190
       XBAR=XBAR/FLOAT(NC)                                                 CFP192
       YBAR=YBAR/FLOAT(NC)                                                 CFP194
C------UPDATE TEST DATA NUMBER                                            CFP194
       NPAGE=NPAGE+1                                                       CFP195
       NDATA=NDATA+1                                                       CFP196
       DATN=NDATA                                                          CFP197
C------OUTPUT PROGRAM TITLE AND DATA ON 1ST CARD
       WRITE(3,2OOO)NDATA,DAY,NPAGE,NP,XERR,YERR                           CFP198
2000   FORMAT(9H1TEST NO ,I1,41X,5HDATA ,A8,37X,5HPAGE ,I1//               CFP200
      *       20H NUMBER OFPOINTS = ,I3/                                   CFP201
      *       18H X-ERROR MARGIN = ,F6.4/                                  CFP202
      *       18H Y-ERROR MARGIN = ,F6.4)                                  CFP203
C------OUTPUT CO-ORDINATES OF POINTS AND FREQUENCIES
```

```
      WRITE(3,2010)                                                    CFP205
2010  FORMAT(39HOCO-ORDINATES OF POINTS AND FREQUENCIES/               CFP208
     *       31H  NN  FREQ(NN)   XP(NN)   YP(NN))                     CFP209
      DO 65 NN=1,NP                                                    CFP210
65    WRITE(3,2020)NN,FREQ(NN),XP(NN),YP(NN)                           CFP212
2020  FORMAT(1X,I3.1X,F8.4,2(1X,F8.3))                                 CFP214
C------FIND POINT NEAREST TO RESONANT FREQUENCY
      DO 70 NN=2,NP-1                                                  CFP215
      RAT1=DIST(XP(NN-1),YP(NN-1),XP(NN),YP(NN))/(FREQ(NN)-FREQ(NN-1)) CFP216
      RAT2=DIST(XY(NN+1),YP(NN+1),XP(NN),YP(NN))/(FREQ(NN+1)-FREQ(NN)) CFP218
C------AVERAGE VALUE OF DS/DF
      RAT=0.5*(RAT1+RAT2)                                              CFP220
      IF (RAT.LE.RMAX) GOT0 70                                         CFP221
      NRES=NN                                                          CFP222
      RMAX=RAT                                                         CFP224
70    CONTINUE                                                         CFP225
C------OUTPUT MEAN CIRCLE CENTRE
      WRITE(3,2030)XBAR,YBAR                                           CFP228
2030  FORMAT(19HOMEAN CIRCLE CENTRE/8H XBAR = ,F8.3/8H YBAR = ,F8.3)   CFP230
C------FIND MEAN RADIUS OF POINTS FROM CENTRE
      RAD=0.0                                                          CFP235
      DO 72 NN=1,NP                                                    CFP238
72    RAD=DIST(XBAR,YBAR,XP(NN),YP(NN))+RAD                            CFP240
      RAD=RAD/FLOAT(NP)                                                CFP242
C------CHECK RADIUS IS WITHIN RANGE
      IF (RAD.GE.1.0.AND.RAD.LE.10.0) GOT0 75                          CFP243
      WRITE(3,198))STAR,RAD,STAR                                       CFP244
1980  FORMAT(1X,A4,10H RADIUS = ,F6.3,18H IS OUTSIDE RANGE ,A4)        CFP245
      GOT0 999                                                         CFP246
75    WRITE(3,2040)RAD                                                 CFP248
2040  FORMAT(37HOMEAN RADIUS OF POINTS FROM CENTRE = ,F8.3)            CFP250
C------CALCULATE ABSOLUTE ERROR FOR MEAN RADIUS
      RERR=DIST(0.0,0.0,XERR,YERR)                                     CFP252
C------FIND HORIZONTAL SPAN OF CIRCLE
      XMIN=XBAR-RAD-RERR                                               CFP255
      XMAX=XBAR+RAD+RERR                                               CFP258
C------CHECK FOR MARGINAL ERROR CIRCLES
      IF (RERR.LT.PREC) GOT0 76)                                       CFP262
      WRITE(3,2050)RERR                                                CFP263
2050  FORMAT(24H ERROR IN MEAN RADIUS = ,F6.4)                         CFP264
C------OUTPUT RESONANT FREQUENCY
76    WRITE(3,2055)NRES,FREQ(NRES)                                     CFP265
2055  FORMAT(7HOPOINT ,I2,24M - RESONANT FREQUENCY = ,F7.4)            CFP266
C------FIND LARGEST ABSOLUTE VALUE OF Y
      YLIM=RAD+RERR+YBAR                                               CFP267
      YLIM=AMAX1(YLIM,2.0*RAD)                                         CFP2675
C------FIND APPROPRIATE SCALING FACTOR
      MRAD=20.0*YLIM+0.5                                               CFP268
      IF (MRAD.LT.40) MRAD=40                                          CFP269
      DO 77 NS=2,11                                                    CFP270
      IF (MRAD.LE.IRAD(NS).AND.MRAD.GT.IRAD(NS-1)) GOT0 78             CFP271
77    CONTINUE                                                         CFP272
      NS=1                                                             CFP273
78    SCALE=SF(NS)                                                     CFP274
      DS=0.005*FLOAT(IRAD(NS))                                         CFP275
```

```
C------CONVERT SCALE-FACTOR INTO CHARACTERS
       CALL COPY8(SFS(1),SFCAP(NS))                                    CFP276
       CALL HGPSYMBL(0.0,-22.o,0.7,SFC,0.0,16)                         CFP277
       CALL HGPSYMBL(9.6,-22.0,0.7,SFS,0.0,5)                          CFP278
C------CALCULATE PARAMETERS FOR AXES
       NXY=INT(YLIM/DS)+1                                              CFP279
       SYAX=2.O*FLOAT(NSY)                                             CFP280
C------FIND POSITION OF Y-AXIS
       IF (XMIN.GT.O.O) GOT0 82                                        CFP281
       NS1=1-INT(XMIN/DS)                                              CFP282
       XLIM=-DS*FLOAT(NS1)                                             CFP283
       IF (XMAX.GT.O.O) GOT0 81                                        CFP284
C------CIRCLE OFFSET ON -VE SIDE OF Y-AXIS
       SXAX,XYAX=NS1+NS1                                               CFP285
       GOT0 84                                                         CFP286
C------CIRCLE IN NORMAL POSITION
81     NS2=NS1+INT(XMAX/DS)+1                                          CFP287
       XYAX=NS1+NS1                                                    CFP288
       SXAX=NS2+NS2                                                    CFP290
       GOTO 84                                                         CFP291
C------CIRCLE OFFSET ON +VE SIDE OF Y-AXIS
82     NS2=INT(XMAX/DS)+1                                              CFP292
       XLIM,XYAX=O.O                                                   CFP294
       sxax=NS2+NS2                                                    CFP296
C------SCALE PARAMETERS FOR GRAPH-PLOTTING
84     XBG=(XBAR-XLIM)*SCALE                                           CFP298
       YBG=-YBAR*SCALE                                                 CFP300
       RAG=RAD*SCALE                                                   CFP301
       RAG1=(RAD-RERR)*SCALE                                           CFP302
       RAG2=(RAD+RERR)*SCALE                                           CFP303
c------PLOT POINTS AND CENTRE FOR GRAPH-PLOTTER
       DO 90 NN=1,NP                                                   CFP306
       XX=(XP(NN)-XLIM)*SCALE                                          CFP307
       XS=XX-0.12                                                      CFP308
       YY=-YP(NN)*SCALE                                                CFP309
       YS=YY-0.21                                                      CFP310
       CALL HGPSYMBL(XS,YS,0.42,PL,0.0.1)                              CFP311
C------FIND DIRECTION OF ANNOTATION
       IF (INOT.EQ.O.AND.NN.NE.NRES) GOT0 90                           CFP3115
C------ANNOTATE FREQUENCY VALUE
       DX=XX-XBG                                                       CFP312
       DY=YY-YBG                                                       CFP313
       VECT=DIST(O.O,O.O,DX,DY)                                        CFP314
       IF (DX,LT,O.O) GOT0 85                                          CFP3145
C------THETA TAKEN AS -VE
       THETA=ATAN2(DY,DX)                                              CFP315
       RAI=VECT+O.2                                                    CFP316
       XF=XBG+RAI*COS(THETA)                                           CFP317
       YF=YBG+RAI*SIN(THETA)                                           CFP318
       GOT0 88                                                         CFP3185
C------THETA TAKEN AS +VE
85     DX=-DX                                                          CFP319
       DY=-DY                                                          CFP319:
       THETA=ATAN2(DY,DX)                                              CFP320
       RAO=VECT+1.7                                                    CFP321
```

```
      XF=XBG-RAO*COS(THETA)                                              CFP322
      YF=YBG-RAO*SIN(THETA)                                              CFP323
88    ANGLE=90.0*THETA/HPI                                               CFP324
      CALL HGPNUMBER(XF,YF,0.21,FREQ(NN),ANGLEO,2,4)                     CFP325
      IF (NN.NE.NRES) GOT0 90                                            CFP3255
C-----UNDERLINE RESONANT FREQUENCY
      XA=XF+0.1*SIN(THETA)                                               CFP326
      YA=YF-0.L*COS(THETA)                                               CFP327
      XB=XA+1.5*COS(THETA)                                               CFP328
      YB=YA+1.5*SIN(THETA)                                               CFP329
      CALL HGPDASHLN(ZA,YA,XB,YB,0.0)                                    CFP330
90    CONTINUE                                                           CFP331
C-----PLOT MEAN CIRCLE ON GRAPH-PLOTTER
      XS=XBG-0.12                                                        CFP332
      YS=YBG-0.21                                                        CFP338
      CALL HGPSYMBL(XS,YS,0.42.AST,0.0,1)                                CFP340
      XO=XBG+RAG                                                         CFP350
      YO=YBG                                                             CFP355
      CALL HGPCIRCLE(XO,YO,0.0,360.0,RAG,RAG,0.0)                        CFP360
      IF(RERR.LT.PREC) GOT0 95                                           CFP362
C-----PLOT MARGINAL CIRCLES ON GRAPH-PLOTTER
      XO=XBG+RAG1                                                        CFP385
      CALL HGPCIRCLE(XO,YO,0.0,360.0,RAG1,RAG1,0.5)                      CFP390
      XO=XBG+RAG2                                                        CFP395
      CALL HGPCIRCLE(XO,YO,0.0,360.0,RAG2,RAG2,0.5)                      CFP400
C------PLOT TITLE OF GRAPH AND CO-ORDINATE AXES
95    CALL HGPSYMBL(0.0,2.0,0.7,TEST,0.0,8)                              CFP405
      CALL HGPNUMBER(4.2,2.0,0.7,DATN,0.0,0,1,0)                         CFP410
      CALL HGPAXISV(XYAX,0.0,YAX,-4,SYAX,-90.0,0.0,DS,2.0,4)             CFP415
      CALL PGHAXISV(0.0,0.0,XAX,4,SXAX,0.0,XLIM,DS,2.0,4)                CFP420
C-----PROJECTIONS OF RESONANT FREQUENCY VECTOR
      DXO=XP(NRES)-XBAR                                                  CFP422
      DYO=YP(NRES)-YBAR                                                  CFP424
      DFAC=0.0                                                           CFP426
      FACT=2.0/FREQ(NRES)                                                CFP427
      NTERM=0                                                            CFP428
C-----ANGLE OF ROTATION IS ANTICLOCKWISE
      DO104NO=1,NRES-1                                                   CFP430
      Nl=NRES-NO                                                         CFP432
C-----PROJECTIONS OF LOWER FREQUENCY VECTOR
      DX1=XP(N1)-XBAR                                                    CFP434
      DY1=YP(N1)-YBAR                                                    CFP436
      HOR1=DXO*DX1+DYO*DY1                                               CFP437
      VER1=DX1+DYO-DXO*DY1                                               CFP438
      IF (ABS(HOR1).LE.PREC) TH1=2,0*QPI                                 CFP439
      IF (ABS(HOR1).GT.PREC) TH1=ATAN2(VER1,HOR1)                        CFP440
      IF(TH1,GT.QPI) GOT0 110                                            CFP441
      TAN1-TAN(0.5*TH1)                                                  CFP442
C-----ANGLE OF ROTATION IS CLOCKWISE
      DO 100 N2=NRES+1,NP                                                CFP444
C-----PROJECTIONS OF HIGHER FREQUENCY VECTOR
      DX2=XP(N2)-XBAR                                                    CFP446
      DY2=YP(N2)-YBAR                                                    CFP448
      HOR2=DXO*DX2+DY2*DYO                                               CFP449
      VER2=DXO*DY2-DX2*DYO                                               CFP450
```

```
      IF (ABS(HOR2),LE.PREC) TH2=2.0*QPI                                CFP451
      IF (ABS(HOR2).GT.PREC) TH2=ATAN2(VER2,HOR2)                       CFP452
      IF (TH2.GT.QPI) GOT0 100                                          CFP453
      TSUM=TAN(0.5*TH2)+TAN1                                            CFP456
C-----SUMMATION TO OBTAIN AVERAGE DAMPING FACTOR
      DFAC=FACT*(FREQ)N2)-FREQ(N1))/TSUM+DFAC                           CFP458
      TERM=NTERM+1                                                      CFP460
100   CONTINUE                                                          CFP462
105   CONTINUE                                                          CFP465
C-----CHECK WHETHER DAMPING FACTOR IS CALCULABLE
110   IF (NTERM.GT.0) GOT0 120                                          CFP466
      WRITE(3,1950)STAR,STAR                                            CFP467
1950  FORMAT(1X,A4,31H DAMPING FACTOR NOT CALCULABLE ,A4)               CFP468
      GOT0 125                                                          CFP469
C-----AVERAGE DAMPING FACTOR
120   DFAC=DFAC/FLOAT(NTERM)                                            CFP470
      WRITE(3,2060)DFAC                                                 CFP480
2060  FORMAT(26HOAVERAGE DAMPING FACTOR = ,F6.4)                        CFP485
C-----CHECK POSITION ON GRAPH-PLOTTER
125   CALL HGPWHERE(XW,YW)                                              CFP510
      XW=XW-SXAX-5.0                                                    CFP515
C-----RESET ORIGIN FOR NEXT SET OF DATA (IF ANY)
      CALL HGPLOT(XW,YW,0.4)                                            CFP520
      GOT0 10                                                           CFP525
C-----FINISH OF GRAPH-PLOTTER
999   CALL HGPLOT(10.0,0.0,3,0)                                         CFP530
      CALL HGPLOT(0.0,0.0,0,0,2)                                        CFP535
      CALL HGPDISC(1,FILE,0)                                            CFP540
      STOP                                                              CFP545
      END                                                               CFP550
```

APPENDIX IV

DETERMINATION OF THE DAMPING RATIO BY THE METHOD OF COMPLEX POWER

For a single degree-of-freedom system the displacement response is given by:

$$u = \frac{\frac{F}{k}}{1 - (\frac{\omega}{\omega_n})^2 + j2\zeta\frac{\omega}{\omega_n}} \quad .. \quad .. \quad .. \quad .. \quad .. \quad \text{(A.IV.1)}$$

Now Power (W) = $F\dot{x}u = jF\omega u$

$$W = \frac{j\frac{F^2\omega}{k}}{1 - (\frac{\omega}{\omega_n})^2 + j2\zeta\frac{\omega}{\omega_n}} \quad .. \quad \text{(A.IV.2)}$$

In terms of the real and imaginary parts,

$$W = W' + jW'' \quad .. \quad .. \quad .. \quad .. \quad .. \quad .. \quad .. \quad \text{(A.IV.3)}$$

$$\text{i.e.} \quad W = \frac{j\frac{F^2\omega}{k}\left\{(1-(\frac{\omega}{\omega_n})^2) - j2\zeta\frac{\omega}{\omega_n}\right\}}{(1-(\frac{\omega}{\omega_n})^2)^2 + 4\zeta^2(\frac{\omega}{\omega_n})^2} \quad .. \quad \text{(A.IV.4)}$$

$$\therefore \quad W' = \frac{2\frac{\omega}{\omega_n}\frac{F^2\omega}{k}}{(1-(\frac{\omega}{\omega_n})^2)^2 + 4\zeta^2(\frac{\omega}{\omega_n})^2} \quad .. \quad .. \quad .. \quad .. \quad \text{(A.IV.5)}$$

and $W'' = \dfrac{\frac{F^2\omega}{k}(1-(\frac{\omega}{\omega_n})^2)}{(1-(\frac{\omega}{\omega_n})^2)^2 + 4\zeta^2(\frac{\omega}{\omega_n})^2}$ .. .. (A.IV.6)

At resonance, $\omega = \omega_n$ and,

$$W' = \frac{F^2\omega_n}{2\zeta k} \; ; \; W'' = 0 \quad .. \quad .. \quad .. \quad .. \quad .. \quad \text{(A.IV.7)}$$

Now $-W'\dfrac{2\zeta\frac{\omega}{\omega_n}\frac{F^2\omega}{k_n}}{r}$ .. .. (A.IV.8)

where $r = (1 - (\frac{\omega}{\omega_n})^2)^2 + 4\zeta^2(\frac{\omega}{\omega_n})^2$

$$\therefore \frac{dW'}{d\omega} = \frac{r.4\zeta\frac{\omega}{\omega_n}.\frac{F^2}{k} - 2\zeta\frac{\omega}{\omega_n}^2.\frac{F^2}{k}.\frac{dr}{d\omega}}{r^2} \quad .. \quad .. \quad .. \quad .. \quad \text{(A.IV.9)}$$

Again, at $\omega = \omega_n$

$$\frac{dW'}{d\omega} = \frac{r.4\zeta\frac{F^2}{k} - 2\zeta\omega\frac{F^2}{k}.\frac{dr}{d\omega}}{16\zeta^4} \quad .. \quad .. \quad .. \quad .. \quad .. \quad \text{(A.IV.10)}$$

Now, $\frac{dr}{d\omega} = 2(1 - (\frac{\omega}{\omega_n})^2)(-\frac{2\omega}{\omega_n^2}) + (8\zeta^2\frac{\omega}{\omega_n^2})$

and at $\omega = \omega_n$,

$$\frac{dr}{d\omega} = \frac{8\zeta^2}{\omega_n}$$

$$\therefore \frac{dW'}{d\omega} = \frac{4\zeta^2 . 4\zeta\frac{F^2}{k} - 2\zeta . \frac{F^2}{k} . \frac{8\zeta^2}{\omega_-}}{16\zeta^4}$$

$$= \frac{16\zeta^3\frac{F^2}{k} - 16\zeta^3\frac{F^2}{k}}{16\zeta^4} = 0$$

$$\therefore \frac{dW'}{d\omega} = 0 \text{ at resonance}$$

$$\text{i.e. } \frac{dW'}{d\omega}\Big|_{\omega=\omega_n} = 0 \quad \ldots\ldots\ldots\ldots \quad (A.IV.11)$$

$$\text{Now, } \frac{dW''}{d\omega} = \frac{r . \frac{F^2}{k} - 3\frac{F^2}{k} . \frac{\omega^2}{\omega_n^2} - \frac{F^2\omega}{k}(1 - (\frac{\omega}{\omega_n})^2\frac{dr}{d\omega}}{r^2}$$

$$\text{at } \omega = \omega_n; \quad r = 4\zeta^2, \quad \frac{dr}{d\omega} = \frac{8\zeta^2}{\omega_n}$$

$$\therefore \frac{dW''}{d\omega} = \frac{4\zeta^2(\frac{}{k}F^2 - 3\frac{F^2}{k})}{16\zeta^4}$$

$$\frac{dW''}{d\omega} = -\frac{F^2}{2k\zeta^2} \quad \ldots\ldots\ldots\ldots \quad (A.IV.12)$$

$$\text{Now } \frac{F^2\omega_n}{2\zeta k} = W' \text{ from A.IV.7}$$

$$\therefore \frac{dW''}{d\omega} = \frac{W'}{\zeta\omega_n}$$

$$\therefore \frac{dW'}{d\omega} = \frac{4\zeta^2 . 4\zeta \frac{F^2}{k} - 2\zeta . \frac{F^2}{k} . \frac{8\zeta^2}{\omega}}{16\zeta^4}$$

$$= \frac{16\zeta^3 \frac{F^2}{k} - 16\zeta^3 \frac{F^2}{k}}{16\zeta^4} = 0$$

$$\therefore \frac{dW'}{d\omega} = 0 \text{ at resonance}$$

$$\text{i.e. } \frac{dW'}{d\omega}\Big|_{\omega=\omega_n} = 0 \quad \text{(A.IV.11)}$$

$$\text{Now, } \frac{dW''}{d\omega} = \frac{r . \frac{F^2}{k} - 3\frac{F^2}{k} . \frac{\omega^2}{\omega_n^2} - \frac{F^2\omega}{k}\left(1 - \left(\frac{\omega}{\omega_n}\right)^2\right)\frac{dr}{d\omega}}{r^2}$$

$$\text{at } \omega = \omega_n; \quad r = 4\zeta^2, \quad \frac{dr}{d\omega} = \frac{8\zeta^2}{\omega_n}$$

$$\therefore \frac{dW''}{d\omega} = \frac{4\zeta^2\left(\frac{F^2}{k} - 3\frac{F^2}{k}\right)}{16\zeta^4}$$

$$\frac{dW''}{d\omega} = -\frac{F^2}{2k\zeta^2} \quad \text{(A.IV.12)}$$

$$\text{Now } \frac{F^2\omega_n}{2\zeta k} = W' \text{ from A.IV.7}$$

$$\therefore \frac{dW''}{d\omega} = -\frac{W'}{\zeta\omega_n}$$

$$\therefore \quad \zeta = -\frac{W'}{\omega_n \cdot \frac{dW''}{d\omega}} \quad \text{at resonance,}$$

$$\text{i.e. } \zeta = \frac{1}{\omega_n} \left.\frac{W'}{dW''/d\omega}\right|_{\omega=\omega_n} \quad \left(\frac{dW''}{d\omega} \text{ is a negative slope}\right) \qquad \text{(A.IV.13)}$$

APPENDIX V

IDENTIFICATION OF A MULTI DEGREE-OF-FREEDOM SYSTEM WITH COULOMB FRICTION ELEMENTS

Consider a three degree-of-freedom lumped parameter system which has only hysteretic damping and Coulomb damping.

CASE 1 - GROUNDED COULOMB ELEMENTS

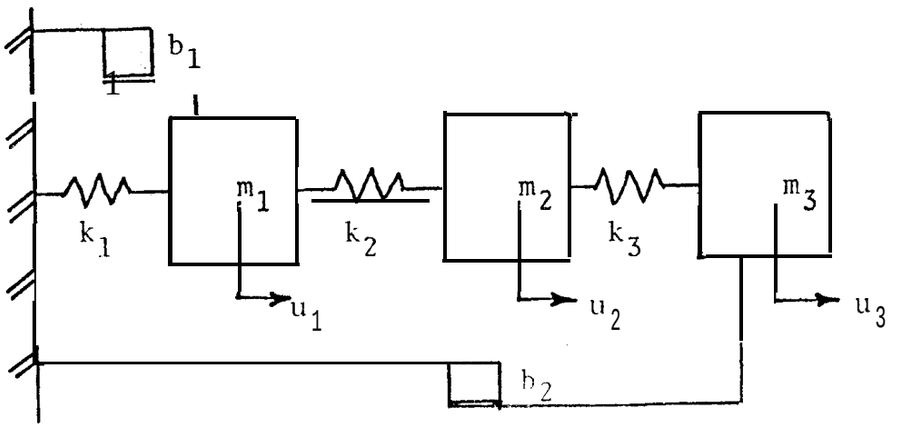

where k = elastic stiffness
u = displacement

The Coulomb friction elements are linearised by the method of harmonic balance and are denoted by the constants b_i which represent the level of the Coulomb friction forces i.e.:

$$b_i = \frac{4\mathcal{F}_i}{\pi} \cdot \quad i = 1, 2 \ldots \qquad \text{(A.VI.1)}$$

The structural damping matrix S is given by:

$$\underset{\sim}{S} = \delta \begin{bmatrix} k_1+k_2 & -k_2 & 0 \\ -k_2 & k_2+k_3 & -k_3 \\ 0 & -k_3 & k_3 \end{bmatrix} \quad \ldots \ldots \quad \text{(A.VI.2)}$$

where δ is the structural damping coefficient; and the frictional damping matrix F is given by:

$$F = \begin{bmatrix} \frac{b_1}{u_1} & 0 & 0 \\ 0 & 0 & 0 \\ 0 & 0 & \frac{b_3}{u_3} \end{bmatrix} \quad .. \quad .. \quad .. \quad .. \quad \text{(A.VI.3)}$$

If the force vector corresponds to a normal mode excitation vector at a normal mode frequency ω_i, then:

$$\underset{\sim}{u_i} = \lambda \underset{\sim}{v_i} = \lambda \begin{bmatrix} v_1 \\ v_2 \\ v_3 \end{bmatrix} \quad .. \quad .. \quad .. \quad .. \quad \text{(A.VI.4)}$$

and $$\underset{\sim}{F_i} = \lambda \begin{bmatrix} \frac{b_1}{v_1} & 0 & 0 \\ 0 & 0 & 0 \\ 0 & 0 & \frac{b_3}{v_3} \end{bmatrix} \quad .. \quad .. \quad .. \quad \text{(A.VI.5)}$$

If one now considers equation (177) i.e.:

$$\frac{W_{ir}}{\lambda\omega_i} = \lambda \underset{\sim}{v}_i^{t} \underset{\sim}{S}_r v_{ir} + \underset{\sim}{v}_i^{t} \underset{\sim}{F}_{ir} v_{ir} \quad \ldots\ldots \quad \text{(A.VI.6)}$$

then the power input at each co-ordinate is obtained from equations A.VI.2, A.VI.4 and A.VI.5 as:

$$\frac{W_{i1}}{\omega_i \lambda} = \lambda \begin{bmatrix} v_i & v_2 & v_3 \end{bmatrix} \begin{vmatrix} \delta(k_1+k_2) \\ -\delta k_2 \\ 0 \end{vmatrix} (v_1) +$$

$$\begin{bmatrix} v_1 & v_2 & v_3 \end{bmatrix} \begin{bmatrix} \frac{b_1}{v_1} \\ 0 \\ 0 \end{bmatrix} (v_1) \quad .. \quad .. \quad .. \quad \text{(A.VI.7)}$$

$$\therefore \quad \frac{W_{i1}}{\omega_i \lambda} = \lambda v_1 \delta\{k_2(v_1 - v_2) + k_1 v_1\} + b_1 v_1 \quad .. \quad \text{(A.VI.8)}$$

Similarly,

$$\frac{W_{12}}{\omega_i \lambda} = \lambda v_2 \delta\{k_2(v_2 - v_1) - k_3 v_3\} \quad .... \quad \text{(A.VI.9)}$$

$$\frac{W_{i3}}{\omega_i \lambda} = \lambda v_3 \delta\{k_3(v_3 - v_2)\} + b_3 v_3 \quad .... \quad \text{(A.VI.10)}$$

If the left hand side of equations A.VI.8, A.VI.9 and A.VI.10 are plotted as a function of λ, the resulting curves are given as:

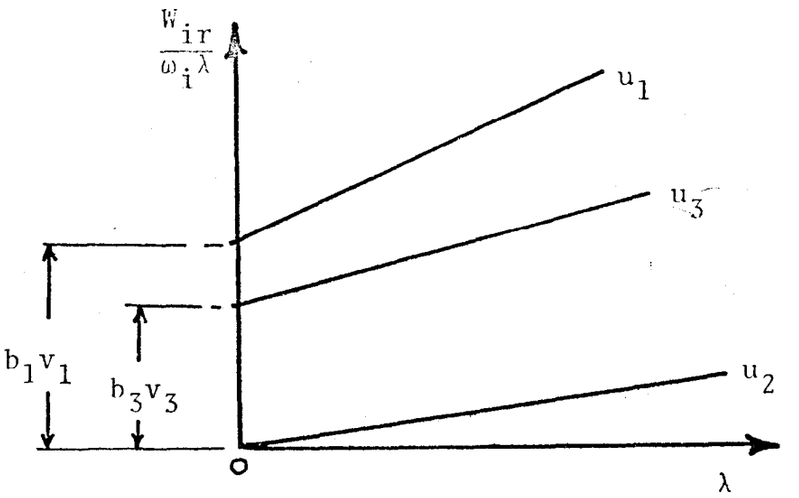

Thus the non-zero intercepts allow the non-linear Coulomb friction force levels to be evaluated.

CASE 2 - COUPLED COULOMB ELEMENT

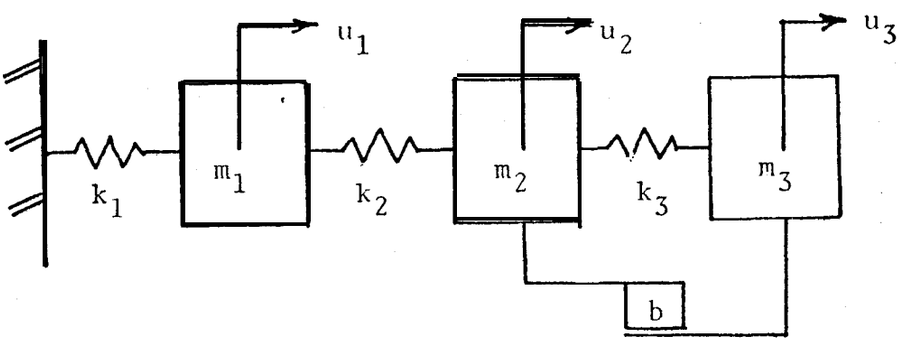

The structural damping matrix is given by equation A.VI.2 and the frictional damping matrix is:

$$F = \begin{bmatrix} 0 & 0 & 0 \\ 0 & \frac{b}{|u_2-u_3|} & \frac{-b}{|u_2-u_3|} \\ 0 & \frac{-b}{|u_2-u_3|} & \frac{b}{|u_2-u_3|} \end{bmatrix} \quad .. \quad .. \quad \text{(A.VI.11)}$$

Again if a normal mode vector, given by equation A.VI.4, is employed, equation A.VI.ll becomes,

$$F_i = \lambda \begin{bmatrix} 0 & 0 & 0 \\ 0 & \frac{b}{|v_2-v_3|} & \frac{-b}{|v_2-v_3|} \\ 0 & \frac{-b}{|v_2-v_3|} & \frac{b}{|v_2-v_3|} \end{bmatrix} \quad .. \quad \text{(A.VI.12)}$$

Employing equation (177) gives for the power input to each co-ordinate,

$$\frac{W_{11}}{\omega_i \lambda} = \lambda v_1 \delta\{k_1 + k_2(v_1 - v_2)\} \quad .. \quad .. \quad \text{(A.VI.13)}$$

$$\frac{W_{i2}}{\omega_i \lambda} = \lambda v_2 \delta\{k_2(v_2 - v_1) + k_3(v_2 - v_3)\} + bv_2 \quad \text{(A.VI.14)}$$

$$\frac{W_{i3}}{\omega_i \lambda} = \lambda v_3 \delta\{k_3(v_3 - v_2)\} - bv_3 \quad .. \quad .. \quad \text{(A.VI.15)}$$

Expressing the above quantities graphically as a function of A gives,

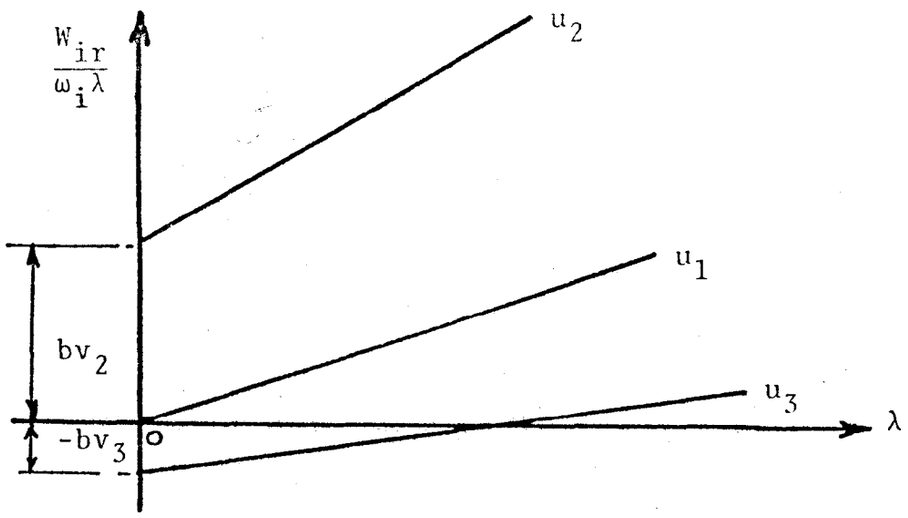

from which the intercepts again provide the values of the non-linear friction force levels.

APPENDIX VI

DESIGN CALCULATIONS FOR EXPERIMENTAL RIG

1. TRANSVERSE MODE CALCULATIONS

The requirement for the transverse mode, based on the results of Table 4.1, Chapter 4, is that the modal stiffness ≥ 300 kN/m. The value chosen for the modal stiffness was 350 kN/m.

From reference (79), the stiffness'of a beam between C and D for the boundary conditions given by,

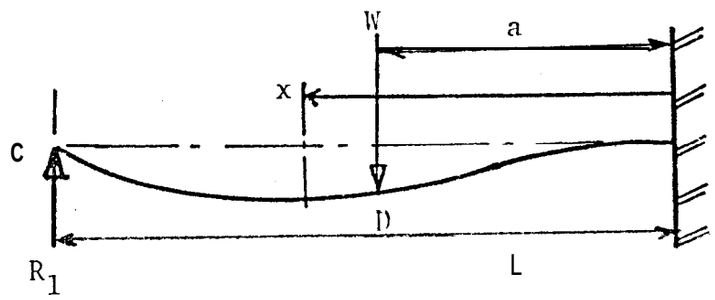

is:

$$K_B = \frac{6EI}{R_1(x^3 - 3L^2x) + 3a^2x} \quad a \leq x \leq L \quad . \quad . \qquad (A.VI.1)$$

where Rl = $\frac{W}{2L^3}(3a^2L - a^3)$.

The second moment of area for the hollow beam is:

$$I = \frac{BD^3}{12} - \frac{bd^3}{12} \qquad . \quad . \quad . \quad . \quad . \quad . \quad . \quad . \quad . \quad . \qquad (A.VI.2)$$

where the cross-section of the hollow beam is:

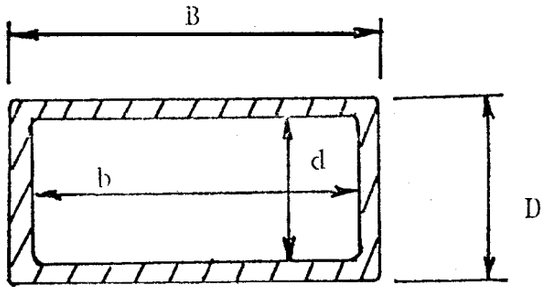

and B = 50.8 mm; D = 25.4 mm
b = 47.6 mm; d = 22.2 mm

$$\therefore \underline{T = 26 \times 10^{-9} m^4}$$

From equation A.VI.l, with a = b = $\frac{L}{2}$,

$$K_B = \frac{76SEI}{7L^3}$$

Assuming a value for Young's Modulus of steel as 210GN/m^2, the required length of the hollow steel beam is given as:

$$L = \left(\frac{768 \times 210 \times 10^9 \times 26 \times 10^{-9}}{7 \times 350 \times 10^3} \right)^{1/3}$$

$$\underline{L = 1.2m}$$

This hollow beam supports a solid steel cross beam at L/Z whose cross-sectional dimensions were chosen as 50.8 mm square to allow the hollow beam to slot through this and be located securely.

Assuming a transverse mode natural frequency of 25Hz gives the length of the solid steel cross beam as:

m_B = mass of cross beam = $\rho A \ell$

$$\therefore \quad \rho A \ell = \frac{K_B}{\omega_B^2}$$

$$\therefore \quad \ell = \frac{350 \times 10^5}{(25 \times 2\pi)^2 \times 7.84 \times 10^3 \times (0.0508)^2}$$

$$\underline{\ell = 0.7\text{m}}$$

2. TORSIONAL MODE CALCULATIONS

The natural frequency of vibration in the torsional mode will already be defined by the transverse mode physical parameters.

The polar second moment of area, from Bredt Batho theory (80) is:

$$J_p = \frac{4A^2}{\oint \frac{ds}{t}}$$

$\oint$ = surface integral
ds = surface contour
t = thickness
A = cross sectional area

$$\therefore \quad J_p = \frac{4(5).8 \times 25.4)^2}{\frac{2}{1.6}(50.8 + 25.4)}$$

$$J_p = 69{,}920 \text{ mm}^4 = 69.92 \times 10^{-9} \text{ m}^4$$

The torsional mode stiffness is given by:

$$K_T = \frac{4GJ_p}{L}$$

Assuming a value for the Modulus of Rigidity for steel as $G = 8OGN/m^2$:

$$K_T = \frac{4 \times 80 \times 10^9 \times 69.92 \times 10^{-9}}{1.2}$$

K_T = 18.65 kNm/rad.

The mass moment of inertia of the cross-beam (the inertia effects of the hollow support tube being negligible) is given by:

$$I_{PP} = \frac{m_B}{12}(a^2 + L^2)$$

$$= \frac{14}{12}(.051^2 + 0.72)$$

$$I_{PP} = 0.575 \text{ kgm}^2$$

$\therefore$ the torsional mode natural frequency,

$$f_t = \frac{1}{2\pi}\left\{\frac{J_p}{I_{pp}}\right\}^{\frac{1}{2}}$$

$$\therefore f_T = \frac{1}{2\pi}\left\{\frac{18.65 \times 10^3}{0.575}\right\}^{\frac{1}{2}}$$

$$\underline{f_T = 28.7 \text{ Hz.}}$$

3. EFFECT OF ADDITIONAL MASSES

The basic experimental rig had design natural frequencies in the transverse and torsional mode respectively of 25Hz and 28.7Hz. In order to 'tune' these so that these natural frequencies could be either well separated or made almost equal, masses were added to the cross-beam which varied the inertia and mass effects:

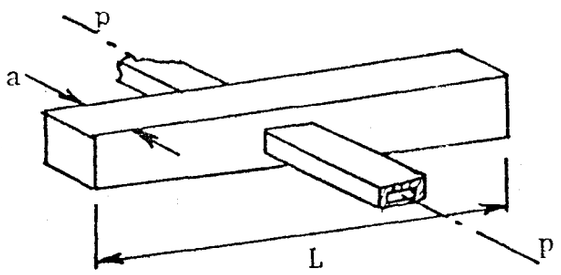

Thus the mass moment of inertia became:

$$I_{PP} = \frac{m_B}{12}(a^2 + L^2) + 2m_A h^2$$

and the effective mass of the beam became:

$$m_B' = m_B + 2m_A$$

The values of m_A used in the tests were chosen as 6kg. at a radius of 0.33m. This gave the design natural frequencies of vibration in the torsional and transverse modes respectively as:

$$f_T = \frac{1}{2\pi}\left(\frac{18.65 \times 10^2}{0.575 + (2 \times 6 \times 0.33^2)}\right)^{\frac{1}{2}}$$

$$\underline{f_T = 15.84 \text{ Hz.}}$$

$$f_B = \frac{1}{2\pi}\left(\frac{346 \times 10^3}{4 + 2 \times 6)}\right)^{\frac{1}{2}}$$

$$\underline{f_b = 18.36 \text{ Hz.}}$$

The actual natural frequencies of the rig with the above physical parameters from initial tests were:

$f_T = 15.54$ Hz
$f_B = 18.24$ Hz

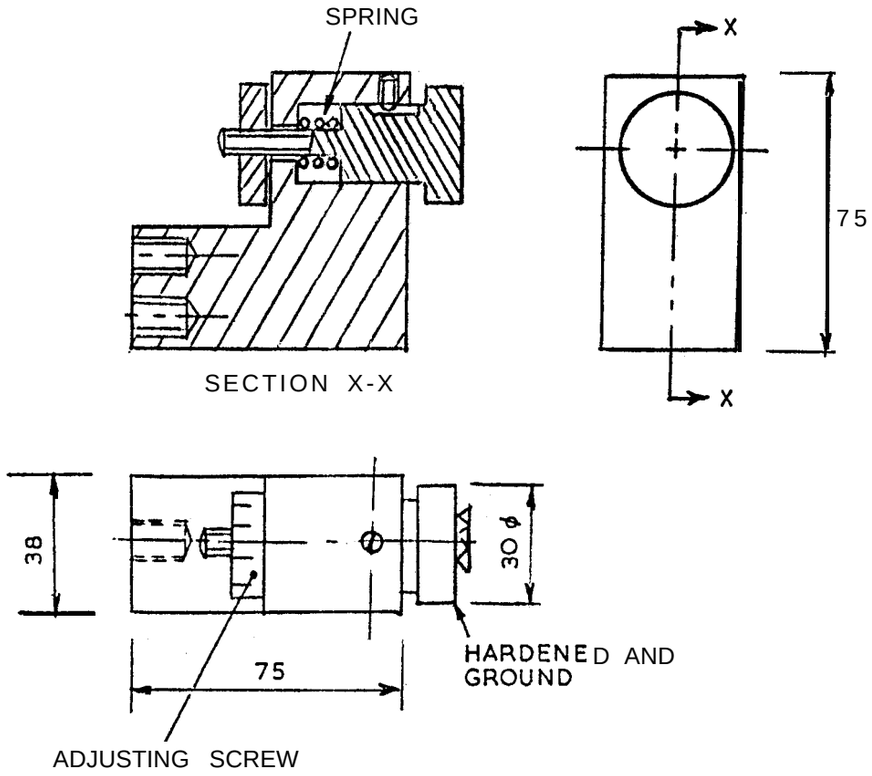

DETAIL OF COULOMB FRICTION DEVICE
MAT' L : M.S.

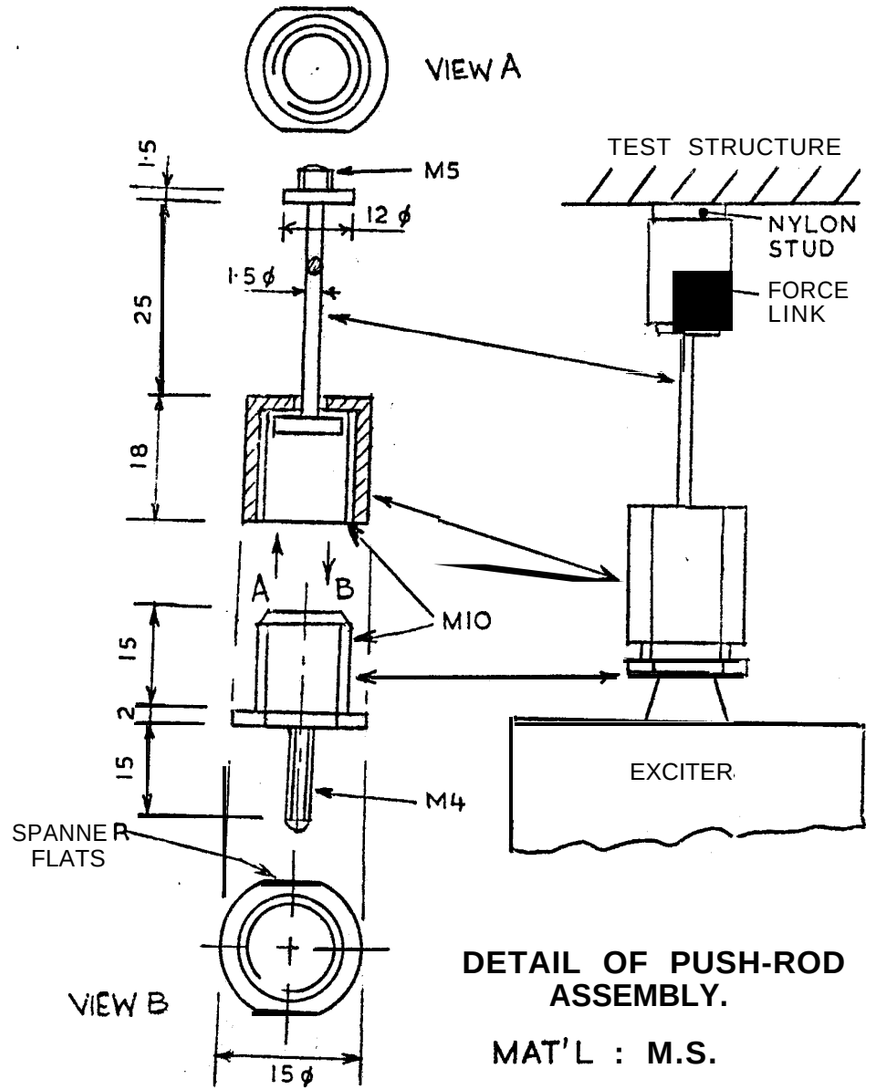

DETAIL OF PUSH-ROD ASSEMBLY.

MAT'L : M.S.

APPENDIX VII

Transducer Calibration Curves

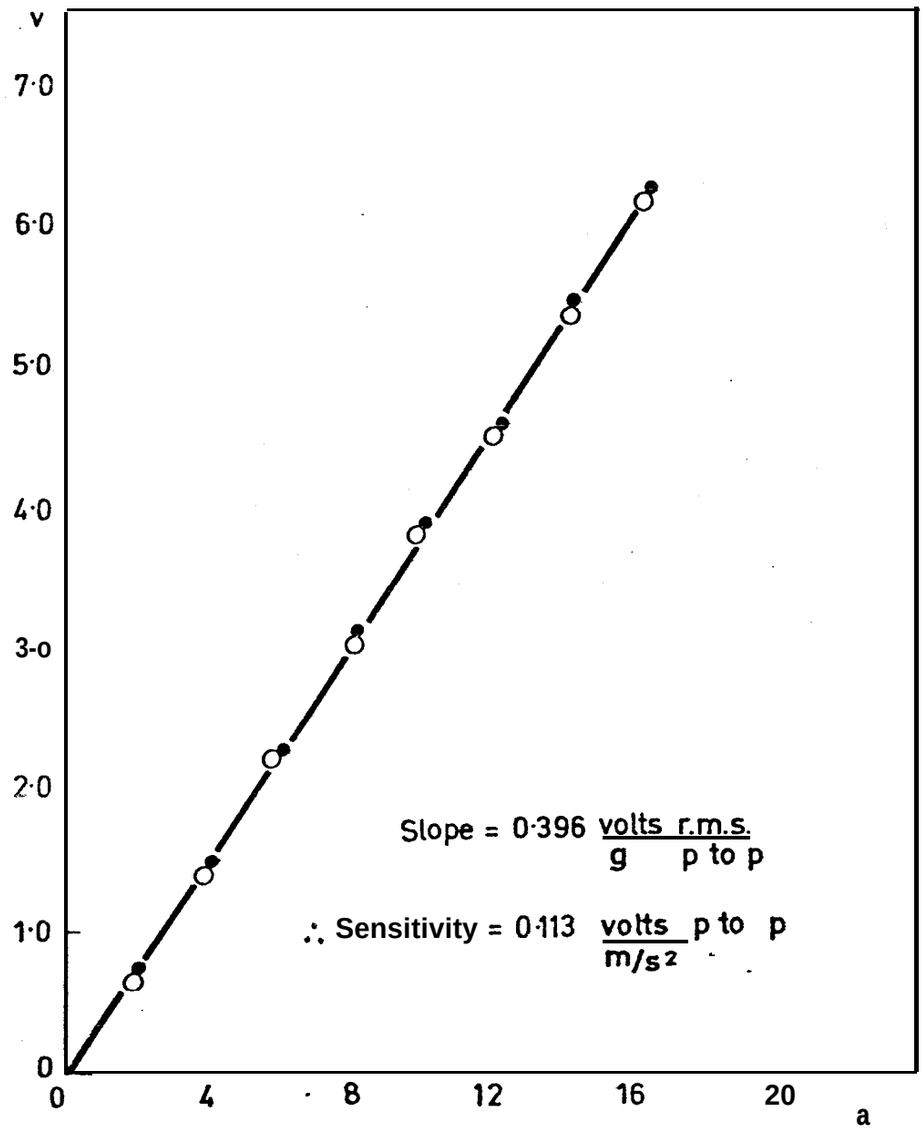

FIGURE A.VII.l

CALIBRATION CURVES FOR ACCELEROMETERS.

V IS THE OUTPUT r.m.s. VOLTAGE OF THE ACCELEREOMETERS
a **IS THE INPUT ACCELERATION IN 'g's PEAK-TO-PEAK**
(p **to** p) (lg = **9.81** m/s^2)
● **ACCELEROMETER** a_1
o **ACCELEROMETER** a_2

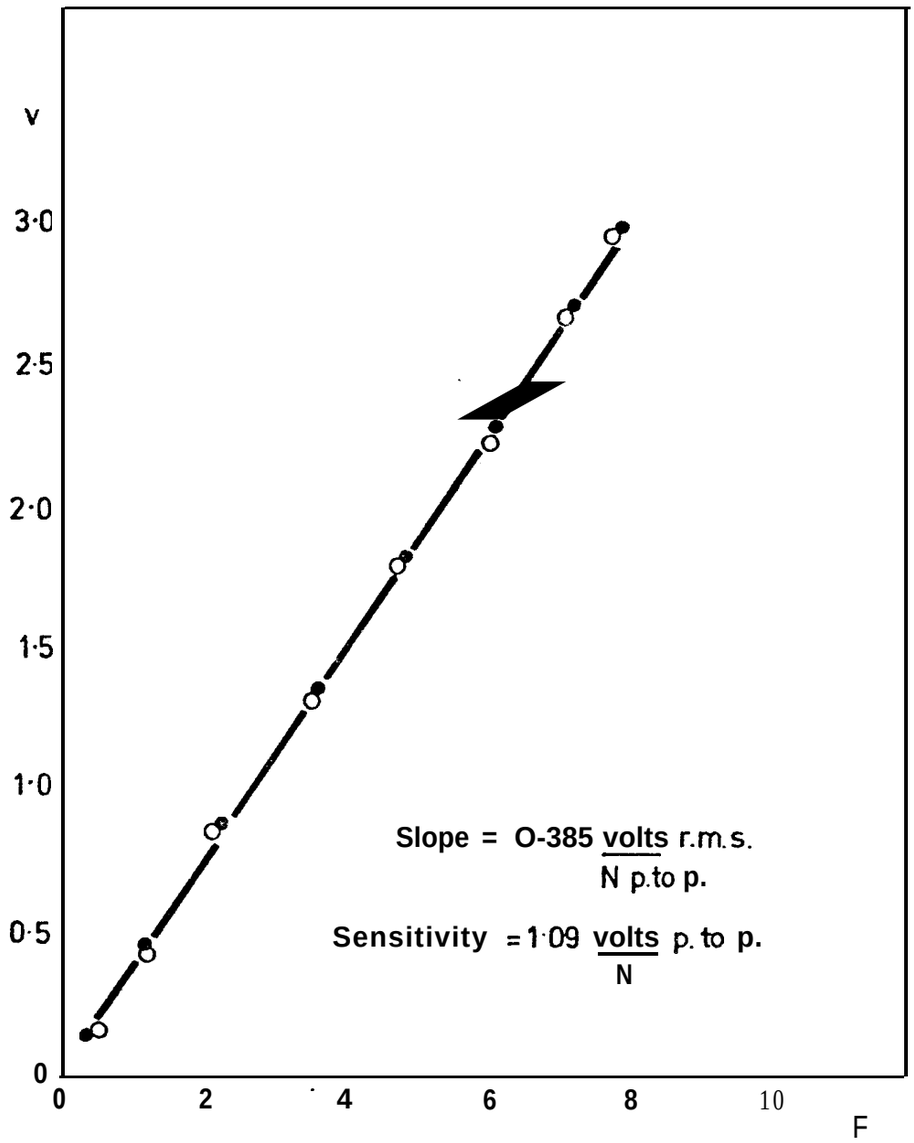

FIGURE A.VII.2

CALIBRATION CURVES FOR FORCE TRANSDUCERS

V IS THE OUTPUT r.m.s. **VOLTAGE**
F IS THE APPLIED FORCE IN NEWTONS PEAK-TO-PEAK
● **FORCE TRANSDUCERS** F_1
o **FORCE TRANSDUCERS** F_2

APPENDIX VIII

Proof Copies of Papers
Accepted for Publication

Journal of Sound and Vibration (1979) **63(3),** *337-350*

FORCE DISTORTION IN RESONANCE TESTING OF STRUCTURES WITH ELECTRO-DYNAMIC VIBRATION EXCITERS

G. R. TOMLINSON †

Department of Mechanical, Production and Chemical Engineering, Manchester Polytechnic, Manchester **M1** *5GD, England*

(Received **1** *June 1978, and in revisedform 7 October 1978)*

Harmonic input force distortion which arises when systems are excited with electro-dynamic exciters is shown to be predominantly second harmonic, the major source of the harmonic distortion being due to the vibration exciter characteristics. These are examined by experimentally determining the magnetic field strength properties of a typical exciter and the results show these to be a non-linear even function. This information is used with the equations of motion of the exciter which are simulated on an analog computer. The computed force characteristics are shown to compare very closely with experimental results. The amount of second harmonic force distortion generated at a system resonance is analyzed by considering a simple single degree-of-freedom model. It is shown that the amount of force distortion is related to the damping of the system under test and the ratio of the exciter stiffness to the system stiffness. It is also shown that the force input to a system near a system resonance can vary considerably, even though the input current to the exciter is constant. These effects are shown to he due to the forces arising from the mass and stiffness characteristics of the exciter being used. Experimental tests on a simple system confirm the theoretical predictions.

1. INTRODUCTION

The use of electro-dynamic vibration exciters for the steady state forced vibration of structures is almost universal [1]. These types of exciters are used as force generators to apply a harmonic force to a structure in order that modal data such as resonant frequencies, impedance data, mode shapes, generalized masses and stiffnesses can be obtained. In theory, measurement of the input force (or forces) and the structural response is straightforward. A sinusoidal voltage applied to an electro-dynamic vibration exciter via an amplifier should generate similar simple harmonic forces and accelerations. However, in practice, when the structure under test resonates, the reaction force (which is equal and opposite to the applied force) between the vibration exciter and the structure tends to become very small [2]. At this very point, i.e., the resonant condition, which is the point of greatest interest as regards test data, harmonics of the forcing frequency become very predominant. This harmonic distortion must be accounted for by suitable signal processing, especially when impedance tests are being carried out in order that reliable experimental results are obtained and techniques for filtering out unwanted harmonics are well established [2, 3].

In the past the source of the major harmonic force distortion was erroneously attributed to the stiffness of the force transducer [4] and to harmonics being generated within the amplifier plus oscillator together with some distortion within the vibration exciter. In this paper it is shown that the distortion is predominantly second harmonic which is generated due to non-linearities in the vibration exciter, and that the magnitude of the harmonic distortion depends basically upon the damping and stiffness of the structure under test.

† Now at the Department of Mechanical Engineering, University of Manchester, Manchester, England.

0022-460X/79/070337 +14 $02.00/0

It is often assumed that the use of high output impedance amplifiers used in connection with constant input current drive to an exciter will provide a constant input force to the system under test. With lightly damped structures, where the amplitudes of vibration may be relatively high, this assumption does not hold true and it is shown that if a constant current source is used to drive the exciter then large variations in the magnitude of the force input at the point of application of the structure may be encountered. These effects are shown to be due to the forces arising from the mass and stiffness characteristics of the exciter which modify the constant force generated in the coil of the exciter. Experimental results from a set of tests on a simple cantilever beam are compared with the theoretical predictions.

2. FORCE DISTORTION ENCOUNTERED DURING RESONANCE TESTING

Resonance testing of structures by use of electro-dynamic vibration exciters must, out of necessity, rely upon a rigid connection between the exciter and test structure along the line of action of the applied force. This often results in a type of force distortion arising from misalignment known as "side-stressing", and is due to the moving coil of the vibration exciter coming into contact with and rubbing against the centre pole magnet. In order to detect, and hence correct, side-stressing it is necessary to include a force detecting device between the vibration exciter and the structure under test, since monitoring of the current in the exciter coil gives little information relating to the actual input force level and also does not convey to the investigator the quality of the signal being applied to the structure under test. Side-stressing can be easily avoided by employing techniques which restrict the lateral movement of the vibration exciter armature [5] and by increasing the air gap between the centre pole magnet and the armature coil, although this latter method does reduce the efficiency of the exciter at high frequencies. A common method of reducing the interaction between the structure under test and the vibration exciter (often used in conjunction with the above techniques) is to use push-rods [6–8]. These are rods of high axial stiffness but allow lateral and rqtational motion between their ends.

When structures which have low modal stiffnesses are tested one finds that the force levels at resonance are very small, with correspondingly large amplitudes, and this often is the main cause of harmonic force distortion. The level of this distortion can be very considerable (e.g., over 100 % relative to the fundamental component) and is predominantly second harmonic [9]. A typical input force signal with predominantly second harmonic distortion and the resulting output response of the same point of a structure at resonance is shown in Figure 1 together with a case of "side-stressing".

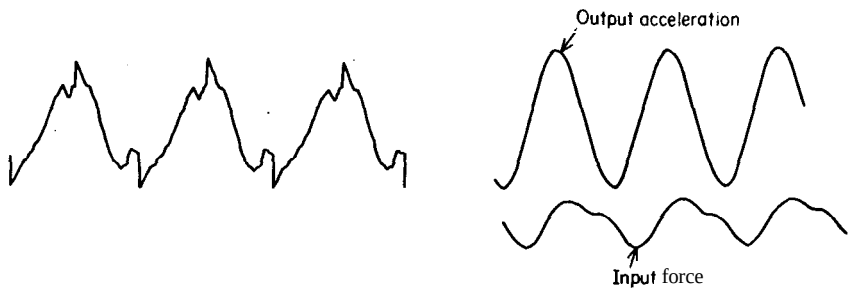

Figure 1. (a) Force distortion due to "side-stressing"; (b) input force at resonance and resulting motion at the same point.

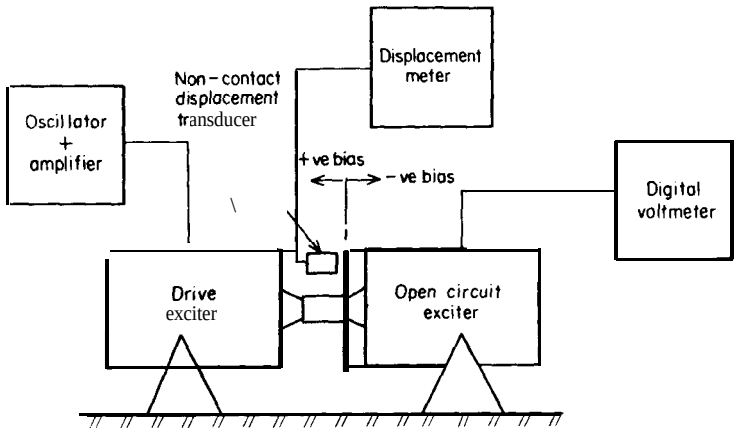

Figure 2. Experimental arrangement to determine magnetic field characteristics of an electro-dynamic exciter.

In the theory of electro-dynamic exciters it is assumed that the force generated is proportional to the input current, the constant of proportionality being a function of both the armature coil design and the magnetic field structure design [10]. If the magnetic flux field is assumed constant then a constant current produces a constant force. However, if the magnetic field structure does not produce a uniform flux density field, then a more fundamental approach is required in which the properties of the magnetic flux field are considered.

In order to examine the characteristics of the vibration exciter magnetic flux field, two vibration exciters with similar characteristics were connected together via a piezoelectric force transducer as shown in Figure 2. One of the exciters was used to "drive" the other exciter, whose armature was open-circuited, with a constant peak-to-peak amplitude at a given frequency, the amplitudes being measured by a non-contact displacement transducer. By superimposing a d.c. bias voltage on to the drive signal, the mean position of the open-circuit exciter armature (i.e., the static equilibrium point about which the vibration takes place) could be varied throughout its working displacement range for that particular exciter model. For each mean position of the open-circuited exciter armature a constant peak-to-peak amplitude of vibration was applied, this amplitude representing 15 % of the rated maximum peak-to-peak displacement range of the exciter. Tests were carried out at different frequencies (for the same mean armature positions and amplitudes of vibration) and the results for two different frequencies are shown on Figure 3. These curves, which are even functions with a square-law characteristic, are related to the back emf generated by the velocity of the armature and the position of the armature in the flux field.

The characteristics of Figure 3 show that the assumption of a constant magnetic field are invalid and that there is a variation in the magnetic field structure which is related to the position of the exciter armature in the magnetic field. In the case of lightly damped structures where the amplitudes of vibration are large and the level of the input forces are small, the normal governing electrodynamic equations are inapplicable and one must resort to electromagnetic theory to include the resulting variations.

From simple electromagnetic theory, the voltage arising as a consequence of the change of flux linkage is given as [11]:

$$v = (d\psi/dx)(dx/dt), \tag{1}$$

where ψ is the flux linkage, x is the instantaneous displacement within the magnetic flux and v is the voltage. Since for each test the velocity was constant, the characteristics of

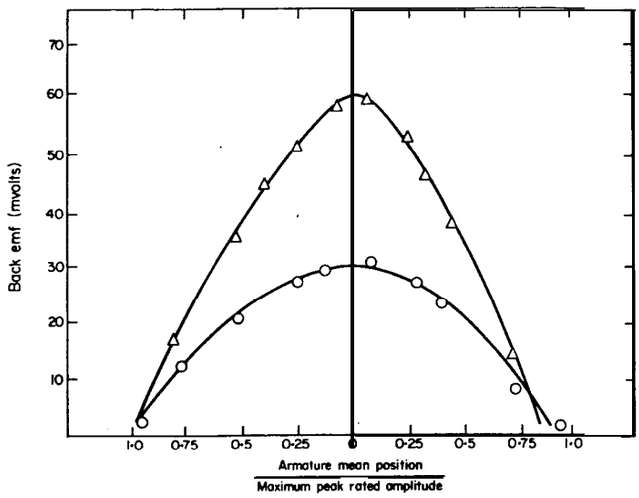

Figure 3. Back emfgenerated *vs.* mean position of open-circuit exciter as a function of maximum rated displacement of exciter.

Figure 3 must represent $d\psi/dx$: i.e.,

$$d\psi/dx = C\{1 - \alpha(x_0 + x)^2\}, \tag{2}$$

where

Ja = constant

= 1/ (maximum rated peak displacement of the exciter) $\geqslant 1/(x_0 + x)$,

due to the constraints imposed by the exciter design (i.e., the armature "bottoms" on the centre pole magnet if $(x_0 + x) > 1/\sqrt{\alpha}$), and where x_0 is the mean position of the armature, x is the instantaneous peak displacement of the armature and C is a constant related to the maximum back emf generated. Thus the back emf generated as a result of the motion of the armature in the magnetic flux field of Figure 3 is

$$v_B = (d\psi/dx)(dx/dt) = C\{1 - \alpha(x_0 + x)^2\}\dot{x}. \tag{3}$$

If the well known basic equations of motion (see Appendix 1) of an electro-dynamic vibration exciter are modified to include the terms of equation (3) one obtains the following expression for the armature equation of motion:

$$\ddot{x} + (k/m)x + (K/mR)\{1 - \alpha(x_0 + x)^2\}\dot{x} = (k_F/mR)v \cos \omega t, \tag{4}$$

where the constant K combines the force current and the back emf constant (these being assumed to be equal in this analysis). Equation (4) represents the motion of the exciter armature, which actually consists of a series of harmonic components. However, due to the fact that the magnitude of the fundamental component of the armature motion is very much greater than the square law terms and the higher harmonics, these become insignificant.

An analysis of the effects of the characteristics derived for the exciter was carried out by using an **analog** computer. The model analyzed represented a single degree-of-freedom system excited by an electro-dynamic vibration exciter via a force transducer. The model is shown in Figure 4 where the stiffness of the force transducer is assumed to be infinite

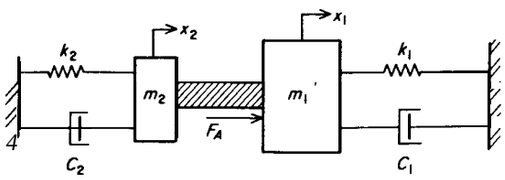

Figure 4. Simple model of single degree-of-freedom system and vibration exciter.

(piezoelectric force transducers have nominal stiffnesses $>10^8$ N/m). In Figure 4, m_1 is the mass of the test structure plus the effective mass of the force transducer above the crystal, m_2 is the mass of the vibration exciter coil assembly plus the effective mass of the force transducer below the crystal, k_1 is the stiffness of the test structure, k_2 is the flexure stiffness of the exciter, c_1 is the damping associated with the test structure, c_2 is the damping associated with the vibration exciter, and F_A is the total force applied to the test structure from the exciter.

Since the force transducer is assumed to have infinite stiffness then $x_1 = x_2 = x$, and the equation of motion of the mass and armature, the vibration being assumed to occur about the zero mean (i.e., $x_0 = 0$), is

$$\ddot{x} + \left\{\frac{C_1}{m_1 + m_2} + \frac{K}{R(m_1 + m_2)}(1 - \alpha x^2)\right\}\dot{x} + \frac{(k_1 + k_2)x}{m_1 + m_2} = \frac{k_F v \cos \omega t}{m_1 + m_2}. \qquad (5)$$

Simulation studies of equation (5) were carried out on an EAL 380 Analog Computer. The physical quantities expressed by the various constants in equation (5) were obtained from data supplied by the manufacturers of the vibration exciters used, and from tests carried out on the exciters. These quantities, together with the simulation diagram used are given in Appendix I. Figure 5 shows a sample set of results from the analog simulation. The simulation predicts the pattern of behaviour which was observed during the experimental tests where, at frequencies above and below the test structure resonant frequency, the force signal is predominantly the fundamental component. At the test structure resonant frequency the magnitude of the fundamental component reduces considerably and the harmonic distortion becomes predominantly second harmonic.

3. ESTIMATION OF HARMONIC DISTORTION MAGNITUDES

In order to establish the levels of harmonic force distortion which can occur during testing, an analysis of the system shown in Figure 4 was carried out. The force generated by the

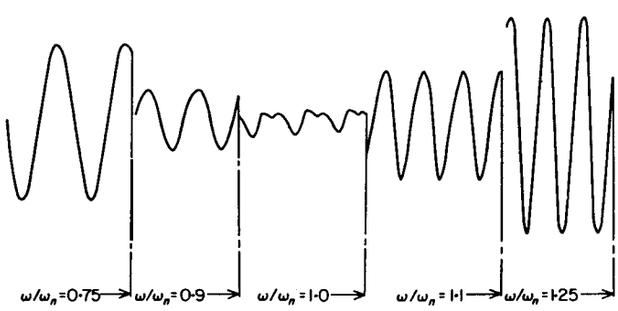

Figure 5. Analog simulation results showing the pattern of behaviour of the force. input signal around resonance for the system shown in Figure 4.

vibration exciter can be assumed to be represented by a harmonic series

$$F_A = \sum_{n=1}^{\infty} F_{A_n} e^{j(n\omega t + \phi_n)}, \qquad n = 1, 2, \ldots, \infty, \tag{6}$$

where

$$F_{A_n} = F_n e^{j(n\omega t + \phi_n)} - (m_2 D^2 + c_2 D + k_2)x e^{j(n\omega t + \phi_n)} \tag{7}$$

and F_n is the magnitude of the nth harmonic component, ω is the excitation frequency, and ϕ_n is the phase angle between the nth force and displacement components, respectively. The force F_{A_n} reacts against the test structure to give

$$F_{A_n} = (m_1 D^2 + c_1 D + k_1)x e^{j(n\omega t + \phi_n)}, \tag{8}$$

and therefore

$$x e^{j(n\omega t + \phi_n)}(F_n/x - m_2 D^2 - c_2 D - k_2) = (m_1 D^2 + c_1 D + k_1)x e^{j(n\omega t + \phi_n)}. \tag{9}$$

For harmonic motion $Dnx = j n\omega x$ and hence

$$F_{A_n} = (m_1 D^2 + c_1 D + k_1)F_n e^{j(n\omega t + \phi_n)}/[(k_1 + k_2) - (m_1 + m_2)n^2\omega^2 + (c_1 + c_2)\, jn\omega] \tag{10}$$

Upon introducing the notation

$$\omega_2^2 = k_2/m_2 \text{ (vibration exciter natural frequency)},$$

$$\omega_1^2 = k_1/m_1 \text{ (structure natural frequency)},$$

$$m_2/m_1 = m', \qquad k_2/k_1 = k', \qquad \beta_n = n\omega/\omega_1, \qquad c_1/k_1 = 2\zeta/\omega_1, \qquad c_2/k_2 = 2\zeta_2/\omega_2,$$

equation (10) becomes:

$$F_{A_n} = (1 - \beta_n^2 + j\beta_n 2\zeta_1)F_n e^{j(n\omega t + \phi_n)}/[(1 + k') - \beta_n^2(1 + m') + j\{2\zeta_1\beta_n + 2\zeta_2 n(\omega/\omega_2)k'\}]. \tag{11}$$

At the structural resonant frequency w = ω_1 and $\beta_1 = 1$; thus the fundamental harmonic force component is

$$F_{A_1} = (j2\zeta_1)F_1 e^{j(\omega t + \phi_1)}/[(1 + k') - (1 + m') + j\{2\zeta_1 + 2\zeta_2(\omega_1/\omega_2)k'\}]. \tag{12}$$

The second harmonic force component is

$$F_{A_2} = (-3 + j4\zeta_1)F_2 e^{j(2\omega t + \phi_2)}/[(1 + k') - 4(1 + m') + j\{4\zeta_1 + 4\zeta_2(\omega_1/\omega_2)k'\}]. \tag{13}$$

Substituting for $(\omega_1/\omega_2)k' = \sqrt{m'k'}$ in equations (12) and (13) gives, for the ratio of the second harmonic component to the fundamental,

$$\frac{F_{A_2}}{F_{A_1}} = \frac{F_2 e^{j(\omega t + \phi)}}{F_1} \frac{(-3 + j4\zeta_1)}{j(2\zeta_1)} \frac{[(k' - m') + j(2\zeta_1 + 2\zeta_2\sqrt{m'k'})]}{[(k' - 4m' - 3) + j(4\zeta_1 + 4\zeta_2\sqrt{m'k'})]}. \tag{14}$$

Equations similar to equation (14) may be written for the higher harmonics but the effects of these are obviously lower than the second harmonic contribution.

If one considers that generally $m' < k' \ll 1$, then equation (14) reduces to

$$|F_{A_2}/F_{A_1}| \simeq (k'/2\zeta_1)|F_2/F_1|. \tag{15}$$

Equation (15) indicates that for the second harmonic distortion to be less than 100%, the stiffness ratio $k' \leqslant 2\zeta_1$. For lightly damped structures, where the equivalence 2ζ = g (g being the structural damping factor) can be made, then $k' \leqslant$ g and, since structural

damping forces increase with stiffness, the stiffer the structure the lower will be the harmonic force distortion.

The reason behind the harmonic.distortion becoming predominant at a system resonance is easily shown by considering equation (11). Equation (1 I) represents the harmonic force components applied to the system under test. If one assumes that the exciter is being driven by a high output impedance amplifier then electrical damping effects can be ignored [12, 133. Also, if one considers the mechanical damping of the exciter to be negligible, equation (1 1), for the fundamental harmonic force component, reduces to

$$F_{A_1} = (1 - \beta_1^2 + j\beta_1 2\zeta_1)F_1 e^{j(\omega t + \phi)}/[(1 + k') - \beta_1^2(1 + m') + j(2\zeta_1\beta_1)], \quad (16)$$

or

$$|F_{A_1}| = [(1 - \beta_1^2)^2 + (\beta_1 2\zeta_1)^2]^{1/2}|F_1|/[((1 + k') - \beta_1^2(1 + m'))^2 + (2\zeta_1\beta_1)^2]^{1/2} \quad (17)$$

where $\beta_1 = \omega/\omega_1$. Equation (17) is shown plotted on Figure 6 as a function of the frequency ratio (ω/ω_1) for different values of the system damping ratio for the cases when the system natural frequency is greater and less than the exciter natural frequency. It can be seen from

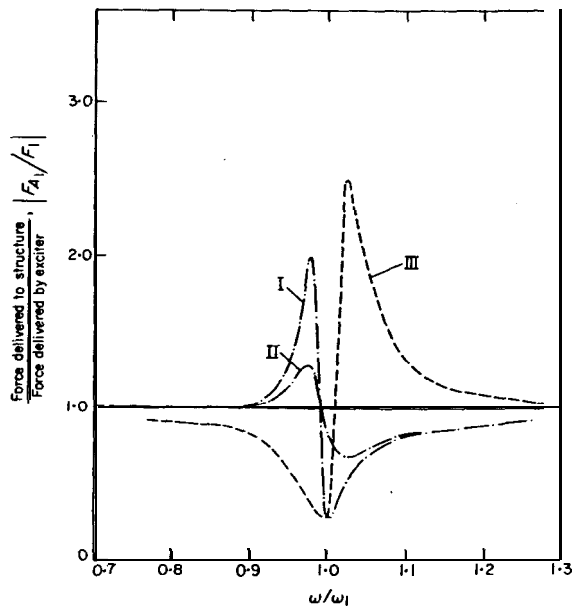

Figure 6. Theoretical curves of equation (11) showing input force variation at a structural resonance. –·–·. Exciter natural frequency < structure natural frequency; ———, exciter natural frequency > structure natural frequency. Curve 1, $\zeta = 0{\cdot}01, m' = 0175, k' = 0{\cdot}14$; curve II, $\zeta = 0{\cdot}05, m' = 0{\cdot}175, k' = 0.14$; curve III, $\zeta = 0{\cdot}01$, $m' = 0{\cdot}005, k' = 0{\cdot}06$.

Figure 6 that there is a large variation in the input force in both cases which reduces as the system damping is increased (i.e., the amplitudes of forced vibration, for a given force, are reduced). Also, the force characteristic is "inverted" when the system natural frequency changes from a value above to a value below that of the exciter natural frequency. These effects have been noted by other researchers [12, 14) and were attributed to the mass and stiffness effects of the exciter.

An analysis of the effects of an exciter's mass and stiffness properties on the force injected into a system has been carried out in Appendix 2. In the analysis it is assumed that a con-

stant current source is used. The analysis shows, with the aid of vector diagrams, that when lightly damped structures are excited with electro-dynamic exciters then considerable variation in both the magnitude and phase of the actual input force to the system under test is encountered.

4. EXPERIMENTAL INVESTIGATION

Tests were carried out on a simple cantilever beam in order to test the validity of the above analyses. The tests allowed the stiffness ratio k' to be varied by changing the flexural stiffness of a standard electro-dynamic vibration exciter. **This method** of varying k' was used in preference to simply changing the beam length in order to alter the value of k since this had more practical significance, and also the mass ratio m' was constant. The cantilever beam used in the tests was 25 mm wide, 50 mm deep and 1·25 m long. It was excited at its tip via a piezoelectric force transducer and push-rod assembly with a standard (commercial) electro-dynamic vibration exciter. The flexure stiffness and effective armature mass of the exciter were 14 N/mm and 0·2 kg respectively. During the tests the beam ivas excited over its fundamental frequency range with a constant displacement and the first and second harmonic components of the input force signal were measured on an harmonic analyzer. In order to provide a variation in k', the stiffness of the exciter was modified by removing one of the fibre flexure supports. This reduced the stiffness of the exciter by approximately 50 %. As a result of this modification the lateral stiffness of the exciter was reduced to such an extent that a linear ball-race guide had to be used to provide lateral support and hence prevent side-stressing of the exciter coil. This obviously increased the exciter frictional damping but transient results indicated that this was minimal for steady state vibrations. The results of the tests are shown on Figure 7 and it can be seen that there is good correlation between the theoretical and experimental results.

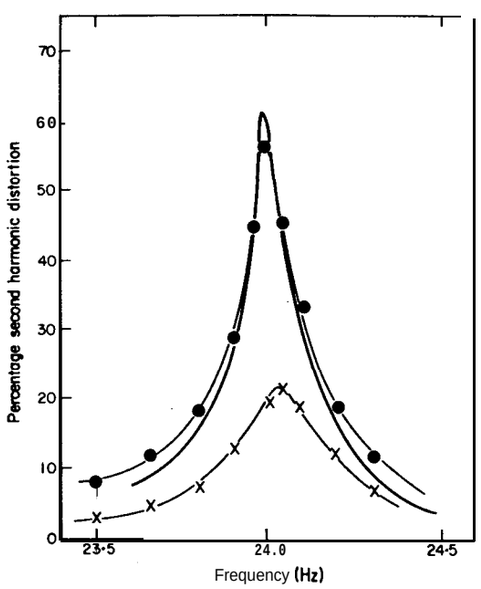

Figure 7. Results from tests on simple cantilever beam. Variation in second harmonic force distortion with exciter stiffness. ●——●, Standard exciter with k' = 0·160, m' = 0·016, ζ_1 = 0·0013; x-x, modified exciter with k' = 0·07, m' = 0·016, ζ_1 = 04013; ———, theoretical curve from equation (11) with k' = 0·160, m' = 0016, ζ_1 = 0·0013, ζ_2 = 0·0.

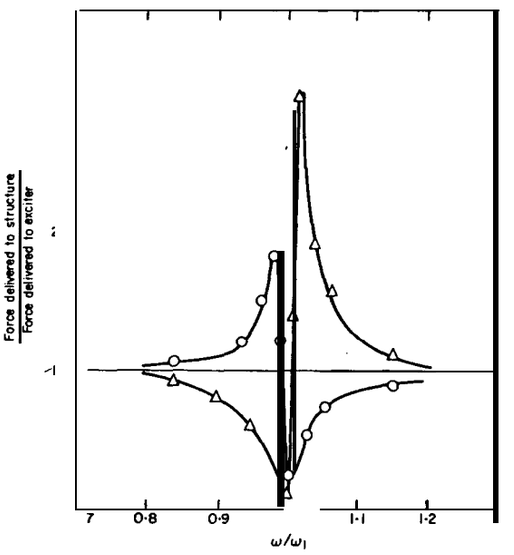

Figure 8. Constant current experimental results showing variation in the input force to a structure at the structural resonance. O———O, Exciter natural frequency < structure natural frequency: A-A, exciter natural frequency > structure natural frequency.

Constant current tests were also carried out and the magnitude of the fundamental harmonic input force component, measured by the piezoelectric force transducer at the tip of the beam, was obtained as the excitation frequency was swept over the fundamental natural frequency of the beam. These tests were carried out with the beam fundamental natural frequency above and below that of the exciter being used in the tests. Figure 8 shows the experimental results obtained in these tests and if a comparison between these and the theoretical curves of Figure 6 is made it can be seen that there is excellent agreement.

5. DISCUSSION

The work reported in this paper has shown that harmonic distortion of the input force signal at a system resonance is primarily due to the non-linear characteristics of the electrodynamic vibration exciter. These non-linearities, which characterize the -magnetic field strength of the exciter, are basically square-law in nature, which results in the force distortion being predominantly second harmonic. Higher harmonics will be present in the force signal due to the fact that distortions of the square-law characteristic will occur during testing, these distortions arising from such things as armature misalignment, higher order terms in the magnetic field strength characteristics and variations in characteristics from one vibrator to another.

It is shown that the damping in the system under test is a very important factor and in order to minimize the harmonic force distortion occurring at resonance this must be significantly greater than the ratio of the vibration exciter stiffness to the test structure stiffness. If the amplitudes of vibration are small, e.g., as a result of exciting higher modes, the harmonic distortion is reduced as a result of two factors. Small amplitudes of vibration restrict the armature movement in the non-linear magnetic field: i.e., movement is restricted to the region around the zero mean position of the curve on Figure 3 and hence the non-

linearities are minimized. The second factor is that higher modes of vibration tend to produce larger damping forces which result in an increase in the fundamental force component, whereas the second and higher order components remain approximately constant.

Further, it has been shown that regardless of whether or not a high output impedance amplifier is used to supply a constant current source, large variations in the magnitude and phase of the input force can occur when testing lightly damped systems. This has been confirmed to be due to the forces arising from the mass and stiffness characteristics of the vibration exciter which modify the resultant force applied to the system at the system resonance. If the natural frequency of the vibration exciter were to be the same as that of the system under test then a constant force would be applied to the system since the vibration exciter effects would be self-compensating.

The importance of these factors is that if a constant current source is used as a reference force condition, then, in the case of a lightly damped single degree-of-freedom system, a ninety degree phase shift between the input current and the output displacement (or acceleration) does not necessarily indicate a natural frequency. Only if the input force measured at the point of application on the test system and the corresponding response are used can this criterion be applied.

However, in terms of the harmonic force distortion levels at resonance, some improvement would be achieved by employing a constant current source since the magnitude of the non-linear term of equation (5) would be reduced. This is because the non-linear term would be a function of the force current constant only as opposed to a combination of this and the back emf constant which would be the case with a voltage source (see Appendix 1).

ACKNOWLEDGMENTS

The author would like to acknowledge Dr J. W. Golten and Mr F. J. Swift for their interest and helpful discussions on this topic.

REFERENCES

1. W. TUSKIN 1977 ***Shock and Vibration Digest*** **9**, 3–10. A comparison of techniques and equipment for generating vibration.
2. D. J. EWINS 1974 ***Solatron Schlumberger Dynamic Analysis Monograph.*** A short guide to mechanical impedance testing.
3. L. R. BURROW, JR. 1964 ***Test Engineering 16-19, 6263.*** Tracking filters standardize sinusoidal vibration tests.
4. W. G. ASHER 1958 ***Institute of Aeronautical Science Proceedings, Specialists' Meeting on Dynamics and Aeroelasticity, Fort Worth 69-76.*** A method of normal mode excitation utilizing admittance measurements.
5. A. PETRUSEWICZ and D. K. ONGMORE 1974 ***Noise and Vibration Controlfor Industrialists.*** London: Elek Scientific Books.
6. D. J. EDWINS 1975 ***Journal of the Society of Environmental Engineers 14, 3-12.*** Measurement and application of mechanical impedance data: Part I: Introduction and ground rules.
7. D. J. EWINS 1976 ***Journal of the Society of Environmental Engineers*** **15**, 13-21. Measurement and application of mechanical impedance data: Part II: Measurement techniques.
8. D. J. EWINS 1976 ***Journal of the Society of Environmental Engineers 15, 22-32.*** Measurement and application of mechanical impedance data: Part III: Interpretation and application of measured data.
9. W. F. BANGS 1964 ***Shock and Vibration Bulletin*** **33**-3, 195–202. Sinusoidal vibration testing of nonlinear spacecraft structures.
10. R. C. LEWIS and D. L. WRISLEY 1950 ***Journal of the Aeronautical*** **Sciences 17**, 705–722. A system **for the excitation of pure natural modes of complex structures.**

11. M. G. SAY 1971 ***Introduction to the Unified Theory of Electromagnetic Machines.*** London : Pitman Press, first edition.
12. G. A. TAYLOR, D. R. GAUKROGER and C. W. SKINGLE 1967 ***R.A.E. Technical Report 67211. M.A.M.A.*** A semi-automatic technique for exciting the principal modes of vibration ofcomplex structures.
13. P. J. HOLMES and R. G. WHITE 1972 ***Journal of Sound and Vibration 25, 217-243.*** Data analysis criteria and instrumentation requirements **for the transient measurement of** mechanical impedance.
14. H. G. NATKE 1969 ***V.K. W. Report*** EY-Bll. Description of a vibration test unit and its use for the third stage of Europa 1. (English translation FLS number 29436.)

APPENDIX 1: BASIC EQUATIONS OF MOTION OF AN ELECTRO-DYNAMIC VIBRATION EXCITER AND ANALOG SIMULATION DIAGRAM

The physical model of an electro-dynamic exciter can be considered simply as a resistor, representing the coil, with an additional voltage drop due to the velocity of the coil moving through the magnetic field of the permanent magnet. The mechanical sub-system is merely a mass and a spring driven by a force proportional to the current, damping effects due to the flexure stiffness hysteresis and the rubber dust cap being ignored. The basic equations of motion are

$$m\dot{x} + kx = k_F i, \qquad Ri + k_B\dot{x} = v\cos\omega t, \tag{A1, 2}$$

where m is the effective armature mass, k is the flexural stiffness, k_F is the force current constant, k_B is the back emf constant, i is the armature current, v is the applied voltage at frequency ω, and R is the exciter coil resistance plus the drive amplifier output resistance. Thus the equation of motion of the armature, from equations (Al) and (A2) is

$$\ddot{x} + (kx/m) + (k_F k_B/mR)\dot{x} = (k_F/mR)\ cos\ ot. \tag{A3}$$

If the electrical power developed in the armature is assumed to be equal to the mechanical power absorbed, then

$$k_B\dot{x}i = k_F\dot{x}i: \qquad \text{i.e., } k_B = k_F \tag{A4}$$

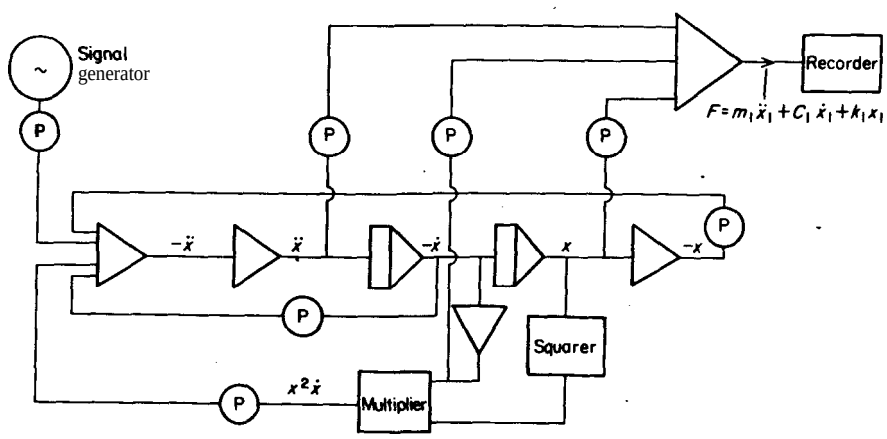

Figure **Al. Analog simulation block diagram used to compute tbe force arising from equation (4). Ⓟ indicates a potentiometer. Values** used in the simulation were m_1 = 0·1 kg, m_2 = 0·02 kg, k_1 = 1 kN/m, k_2 = 3 kN/m, C_1 = O-2. **Ns/m, $k_F = k_B$** = 8 **N/A,** R = **4 ohms. $\alpha = 025 \times 10^6/m^2$.**

Both k_B and k_F are dependent upon the characteristic of the magnetic flux field of the exciter and these effects, given by equation (2) of section 2, can be combined in equation (A3) to give equation (4) of section 2: i.e.,

$$\ddot{x} + (kx/m) + (K/mR)\{1 - \alpha(x_0 + x)'\}\ \dot{x} = (k_F/mR)\, v \cos \omega t. \quad \text{(A5)}$$

The block diagram **used** in the analog simulation of equation (5) is shown in Figure Al together with the values of the various physical constants used in the simulation.

APPENDIX 2: THE EFFECTS OF AN ELECTRO-DYNAMIC EXCITER ON A VIBRATING STRUCTURE

The force necessary to vibrate a structure is produced by the current through the exciter coil. The moving elements of the exciter, namely the armature and some fraction of the flexure mass and the push-rod assembly (which incorporates the force gauge), are rigidly attached to the structure under test and as a result some of the force is used to accelerate these additional masses. If the structure under test is at resonance then the displacement of the excitation point is in quadrature with the exciting force. The additional masses of the moving elements of the exciter are in phase with the structure but the acceleration forces of these additional masses oppose the forces arising from the effects of the **flexural** stiffness of the exciter. This results in the oscillator current vector not being in quadrature with the displacement of the structure at resonance. This can be explained by considering a single degree-of-freedom system excited by an electro-dynamic exciter. The model of the system under analysis is shown in Figure 4.

The resultant force R applied to the structure is

$$R = F\, e^{j\omega t} - m_2\ddot{x}_2 - c_2\dot{x}_2 - k_2x_2, \quad \text{(A6)}$$

where F is the force delivered to the moving parts of the exciter as a result of the oscillator current {which is held constant in magnitude and phase with the oscillator reference voltage). If the stiffness of the force transducer is considered to be infinite compared to the exciter and test structure stiffness, then the displacements within the system are common: i.e.,

$$x_2 = x_1 = x. \quad \text{(A7)}$$

The displacement of the armature(and structure) is related to the oscillator reference current by

$$x = X\, e^{j(\omega t - \psi)}, \quad \text{(A8)}$$

where ψ is the phase angle between the oscillator reference current and the displacement, X is the peak amplitude of the displacement and ω is the radian frequency. With the aid of the vector diagram in Figure A2 the resultant force applied to the structure can be obtained. as

$$R = F \cos \omega t + m_2\omega^2 X \cos(\omega t - \psi) - k_2 X \cos(\omega t - \psi) + c_2\omega X \sin(\omega t - \psi). \quad \text{(A9)}$$

The reaction force of the structure, which will be equal and opposite to R, will be

$$R_F = -R = m_1\omega^2 X \cos(\omega t - \psi) - k_1 X \cos(\omega t - \psi) + c_1\omega X \sin(\omega t - \psi). \quad \text{(A10)}$$

If the forces are expressed relative to the oscillator reference then at a given frequency there will be a phase angle between the force delivered from the exciter and the resultant force as a result of equation **(A9),** and as shown on Figure A3.

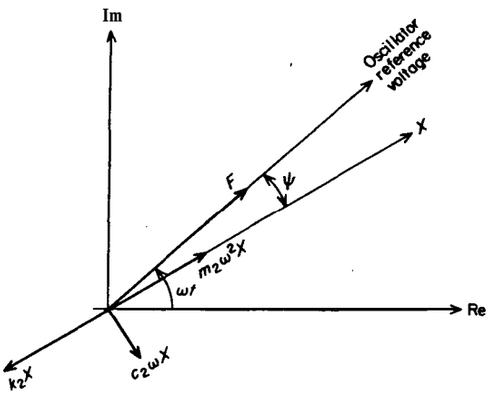

Figure A2. Vector diagram for equations (A6), (A7) and (A8).

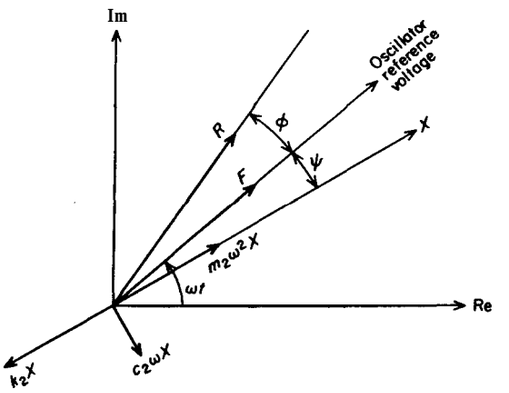

Figure A3. Vector diagram showing the force applied to the structure (R) and the force delivered to the exciter (F).

From Figure A3 the resultant force applied to the structure expressed relative to the oscillator reference is

$$R \sin\phi = m_2\omega^2 X \sin\psi - k_2 X \sin\psi - c_2 X\omega \cos\psi, \quad \text{(A11)}$$

$$R \cos\phi = -m_2\omega^2 X \cos\psi + k_2 X \cos\psi - c_2\omega X \sin\psi + F. \quad \text{(A12)}$$

For a lightly damped single degree-of-freedom system resonance occurs when the phase angle between the resulting displacement and the applied force is 90°: i.e., when

$$\phi + \psi = 90^\circ. \quad \text{(A13)}$$

Substituting $\psi = 90^\circ - \phi$ in equations (Al I) and (A12) gives

$$R \sin\phi = (m_2\omega^2 - k_2)X \cos\phi - c_2 X \sin\phi, \quad \text{(A14)}$$

$$R \cos\phi = -(m_2\omega^2 - k_2)X \sin\phi - c_2 X \cos\phi + F. \quad \text{(A15)}$$

Multiplying equation (A14) by cos ϕ and equation (A15) by sin ϕ and rearranging gives

$$(m_2\omega^2 - k_2)X = F \sin\phi. \quad \text{(A16)}$$

With the exciter and structure natural frequencies denoted, respectively, by

$$\omega_2^2 = k_2/m_2, \qquad \omega_1^2 = k_1/m_1, \tag{A17}$$

equation (A16) can be written as

$$k_2 X((\omega_1/\omega_2)^2 - 1) = F \sin \phi. \tag{A18}$$

Thus the force which is applied to the structure is only in phase with the force delivered by the exciter when one or more of the following conditions arises: (a) $\phi = 0$; (b) $\omega_1 = \omega_2$; (c) x = 0.

Journal of Sound and Vibration (1979) 64(2), 233-242

IDENTIFICATION OF THE DYNAMIC CHARACTERISTICS OF A STRUCTURE WITH COULOMB FRICTION

G. R. TOMLINSON†

Department of Mechanical, Production and Chemical Engineering, Manchester Polytechnic, Manchester M1 5GD, England

AND

J. H. HIBBERT

Department of Mechanical and Aeronautical Engineering, University of Salford, Salford M5 4 WT, England

(Received 3 August 1978, and in revisedform 7 December 1978)

The effect of coulomb friction on the Kennedy and Pancu vector plot of a single degree-of-freedom system is analyzed by using the method of harmonic balance. It is shown that the resulting diagram no longer conforms to a locus of a circle in the resonant region, which restricts the usual methods of analysis. A technique, based upon the in-phase and quadrature power dissipated when exciting a normal mode, is presented which allows the magnitude of the non-linear friction force and the hysteretic damping constant to be evaluated. The technique is also applied to systems having several degrees-of-freedom and it shows that it is possible to identify the characteristics of a single non-linear coulomb device situated within a structure, but in the case of more than one device, the technique has some restrictions. The theoretical results are compared with experimental data from a structure containing a non-linear coulomb device.

1. INTRODUCTION

The estimation of modal parameters from frequency or transient response data has relied heavily on the use of vector plots derived by Kennedy and Pancu [1]. This technique, which has been applied to a wide number of applications [2], relies upon a circular arc being curve-fitted to experimental data in the resonant regions [3]. Any deviation in the experimental data from the locus of a circle in these regions will automatically evoke errors, and in certain cases, will restrict the application of this technique.

Such a case arises with systems comprising non-linear elements [4], for which the best curve fit to the experimental data may result in figures resembling elongated circles (elliptical shapes) or combinations of circles with distorted regions, White [5] showed such effects from the results of a structure subjected to large deflections and concluded that as a result of thii the methods which are normally used to obtain certain modal parameters, such as the maximum frequency spacing criterion for estimation of the modal frequency, did not hold true.

Methods for identifying modal parameters of systems which display non-linear characteristics have, in the past, been only partially successful in the sense that the analysis either was concerned with ideal systems [6, 7] or was restricted to single degree of freedom systems

Other techniques [9] have shown that it is theoretically possible to ascertain the position and the characteristics of the non-linear element, but only if the characteristics of the non-linearity are dependent upon the absolute amplitude of the element: i.e., it is grounded.

In this paper the effects of a non-linear coulomb friction device on the Kennedy and Pancu plot of a single degree-of-freedom system are analyzed by using the method of harmonic balance, and this principle is then applied to the normal mode response of a multidegree-of-freedom system. A technique is thereby derived for locating and identifying the characteristics of a single coulomb frictional device, which may be situated anywhere in the structure, and the application of the technique to systems comprising more than one frictional device is discussed It must be realized however that the types of system to which the technique is applicable are restricted to those where the elastic elements are assumed to be linear, and where, besides coulomb friction, there exists only linear damping. The results from experimental tests on a two degree-of-freedom model, having a controlled coulomb frictional device, are compared with the theoretically predicted characteristics

2. NORMAL MODE RESPONSE OF A SYSTEM WITH COULOMB FRICTION

The conditions for the existence of classical normal modes in structures where frictional energy is dissipated [10,11], appear to have no physical justification but systems can frequently be described adequately by equivalent single degree-of-freedom models providing that the modes are well separated or the frictional forces are not excessive [12]. In the following analysis it is assumed that the frictional mechanism is of the coulomb form: that is, the frictional force $f(\dot{x})$ is defined by the relationships

$$f(\dot{x}) = q \quad \text{for } \dot{x} > 0, \qquad f(\dot{x}) = -q \quad \text{for } \dot{x} < 0, \tag{I}$$

where q is the peak magnitude of the frictional force. By using the method of harmonic balance, this characteristic can be represented by an equivalent hysteretic damping constant h^*, where

$$h^* = 4q/\pi|u| \tag{2}$$

and $|u|$ is the peak displacement.

If the elastic and non-frictional dissipative properties of the structure are to be represented by a massless element of complex stiffness the equivalent single degree-of-freedom model for a particular mode may be represented by a body of mass m supported by an element of complex stiffness, given as

$$k + jh^* = k'(1 + j\delta^*), \tag{3}$$

where k is the elastic component of stiffness and the equivalent loss factor δ^* has the form

$$\delta^* = (6 + 4q/\pi k'|u|), \tag{4}$$

δ being the structural (non-frictional) loss factor. When a harmonic force $pe^{j\omega t}$ is applied to the body of mass m, the equation of motion is

$$m\ddot{x} + k'(1 + j\delta^*)x = pe^{j\omega t}, \tag{5}$$

which has the solution $x = ue^{j\omega t}$, where $u = |u|e^{j\phi}$,

$$|u| = (p/k')/[(1 - \Omega^2)^2 + \delta^{*2}]^{1/2}, \tag{6}$$

and $\tan \phi = \delta^*/(1 - \Omega^2)$, where $\Omega = \omega\sqrt{m/k'}$.

Equation (4) may now be substituted into equation (6) to give:

$$|u| = \frac{-\delta r + \sqrt{(p/k')^2[(1-\Omega^2)^2 + \delta^2] - r^2(1-\Omega^2)^2}}{(1-\Omega^2)^2 + \delta^2}, \tag{7}$$

where $r = 4q/\pi k'$.

A solution for $|u|$ is only possible when $r < p/k'$. In practical situations this means that the applied force p must be greater than the magnitude of the friction force q in order for any relative motion to exist The phase angle, for equations (4) and (6), is given by

$$\tan \phi = [\delta + (r/|u|)]/(1-\Omega^2). \tag{8}$$

When the vector response, from equations (7) and (8), is plotted in the phase plane it is found that the locus **has a form similar to that** shown in Figure 1. Clearly, the effect of the

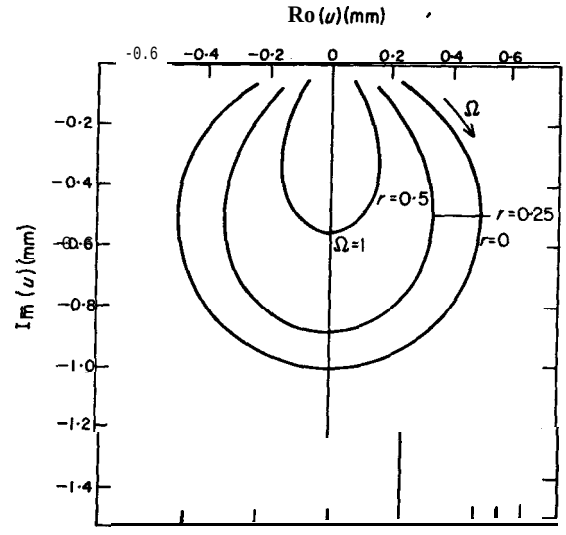

Figure 1. Effect of coulomb friction on the vector response locus of a single degree-of-freedom system with hysteretic damping r being proportional to the friction force level (r 4q/πk').

coulomb frictional forces is to produce an elongation, parallel to the imaginary axis, of the familiar circular locus which is obtained for lightly damped linear systems. As a result of this distortion, the system parameters **cannot** be determined as readily from this vector response locus as they can when the system is linear.

An alternative approach is that based upon the measurement of complex power in the region of resonance as proposed by Bonneau [13]. In this method, the total input power W to a mode is determined by obtaining the product of the applied force **and** the associated velocity. It is evident that the power must be a complex quantity having real and imaginary components W' and W'' respectively. It can be easily shown [13) that for a viscously damped single degree-of-freedom system the following conditions apply at resonance $(\omega = \omega_n)$:

$$W''|_{\omega=\omega_n} = dW'/d\omega|_{\omega=\omega_n} = 0, \tag{9}$$

$$dW''/d\omega|_{\omega=\omega_n} = \text{a maximum.} \tag{10}$$

These conditions can be shown to give the damping ratio ζ as

$$\zeta = (1/\omega_n)\{W'/(dW''/d\omega)\}|_{\omega=\omega_n}. \tag{11}$$

Thus **plots of the in-phase and quadrature power against frequency will provide estimates of the damping and the natural frequency. Typical plots of the in-phase and quadrature components from a set of experimental results are shown on Figure 6 of section 6.** The obvious advantages resulting from this technique are that the curve fitting procedures involved are **simple and do not need to be modified for the type of non-linearity under investigation.**

It is evident from equations (7) and (8) that when a frictionally damped single degree-of-freedom system is excited at its resonant frequency, the displacement and force are in quadrature and

$$|u| = [(p/k') - r]/\delta. \tag{12}$$

It follows therefore that since at resonance

$$p = k'(\delta|u| + r),$$

then

$$W'|_{\omega=\omega_n} = \omega_n k'(\delta|u|^2 + r|u|) \tag{13}$$

and since also $W''_{\omega=\omega_n} = 0$, equation (13) can be expressed in the form

$$(W'/\omega_n|u|)_{\omega=\omega n} = k'\delta|u| + k'r. \tag{14}$$

If, therefore, $W'/\omega_n|u|$ is plotted against $|u|$, at the resonant frequency, the resulting curve will be a straight line with an intercept equal to the value of k'r. The results may then be substituted into equation (14) to obtain the value of the linear hysteretic damping constant $k'\delta$.

3. THE EFFECT OF COULOMB FRICTION ON SYSTEMS HAVING SEVERAL DEGREES-OF-FREEDOM

The procedure described in the previous section can be used to analyze complex structures when modal interaction is not particularly strong. However, there are many cases where the frictional coupling is such that a more refined dynamical model needs to be identified In such cases, it is necessary to represent the structure by a lumped parameter system with *n* degrees-of-freedom The system may then be defined by mass, stiffness and damping matrices M, K and **H** respectively. If the system is assumed to be linear, the harmonic solution $x = u e^{j\omega t}$ gives the resulting matrix equations

$$-\omega^2\mathbf{Mu} + \mathbf{Ku} + j\mathbf{Hu} = \mathbf{p}. \tag{15}$$

When the system is excited at its *ith* natural frequency ω_i by the forces $\mathbf{p}_i$ such that the peak displacements are given by $\lambda\mathbf{v}_i$, where $\mathbf{v}_i$ is the *ith* normalized mode shape and λ is a constant, equation (15) reduces to

$$j\lambda\mathbf{Hv}_i = \mathbf{p}_i, \tag{16}$$

since $\omega_i^2\mathbf{Mv}_i = \mathbf{Kv}_i$. **Thus,** providing that $\mathbf{p}_i$ **is real,** all the displacements *will be in* phase with each other and in quadrature with the forces.

If it is assumed that the damping is a combination of structural (hysteretic) damping and frictional damping, denoted by the matrices S and **F** respectively, the matrix **F can be** formed by linearizing the coulomb friction elements. The elements of the **F** matrix may be expressed in terms of the displacements in the following manner:

$$f_{kl} = \sum[b_{kl}/g_{kl}(u_1, u_2, \ldots, u_n)], \tag{17}$$

where f_{kl} is the element in the kth row and lth column, b_{kl} is a constant and g_{kl} is a linear function of amplitudes. Thus, when the system is excited at its ith natural frequency,

$$f_{kl} = \sum [b_{kl}/\lambda \mathbf{g}_{kl}^t \mathbf{v}_i], \tag{18}$$

where $\mathbf{g}_{kl}^t$ is a transposed vector of constants. The frictional damping matrix can then be expressed in the form

$$\mathrm{F} = (1/\lambda)\mathbf{F}_i, \tag{19}$$

where the elements of $\mathbf{F}_i$ have the amplitude independent form

$$b_{kl}/\mathbf{g}_{kl}^t \mathbf{v}_i. \tag{20}$$

Equation (16) may therefore be stated as

$$\mathrm{j}(\lambda \mathbf{S} + \mathbf{F}_i)\mathbf{v}_i = \mathbf{p}_i \tag{21}$$

Since the power dissipated, W_i, when the system is vibrating at its ith natural frequency, is given by

$$W_i = -\dot{\mathbf{u}}_i^t \mathbf{p}_i = -\mathrm{j}\omega_i \lambda \mathbf{v}_i^t \mathbf{p}_i,$$

it follows that

$$W_i = \omega_i \mathbf{v}_i^t (\lambda^2 \mathbf{S} + \lambda \mathbf{F}_i)\mathbf{v}_i, \tag{22}$$

$$W_i/\lambda\omega_i = \lambda \mathbf{v}_i^t \mathbf{S} \mathbf{v}_i + \mathbf{v}_i^t \mathbf{F}_i \mathbf{v}_i \tag{23}$$

Clearly, equation (23) can be used to evaluate the n values of $\mathbf{v}_i^t$, $\mathbf{F}_i$ and $\mathbf{v}_i$ corresponding to n modes of the system. However, this information is not sufficient to completely define the form of the coulomb damping matrix $\mathbf{F}_i$ unless there is additional information relating to the location of the frictional mechanisms. For example, if it is known that all such mechanisms couple the structure to ground, $\mathbf{F}_i$ must be diagonal and a unique solution can readily be found to give the values of the corresponding hysteretic damping constants. Unfortunately, it would appear that no such general unique solution exists when the system also possesses frictional devices which couple one co-ordinate to another. However, the co-ordinates which are coupled either to ground or to other co-ordinates by frictional devices can easily be identified by measuring the power input, W_{ir} to each co-ordinate; when only the power to the rth co-ordinate is considered, equation (23) takes the form

$$W_{ir}/\lambda\omega_i = \lambda \mathbf{v}_i^t \mathbf{S}_r v_{ir} + \mathbf{v}_i^t \mathbf{F}_{ir} v_{ir}, \tag{24}$$

where v_{ir} is the rth element of $\mathbf{v}_i$, $\mathbf{F}_{ir}$ is the rth column of the matrix $\mathbf{F}_i$ and $\mathbf{S}_r$ is the rth column. of the matrix S. Equation (24) is now of the same form as equation (14) and when this result is plotted, a non-zero $\mathbf{v}_i^t \mathbf{F}_{ir} v_{ir}$ intercept indicates that a frictional device is coupled to the rth co-ordinate. Further, in the case of only a single frictional device being present in the system, which couples a pair of co-ordinates, say the rth and sth, the only non-zero intercepts would be those associated with these two co-ordinates and the magnitude q of the frictional device can be evaluated directly since

$$F_{i_{rr}} = F_{i_{ss}} = -F_{i_{rs}} = -F_{i_{sr}} = 4q/\pi(v_r - v_s). \tag{25}$$

4. EXPERIMENTAL INVESTIGATION

A series of tests were carried out in order that the identification method described in this paper could be applied to a practical system which included a coulomb frictional

device. The rig was designed to have two principal modes of vibration, a torsional mode and a transverse ***mode*** which could be tuned to provide close or well separated natural frequencies.

The essential features of the rig comprised a hollow steel rectangular tube which was securely connected to a rigid steel cross beam This assembly was mounted on a massive base and the ends of the tube were constrained so as to produce an encastre-pinned beam. Thus the hollow beam acted as both a spring in bending and torsion, the rigid steel cross beam providing the mass and inertia properties. Load masses, which were adjustable in position, were attached to the steel cross beam to provide a means of tuning the natural frequencies. The coulomb frictional device, which was located close to one end of the rigid cross beam, consisted of a highly polished hardened steel disc held in contact by a spring against a Teflon coated aluminium pad which was attached to the cross beam. In order to excite the normal modes of vibration of the system two electro-dynamic vibration exciters were connected to the cross beam via push-rod and piezoelectric force link assemblies, the output responses of the system being measured at the input points by piezoelectric accelerometers.

5. EXPERIMENTAL PROCEDURE

The criterion used for establishing when a normal mode of vibration was excited was the classical phase-resonance criterion [14]. By employing this criterion, the input powers in each normal mode were determined as a function of a reference modal amplitude. A typical set of results from these tests are shown on Figure 2. In order to determine the actual coulomb friction force magnitudes used in the tests, quasi-static measurements were carried out. These consisted of measuring the displacement of the cross beam and the input force at an excitation frequency of 20 **mHz.** The input force was plotted directly against the output displacement on an X-Y recorder which resulted in a hysteresis curve from which

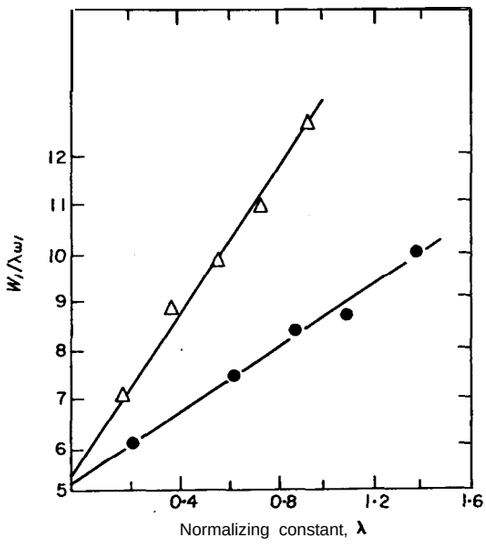

Figure 2 Experimental modal input powers from the transverse (-A-) and torsional (——●——) normal mode tests. The results are plotted according to the form ofequation (23).

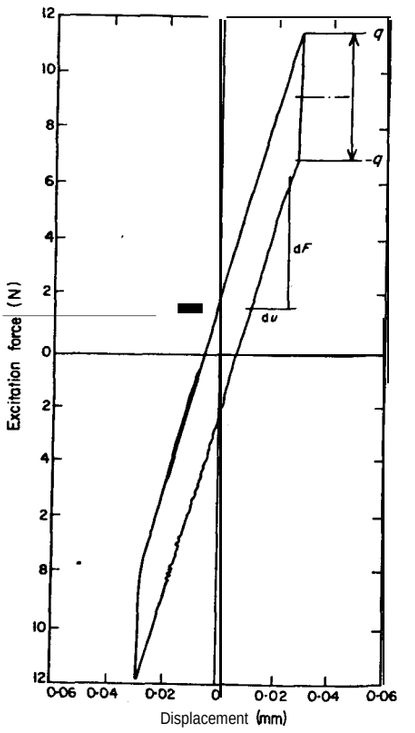

Figure 3. Hysteresis curve obtained from the quasi-static transverse mode test with the friction pad in contact. Frequency of excitation force is 20 mHz. dF/du = static stiffness.

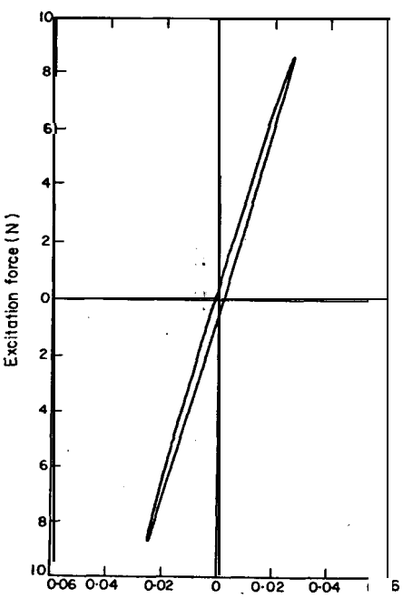

Figure 4. Hysteresis curve from the transverse mode without the friction pad in contact. The slope (as in Figure 4) represents the static stiffness of this mode. Frequency of excitation force is 20 mHz.

the frictional damping element characteristics could be obtained, Figures 3 and 4 show the hysteresis curves obtained from the quasi-static tests with and without the frictional device in operation.

6. ANALYSIS OF RESULTS

The form of the $\mathbf{F}_i$ matrix for the system under test is obtained by using the intercepts of the *curves* on Figure 2 and equation (25). The magnitude q of the frictional force is then given directly by using the information from either of the two modes since in this case

TABLE 1

Method of evaluation		Coulomb friction force level (N peak-to-peak)
Normal mode power curve (Figure 2)	Transverse mode	4·4
	Torsional mode	4.16
Quasi-static tests		4·5

$\mathbf{v}_1^t = [1{\cdot}0\ 1{\cdot}0]$, $\mathbf{v}_2^t = [1{\cdot}0\ -1{\cdot}0]$ and $F_i = 4q/\pi$. The values of q obtained from this analysis for both the torsional and transverse modes are shown in Table 1 together with the value of q obtained from the quasi-static tests. The results from one set of normal mode tests in the transverse mode were plotted in terms of the vector response in the phase plane,

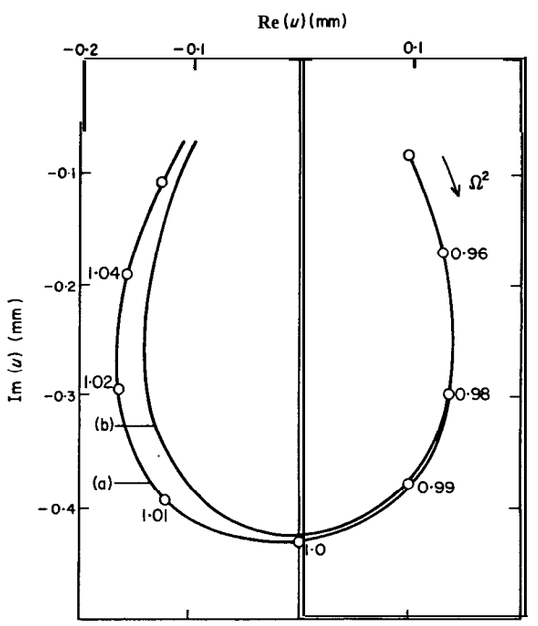

Figure 5. Distortion of a single mode vector response as a result of coulomb friction, curve (a) experimental results and (b) theoretical response using equations (7) and (8) with values of 6, r and P/k' obtained from test (a) results.

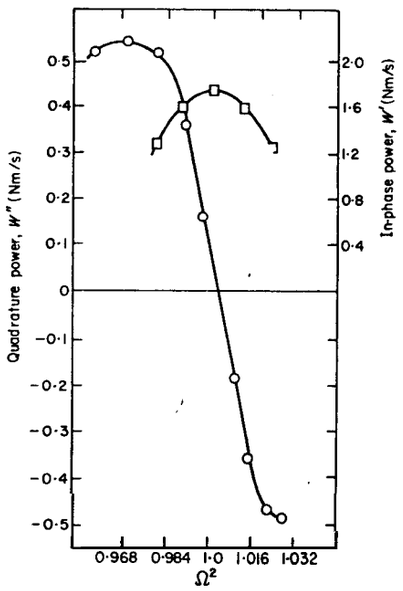

Figure 6. Experimental results from curve (a) of Figure 5 plotted in terms of the complex power components. □——□, In-phase component; ○——○, quadrature component.

together with the curve from equations (7) and (8). Figure 5 displays the similarity between the measured and theoretical results, and the same experimental data, in terms of the in-phase and quadrature powers is shown plotted on Figure 6.

7. CONCLUSIONS

The work described in this paper has shown that it is possible to analyze systems which include non-linear elements characterized by coulomb friction devices. In the case of a system comprising only one such device it has been shown that not only can the magnitudes of the frictional forces involved be evaluated but also the actual location of the non-linear element within the system is obtained In the case of more than one frictional device being present, it is necessary to have a ***priori*** knowledge regarding the location of those non-linearities in order that their characteristics can be evaluated In some cases these locations may be obvious, for example, a hinge or a guideway would provide the necessary mechanism, in which case their characteristics could be identified The application of complex power techniques to the frequency response testing of both linear and non-linear systems appears to offer advantages over the Kennedy and Pancu type plots, where, in the case of non-linearities, the response locus becomes disturbed to such an extent that damping and natural frequency estimates incur large errors. The mechanism of obtaining the power dissipation experimentally is exactly the same as that for obtaining the Kennedy and Pancu information, whether multi-point or single point excitation methods are used; thus no deviation in experimental technique is required.

The results of the experimental programme gave very encouraging results, and in the analysis of complex structures such as the ground resonance testing of aircraft the technique could be utilized, to aid the present identification schemes already employed.

REFERENCES

1. C. C. KENNEDY and C. D. P. PANCU 1947 *Journal of Aeronautical Sciences 14, 603625.* Use of vectors and vibration measurement and analysis.
2. M. RADES 1976 Shock *and Vibration Digest 8, 73-88.* Methods for the analysis of structural frequency-response measurement data.
3. H. G. D. GOYDER 1976 *Institute of Sound and Vibration Research Technical Report No. 87.* Structural modelling by the curve fitting of measured response data.
4. G. DE VRIES 1955 *La Recherche Aerospatiale 44, 5559.* Harmonic analysis applied to vibration testing of non-linear structures.
5. R. G. WHITE 1971 *Journal of Sound and Vibration 16, 255267.* Effects of non-linearity due to large deflections in the resonance testing of structures.
6. J. P. DEN HARTOG 1931 *Transactions of the American Society of Mechanical Engineers 53,107-l* 15. Forced vibrations with combined coulomb and viscous friction.
7. G. C. K. YEH 1966 *Journal of the Acoustical Society of America 39, 14-24.* Forced vibrations of a two degree-of-freedom system with combined coulomb and viscous damping.
8. A. TONDL 1975 *Shock and Vibration Digest* **7, 3–20**. *The* application of skeleton curves and limit envelopes to the analysis of non-linear vibrations.
9. L. PUST 1974 *Proeeedings of the 4th World Congress for the Theory of Machines and Mechanisms, Yugoslavia, 16-24.* Properties of the dynamic compliance matrix of non-linear systems.
10. T. K. CAUGHEY and M. E. J. O'KELLY 1965 *Journal of Applied Mechanics, Transactions of the American Society of Mechanical Engineers 32, 583-588.* Classical normal modes in damped linear systems.
11. L. Y. BAHER and R. L. MALLETT 1978 *Journal of Applied Mechanics, Transactions of the American Society of Mechancial Engineers* **45, 225–226**. Discussion of "A theorem on the free vibration of damped systems".
12. T. K. HASSELMAN 1974 *AIAA/ASME/SAE 15th—Structures, Structural Dynamics and Material, Conferences, Las Vegas, Nevada. AIAA Paper No, 74-387.* Damping synthesis from substructure tests.
13. E. BONNEAU 1969 *La Recherche Aerospatiale* **130, 45–51**. Determination of the vibration characteristics of a structure from the expression of the complex power supplied.
14. R. C. LEWIS and D. L. WRISLEY 1950 *Journal of Aeronautical Sciences* **17, 705–736.** A system for the excitation of pure natural modes of complex structures.